中央大学博士論文

Electromagnetic Plane Wave Scattering by Aperture on Thick Conducting Screen

NGUYEN Nam Khanh

博士 (工学)

中央大学大学院 理工学研究科 電気・情報系専攻

Electrical Engineering and Information System Course

Graduate School of Science and Engineering

Chuo University

March 2021

Contents

List of Figures

Chapter 1

Introduction

1.1 Electromagnetic Wave Scattering

Scattering of electromagnetic waves is the process of re-radiation of an incident wave by an obstacle (scatterer). Depend on the scatterer's shape and material, the propagation direction, amplitude, phase, polarization of the incident electromagnetic wave can be changed. In some special cases, the incident plane wave can even be changed into the spherical or cylindrical waves. The purpose of solving a scattering problem is to determine those variations by combining physical knowledge and mathematical tools. In electromagnetism, the term scattering can be used as a synonym of diffraction, while there is a distinction between them in the optical area. It is necessary to understand the electromagnetic scattering characteristics by a certain material body to design microwave, and radio devices and systems.

Electromagnetic scattering is an interdisciplinary topic that has been researched for decades and utilized in various applications. Remote sensing technologies use the scattered electromagnetic fields from the object to remotely and non-destructively observe and predict the surrounding space and material scatterers. Understanding how electromagnetic waves interact with the objects and how to get scattered waves from them helps us to extract their encoded information (shape, material, position, orientation, speed, etc.) in the scattered fields. An efficient scattered field simulation also plays an important role. Radar systems in this application generally operate at microwave frequencies between 100 MHz and 100 GHz corresponding to wavelength from 3 m to 3 mm which is comparable to the ordinary scatterer's size. Moreover, frequencies from 430 THz to

770 THz of the visible spectrum corresponding to wavelength from 390 nm to 700 nm is applicable in the nanoscience area. In these cases, the wave nature of electromagnetic fields is recognizable via the scattering effects, for example, wave penetration into shadow region, where framework of simple ray optical constructions cannot explain appropriately. The inability of simple ray-based concepts to sufficiently describe these wave phenomena has led to the creation of electromagnetic scattering theory. Electromagnetic scattering theory is a branch of electromagnetics that describes, explains, and predicts electromagnetic field behavior in the existence of objects by fully considering the wave nature of the electromagnetic field. Electromagnetic scattering theory includes knowledge of physics (particularly, electromagnetics and optics) and mathematics. During its history, many outstanding researchers, including Rene Descartes (1596–1650), Christiaan Huygens (1629–1695), Thomas Young (1773–1829), Augustin-Jean Fresnel (1788–1827), Hermann von Helmholtz (1821–1894), Gustav Kirchhoff (1824–1887), James Clerk Maxwell (1831–1879), Heinrich Hertz (1857–1894), and Arnold Sommerfeld (1868–1951), have contributed to the establishment of the wave theory of electromagnetic scattering. The theory is still in the process of development motivated by new application fields, from stealthy aircraft and ships to metamaterials in photonics and nanoscience. This thesis concentrates on radio wave propagation application where analysis of electromagnetic scattering features from outdoor buildings, trees, and indoor furniture is necessary to build an efficient wave propagation model.

To be applied to the practical problems with complicated scatterers, it is necessary to solve the theoretical problems for canonical objects. One of the original research on electromagnetic scattering solution is related to the classical study of circular cylinder or sphere diffraction. As introduced in [1], a dielectric circular cylinder diffraction was first considered by Rayleigh [2], and that of a dielectric sphere was first determined by Lorenz [3]. Besides, wave diffraction by conducting circular cylinder and sphere was solved by Thomson [4]. Also, a solution published by Mie [5] became widely known as theoretical Mie scattering for sphere diffraction. After that, much simpler and more compact mathematical formulation have been developed to solve the above canonical scattering problems, and they are introduced in some textbooks, for example, [1], [6]–[9].

1.2 Research Background

In recent years, wireless communication in metropolitan area has been studied and improved continuously to suffice the quantity and quality demand of device connection. A representative example is that the researchers and developers are creating new equipment and techniques, ready for the era of 5G (the fifth generation technology standard for broadband cellular networks) with a huge number of devices connected at high speed. One of the most important aspects is the research on the radio wave behavior with the existence of the objects in the urban environment. In fact, the radio waves are strongly affected by the walls and windows of high-rise buildings. Here, window apertures can be considered as the primary communicating path for indoor-outdoor mobile radio wave propagation while building walls cause reflection for almost all of the high frequency signals. Accurately estimating these effects will lead to stable and higher-speed wireless communication services. Moreover, window scattering analyses help mobile service providers to determine base station arrangement and plan a suitable communication frequency.

A suitable electromagnetic wave scattering calculation method plays the main role in the efficiency of a wave prediction model. The aperture scattering problem has been approached by various calculation methods that depend on the corresponding application. An eigenfunction expansion solution in terms of Mathieu functions [10] has been applied by Morse and Rubinstein, while Kobayashi Potential (KP) method with Weber-Schafheitlin discontinuous integrals [11] has been given by Nomura and Katsura to analyze the scattering characteristic by an infinitely thin slit. The KP method is also an effective solution in more complicated cases of the two-dimensional thick conducting slits [12], [13] or three-dimensional hole [14]. To analyze the thickness effect, Wiener-Hopf and generalized matrix technique [15], and Fourier transform technique [16], [17] may also be applied. Nevertheless, the above results have mainly considered relatively narrow slit apertures.

The exact solution is desirable everywhere. An exact solution of the aperture scattering problem may be represented in the form of wave equation eigenfunction series. However, when the aperture width is electrically large, the rate of series convergence is slow which leads to difficult numerical evaluation. Considering the feasibility, approximation methods have been used widely to solve various problems. Finite Difference Time Domain (FDTD), Finite Element Method (FEM), Method of Moment (MOM), Finite Difference Method

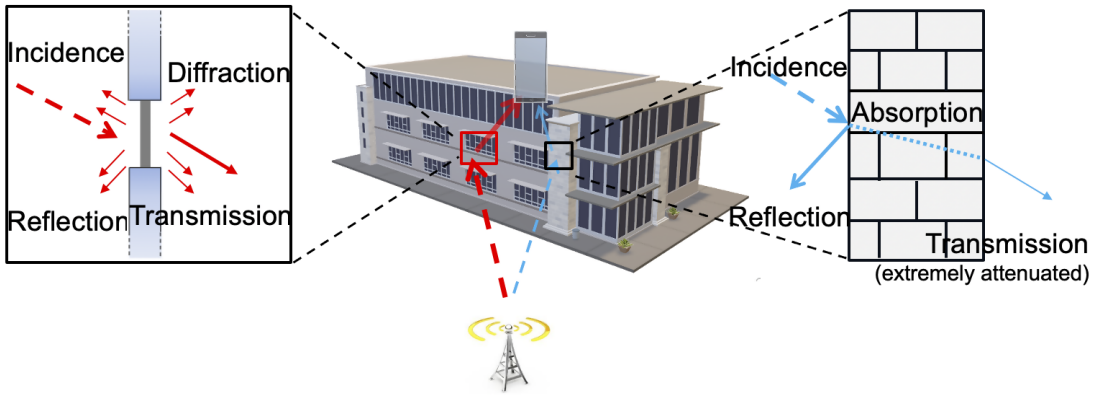

Figure 1.1: Outdoor-indoor electromagnetic wave propagation model with effect of building windows and walls.

(FDM) are among the famous numerical methods. Some numerical methods are developed to estimate the scattering by the objects of small size compared with wavelength [18]–[24]. However, these numerical methods may have a problem applying for the scattering by electrically large objects because of unrealistic execution time and heavy memory requirement. Additionally, the numerical solutions cannot provide qualitative, physical insight into the basic mechanisms of scattering and diffraction.

Besides, asymptotic high frequency methods also provide powerful and fast ability in analyzing a wide variety of electromagnetic scattering problems of electrically large objects. These approaches can be grouped into two categories. One is the ray optical methods group containing Geometrical Optics (GO), Geometrical Theory of Diffraction (GTD) and Uniform version of the GTD, which is further divided into UTD and UAT. There is another group using the wave optical method, in which we can list the Physical Optics (PO) and the Physical Theory of Diffraction (PTD). Around 1883, Kirchhoff had generalized the integral representation of equivalent source. This integral representation of equivalent source is later known as Kirchhoff approximation (KA) or physical optics approximation which serves well the derivation of scattering integral using incident wave. The high frequency asymptotic solution obtained from this scattering integral represents the diffracted waves. The GO ray field consists of direct, reflected and diffracted rays. The method describes reflection and refraction of high frequency EM waves but not the diffraction of waves around edges and smooth objects. Meanwhile, the wave-based physical optics approach finds the scattered field by directly integrating currents induced when

a metallic body is illuminated by external electromagnetic source. GTD is an upgraded version of GO and it overcame the failure of GO in the shadow region; and it illustrates nicely the mechanism of radiation and scattering.

For practical applications of indoor-outdoor mobile radio wave propagation through windows, one has to pay attention that the window dimension is large with respect to the wavelength. Then the numerical methods and eigenfunction methods are not efficient for this scenario, high frequency asymptotic techniques may be more suitable. Clemmow solved the problem of scattering of electromagnetic plane waves by an infinite slit constructed from two perfectly conducting semi-infinite coplanar screens of zero thickness for the special case of normal incidence using asymptotic series [26]. Levine extended the solution for all angles of incidence by applying Wiener-Hopf technique to the integral equation combined with Taylor's series [27]. That method was also used in a simple representation with less algebraic manipulations by Seshadri [28] and with Wu [29] for both E and H-polarization. Wiener-Hopf technique of higher order asymptotic is also applied for high frequency diffraction by a strip [30]. However, as mentioned, the above approaches have only considered infinitely thin slit. More realistic approaches where the thickness is considered such as Geometrical Theory of Diffraction (GTD) [25]–[33] and Kirchhoff approximation (KA) method [34] may be convenient to use. GTD is known to yield accurate results in slit diffraction, if the effect of the multiple edge diffraction is included [25], [33]. However, GTD may not be applicable for the case of the rectangular holes, since the accurate diffraction coefficient of the corner is not available yet.

In this study, we utilize the KA method to analyze the plane wave scattering by the window aperture. KA is one of the representative methods to calculate the scattering fields. Using KA (sometimes known as PO since there is no clear distinction between them) to solve the electromagnetic scattering problem, the radiation from equivalent electric and magnetic currents approximated from incident wave can be represented in the integral form. This integral form cannot be evaluated analytically. By evaluating by numerical integral with large value of wave number k, the asymptotic solution for high frequencies can be obtained. According to this asymptotic evaluation of the integral expression, scattering fields, in general, include the components of incident plane wave, reflected plane wave from conducting surface and diffracted wave from the object's edge. As presented in [35], the KA method is applied to derive scattering fields from a conducting wedge in

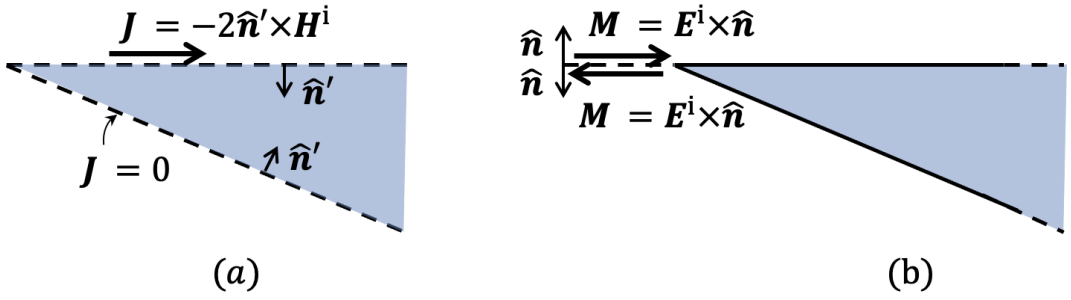

Figure 1.2: Equivalent current sources in the KA method. (a) Electric currents postulated on the virtual surface on the conducting wedge. (b) Magnetic currents postulated on the aperture virtual surface.

two ways. The first one is that the scattering field is conducted from the equivalent electric currents ($\boldsymbol{J}$) exist on the virtual surface postulated on the conducting wedge surface. These electric current sources result from the magnetic component of the incident plane wave. Another way to derive the scattering field is using the equivalent magnetic currents ($\boldsymbol{M}$) exist on the virtual extended surface (the aperture) of the conducting surface. These magnetic current sources result from the electric component of the incident plane wave. The latter method is suitable to be utilized in this thesis to derive the scattering fields at both upper and lower half-space of the slit/hole. The primary scattering fields can be considered as field radiations from equivalent magnetic current sources postulated on the closing aperture. In order to obtain the diffracted field from the lower aperture of the thick slit/hole, conversion into waveguide modes can be used to obtain the internal waveguide fields inside the slit/hole, and the magnetic current is postulated again at the lower aperture from them. The numerically obtained results are compared with those of other methods to evaluate the accuracy of the proposed formulation in different conditions of the slit/hole dimension. The KA method has great advantages for general scattering analyses, since the formulation is simpler than that of the GTD, and easy to adapt to complicated problems. By our analysis, it has been shown that the KA method can be applied confidently for large aperture cases especially for estimating the main diffraction beam behavior. Also, the simple formulation leads to a short calculation time. Accordingly, the method has been successfully applied to investigate the plane wave scattering by complicated and realistic objects such as thick loaded slits which can be considered as a model of window aperture with glass layers. A further step to study more practical

diffraction analysis by three-dimensional rectangular holes in a thick conducting screen has been established. More realistic aspects are under investigation.

1.3 Thesis Contents

This thesis consists of four chapters.

In Chapter 2, the KA method has been applied to formulate plane wave scattering by loaded conducting thick slits. This is the model of a two-dimensional window aperture with a glass layer inserted. Here, the far-field scattering in the upper, lower, and inner region of the slit has been formulated as field radiations from equivalent magnetic current sources postulated on the upper and lower apertures. The effect of the loaded layer on the scattering fields has also been investigated. Both E and H polarization of the incident wave has been taken into the formulation. Numerical calculations and discussion are carried out, and the accuracy of the presented method is evaluated by comparison with the results from reference solutions of GTD and KP methods. Special cases of infinitely thin slit, as well as empty slit, have also been considered to evaluate the accuracy.

The KA method is extended to solve the plane wave scattering problem from a rectangular hole perforated in a thick conducting screen which is the three-dimension of the building window in Chapter 3. This is a very important step where the KA method is proved to be able to solve a practical problem of three-dimensional model. Based on that, more practical problems can be solved using this calculation method. Also, the KA efficiency can be evaluated since calculation for 3D objects is obviously much more complicated compared with those of 2D objects. The calculation process is similar to which shown in Chapter 2 where the scattering field can be derived using the equivalent magnetic current sources. However, the detailed formulation is different since the scattered object is three-dimensional. Both E and H polarization of the incident wave has been taken into the formulation. Relation between the above two-dimensional and three-dimensional scattering formulation has also been shown. Here, conversion equations between 2D and 3D formulations are expressed. This is not only to self-validate the formulation but also help to estimate the complicated 3D scattering results from the simpler 2D results. Then the calculation speed is reduced especially when more practical problems are taken into account. Numerical calculations and discussion are carried out, and the accuracy of pre-

sented method is evaluated by comparison with the results from reference solution of the KP method.

Finally, Chapter 4 shows conclusions and discussions on our research. In the following discussion, the time-harmonic factor $e^{-i\omega t}$ is assumed and suppressed throughout the text.

Chapter 2

Analysis of Plane Wave Scattering by Loaded Conducting Thick Slits

In this chapter, the KA method has been applied to formulate plane wave scattering by loaded conducting thick slits. The scattering field can be obtained by the radiation from equivalent magnetic current sources on the aperture of the slit. Equivalent magnetic currents are also applied to calculate the penetrating fields inside the slit and the subsequent transmitted field in the lower region. Both E and H polarized incident plane wave have been formulated, and formulation of a special case of infinite screen has been derived. The formulas derived in Sects. 2.1 and 2.2 are used to obtain some numerical results for the scattering far-fields in Sect. 2.3. The KA method results have been compared with those of GTD and KP method for validation.

As illustrated in Fig. 2.1, a plane wave with a unit amplitude:

$$\phi_y^{\mathrm{i}} = e^{-ik(x\cos\theta_0 + z\sin\theta_0)} \tag{2.1}$$

impinges upon a slit perforated on an infinitely long perfectly conducting thick screen with incident angle θ_0. The width and thickness of the slit are a and b, respectively, and k is the free space wavenumber. ϕ_y^{i} represents for $E_y^{\mathrm{i}}(H_y^{\mathrm{i}})$ for E(H) polarization. Inside the slit, there exists a medium layer of permittivity ε_r and permeability μ_r and its thickness is $b_2 - b_1$. In order to determine the scattering contributions ϕ_y^{s}, the KA method is utilized here. Consequently, the scattering fields are obtained as radiations from the equivalent magnetic current sources on the virtually closed apertures.

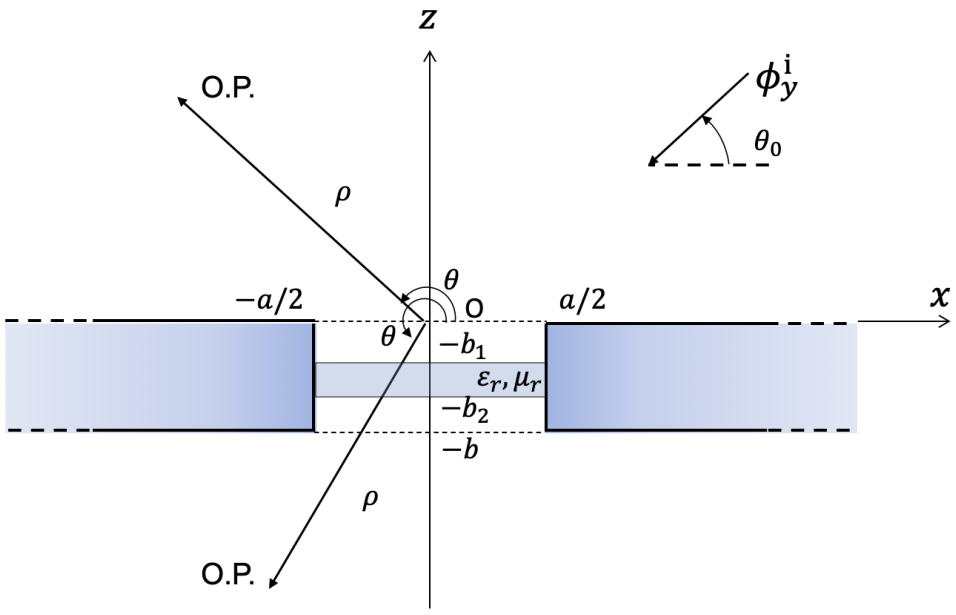

Figure 2.1: Plane wave scattering by a loaded slit in a thick conducting screen.

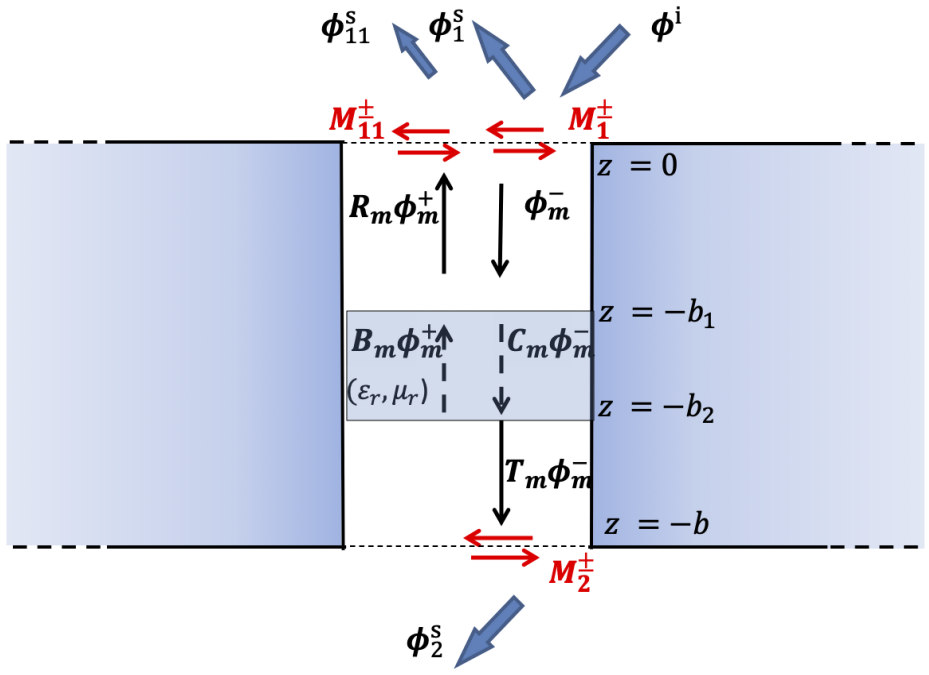

Figure 2.2: Scattering field at upper and lower regions of the slit (radiation from the equivalent magnetic current sources at the slit apertures).

By doing so, there exists a reflected field $\boldsymbol{\phi}^{\mathrm{r}}$ due to the reflection from the screen's surface at $z = 0$ in the upper half-space ($z > 0$) as

$$\phi_y^r = \begin{pmatrix} E_y^r \\ H_y^r \end{pmatrix} = \mp e^{-ik(x\cos\theta_0 + z\sin\theta_0)}, \tag{2.2}$$

for E and H polarizations. This contribution will be omitted in the following analysis.

2.1 E Polarization

In this case, we have a Transverse Electric (TE) incident plane wave where electric vectors $\boldsymbol{E}^{\mathrm{i}}$ are perpendicular with the wave propagation direction. Eq. (2.1) becomes

$$E_y^{\mathrm{i}} = e^{-ik(x\cos\theta_0 + z\sin\theta_0)}. \tag{2.3}$$

2.1.1 Primary Upper Scattering Far-field

The equivalent magnetic current sources on the closed upper side of the upper aperture $\boldsymbol{M}_1^+$ can be expressed in terms of incident electric field as:

$$\begin{aligned} \boldsymbol{M}_1^+(x, z = 0_+) &= E_y^{\mathrm{i}}\big|_{z=0}\hat{\boldsymbol{y}} \times (+\hat{\boldsymbol{z}}) = E_y^{\mathrm{i}}\big|_{z=0}\hat{\boldsymbol{x}} \\ &= e^{-ikx\cos\theta_0}\hat{\boldsymbol{x}}, \quad (|x| < \frac{a}{2}, z = 0_+), \end{aligned} \tag{2.4}$$

where ' $\hat{}$ ' denotes the corresponding unit vector. With the condition of no equivalent electric current exists, the scattering E-field $\boldsymbol{E}_1^{\mathrm{s}}(\boldsymbol{r})$ can be expressed in terms of the equivalent magnetic current $\boldsymbol{M}_1^+$ as

$$\begin{aligned} \boldsymbol{E}_1^{\mathrm{s}}(\boldsymbol{r}) &= -\int_{S'} \{\boldsymbol{M}_1^+(\boldsymbol{r'}) \times \boldsymbol{\nabla}' G\} dS' \\ &= -\int_{S'} M_{1x}^+(\boldsymbol{r'})\hat{\boldsymbol{x}} \times \left(\frac{\partial G}{\partial x'}\hat{\boldsymbol{x}} + \frac{\partial G}{\partial y'}\hat{\boldsymbol{y}} + \frac{\partial G}{\partial z'}\hat{\boldsymbol{z}}\right) dS' \\ &= -\int_{S'} M_{1x}^+(\boldsymbol{r'}) \left(\frac{\partial G}{\partial y'}\hat{\boldsymbol{z}} - \frac{\partial G}{\partial z'}\hat{\boldsymbol{y}}\right) dS', \end{aligned} \tag{2.5}$$

where S' is the aperture ($|x'| < a/2, z' = 0_+$) on which the equivalent source $\boldsymbol{M}_1^+$ exists, $\boldsymbol{r}$ is the vector directed to the observation point, $\boldsymbol{r'}$ is the position vector to the aperture source point $(x', z' = 0)$ on S', and G is the two-dimensional half-space Green's function, considering the imaging effect of the magnetic current on the boundary

$$G(x, z; x', z') = \frac{i}{2} H_0^{(1)}(k\sqrt{(x - x')^2 + (z - z')^2}). \tag{2.6}$$

The scattering E-field $\boldsymbol{E}_1^{\rm s}(\boldsymbol{r})$ has only y component $E_{1y}^{\rm s}$[35]

$$E_{1y}^{\rm s} = \int_{-a/2}^{a/2} M_{1x}^{+}(x') \frac{\partial}{\partial z'} \left\{ \frac{i}{2} \mathrm{H}_0^{(1)}(k\sqrt{(x-x')^2+(z-z')^2}) \Big|_{z'=0} \right\} dx', \tag{2.7}$$

where the zeroth-order Hankel function of the first kind $\mathrm{H}_0^{(1)}(\chi)$ for variable x' is evaluated by the special integral for variable η with saddle point method as

$$H_0^{(1)}(k\sqrt{(x-x')^2+(z-z')^2}) = \frac{1}{\pi} \int_{-\infty}^{\infty} \frac{e^{i\eta(x-x')+i\sqrt{k^2-\eta^2}|z-z'|}}{\sqrt{k^2-\eta^2}} d\eta. \tag{2.8}$$

Then Eq.(2.7) becomes, in case of $z > 0$, $z' = 0$

$$\begin{aligned}
E_{1y}^{\rm s} &= -\frac{i}{2\pi} \int_{-a/2}^{a/2} e^{-ikx'\cos\theta_0} \frac{\partial}{\partial z'} \left\{ \int_{-\infty}^{\infty} \frac{e^{i\eta(x-x')+i\sqrt{k^2-\eta^2}(z-z')}}{\sqrt{k^2-\eta^2}} \Big|_{z'=0} \right\} d\eta dx' \\
&= \frac{-i^2}{2\pi} \int_{-a/2}^{a/2} e^{-ikx'\cos\theta_0} \int_{-\infty}^{\infty} e^{i\eta(x-x')+i\sqrt{k^2-\eta^2}z} d\eta dx' \\
&= \frac{1}{2\pi} \int_{-\infty}^{\infty} e^{i\eta x+i\sqrt{k^2-\eta^2}z} \int_{-a/2}^{a/2} e^{-i(k\cos\theta_0+\eta)x'} dx' d\eta \\
&= \frac{1}{2\pi} \int_{-\infty}^{\infty} e^{i\eta x+i\sqrt{k^2-\eta^2}z} \frac{e^{-i(k\cos\theta_0+\eta)x'}}{-i(k\cos\theta_0+\eta)} \Big|_{-a/2}^{a/2} \\
&= \frac{1}{2\pi} \int_{-\infty}^{\infty} e^{i\eta x+i\sqrt{k^2-\eta^2}z} \frac{e^{i(k\cos\theta_0+\eta)a/2} - e^{-i(k\cos\theta_0+\eta)a/2}}{i(k\cos\theta_0+\eta)} \\
&= \frac{-i}{2\pi} \int_{-\infty}^{\infty} \frac{e^{(ika\cos\theta_0)/2+i\eta(x+a/2)+i\sqrt{k^2-\eta^2}z} - e^{(-ika\cos\theta_0)/2+i\eta(x-a/2)+i\sqrt{k^2-\eta^2}z}}{(k\cos\theta_0+\eta)} d\eta \\
&= I_1 + I_2.
\end{aligned} \tag{2.9}$$

where

$$I_1 = \frac{-i}{2\pi} \int_{-\infty}^{\infty} \frac{e^{(ika\cos\theta_0)/2+i\eta(x+a/2)+i\sqrt{k^2-\eta^2}z}}{(k\cos\theta_0+\eta)} d\eta, \tag{2.10}$$

$$I_2 = \frac{i}{2\pi} \int_{-\infty}^{\infty} \frac{e^{(-ika\cos\theta_0)/2+i\eta(x-a/2)+i\sqrt{k^2-\eta^2}z}}{(k\cos\theta_0+\eta)} d\eta. \tag{2.11}$$

Calculate above integral with saddle point method with

$$\begin{aligned}
&\eta = k\sin\omega, \quad d\eta = k\cos\omega d\omega, \quad x \mp a/2 = \rho_\pm \cos\theta_\pm, \quad z = \rho_\pm \sin\theta_\pm, \\
&\sqrt{k^2-\eta^2} = \sqrt{k^2-k^2\sin^2\omega} = k\cos\omega, \\
&i\eta(x \pm a/2) + i\sqrt{k^2-\eta^2}z = ik\sin\omega\rho_\mp\cos\theta \mp + ik\cos\omega\rho_\mp\sin\theta_\mp \\
&\qquad\qquad = ik\rho_\mp \sin(\omega+\theta_\mp).
\end{aligned} \tag{2.12}$$

Then I_1, I_2 become

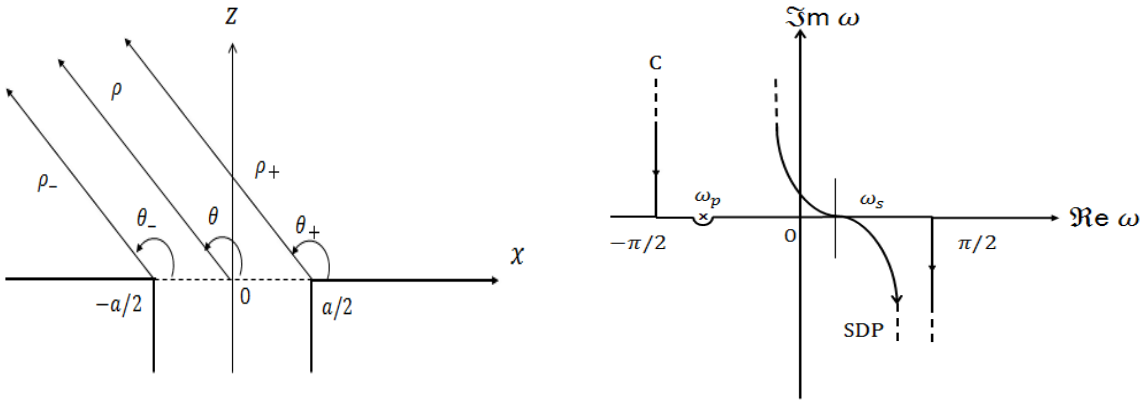

(a) (b)

Figure 2.3: Saddle point method integral evaluation (upper region).

$$I_1 = \frac{-i}{2\pi}\int_C \frac{e^{(ika\cos\theta_0)/2+ik\rho_-\sin(\omega+\theta_-)}}{(k\cos\theta_0 + k\sin\omega)} k\cos\omega d\omega$$
$$= \frac{-i}{2\pi}\int_C \frac{e^{(ika\cos\theta_0)/2+ik\rho_-\sin(\omega+\theta_-)}}{(\cos\theta_0 + \sin\omega)} \cos\omega d\omega, \tag{2.13}$$
$$I_2 = \frac{i}{2\pi}\int_C \frac{e^{(-ika\cos\theta_0)/2+ik\rho_+\sin(\omega+\theta_+)}}{(k\cos\theta_0 + k\sin\omega)} k\cos\omega d\omega$$
$$= \frac{i}{2\pi}\int_C \frac{e^{(-ika\cos\theta_0)/2+ik\rho_+\sin(\omega+\theta_+)}}{(\cos\theta_0 + \sin\omega)} \cos\omega d\omega. \tag{2.14}$$

The position of the pole in the ω plane yields $-\cos\theta_0 = \sin\omega_p$, then

$$\omega_p = \arcsin(-\cos\theta_0) = -\arcsin(\cos\theta_0), \tag{2.15}$$

θ_0	0	$\frac{\pi}{2}$	π
ω_p	$-\frac{\pi}{2}$	0	$\frac{\pi}{2}$

One can find the saddle point from

$$\frac{\partial}{\partial\omega}(ik\rho_\pm\sin(\omega+\theta_\pm)) = ik\rho_\pm\cos(\omega+\theta_\pm) = 0$$
$$\cos(\omega_s+\theta_\pm) = 0, \quad \omega_s+\theta_\pm = \pm\frac{\pi}{2}. \tag{2.16}$$

Since the observation point is in the upper half-plane, the saddle point in $-\frac{\pi}{2} < \omega < \frac{\pi}{2}$ is With $\theta > 0$:

$$\omega_s = \frac{\pi}{2} - \theta_\pm, \quad \sin\omega_s = \sin\left(\frac{\pi}{2}-\theta_\pm\right) = \cos\theta_\pm, \quad \cos\omega_s = \cos\left(\frac{\pi}{2}-\theta_\pm\right) = \sin\theta_\pm,$$
$$ik\rho_\pm\sin(\omega+\theta_\pm) \sim ik\rho_\pm\sin(\omega_s+\theta_\pm) - \frac{ik\rho_\pm}{2}\sin(\omega_s+\theta_\pm)(\omega-\omega_s)^2,$$
$$= ik\rho_\pm - \frac{ik\rho_\pm}{2}(\omega-\omega_s)^2. \tag{2.17}$$

Then

$$
\begin{aligned}
I_1 &= \frac{-i}{2\pi} e^{(ika\cos\theta_0)/2} \int_{SDP} \frac{e^{ik\rho_- - ik\rho_-(\omega-\omega_s)^2/2}}{\cos\theta_0 + \sin\omega_s} \cos\omega d\omega \\
&\sim \frac{-i}{2\pi} e^{(ika\cos\theta_0)/2} \cdot \frac{\sin\theta_-}{\cos\theta_0 + \cos\theta_-} e^{ik\rho_-} \sqrt{\frac{2\pi}{ik\rho_-}} \\
&= \frac{-2\sin\theta_-}{\cos\theta_0 + \cos\theta_-} \sqrt{\frac{1}{8\pi k\rho_-}} \cdot e^{ik\rho_- + (ika\cos\theta_0)/2 + i\pi/4},
\end{aligned} \tag{2.18}
$$

$$
\begin{aligned}
I_2 &= +\frac{i}{2\pi} e^{-(ika\cos\theta_0)/2} \int_{SDP} \frac{e^{ik\rho_+ - ik\rho_+(\omega-\omega_s)^2/2}}{\cos\theta_0 + \sin\omega_s} \cos\omega d\omega \\
&\sim \frac{i}{2\pi} e^{-(ika\cos\theta_0)/2} \cdot \frac{\sin\theta_+}{\cos\theta_0 + \cos\theta_+} e^{ik\rho_+} \sqrt{\frac{2\pi}{ik\rho_+}} \\
&= \frac{2\sin\theta_+}{\cos\theta_0 + \cos\theta_+} \sqrt{\frac{1}{8\pi k\rho_+}} \cdot e^{ik\rho_+ - (ika\cos\theta_0)/2 + i\pi/4}.
\end{aligned} \tag{2.19}
$$

If the observation point is sufficiently far, considering the phase only, one gets

$$
\rho_\pm \sim \rho \mp \frac{a}{2}\cos\theta, \quad \theta_\pm \sim \theta. \tag{2.20}
$$

Then the scattering E far-field is

$$
\begin{aligned}
E^{\mathrm{s}}_{1y} &= I_1 + I_2 \\
&= \frac{2\sin\theta}{\cos\theta_0 + \cos\theta} \sqrt{\frac{1}{8\pi k\rho}} e^{ik\rho + i\pi/4} \left(e^{-(ika\cos\theta_0)/2 + (ika\cos\theta)/2} - e^{(ika\cos\theta_0)/2 - (ika\cos\theta)/2} \right) \\
&= \frac{-4i\sin\theta\sin\left\{ka(\cos\theta_0 + \cos\theta)/2\right\}}{\cos\theta_0 + \cos\theta} \sqrt{\frac{1}{8\pi k\rho}} e^{ik\rho + i\pi/4} \\
&= \frac{-4i\sin\theta\sin\left\{ka(\cos\theta_0 + \cos\theta)/2\right\}}{\cos\theta_0 + \cos\theta} C(k\rho),
\end{aligned} \tag{2.21}
$$

where

$$
C(k\rho) = \sqrt{\frac{1}{8\pi k\rho}} e^{ik\rho + i\pi/4}. \tag{2.22}
$$

On the shadow boundary ($\theta = \pi - \theta_0$):

$$
\sin\theta = \sin(\pi - \theta_0) = \sin\theta_0,
$$

$$
\cos\theta = \cos(\pi - \theta_0) = -\cos\theta_0.
$$

Then

$$\begin{aligned}\lim_{\theta\to\pi-\theta_0} E^{\rm s}_{1y} &= \sqrt{\frac{1}{8\pi k\rho}}e^{ik\rho+i\pi/4}\lim_{\theta\to\pi-\theta_0}\frac{-4i\sin\theta\sin\left\{ka(\cos\theta_0+\cos\theta)/2\right\}}{\cos\theta_0+\cos\theta}\\ &= \sqrt{\frac{1}{8\pi k\rho}}e^{ik\rho+i\pi/4}\frac{-4i\sin\theta\cos\left\{ka(\cos\theta_0+\cos\theta)/2\right\}ka(-\sin\theta)/2}{-\sin\theta}\Big|_{\theta\to\pi-\theta_0}\\ &= -2ika\sin\theta\ C(k\rho). \end{aligned} \tag{2.23}$$

2.1.2 Modal Excitation in Slit Region

A part of the incident plane wave penetrates through the upper aperture and propagates into the slit. This field impinges the loaded medium and eventually leads to the scattering field in the lower half-space and a secondary contribution in the upper half-space. In the previous study by GTD [31]–[33], the field in the slit has been considered to be excited by the aperture edges ($x=\pm a/2, z=0$), and the exciting waveguide modes have been derived from the ray-mode conversion method. In this investigation, however, the modal excitation is given by equivalent magnetic source $\boldsymbol{M}_1^-$ on the closed aperture expressed as

$$\begin{aligned}\boldsymbol{M}_1^-(x,z=0_-) &= E_y^{\rm i}\big|_{z=0}\hat{\boldsymbol{y}}\times(-\hat{\boldsymbol{z}}) = -E_y^{\rm i}\big|_{z=0}\hat{\boldsymbol{x}}\\ &= -e^{-ikx\cos\theta_0}\hat{\boldsymbol{x}},\quad (|x|<\frac{a}{2}, z=0_-),\end{aligned} \tag{2.24}$$

The excited field $\boldsymbol{\phi}^{\rm w}=\boldsymbol{E}^{\rm w}$ inside a semi-infinitely long ($b\to\infty$) parallel plane waveguide may be expressed as

$$E_y^{\rm w} = \int_{-a/2}^{a/2} M_{1x}^-(x')\frac{\partial}{\partial z'}G^{\rm w}(x,z;x',z'=0_-)dx', \tag{2.25}$$

where $G^{\rm w}$ is the Green's function for a parallel plane waveguide considering the imaging effect for the metal closure at the aperture, namely

$$G^{\rm w}(x,z;x',z') = \sum_{m=1}^{\infty}\frac{2i}{a\zeta_m}\sin\frac{m\pi}{a}\left(x+\frac{a}{2}\right)\sin\frac{m\pi}{a}\left(x'+\frac{a}{2}\right)e^{i\zeta_m|z-z'|}, \tag{2.26}$$

and ζ_m denotes the wave number in z-direction as

$$\zeta_m = \sqrt{k^2-\left(\frac{m\pi}{a}\right)^2}. \tag{2.27}$$

The field propagating downward inside the slit may be derived as

$$E_y^{\rm w} = \sum_{m=1}^{\infty}E_m^-, \tag{2.28}$$

where

$$E_m^{\pm} = F_m \sin\frac{m\pi}{a}\left(x+\frac{a}{2}\right)e^{\pm i\zeta_m z}. \tag{2.29}$$

Here, F_m is the excitation coefficient of the $\mathrm{TE_m}$ waveguide modal field. F_m can be calculated by integrating the equivalent source $\boldsymbol{M}_1^-$ over the aperture ($|x| \leqslant a/2, z = 0_-$), one gets

$$\begin{aligned} F_m = &-\frac{2m\pi}{\{(m\pi)^2 - (ka\cos\theta_0)^2\}} \\ &\cdot\left\{(-1)^m e^{(-ika\cos\theta_0)/2} - e^{(ika\cos\theta_0)/2}\right\}. \end{aligned} \tag{2.30}$$

2.1.3 Secondary Upper Scattering Far-field and Lower Scattering Far-field

The waveguide modes $\phi_m^- = E_m^-$ impinge the loaded medium as in Fig. 2.2. Then the internal field inside the slit may be expressed as:

$$E_y^{\mathrm{L}} = R_m E_m^+ + E_m^- = (R_m e^{i\zeta_m z} + e^{-i\zeta_m z})F_m \sin\frac{m\pi}{a}\left(x+\frac{a}{2}\right), \quad (z > -b_1), \tag{2.31}$$

$$\begin{aligned} E_y^{\mathrm{L}} &= B_m E_m^+ + C_m E_m^- \\ &= (B_m e^{i\zeta'_m z} + C_m e^{-i\zeta'_m z})F_m \sin\frac{m\pi}{a}\left(x+\frac{a}{2}\right), \quad (-b_1 > z > -b_2), \end{aligned} \tag{2.32}$$

$$E_y^{\mathrm{L}} = T_m E_m^- = T_m e^{-i\zeta_m z} F_m \sin\frac{m\pi}{a}\left(x+\frac{a}{2}\right), \quad (z < -b_2), \tag{2.33}$$

where ζ'_m denote the wave number inside the loaded medium in z-direction as

$$\zeta'_m = \sqrt{\varepsilon_r\mu_r k^2 - \left(\frac{m\pi}{a}\right)^2}. \tag{2.34}$$

The corresponding magnetic field in x-direction $H_x = -\partial E_y / i\omega\mu\partial z$ can be expressed as

$$H_x^{\mathrm{L}} = \frac{\zeta_m}{\omega\mu_0}(-R_m e^{i\zeta_m z} + e^{-i\zeta_m z})F_m \sin\frac{m\pi}{a}\left(x+\frac{a}{2}\right), \quad (z > -b_1), \tag{2.35}$$

$$H_x^{\mathrm{L}} = \frac{\zeta'_m}{\omega\mu_0\mu_r}(-B_m e^{i\zeta'_m z} + C_m e^{-i\zeta_m z})F_m \sin\frac{m\pi}{a}\left(x+\frac{a}{2}\right), \quad (-b_1 > z > -b_2), \tag{2.36}$$

$$H_x^{\mathrm{L}} = \frac{\zeta_m}{\omega\mu_0} T_m e^{-i\zeta_m z} F_m \sin\frac{m\pi}{a}\left(x+\frac{a}{2}\right), \quad (z < -b_2). \tag{2.37}$$

Apply boundary condition at $z=-b_1$ and $z=-b_2$ for the above field equations:

$$E_y^{\mathrm{L}}\big|_{z=-b_1^+} = E_y^{\mathrm{L}}\big|_{z=-b_1^-}, \tag{2.38}$$

$$H_x^{\mathrm{L}}\big|_{z=-b_1^+} = H_x^{\mathrm{L}}\big|_{z=-b_1^-}, \tag{2.39}$$

$$E_y^{\mathrm{L}}\big|_{z=-b_2^+} = E_y^{\mathrm{L}}\big|_{z=-b_2^-}, \tag{2.40}$$

$$H_x^{\mathrm{L}}\big|_{z=-b_2^+} = H_x^{\mathrm{L}}\big|_{z=-b_2^-}. \tag{2.41}$$

One gets the reflection coefficient R_m and the transmission coefficient T_m as

$$R_m = \frac{(\zeta_m^2\mu_r^2 - \zeta_m'^2)2i\sin\{\zeta_m'(b_1-b_2)\}e^{2i\zeta_m b_1}}{(\mu_r\zeta_m+\zeta_m')^2 e^{i\zeta_m'(b_1-b_2)} - (\mu_r\zeta_m-\zeta_m')^2 e^{i\zeta_m'(b_2-b_1)}}, \tag{2.42}$$

$$T_m = \frac{4\mu_r\zeta_m\zeta_m' e^{i\zeta_m(b_1-b_2)}}{(\mu_r\zeta_m+\zeta_m')^2 e^{i\zeta_m'(b_1-b_2)} - (\mu_r\zeta_m-\zeta_m')^2 e^{i\zeta_m'(b_2-b_1)}}. \tag{2.43}$$

In case of empty slit ($\varepsilon_r=\mu_r=1$ or $b_1=b_2$), one gets immediately $R_m=0$, $T_m=1$, and the internal waveguide field $\boldsymbol{E}^{\mathrm{w}}$ propagates directly down to the lower aperture ($z=-b$).

In the case of loaded slit, the reflected waveguide modes $R_m E_m^+$ bounce back to the upper aperture and excite there secondary equivalent magnetic current $\boldsymbol{M}_{11}^{\pm}$

$$\begin{aligned}\boldsymbol{M}_{11}^{\pm}(x, z=0_{\pm}) &= \sum_{m=1}^{\infty} R_m E_m^+ \hat{\boldsymbol{y}}\big|_{z=0} \times (\pm\hat{\boldsymbol{z}}) \\ &= \pm\sum_{m=1}^{\infty} R_m F_m \sin\frac{m\pi}{a}\left(x+\frac{a}{2}\right)\hat{\boldsymbol{x}}, \quad \left(|x|<\frac{a}{2}\right).\end{aligned} \tag{2.44}$$

Similarly to the primary upper scattering field derivation from equivalent magnetic current, the secondary upper scattering field caused by $\boldsymbol{M}_{11}^+$ at $z=0_+$ can be expressed as

$$E_{11y}^{\mathrm{s}} = \int_{-a/2}^{a/2} M_{11x}^+(x')\frac{\partial}{\partial z'}G(x,z;x',z'=0_+)dx'. \tag{2.45}$$

Substituting Eqs. (2.6) and (2.44) into Eq. (2.45) and evaluating the integral by the saddle point method asymptotically, one can derive the secondary scattering far field in the upper half-space ($z>0$) as

$$\begin{aligned}E_{11y}^{\mathrm{s}} &= 2ika\sin\theta\; C(k\rho)\sum_{m=1}^{\infty}\frac{R_m F_m m\pi}{(m\pi)^2-(ka\cos\theta)^2} \\ &\quad\cdot\left\{(-1)^m e^{(-ika\cos\theta)/2} - e^{(ika\cos\theta)/2}\right\}.\end{aligned} \tag{2.46}$$

On the other hand, the transmitted waveguide modes $T_m E_m^-$ propagate down to the lower aperture ($z=-b$) and excite there scattering fields $\boldsymbol{E}_2^{\mathrm{s}}$ to the lower half-space

($z < -b$). These scattering fields are again calculated from the equivalent magnetic currents $\boldsymbol{M}_2^{\pm}$ on the closed aperture at $z = -b$, as in Fig. 2. The equivalent magnetic current $\boldsymbol{M}_2^{\pm}$ can be found from

$$\begin{aligned}\boldsymbol{M}_2^{\pm}(x, z = -b_{\pm}) &= \sum_{m=1}^{\infty} T_m E_m^{-} \hat{\boldsymbol{y}}\big|_{z=-b} \times (\pm\hat{\boldsymbol{z}}) \\ &= \pm \sum_{m=1}^{\infty} T_m F_m \sin\frac{m\pi}{a}\left(x + \frac{a}{2}\right) e^{i\zeta_m b}\hat{\boldsymbol{x}}, \quad \left(|x| < \frac{a}{2}\right). \end{aligned} \tag{2.47}$$

The radiation field $\boldsymbol{E}_2^{\mathrm{s}}$ in the lower half-space can be derived from the equivalent source $\boldsymbol{M}_2^{-}$ in Eq. (2.47) like the primary scattering field $\boldsymbol{E}_1^{\mathrm{s}}$ in Sect. 2.1.1. $\boldsymbol{E}_2^{\mathrm{s}}$ becomes

$$E_{2y}^{\mathrm{s}} = \int_{-a/2}^{a/2} M_{2x}^{-}(x') \frac{\partial}{\partial z'} G(x, z; x', z' = -b_{-}) dx'. \tag{2.48}$$

Once again, the integral in Eq. (2.48) can be evaluated using the saddle point method. One gets the scattering field E_{2y}^{s} for $\theta > \pi$ as From Eq. (2.6) in case of $z < z' = -b$, the lower E-field

$$\begin{aligned} E_{2y}^{\mathrm{s}} &= \int_{-a/2}^{a/2} M_{2x}^{-} \frac{\partial}{\partial z'} \left\{ \frac{i}{2} \mathrm{H}_0^{(1)}(k\sqrt{(x-x')^2 + (z-z')^2}) \Big|_{z'=-b} \right\} dx' \\ &= -\frac{i}{2\pi} \int_{-a/2}^{a/2} \sum_{m=1}^{\infty} T_m F_m \sin\frac{m\pi}{a}\left(x' + \frac{a}{2}\right) e^{i\zeta_m b} \\ &\qquad \frac{\partial}{\partial z'} \left\{ \int_{-\infty}^{\infty} \frac{e^{i\eta(x-x') + i\sqrt{k^2-\eta^2}(-z+z')}}{\sqrt{k^2-\eta^2}} \Big|_{z'=-b} \right\} d\eta dx' \\ &= -\frac{i^2}{2\pi} \int_{-a/2}^{a/2} \sum_{m=1}^{\infty} T_m F_m \sin\frac{m\pi}{a}\left(x' + \frac{a}{2}\right) e^{i\zeta_m b} \\ &\qquad \int_{-\infty}^{\infty} e^{i\eta(x-x') + i\sqrt{k^2-\eta^2}(-z-b)} d\eta dx' \\ &= \frac{1}{2\pi} \int_{-\infty}^{\infty} \sum_{m=1}^{\infty} T_m F_m e^{i\zeta_m b} e^{i\eta x - i\sqrt{k^2-\eta^2}(z+b)} \\ &\qquad \left\{ \int_{-a/2}^{a/2} \sin\frac{m\pi}{a}\left(x' + \frac{a}{2}\right) e^{-i\eta x'} dx' \right\} d\eta \\ &= \frac{1}{2\pi} \int_{-\infty}^{\infty} \sum_{m=1}^{\infty} T_m F_m e^{i\zeta_m b} e^{i\eta x - i\sqrt{k^2-\eta^2}(z+b)} \\ &\qquad \left\{ \frac{-\frac{m\pi}{a}}{\left(\frac{m\pi}{a}\right)^2 - \eta^2} \left(\cos m\pi \cdot e^{-i\eta a/2} - e^{i\eta a/2}\right) \right\} d\eta \\ &= -\frac{1}{2\pi} \int_{-\infty}^{\infty} \sum_{m=1}^{\infty} T_m F_m e^{i\zeta_m b} \frac{\frac{m\pi}{a}}{\left(\frac{m\pi}{a}\right)^2 - \eta^2} \\ &\qquad \left\{ \cos m\pi e^{i\eta(x-a/2) - i\sqrt{k^2-\eta^2}(z+b)} - e^{i\eta(x+a/2) - i\sqrt{k^2-\eta^2}(z+b)} \right\} d\eta \end{aligned}$$

$$= I_1 + I_2. \tag{2.49}$$

where

$$I_1 = -\frac{1}{2\pi}\int_{-\infty}^{\infty}\sum_{m=1}^{\infty} T_m F_m e^{i\zeta_m b}\frac{\frac{m\pi}{a}}{\left(\frac{m\pi}{a}\right)^2-\eta^2}\cos m\pi e^{i\eta(x-a/2)-i\sqrt{k^2-\eta^2}(z+b)}d\eta, \tag{2.50}$$

$$I_2 = \frac{1}{2\pi}\int_{-\infty}^{\infty}\sum_{m=1}^{\infty} T_m F_m e^{i\zeta_m b}\frac{\frac{m\pi}{a}}{\left(\frac{m\pi}{a}\right)^2-\eta^2}e^{i\eta(x+a/2)-i\sqrt{k^2-\eta^2}(z+b)}d\eta. \tag{2.51}$$

Calculate above integral with saddle point method with

$$\begin{aligned}
&\eta = k\sin\omega, \quad d\eta = k\cos\omega d\omega, \quad x \mp \frac{a}{2} = \rho'_{\pm}\cos\theta_{\pm}, \quad z+b = \rho'_{\pm}\sin\theta_{\pm},\\
&\sqrt{k^2-\eta^2} = \sqrt{k^2-k^2\sin^2\omega} = k\cos\omega,\\
&i\eta(x\pm\frac{a}{2}) - i\sqrt{k^2-\eta^2}(z+b) = ik\sin\omega\rho'_{\mp}\cos\theta_{\mp} - ik\cos\omega\rho'_{\mp}\sin\theta_{\mp}\\
&\qquad\qquad = ik\rho'_{\mp}\sin(\omega-\theta_{\mp}).
\end{aligned} \tag{2.52}$$

Then I_1, I_2 become

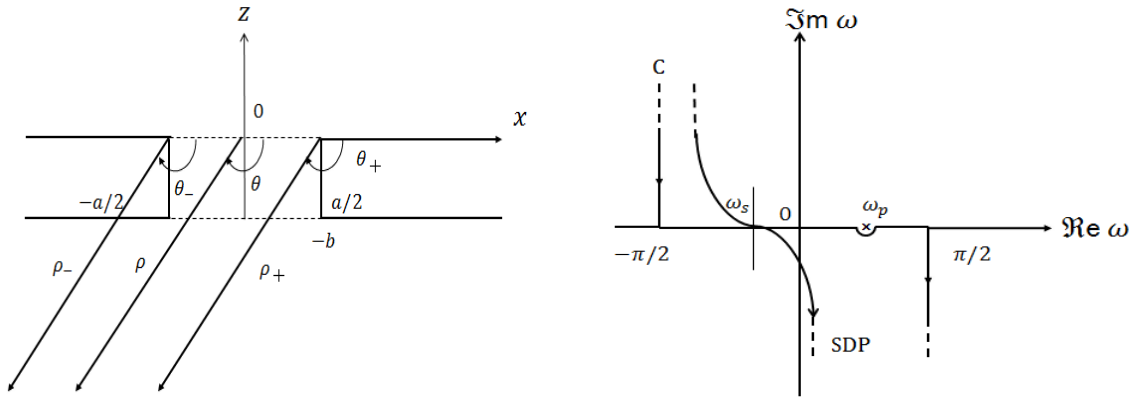

(a) (b)

Figure 2.4: Saddle point method integral evaluation (lower region).

$$I_1 = -\frac{1}{2\pi}\int_C\sum_{m=1}^{\infty} T_m F_m e^{i\zeta_m b}\frac{m\pi}{a}\frac{k\cos\omega}{\left(\frac{m\pi}{a}\right)^2-(k\sin\omega)^2}\cos m\pi\cdot e^{ik\rho'_+\sin(\omega-\theta_+)}d\omega, \tag{2.53}$$

$$I_2 = \frac{1}{2\pi}\int_C\sum_{m=1}^{\infty} T_m F_m e^{i\zeta_m b}\frac{m\pi}{a}\frac{k\cos\omega}{\left(\frac{m\pi}{a}\right)^2-(k\sin\omega)^2}e^{ik\rho'_-\sin(\omega-\theta_-)}d\omega. \tag{2.54}$$

The position of the pole in ω plane yields $\left(\frac{m\pi}{a}\right)^2-(k\sin\omega_p)^2$, then

$$\omega_p = \arcsin\left(\frac{m\pi}{ka}\right)^2. \tag{2.55}$$

One can find the saddle point from

$$\frac{\partial}{\partial\omega}(ik\rho'_{\pm}\sin(\omega-\theta_{\pm}))=ik\rho'_{\pm}\cos(\omega-\theta_{\pm})=0,$$
$$\cos(\omega_s-\theta_{\pm})=0,\quad \omega_s-\theta_{\pm}=\pm\frac{\pi}{2}. \tag{2.56}$$

Since the observation point is in the lower half-plane, the saddle point in $-\frac{\pi}{2}<\omega<\frac{\pi}{2}$ is With $\theta<0$:

$$\omega_s=\frac{\pi}{2}+\theta_{\pm},\quad \sin\omega_s=\sin\left(\frac{\pi}{2}+\theta_{\pm}\right)=\cos\theta_{\pm},\quad \cos\omega_s=\cos\left(\frac{\pi}{2}+\theta_{\pm}\right)=-\sin\theta_{\pm},$$
$$ik\rho'_{\pm}\sin(\omega-\theta_{\pm})\sim ik\rho'_{\pm}\sin(\omega_s-\theta_{\pm})-\frac{ik\rho'_{\pm}}{2}\sin(\omega_s-\theta_{\pm})(\omega-\omega_s)^2$$
$$=ik\rho'_{\pm}-\frac{ik\rho'_{\pm}}{2}(\omega-\omega_s)^2. \tag{2.57}$$

Then

$$I_1=-\frac{1}{2\pi}\sum_{m=1}^{\infty}T_mF_me^{i\zeta_mb}\frac{m\pi}{a}\cos m\pi\int_{SDP}\frac{-k\sin\theta_+}{\left(\frac{m\pi}{a}\right)^2-(k\cos\theta_+)^2}e^{ik\rho'_+-ik\rho'_+(\omega-\omega_s)^2/2}d\omega$$
$$=-\frac{1}{2\pi}\sum_{m=1}^{\infty}T_mF_me^{i\zeta_mb}\frac{m\pi}{a}\cos m\pi\frac{-k\sin\theta_+}{\left(\frac{m\pi}{a}\right)^2-(k\cos\theta_+)^2}e^{ik\rho'_+}\sqrt{\frac{2\pi}{ik\rho'_+}}$$
$$=2k\sin\theta_+\sqrt{\frac{1}{8\pi k\rho'_+}}\sum_{m=1}^{\infty}\frac{T_mF_m\frac{m\pi}{a}\cos m\pi}{\left(\frac{m\pi}{a}\right)^2-(k\cos\theta_+)^2}e^{ik\rho'_++i\zeta_mb-i\pi/4}, \tag{2.58}$$
$$I_2=\frac{1}{2\pi}\sum_{m=1}^{\infty}T_mF_me^{i\zeta_mb}\frac{m\pi}{a}\int_{SDP}\frac{-k\sin\theta_-}{\left(\frac{m\pi}{a}\right)^2-(k\cos\theta_-)^2}e^{ik\rho'_--ik\rho'_-(\omega-\omega_s)^2/2}d\omega$$
$$=\frac{1}{2\pi}\sum_{m=1}^{\infty}T_mF_me^{i\zeta_mb}\frac{m\pi}{a}\frac{-k\sin\theta_-}{\left(\frac{m\pi}{a}\right)^2-(k\cos\theta_-)^2}e^{ik\rho'_-}\sqrt{\frac{2\pi}{ik\rho'_-}}$$
$$=-2k\sin\theta_-\sqrt{\frac{1}{8\pi k\rho'_-}}\sum_{m=1}^{\infty}\frac{T_mF_m\frac{m\pi}{a}}{\left(\frac{m\pi}{a}\right)^2-(k\cos\theta_-)^2}e^{ik\rho'_-+i\zeta_mb-i\pi/4}. \tag{2.59}$$

Since we assumed ρ is the distance from observation point (in both upper and lower half-space) to the origin. Then

$$\rho=\rho'+b\sin\theta. \tag{2.60}$$

If the observation point is sufficiently far, considering the phase only, one gets

$$\rho_{\pm}\sim\rho\mp\frac{a}{2}\cos\theta,\quad \theta_{\pm}\sim\theta. \tag{2.61}$$

Then the scattering E far-field from the lower aperture is

$$
\begin{aligned}
E^s_{2y} =& I_1 + I_2 \\
=& 2k\sin\theta\sqrt{\frac{1}{8\pi k\rho}}\sum_{m=1}^{\infty}\frac{T_m F_m \frac{m\pi}{a}}{\left(\frac{m\pi}{a}\right)^2-(k\cos\theta)^2} \\
& \qquad \left\{\cos m\pi e^{(-ika\cos\theta)/2} - e^{(ika\cos\theta)/2}\right\} e^{ik\rho_+ + i\zeta_m b - i\pi/4 + ikb\sin\theta} \\
=& 2k\sin\theta\sqrt{\frac{1}{8\pi k\rho}}\sum_{m=1}^{\infty} T_m \frac{-2m\pi}{(m\pi)^2-(ka\cos\theta_0)^2}\frac{\frac{m\pi}{a}a^2}{(m\pi)^2-(ka\cos\theta_0)^2} \\
& \cdot \left\{\cos m\pi e^{(-ika\cos\theta_0)/2} - e^{(ika\cos\theta_0)/2}\right\} \\
& \cdot \left\{\cos m\pi e^{(-ika\cos\theta)/2} - e^{(ika\cos\theta)/2}\right\} e^{ik\rho_+ + i\zeta_m b - i\pi/4 + ikb\sin\theta} \\
=& 4ika\sin\theta C(k\rho)\sum_{m=1}^{\infty} T_m \frac{(m\pi)^2}{\{(m\pi)^2-(ka\cos\theta_0)^2\}\{(m\pi)^2-(ka\cos\theta)^2\}} \\
& \cdot \left\{(-1)^m e^{(-ika\cos\theta_0)/2} - e^{(ika\cos\theta_0)/2}\right\} \\
& \cdot \left\{(-1)^m e^{(-ika\cos\theta)/2} - e^{(ika\cos\theta)/2}\right\} \\
& \cdot e^{i\zeta_m b + ikb\sin\theta}.
\end{aligned}
\tag{2.62}
$$

For modal reflection at the lower aperture, one may use the similar formula in Eq. (2.25) with M^+_{2x} in Eq. (2.47). One finds that the modal coefficients obtained from the equivalent magnetic current M^+_{2x} become unit values which cancel the reflection coefficients (-1) of the waveguide modes by closing the lower aperture. Consequently, there is no reflection at all from the lower aperture by the Kirchhoff approximation. Similarly, the modal reflection does not also exist at the upper aperture despite the presence of the equivalent magnetic current M^-_{11x}.

2.1.4 Scattering Far-field from Infinitely Thin Slit

It may be interesting to derive a special circumstance of an infinitely thin slit, one can take the limit $b \to 0$ in Eq. (2.62), and the transmission coefficient $T_m = 1$. On the other hand, the lower scattering field in this case $\boldsymbol{\phi}^{\rm ss}_2 = \boldsymbol{E}^{\rm ss}_2$ can be derived directly from $\boldsymbol{M}^-_1$ in Eq. (2.24) in the similar way of deriving $\boldsymbol{E}^{\rm s}_1$ in Sect. 2.1.1 with $\boldsymbol{M}^+_1$ replaced by $\boldsymbol{M}^-_1$ in Eq. (2.5). Since $\boldsymbol{M}^-_1 = -\boldsymbol{M}^+_1$, one gets for $\theta > \pi$

$$
E^{\rm ss}_{2y} = -E^{\rm s}_{1y} = \frac{4i\sin\theta\sin\{ka(\cos\theta_0+\cos\theta)/2\}}{\cos\theta_0+\cos\theta}C(k\rho). \tag{2.63}
$$

The comparison of results from these two calculations will be shown in Sect. 2.3.

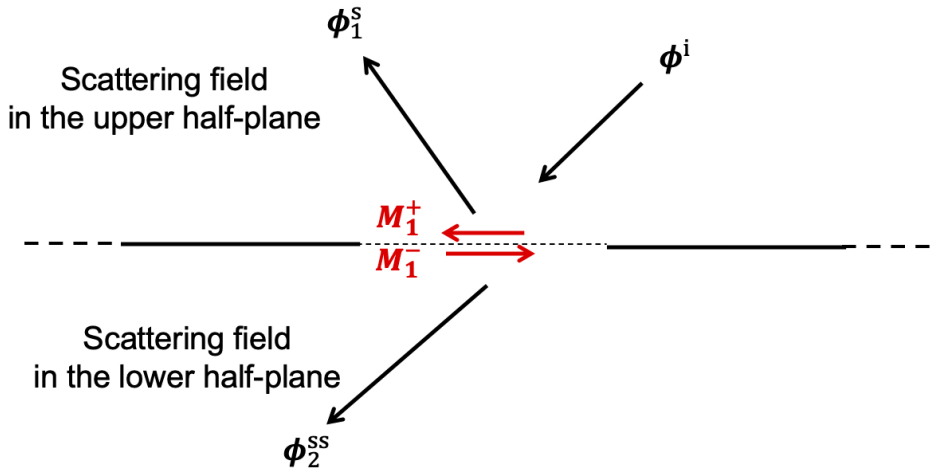

Figure 2.5: Plane wave scattering by an infinitely thin slit.

2.2 H Polarization

In this case, we have a Transverse Magnetic (TM) incident plane wave where magnetic vectors $\boldsymbol{H}^{\mathrm{i}}$ are perpendicular with the wave propagation direction. Eq. (2.1) becomes

$$H_y^{\mathrm{i}} = e^{-ik(x\cos\theta_0 + z\sin\theta_0)}. \tag{2.64}$$

The corresponding incident electric field components can be derived based on Maxwell's equations as:

$$-i\omega\varepsilon_0 \boldsymbol{E}^{\mathrm{i}} = \nabla \times \boldsymbol{H}^{\mathrm{i}} = \begin{vmatrix} \hat{\boldsymbol{x}} & \hat{\boldsymbol{y}} & \hat{\boldsymbol{z}} \\ \frac{\partial}{\partial x} & \frac{\partial}{\partial y} & \frac{\partial}{\partial z} \\ 0 & H_y^{\mathrm{i}} & 0 \end{vmatrix} = \hat{\boldsymbol{x}}\left(-\frac{\partial}{\partial z}H_y^{\mathrm{i}}\right) + \hat{\boldsymbol{z}}\left(\frac{\partial}{\partial x}H_y^{\mathrm{i}}\right). \tag{2.65}$$

Then

$$E_x^{\mathrm{i}} = -\frac{i}{\omega\varepsilon_0}\frac{\partial H_y^{\mathrm{i}}}{\partial z} = -\sqrt{\frac{\mu_0}{\varepsilon_0}}\sin\theta e^{-ik(x\cos\theta_0 + z\sin\theta_0)}, \tag{2.66}$$

$$E_z^{\mathrm{i}} = \frac{i}{\omega\varepsilon_0}\frac{\partial H_y^{\mathrm{i}}}{\partial x} = \sqrt{\frac{\mu_0}{\varepsilon_0}}\cos\theta e^{-ik(x\cos\theta_0 + z\sin\theta_0)}. \tag{2.67}$$

2.2.1 Primary Upper Scattering Faf-field

The equivalent magnetic current sources on the closed upper side of the upper aperture $\boldsymbol{M}_1^+$ can be expressed in terms of incident electric field as:

$$\begin{aligned}\boldsymbol{M}_1^+(x, z=0_+) &= (E_x^{\mathrm{i}}\hat{\boldsymbol{x}} + E_z^{\mathrm{i}}\hat{\boldsymbol{z}})\big|_{z=0} \times (+\hat{\boldsymbol{z}}) = -E_x^{\mathrm{i}}\big|_{z=0}\hat{\boldsymbol{x}} \\ &= \sqrt{\frac{\mu_0}{\varepsilon_0}}\sin\theta_0 e^{-ikx\cos\theta_0}\hat{\boldsymbol{y}}, \quad (|x| < \frac{a}{2}, z = 0_+). \end{aligned} \tag{2.68}$$

With the condition of no equivalent electric current exists, the scattering H-field $\boldsymbol{H}_1^{\mathrm{s}}(\boldsymbol{r})$ can be expressed in terms of the equivalent magnetic current $\boldsymbol{M}_1^+$ as

$$\boldsymbol{H}_1^{\mathrm{s}}(\boldsymbol{r}) = i\omega\varepsilon_0 \int_{S'} \boldsymbol{M}_1^+(\boldsymbol{r'}) G dS' = i\omega\varepsilon_0 \int_{S'} M_{1y}^+(\boldsymbol{r'}) G dS' \hat{\boldsymbol{y}}. \tag{2.69}$$

The scattering H-field $\boldsymbol{H}_1^{\mathrm{s}}(\boldsymbol{r})$ has only y component H_{1y}^{s}[35]

$$\begin{aligned} H_{1y}^{\mathrm{s}} &= i\omega\varepsilon_0 \int_{-a/2}^{a/2} M_{1y}^+(x')\frac{i}{2}\mathrm{H}_0^{(1)}(k\sqrt{(x-x')^2+(z-z')^2})\Big|_{z'=0} dx' \\ &= -\frac{k\sin\theta_0}{2}\int_{-a/2}^{a/2} e^{-ikx'\cos\theta_0}\mathrm{H}_0^{(1)}(k\sqrt{(x-x')^2+(z-z')^2})\Big|_{z'=0} dx'. \end{aligned} \tag{2.70}$$

Then Eq. (2.70) becomes, in case of $z > 0$, $z' = 0$

$$\begin{aligned} H_{1y}^{\mathrm{s}} &= -\frac{k\sin\theta_0}{2}\int_{-a/2}^{a/2} e^{-ikx'\cos\theta_0}\left\{\frac{1}{\pi}\int_{-\infty}^{\infty}\frac{e^{i\eta(x-x')+i\sqrt{k^2-\eta^2}(z-z')}}{\sqrt{k^2-\eta^2}}\Big|_{z'=0} d\eta\right\} dx' \\ &= -\frac{k\sin\theta_0}{2\pi}\int_{-a/2}^{a/2} e^{-i(k\cos\theta_0+\eta)x'}dx' \int_{-\infty}^{\infty}\frac{e^{i\eta x+i\sqrt{k^2-\eta^2}z}}{\sqrt{k^2-\eta^2}}d\eta \\ &= -\frac{k\sin\theta_0}{2\pi}\int_{-\infty}^{\infty}\frac{e^{-i(k\cos\theta_0+\eta)x'}}{-i(k\cos\theta_0+\eta)}\Big|_{-a/2}^{a/2}\frac{e^{i\eta x+i\sqrt{k^2-\eta^2}z}}{\sqrt{k^2-\eta^2}}d\eta \\ &= -\frac{k\sin\theta_0}{2\pi}\int_{-\infty}^{\infty}\frac{e^{i(k\cos\theta_0+\eta)a/2}-e^{-i(k\cos\theta_0+\eta)a/2}}{i(k\cos\theta_0+\eta)}\frac{e^{i\eta x+i\sqrt{k^2-\eta^2}z}}{\sqrt{k^2-\eta^2}}d\eta \\ &= \frac{ik\sin\theta_0}{2\pi}\int_{-\infty}^{\infty}\frac{e^{(ika\cos\theta_0)/2+i\eta(x+a/2)+i\sqrt{k^2-\eta^2}z}-e^{(-ika\cos\theta_0)/2+i\eta(x-a/2)+i\sqrt{k^2-\eta^2}z}}{(k\cos\theta_0+\eta)\sqrt{k^2-\eta^2}}d\eta \\ &= I_1 + I_2. \end{aligned} \tag{2.71}$$

where

$$I_1 = \frac{ik\sin\theta_0}{2\pi}\int_{-\infty}^{\infty}\frac{e^{(ika\cos\theta_0)/2+i\eta(x+a/2)+i\sqrt{k^2-\eta^2}z}}{(k\cos\theta_0+\eta)\sqrt{k^2-\eta^2}}d\eta, \tag{2.72}$$

$$I_2 = -\frac{ik\sin\theta_0}{2\pi}\int_{-\infty}^{\infty}\frac{e^{(-ika\cos\theta_0)/2+i\eta(x-a/2)+i\sqrt{k^2-\eta^2}z}}{(k\cos\theta_0+\eta)\sqrt{k^2-\eta^2}}d\eta. \tag{2.73}$$

Calculate above integral with saddle point method with

$$\eta = k\sin\omega, \quad d\eta = k\cos\omega d\omega, \quad x \mp \frac{a}{2} = \rho_\pm \cos\theta_\pm, \quad z = \rho_\pm \sin\theta_\pm,$$
$$\sqrt{k^2-\eta^2} = \sqrt{k^2 - k^2\sin^2\omega} = k\cos\omega,$$
$$i\eta(x \pm \frac{a}{2}) + i\sqrt{k^2-\eta^2}z = ik\sin\omega\rho_\mp\cos\theta \mp + ik\cos\omega\rho_\mp\sin\theta_\mp$$
$$= ik\rho_\mp\sin(\omega+\theta_\mp). \tag{2.74}$$

Then I_1, I_2 become

$$I_1 = \frac{ik\sin\theta_0}{2\pi}\int_C \frac{e^{(ika\cos\theta_0)/2 + ik\rho_-\sin(\omega+\theta_-)}}{(k\cos\theta_0 + k\sin\omega)k\cos\omega} k\cos\omega d\omega$$
$$= \frac{i\sin\theta_0}{2\pi}\int_C \frac{e^{(ik\cos\theta_0)/2 + ik\rho_-\sin(\omega+\theta_-)}}{(\cos\theta_0+\sin\omega)} d\omega, \tag{2.75}$$
$$I_2 = -\frac{ik\sin\theta_0}{2\pi}\int_C \frac{e^{(-ika\cos\theta_0)/2 + ik\rho_+\sin(\omega+\theta_+)}}{(k\cos\theta_0 + k\sin\omega)k\cos\omega} k\cos\omega d\omega$$
$$= -\frac{i\sin\theta_0}{2\pi}\int_C \frac{e^{(-ika\cos\theta_0)/2 + ik\rho_+\sin(\omega+\theta_+)}}{(\cos\theta_0+\sin\omega)} d\omega. \tag{2.76}$$

The position of the pole in the ω plane yields $-\cos\theta_0 = \sin\omega_p$, then

$$\omega_p = \arcsin(-\cos\theta_0) = -\arcsin(\cos\theta_0), \tag{2.77}$$

θ_0	0	$\frac{\pi}{2}$	π
ω_p	$-\frac{\pi}{2}$	0	$\frac{\pi}{2}$

One can find the saddle point from

$$\frac{\partial}{\partial\omega}(ik\rho_\pm\sin(\omega+\theta_\pm)) = ik\rho_\pm\cos(\omega+\theta_\pm) = 0,$$
$$\cos(\omega_s+\theta_\pm) = 0, \quad \omega_s + \theta_\pm = \pm\frac{\pi}{2}. \tag{2.78}$$

Since the observation point is in the upper half-plane, the saddle point in $-\frac{\pi}{2} < \omega < \frac{\pi}{2}$ is With $\theta > 0$:

$$\omega_s = \frac{\pi}{2} - \theta_\pm, \quad \sin\omega_s = \sin\left(\frac{\pi}{2}-\theta_\pm\right) = \cos\theta_\pm, \quad \cos\omega_s = \cos\left(\frac{\pi}{2}-\theta_\pm\right) = \sin\theta_\pm,$$
$$ik\rho_\pm\sin(\omega+\theta_\pm) \sim ik\rho_\pm\sin(\omega_s+\theta_\pm) - \frac{ik\rho_\pm}{2}\sin(\omega_s+\theta_\pm)(\omega-\omega_s)^2$$
$$= ik\rho_\pm - \frac{ik\rho_\pm}{2}(\omega-\omega_s)^2. \tag{2.79}$$

Then

$$
\begin{aligned}
I_1 &= \frac{i\sin\theta_0}{2\pi} e^{(ika\cos\theta_0)/2} \int_{SDP} \frac{e^{ik\rho_- - ik\rho_-(\omega-\omega_s)^2/2}}{\cos\theta_0 + \sin\omega_s} d\omega \\
&= \frac{i\sin\theta_0}{2\pi} e^{(ika\cos\theta_0)/2} \frac{1}{\cos\theta_0 + \cos\theta_-} e^{ik\rho_-} \sqrt{\frac{2\pi}{ik\rho_-}} \\
&= \frac{2\sin\theta_0}{\cos\theta_0 + \cos\theta_-} \sqrt{\frac{1}{8\pi k\rho_-}} e^{ik\rho_- + (ika\cos\theta_0)/2 + i\pi/4}, \qquad (2.80) \\
I_2 &= -\frac{i\sin\theta_0}{2\pi} e^{(-ika\cos\theta_0)/2} \int_{SDP} \frac{e^{ik\rho_+ - ik\rho_+(\omega-\omega_s)^2/2}}{\cos\theta_0 + \sin\omega_s} d\omega \\
&= -\frac{i\sin\theta_0}{2\pi} e^{(-ika\cos\theta_0)/2} \frac{1}{\cos\theta_0 + \cos\theta_+} e^{ik\rho_+} \sqrt{\frac{2\pi}{ik\rho_+}} \\
&= -\frac{2\sin\theta_0}{\cos\theta_0 + \cos\theta_+} \sqrt{\frac{1}{8\pi k\rho_+}} e^{ik\rho_+ - (ika\cos\theta_0)/2 + i\pi/4}. \qquad (2.81)
\end{aligned}
$$

If the observation point is sufficiently far, considering the phase only, one gets

$$
\rho_\pm \sim \rho \mp \frac{a}{2}\cos\theta, \quad \theta_\pm \sim \theta. \qquad (2.82)
$$

Then the scattering H far-field is

$$
\begin{aligned}
H_{1y}^{\mathrm{s}} &= I_1 + I_2 \\
&= \frac{2\sin\theta_0}{\cos\theta_0 + \cos\theta} \sqrt{\frac{1}{8\pi k\rho}} e^{ik\rho + i\pi/4} \left\{ e^{ika(\cos\theta_0 + \cos\theta)/2} - e^{-ika(\cos\theta_0 + \cos\theta)/2} \right\} \\
&= \frac{4i\sin\theta_0 \sin\left\{ka(\cos\theta_0 + \cos\theta)/2\right\}}{\cos\theta_0 + \cos\theta} C(k\rho). \qquad (2.83)
\end{aligned}
$$

On the shadow boundary ($\theta = \pi - \theta_0$):

$$
\begin{aligned}
\sin\theta &= \sin(\pi - \theta_0) = \sin\theta_0, \\
\cos\theta &= \cos(\pi - \theta_0) = -\cos\theta_0.
\end{aligned}
$$

Then

$$
\begin{aligned}
\lim_{\theta\to\pi-\theta_0} H_{1y}^{\mathrm{s}} &= \sqrt{\frac{1}{8\pi k\rho}} e^{ik\rho + i\pi/4} \lim_{\theta\to\pi-\theta_0} \frac{4i\sin\theta_0 \sin\left\{ka(\cos\theta_0 + \cos\theta)/2\right\}}{\cos\theta_0 + \cos\theta} \\
&= \sqrt{\frac{1}{8\pi k\rho}} e^{ik\rho + i\pi/4} \left. \frac{4i\sin\theta_0 \cos\left\{ka(\cos\theta_0 + \cos\theta)/2\right\} ka(-\sin\theta)/2}{-\sin\theta} \right|_{\theta\to\pi-\theta_0} \\
&= 2ika\sin\theta_0 \; C(k\rho). \qquad (2.84)
\end{aligned}
$$

2.2.2 Modal Excitation in Slit Region

The modal excitation is given by equivalent magnetic source $\boldsymbol{M}_1^-$ on the closed aperture expressed as

$$\begin{aligned}\boldsymbol{M}_1^-(x, z=0_-) &= (E_x^{\mathrm{i}}\hat{\boldsymbol{x}} + E_z^{\mathrm{i}}\hat{\boldsymbol{z}})\big|_{z=0} \times (-\hat{\boldsymbol{z}}) = E_x^{\mathrm{i}}\big|_{z=0}\hat{\boldsymbol{x}} \\ &= -\sqrt{\frac{\mu_0}{\varepsilon_0}}\sin\theta_0 e^{-ikx\cos\theta_0}\hat{\boldsymbol{y}}, \quad (|x| < \frac{a}{2}, z=0_-). \end{aligned} \tag{2.85}$$

The excited field $\boldsymbol{\phi}^{\mathrm{w}} = \boldsymbol{H}^{\mathrm{w}}$ inside a semi-infinitely long ($b \to \infty$) parallel plane waveguide may be expressed as

$$\boldsymbol{H}_y^{\mathrm{w}} = i\omega\varepsilon_0 \int_{S'} \boldsymbol{M}_1^- G^{\mathrm{w}} dS' = i\omega\varepsilon_0 \int_{S'} M_{1y}^- G^{\mathrm{w}} dS'. \tag{2.86}$$

The field propagating downward inside the slit may be derived as

$$H_y^{\mathrm{w}} = \sum_{m=0}^{\infty} H_m^-, \tag{2.87}$$

where

$$H_m^{\pm} = \bar{F}_m \cos\frac{m\pi}{a}\left(x + \frac{a}{2}\right) e^{\pm i\zeta_m z}. \tag{2.88}$$

Here, $\bar{F}_m$ is the excitation coefficient of the $\mathrm{TM_m}$ waveguide modal field. $\bar{F}_m$ can be calculated by integrating the equivalent source $\boldsymbol{M}_1^-$ over the aperture ($|x| \leqslant a/2, z = 0_-$), one gets

$$\begin{aligned}\bar{F}_m &= i\omega\varepsilon_0\left(-\frac{i\epsilon_m}{a\zeta_m}\right)\sqrt{\frac{\mu_0}{\varepsilon_0}}\sin\theta_0\left\{\int_{-a/2}^{a/2}\cos\frac{m\pi}{a}\left(x' + \frac{a}{2}\right)e^{-ikx_0\cos\theta_0}dx'\right\} \\ &= \frac{\epsilon_m k}{a\zeta_m}\sin\theta_0\left[\frac{-ik\cos\theta_0}{(ik\cos\theta_0)^2 + \left(\frac{m\pi}{a}\right)^2}\left\{\cos m\pi e^{(-ika\cos\theta_0)/2} - e^{(ika\cos\theta_0)/2}\right\}\right] \\ &= -\frac{i\epsilon_m k^2 a\sin\theta_0\cos\theta_0}{\zeta_m\left\{(m\pi)^2 - (ka\cos\theta_0)^2\right\}}\left\{(-1)^m e^{(-ika\cos\theta_0)/2} - e^{(ika\cos\theta_0)/2}\right\} \end{aligned} \tag{2.89}$$

In addition, applying Maxwell's Equations in the waveguide area, one can derive E-field components propagating inside the waveguide as

$$-i\omega\varepsilon_0\boldsymbol{E}^{\mathbf{w}} = \nabla\times\boldsymbol{H}^{\mathbf{w}} = \begin{vmatrix}\hat{\boldsymbol{x}} & \hat{\boldsymbol{y}} & \hat{\boldsymbol{z}} \\ \frac{\partial}{\partial x} & \frac{\partial}{\partial y} & \frac{\partial}{\partial z} \\ 0 & H_y^{\mathrm{w}} & 0\end{vmatrix} = \hat{\boldsymbol{x}}\left(-\frac{\partial}{\partial z}H_y^{\mathrm{w}}\right) + \hat{\boldsymbol{z}}\left(\frac{\partial}{\partial x}H_y^{\mathrm{w}}\right)$$

$$E_x^{\mathrm{w}} = \frac{1}{i\omega\varepsilon_0}\frac{\partial H_y^{\mathrm{w}}}{\partial z} = \frac{1}{i\omega\varepsilon_0}\sum_{m=0}^{\infty}\bar{F}_m \cos\frac{m\pi}{a}\left(x+\frac{a}{2}\right)(-i\zeta_m)e^{-i\zeta_m z}$$
$$= \sum_{m=0}^{\infty}\bar{F}_{mx}\cos\frac{m\pi}{a}\left(x+\frac{a}{2}\right)e^{-i\zeta_m z}, \tag{2.90}$$

where

$$\bar{F}_{mx} = -\frac{\zeta_m}{\omega\varepsilon_0}\bar{F}_m, \tag{2.91}$$

$$E_z^{\mathrm{w}} = -\frac{1}{i\omega\varepsilon_0}\frac{\partial H_y^{\mathrm{w}}}{\partial x} = -\frac{1}{i\omega\varepsilon_0}\sum_{m=0}^{\infty}\bar{F}_m\left(\frac{m\pi}{a}\right)\left\{-\sin\frac{m\pi}{a}\left(x+\frac{a}{2}\right)\right\}e^{-i\zeta_m z}$$
$$= \sum_{m=0}^{\infty}\bar{F}_{mz}\sin\frac{m\pi}{a}\left(x+\frac{a}{2}\right)e^{-i\zeta_m z}, \tag{2.92}$$

where

$$\bar{F}_{mz} = \frac{m\pi}{i\omega\varepsilon_0 a}\bar{F}_m. \tag{2.93}$$

2.2.3 Secondary Upper Scattering Far-field and Lower Scattering Field

The waveguide modes $\phi_m^- = H_m^-$ impinge the loaded medium as in Fig. 2.2. Then the internal field inside the slit may be expressed as:

$$H_y^{\mathrm{L}} = \bar{R}_m H_m^+ + H_m^- = (\bar{R}_m e^{i\zeta_m z} + e^{-i\zeta_m z})\bar{F}_m\cos\frac{m\pi}{a}\left(x+\frac{a}{2}\right), \quad (z > -b_1), \tag{2.94}$$

$$H_y^{\mathrm{L}} = \bar{B}_m H_m^+ + \bar{C}_m H_m^-$$
$$= (\bar{B}_m e^{i\zeta'_m z} + \bar{C}_m e^{-i\zeta'_m z})\bar{F}_m\cos\frac{m\pi}{a}\left(x+\frac{a}{2}\right), \quad (-b_1 > z > -b_2), \tag{2.95}$$

$$H_y^{\mathrm{L}} = \bar{T}_m H_m^- = \bar{T}_m e^{-i\zeta_m z}\bar{F}_m\cos\frac{m\pi}{a}\left(x+\frac{a}{2}\right), \quad (z < -b_2). \tag{2.96}$$

The corresponding electric field in x-direction $E_x = \partial H_y / i\omega\varepsilon\partial z$ can be expressed as

$$E_x^{\mathrm{L}} = \frac{\zeta_m}{\omega\varepsilon_0}(\bar{R}_m e^{i\zeta_m z} - e^{-i\zeta_m z})\bar{F}_m\cos\frac{m\pi}{a}\left(x+\frac{a}{2}\right), \quad (z > -b_1), \tag{2.97}$$

$$E_x^{\mathrm{L}} = \frac{\zeta'_m}{\omega\varepsilon_0\varepsilon_r}(\bar{B}_m e^{i\zeta'_m z} - \bar{C}_m e^{-i\zeta'_m z})\bar{F}_m\cos\frac{m\pi}{a}\left(x+\frac{a}{2}\right), \quad (-b_1 > z > -b_2), \tag{2.98}$$

$$E_x^{\mathrm{L}} = -\frac{\zeta_m}{\omega\varepsilon_0}\bar{T}_m e^{-i\zeta_m z}\bar{F}_m\cos\frac{m\pi}{a}\left(x+\frac{a}{2}\right), \quad (z < -b_2). \tag{2.99}$$

Apply boundary condition at $z = -b_1$ and $z = -b_2$ for the above field equations:

$$H_y^{\mathrm{L}}\big|_{z=-b_1^+} = H_y^{\mathrm{L}}\big|_{z=-b_1^-}, \tag{2.100}$$

$$E_x^{\mathrm{L}}\big|_{z=-b_1^+} = E_x^{\mathrm{L}}\big|_{z=-b_1^-}, \tag{2.101}$$

$$H_y^{\mathrm{L}}\big|_{z=-b_2^+} = H_y^{\mathrm{L}}\big|_{z=-b_2^-}, \tag{2.102}$$

$$E_x^{\mathrm{L}}\big|_{z=-b_2^+} = E_x^{\mathrm{L}}\big|_{z=-b_2^-}. \tag{2.103}$$

One gets the reflection coefficient $\bar{R}_m$ and the transmission coefficient $\bar{T}_m$ as

$$\bar{R}_m = \frac{(\zeta_m^2\varepsilon_r^2 - \zeta'^2_m)2i\sin\zeta'_m(b_1-b_2)e^{2i\zeta_m b_1}}{(\varepsilon_r\zeta_m+\zeta'_m)^2e^{i\zeta'_m(b_1-b_2)} - (\varepsilon_r\zeta_m-\zeta'_m)^2e^{i\zeta'_m(b_2-b_1)}}, \tag{2.104}$$

$$\bar{T}_m = \frac{4\varepsilon_r\zeta_m\zeta'_m e^{i\zeta_m(b_1-b_2)}}{(\varepsilon_r\zeta_m+\zeta'_m)^2e^{i\zeta'_m(b_1-b_2)} - (\varepsilon_r\zeta_m-\zeta'_m)^2e^{i\zeta'_m(b_2-b_1)}}. \tag{2.105}$$

In case of empty slit ($\varepsilon_r = \mu_r = 1$ or $b_1 = b_2$), one gets immediately $\bar{R}_m = 0$, $\bar{T}_m = 1$, and the internal waveguide field $\boldsymbol{H}^{\mathrm{w}}$ propagates directly down to the lower aperture ($z = -b$).

In the case of loaded slit, the reflected waveguide modes $\bar{R}_m H_m^+$ bounce back to the upper aperture and excite there secondary equivalent magnetic current $\boldsymbol{M}_{11}^{\pm}$

$$\begin{aligned}\boldsymbol{M}_{11}^{\pm}(x, z=0_\pm) &= \sum_{m=0}^{\infty}\bar{R}_m(E_x^{\mathrm{w}}\hat{\boldsymbol{x}} + E_z^{\mathrm{w}}\hat{\boldsymbol{z}})\big|_{z=0}\times(\pm\hat{\boldsymbol{z}}) \\ &= \pm\sum_{m=0}^{\infty}\bar{R}_m\bar{F}_m\cos\frac{m\pi}{a}\left(x+\frac{a}{2}\right)\hat{\boldsymbol{y}}, \quad \left(|x|<\frac{a}{2}\right).\end{aligned} \tag{2.106}$$

Similarly to the primary upper scattering field derivation from equivalent magnetic current, the secondary upper scattering field caused by $\boldsymbol{M}_{11}^{+}$ at $z = 0_+$ can be expressed as

$$H_{11y}^{\mathrm{s}} = i\omega\varepsilon_0\int_{-a/2}^{a/2}M_{11y}^{+}(x')\frac{i}{2}\mathrm{H}_0^{(1)}(k\sqrt{(x-x')^2+(z-z')^2})\Big|_{z'=0}dx'. \tag{2.107}$$

Substituting Eq. (2.106) into Eq. (2.107) and evaluating the integral by the saddle point method asymptotically as in Sect. 2.1.1, one can derive the secondary scattering far field in the upper half-space ($z > 0$) for H polarization case as

$$\begin{aligned}H_{11y}^{\mathrm{s}} &= 2ka\cos\theta\ C(k\rho)\sum_{m=0}^{\infty}\frac{\bar{R}_m\bar{F}_m\zeta_m a}{(m\pi)^2-(ka\cos\theta)^2} \\ &\quad\cdot\left\{(-1)^m e^{(-ika\cos\theta)/2} - e^{(ika\cos\theta)/2}\right\}.\end{aligned} \tag{2.108}$$

On the other hand, the transmitted waveguide modes $\bar{T}_m H_m^-$ propagate down to the lower aperture ($z = -b$) and excite there scattering fields $\boldsymbol{H}_2^{\mathrm{s}}$ to the lower half-space

($z < -b$). These scattering fields are again calculated from the equivalent magnetic currents $\boldsymbol{M}_2^{\pm}$ on the closed aperture at $z = -b$, as in Fig. 2.2. The equivalent magnetic current $\boldsymbol{M}_2^{\pm}$ can be found from

$$\begin{aligned}\boldsymbol{M}_2^{\pm}(x, z = -b_{\pm}) &= (E_x^{\mathrm{w}}\hat{\boldsymbol{x}} + E_z^{\mathrm{w}}\hat{\boldsymbol{z}})\big|_{z=-b} \times (\pm\hat{\boldsymbol{z}}) \\ &= \mp\sum_{m=0}^{\infty} \bar{T}_m \bar{F}_{mx} \cos\frac{m\pi}{a}\left(x + \frac{a}{2}\right) e^{i\zeta_m b}\hat{\boldsymbol{y}}, \quad \left(|x| < \frac{a}{2}\right). \end{aligned} \tag{2.109}$$

The radiation field $\boldsymbol{H}_2^{\mathrm{s}}$ in the lower half-space can be derived from the equivalent source $\boldsymbol{M}_2^{-}$ in Eq. (2.47) like the primary scattering field $\boldsymbol{H}_1^{\mathrm{s}}$ with $\boldsymbol{M}_1^{+}$in Sect. 2.2.1. $\boldsymbol{H}_2^{\mathrm{s}}$ becomes

$$H_{2y}^{\mathrm{s}} = i\omega\varepsilon_0 \int_{-a/2}^{a/2} M_{2y}^{-}(x') \frac{i}{2} \mathrm{H}_0^{(1)}(k\sqrt{(x-x')^2 + (z-z')^2})\Big|_{z'=0} dx'. \tag{2.110}$$

Once again, the integral in Eq. (2.110) can be evaluated using the saddle point method. One gets the scattering field H_{2y}^{s} for $\theta > \pi$ as

$$\begin{aligned} H_{2y}^{\mathrm{s}} &= \frac{i^2\omega\varepsilon_0}{2} \int_{-a/2}^{a/2} M_{2y}^{-} \mathrm{H}_0^{(1)}(k\sqrt{(x-x')^2 + (z-z')^2})\Big|_{z'=-b} dx' \\ &= -\frac{\omega\varepsilon_0}{2\pi} \int_{-a/2}^{a/2} \sum_{m=0}^{\infty} \bar{T}_m \bar{F}_{mx} \cos\frac{m\pi}{a}\left(x' + \frac{a}{2}\right) e^{i\zeta_m b} \\ &\qquad \cdot \left\{ \int_{-\infty}^{\infty} \frac{e^{i\eta(x-x') + i\sqrt{k^2-\eta^2}(-z+z')}}{\sqrt{k^2-\eta^2}}\Big|_{z'=-b} d\eta \right\} dx' \\ &= -\frac{\omega\varepsilon_0}{2\pi} \int_{-a/2}^{a/2} \sum_{m=0}^{\infty} \bar{T}_m \bar{F}_{mx} \cos\frac{m\pi}{a}\left(x' + \frac{a}{2}\right) e^{i\zeta_m b} \int_{-\infty}^{\infty} e^{i\eta(x-x') + i\sqrt{k^2-\eta^2}(-z-b)} d\eta dx' \\ &= -\frac{\omega\varepsilon_0}{2\pi} \int_{-\infty}^{\infty} \sum_{m=0}^{\infty} \bar{T}_m \bar{F}_{mx} e^{i\zeta_m b} e^{i\eta x - i\sqrt{k^2-\eta^2}(z+b)} \left\{ \int_{-a/2}^{a/2} \cos\frac{m\pi}{a}\left(x' + \frac{a}{2}\right) e^{-i\eta x'} dx' \right\} d\eta \\ &= -\frac{\omega\varepsilon_0}{2\pi} \int_{-\infty}^{\infty} \sum_{m=0}^{\infty} \bar{T}_m \bar{F}_{mx} e^{i\zeta_m b} e^{i\eta x - i\sqrt{k^2-\eta^2}(z+b)} \\ &\qquad \cdot \left\{ \frac{-i\eta}{\left(\frac{m\pi}{a}\right)^2 - \eta^2} \left(\cos m\pi e^{-i\eta a/2} - e^{i\eta a/2}\right) \right\} d\eta \\ &= \frac{i\omega\varepsilon_0}{2\pi} \int_{-\infty}^{\infty} \sum_{m=0}^{\infty} \bar{T}_m \bar{F}_{mx} e^{i\zeta_m b} \frac{\eta}{\left(\frac{m\pi}{a}\right)^2 - \eta^2} \\ &\qquad \cdot \left\{ \cos m\pi e^{i\eta(x-a/2) - i\sqrt{k^2-\eta^2}(z+b)} - e^{i\eta(x+a/2) - i\sqrt{k^2-\eta^2}(z+b)} \right\} d\eta \\ &= I_1 + I_2. \end{aligned} \tag{2.111}$$

Calculate above integral with saddle point method with

$$\eta = k\sin\omega, \quad d\eta = k\cos\omega d\omega, \quad x \mp \frac{a}{2} = \rho'_{\pm}\cos\theta_{\pm}, \quad z + b = \rho'_{\pm}\sin\theta_{\pm},$$
$$\sqrt{k^2-\eta^2} = \sqrt{k^2 - k^2\sin^2\omega} = k\cos\omega,$$
$$i\eta(x \pm \frac{a}{2}) - i\sqrt{k^2-\eta^2}(z+b) = ik\sin\omega\cdot\rho'_{\mp}\cos\theta_{\mp} - ik\cos\omega\cdot\rho'_{\mp}\sin\theta_{\mp}$$
$$= ik\rho'_{\mp}\sin(\omega - \theta_{\mp}). \tag{2.112}$$

Then I_1, I_2 become

$$I_1 = \frac{i\omega\varepsilon_0}{2\pi}\int_C \sum_{m=0}^{\infty} \bar{T}_m\bar{F}_{mx}e^{i\zeta_m b}\frac{k\sin\omega}{\left(\frac{m\pi}{a}\right)^2 - (k\sin\omega)^2}\cos m\pi e^{ik\rho'_+\sin(\omega-\theta_+)}d\omega, \tag{2.113}$$

$$I_2 = -\frac{i\omega\varepsilon_0}{2\pi}\int_C \sum_{m=0}^{\infty} \bar{T}_m\bar{F}_{mx}e^{i\zeta_m b}\frac{k\sin\omega}{\left(\frac{m\pi}{a}\right)^2 - (k\sin\omega)^2}e^{ik\rho'_-\sin(\omega-\theta_-)}d\omega. \tag{2.114}$$

The position of the pole in ω plane yields $\left(\frac{m\pi}{a}\right)^2 - (k\sin\omega_p)^2$, then

$$\omega_p = \arcsin\left(\frac{m\pi}{ka}\right)^2. \tag{2.115}$$

One can find the saddle point from

$$\frac{\partial}{\partial\omega}(ik\rho'_{\pm}\sin(\omega-\theta_{\pm})) = ik\rho'_{\pm}\cos(\omega-\theta_{\pm}) = 0,$$
$$\cos(\omega_s - \theta_{\pm}) = 0, \quad \omega_s - \theta_{\pm} = \pm\frac{\pi}{2}. \tag{2.116}$$

Since the observation point is in the lower half-plane, the saddle point in $-\frac{\pi}{2} < \omega < \frac{\pi}{2}$ is With $\theta < 0$:

$$\omega_s = \frac{\pi}{2} + \theta_{\pm}, \quad \sin\omega_s = \sin\left(\frac{\pi}{2}+\theta_{\pm}\right) = \cos\theta_{\pm}, \quad \cos\omega_s = \cos\left(\frac{\pi}{2}+\theta_{\pm}\right) = -\sin\theta_{\pm},$$
$$ik\rho'_{\pm}\sin(\omega-\theta_{\pm}) \sim ik\rho'_{\pm}\sin(\omega_s-\theta_{\pm}) - \frac{ik\rho'_{\pm}}{2}\sin(\omega_s-\theta_{\pm})(\omega-\omega_s)^2,$$
$$= ik\rho'_{\pm} - \frac{ik\rho'_{\pm}}{2}(\omega-\omega_s)^2. \tag{2.117}$$

Then

$$I_1 = \frac{i\omega\varepsilon_0}{2\pi}\sum_{m=0}^{\infty}\bar{T}_m\bar{F}_{mx}e^{i\zeta_m b}\cos m\pi\int_{SDP}\frac{k\cos\theta_+}{\left(\frac{m\pi}{a}\right)^2 - (k\cos\theta_+)^2}e^{ik\rho'_+ - ik\rho'_+(\omega-\omega_s)^2/2}d\omega$$
$$= \frac{i\omega\varepsilon_0}{2\pi}\sum_{m=0}^{\infty}\bar{T}_m\bar{F}_{mx}e^{i\zeta_m b}\cos m\pi\frac{k\cos\theta_+}{\left(\frac{m\pi}{a}\right)^2 - (k\cos\theta_+)^2}e^{ik\rho'_+}\sqrt{\frac{2\pi}{ik\rho'_+}}$$
$$= 2k\omega\varepsilon_0\cos\theta_+\sqrt{\frac{1}{8\pi k\rho'_+}}\sum_{m=0}^{\infty}\frac{\bar{T}_m\bar{F}_{mx}\cos m\pi}{\left(\frac{m\pi}{a}\right)^2 - (k\cos\theta_+)^2}e^{ik\rho'_+ + i\zeta_m b + i\pi/4}, \tag{2.118}$$

$$
\begin{aligned}
I_2 &= -\frac{i\omega\varepsilon_0}{2\pi}\sum_{m=0}^{\infty}\bar{T}_m\bar{F}_{mx}e^{i\zeta_m b}\int_{SDP}\frac{k\cos\theta_-}{\left(\frac{m\pi}{a}\right)^2-(k\cos\theta_-)^2}e^{ik\rho'_- -ik\rho'_-(\omega-\omega_s)^2/2}d\omega \\
&= -\frac{i\omega\varepsilon_0}{2\pi}\sum_{m=0}^{\infty}\bar{T}_m\bar{F}_{mx}e^{i\zeta_m b}\frac{k\cos\theta_-}{\left(\frac{m\pi}{a}\right)^2-(k\cos\theta_-)^2}e^{ik\rho'_-}\sqrt{\frac{2\pi}{ik\rho'_-}} \\
&= -2k\omega\varepsilon_0\cos\theta_-\sqrt{\frac{1}{8\pi k\rho'_-}}\sum_{m=0}^{\infty}\frac{\bar{T}_m\bar{F}_{mx}}{\left(\frac{m\pi}{a}\right)^2-(k\cos\theta_-)^2}e^{ik\rho'_- +i\zeta_m b+i\pi/4}.
\end{aligned}
\tag{2.119}
$$

Since we assumed ρ is the distance from observation point (in both upper and lower half-space) to the origin. Then

$$
\rho = \rho' + b\sin\theta. \tag{2.120}
$$

If the observation point is sufficiently far, considering the phase only, one gets

$$
\rho_\pm \sim \rho \mp \frac{a}{2}\cos\theta, \quad \theta_\pm \sim \theta. \tag{2.121}
$$

Then the scattering H far-field from the lower aperture is, using Eqs. (2.89) and (2.91)

$$
\begin{aligned}
H^{\mathrm{s}}_{2y} =& I_1 + I_2 \\
=& 2k\omega\varepsilon_0\cos\theta\sqrt{\frac{1}{8\pi k\rho}} \\
& \cdot\sum_{m=0}^{\infty}\frac{\bar{T}_m\bar{F}_{mx}}{\left(\frac{m\pi}{a}\right)^2-(k\cos\theta)^2}\left\{\cos m\pi\cdot e^{(-ika\cos\theta)/2}-e^{(ik\cos\theta)/2}\right\}e^{ik\rho_+ +i\zeta_m b+i\pi/4+ikb\sin\theta} \\
=& 2ka\cos\theta C(k\rho)\sum_{m=0}^{\infty}\bar{T}_m\bar{F}_m\frac{-\zeta_m a}{(m\pi)^2-(ka\cos\theta)^2} \\
& \cdot\left\{(-1)^m e^{-ik\frac{a}{2}\cos\theta}-e^{ik\frac{a}{2}\cos\theta}\right\}e^{i\zeta_m b+ikb\sin\theta}.
\end{aligned}
\tag{2.122}
$$

For modal reflection at the lower aperture, one may use the similar formula in Eq. (2.86) with M^+_{2y} in Eq. (2.109). One finds that the modal coefficients obtained from the equivalent magnetic current M^+_{2x} become unit values which cancel the reflection coefficients (-1) of the waveguide modes by closing the lower aperture. Consequently, there is no reflection at all from the lower aperture by the Kirchhoff approximation. Similarly, the modal reflection does not also exist at the upper aperture despite the presence of the equivalent magnetic current M^-_{11x}.

2.2.4 Scattering Far-field from Infinitely Thin Slit

Special circumstance of an infinitely thin slit has also been considered for H polarization case, one can take the limit $b \to 0$ in Eq. (2.122), and the transmission coefficient $T_m = 1$.

On the other hand, the lower scattering field in this case $\boldsymbol{\phi}_2^{\mathrm{ss}} = \boldsymbol{H}_2^{\mathrm{ss}}$ can be derived directly from $\boldsymbol{M}_1^-$ in Eq. (2.85) in the similar way of deriving $\boldsymbol{H}_1^{\mathrm{s}}$ in Sect. 2.2.1 with $\boldsymbol{M}_1^+$ replaced by $\boldsymbol{M}_1^-$ in Eq. (2.69). Since $\boldsymbol{M}_1^- = -\boldsymbol{M}_1^+$, one gets for $\theta > \pi$

$$H_{2y}^{\mathrm{ss}} = -H_{1y}^{\mathrm{s}} = -\frac{4i \sin\theta_0 \sin\{ka(\cos\theta_0 + \cos\theta)/2\}}{\cos\theta_0 + \cos\theta} C(k\rho). \tag{2.123}$$

The comparison of results from these two calculations will be shown in Sect. 2.3.

2.3 Numerical Results and Discussion

Some numerical results for the scattering far fields by thick loaded conducting slit are obtained by using the formulas derived in the previous section. The scattering field in the upper half-space ($z > 0$) is given by a summation of the primary and secondary upper scattering field $\boldsymbol{\phi}_1^{\mathrm{s}} + \boldsymbol{\phi}_{11}^{\mathrm{s}}$, and the one in the lower half-space ($z < -b$) is by $\boldsymbol{\phi}_2^{\mathrm{s}}$. Firstly, the figures which include numerical results from KA, GTD, and KP method for loaded slit are shown to validate the formulation obtained by the proposed KA method. After that, the other aspects of scattering feature analyzed by the KA method have been shown. Special cases of empty slit ($R_m = 0$, $T_m = 1$) and infinitely thin slit has also been investigated. In the following calculations, a common factor $C(k\rho)$ is omitted.

Figures 2.6–2.8 show the scattering far field for fully loaded slits in E polarization. The aperture widths are set to be $ka = 30$, the screen thickness is $kb = 2$, the complex relative permitivity $\varepsilon_r = 3 + i4$ represents for the lossy loaded layer, the complex relative permeability $\mu_r = 1$, and the incident angle $\theta_0 = 20°$, $50°$, $90°$ are chosen. As can be seen from the figures, in general, the higher incident angle is, the stronger the scattering fields become, especially at the main lobe. One observes that the main lobes direct the corresponding reflected and incident shadow boundary directions. A symmetric pattern with respect to the normal (z) axis is observed in case of normal incidence. When the loaded medium has a loss (denoted by the imaginary part in loaded material parameters), the scattering fields in both half-spaces become weak due to the decay inside the dielectric material. The effect of the loaded layer inside the slit on the scattering field is given by comparison with the case of empty slit. For transmitted region ($180° \leqslant \theta \leqslant 360°$), one sees from the previous section that the scattering fields are given by a summation of the modal re-radiation fields as in Eq. (2.62). The main transmitted lobe is made

by the significant modes whose propagation angles are in the vicinity of the incident angle θ_0, and these modal excitation coefficients become large [34]. Figures 2.9–2.11 show the pattern change when the glass layer becomes lossless with $\varepsilon_r = 3$. Although one can not see the attenuation anymore in both upper and lower half-space, the patterns still slightly change due to the effect of the dielectric-loaded layer characteristic to the incoming electromagnetic waves. The effect of the loaded layer thickness can be observed in Figs. 2.12–2.17. As the loaded layer becomes thicker, there are not so many changes at the upper half-space or in case of lossless load. However, significant decay occurs in lossy case for the transmitted field, especially when the incident field impinges at low angles. The KA method is proved that to be more accurate for electrically large aperture by good agreement with the results derived by the GTD and the KP methods ($ka = 30$). However, one also can assess the KA results in case of narrower aperture ($ka = 7$) from the comparison shown in Figs. 2.18–2.29. Scattering field features change as the aperture width decrease. Fewer diffraction lobes are constructed due to the reduced interference between the radiation fields excited at the edges at $x = \pm a/2$. Also, a clear decrease in the scattering values at all observation angles can be observed.

The attenuation is reduced in case of partially loaded slit as shown in Figs. 2.30–2.33. Also, in order to see the effect of the evanescent modal re-radiation, our KA results are obtained by including the first three evanescent modal re-radiations. Results labeled as "Empty0" and "Loaded0" with dots and crosses symbols, respectively, are calculated without the evanescent modal contribution.

The effect of evanescent modal re-radiation has also been shown in Fig. 2.34–2.41 in case of empty thick slits for both E and H polarization in dB. Here, the aperture widths are set to be $ka = 30$, 7, the screen thickness is $kb = 2$, and the incident angle $\theta_0 = 50°$, 90° are chosen. For comparison, the figures also include the results obtained by the GTD [31], [33], and by the KP method [12]. One can observe that the main scattering characteristic, in this case, is relatively similar to the case with loaded layer considered. The main difference is that the transmitted wave to the lower region experiences no attenuation as they pass through the slit. The main feature of the scattering pattern is almost the same between E and H polarizations. However, the difference occurs at the boundary direction at $\theta = 0°, 180°, 360°$ due to the boundary conditions.

The scattering feature in thin slit case should be considered in the next discussion.

According to the formulation for the lower scattering field, a limit value of the expression can be obtained for taking a limit of a corresponding infinitely thin case ($b \to 0$), while one can get a direct formulation for this case by considering the equivalent currents $\boldsymbol{M}_1^{\pm}$ only, without the current $\boldsymbol{M}_2^{\pm}$ as in Fig. 2.5. Figures 2.42 and 2.43 shows the difference between the limit cases in Eqs. (2.62), (2.122) and the direct formulation cases in Eqs. (2.63), (2.123). Both results are indistinguishable. The scattering patterns with result calculated by the KA method in this special case are shown in comparison with those of the KP method. An agreement can be seen, and one can also observe a symmetry in all scattering patterns with respect to the boundary (x) direction. This feature can be expected when the screen becomes infinitely thin.

Figures 2.44 and 2.45 show the normalized far-field scattering pattern changes with the effect of the slit's thickness. Here, we consider the thickness effect in case of empty slit. Both E and H polarizations are considered using the KA method with a representative aperture width parameter of $ka = 50$ in all figures. Figure 2.44 shows the gradual changes from an infinitely thin case to the finite thin case. For the upper scattering field ($\theta < 180°$), the patterns stay similar with different thickness, since no information of the slit's thickness kb contained in the primary scattering fields excited by $\boldsymbol{M}_1^{+}$. Besides, the symmetric pattern with respect to the boundary (x) direction for an infinitely thin case ($kb = 0$) deteriorates as the thickness parameter increases. This effect occurs even for relatively thin case in Fig. 2.44(b) for $b/a = 0.02$, and this thickness effect seems to be more influential for E polarization. Moreover, Fig. 2.45 shows the pattern changes for pretty thick cases. Three representative thickness cases are chosen here in order to show the incident beam splitting clearly. Due to the slit's thickness, incident plane wave experiences the reflection at the internal slit wall. Accordingly, the geometrical optic (GO) beam yields a splitting. A half splitting can be seen in Fig. 2.45(a) for $kb = 25/\sqrt{3}$ where the lower scattering pattern becomes roughly symmetric with respect to the normal (z) axis. The total GO beam reflection occurs in Fig. 2.45(b) for $kb = 50/\sqrt{3}$, and the GO beam propagation due to the double bouncing can be observed Fig. 2.45(c) for $kb = 100/\sqrt{3}$. While the incident plane wave in the slit's aperture is converted into the waveguide modes, the original GO beam feature is kept by modal re-radiation field correctly.

Figure 2.47 shows the far-field scattering pattern comparison between KA and GTD

methods for the case of aperture width $ka = 50$ and other thickness of $kb = 1$. Again, KA solution predicts well for main diffraction beam directions. When the aperture width parameter increases to $ka = 50$ as in this case, the side lobe levels get lower. Accordingly, the KA accuracy becomes better if one estimates the main feature at the main reflected of transmitted direction of the diffraction pattern, even the multi-edge effect has not been considered. When the proposed KA formulation is put in comparison with those by GTD [31], [33], main difference maybe found in the modal re-radiation field. Since the KA approximation yields no waveguide modal reflections and couplings at the open end, modal re-radiation occurs only once at the lower half-plane. Accordingly, one does not need to solve the matrix equation by GTD method for the successive modal re-radiation field [31]. Then one can expect fast calculation from simple integral form. By comparing the CPU time for numerical evaluation, the present method is 1.5 times faster than the previous GTD formulation [31]. This performs well for wide apertures, since many waveguide modes will be excited inside the slit, and the modal coupling between them become involved to compute.

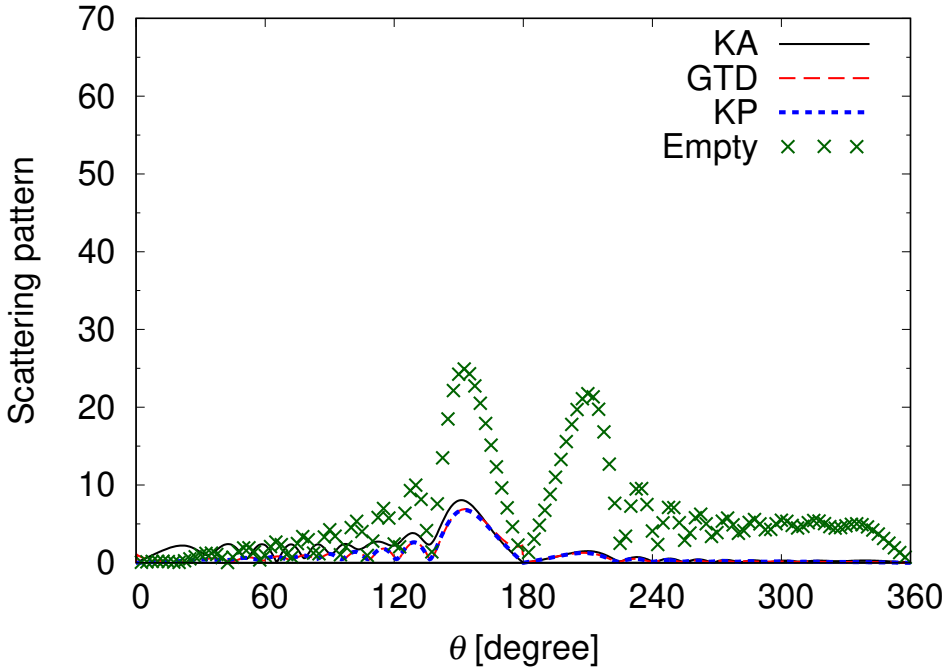

Figure 2.6: Far-field scattering pattern comparison of KA, KP and GTD methods. E polarization. $ka = 30$, $kb_1 = 0$, $kb_2 = kb = 2$, $\varepsilon_r = 3 + i4$, $\theta_0 = 20°$.

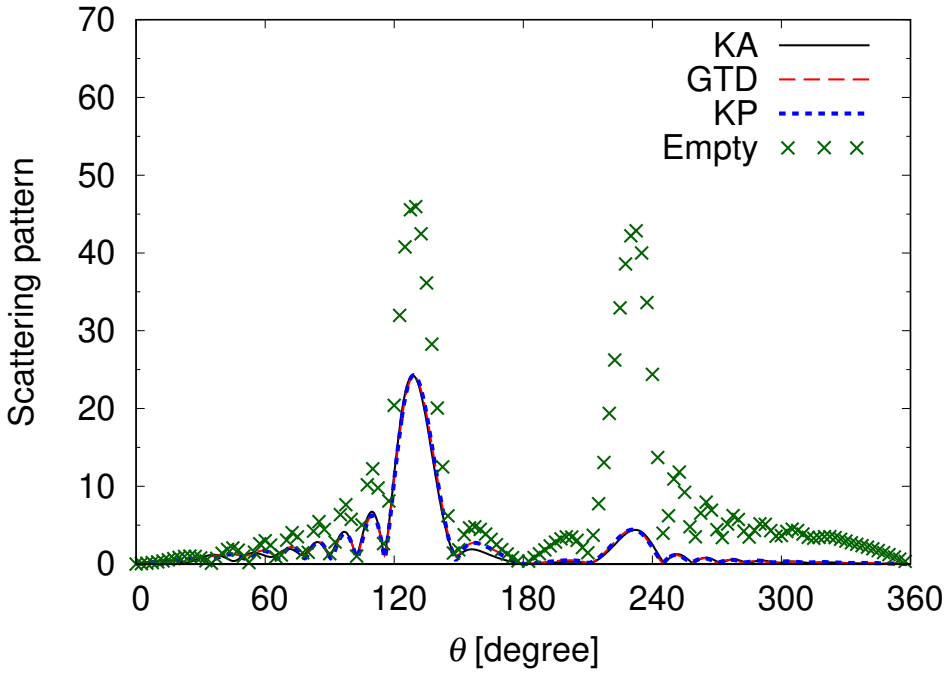

Figure 2.7: Far-field scattering pattern comparison of KA, KP and GTD methods. E polarization. $ka = 30$, $kb_1 = 0$, $kb_2 = kb = 2$, $\varepsilon_r = 3 + i4$, $\theta_0 = 50°$.

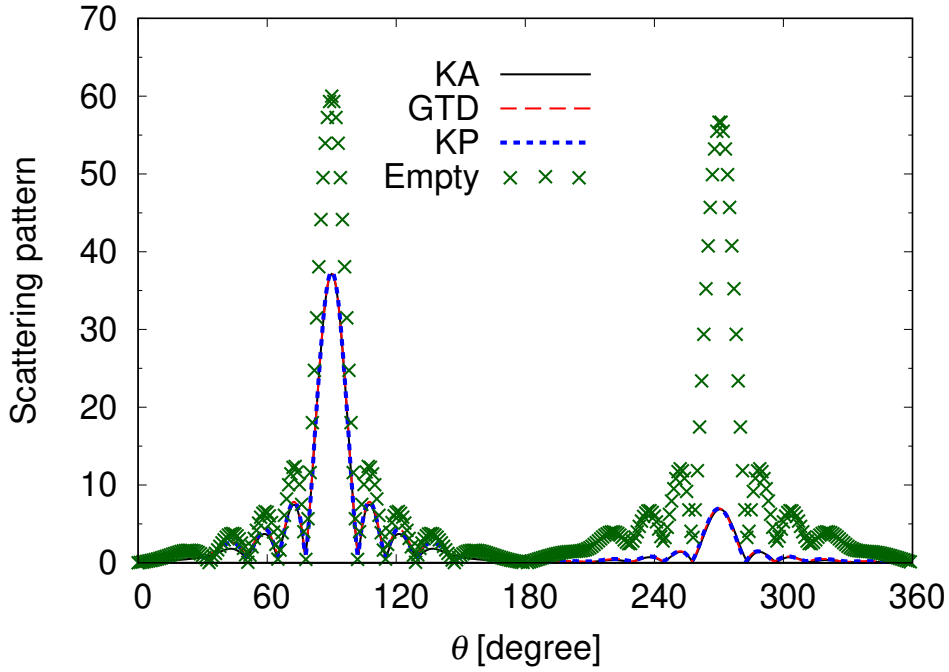

Figure 2.8: Far-field scattering pattern comparison of KA, KP and GTD methods. E polarization. $ka = 30$, $kb_1 = 0$, $kb_2 = kb = 2$, $\varepsilon_r = 3 + i4$, $\theta_0 = 90°$.

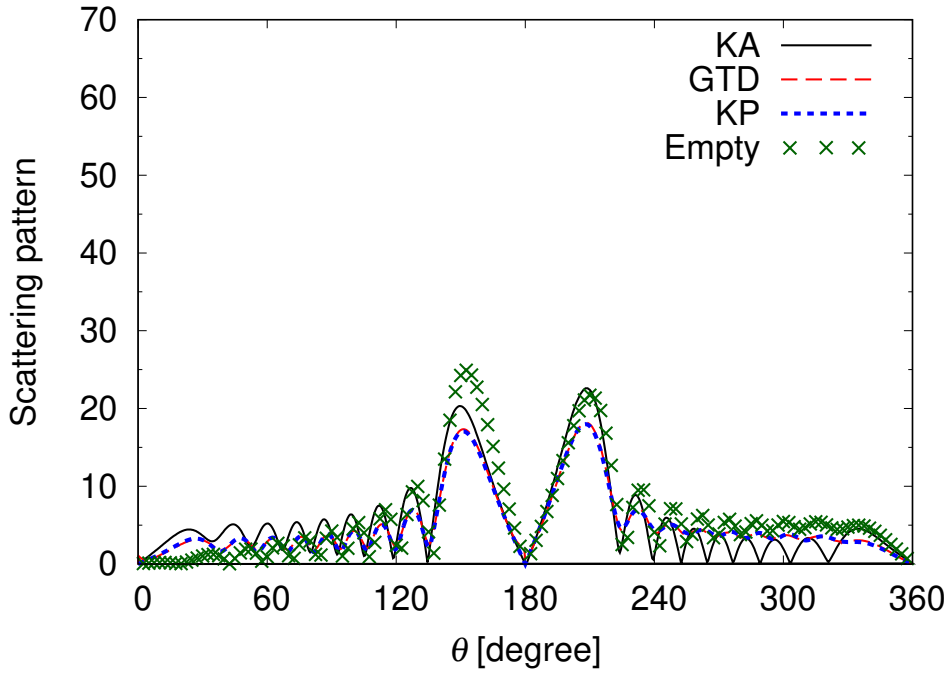

Figure 2.9: Far-field scattering pattern comparison of KA, KP and GTD methods. E polarization. $ka = 30$, $kb_1 = 0$, $kb_2 = kb = 2$, $\varepsilon_r = 3$, $\theta_0 = 20°$.

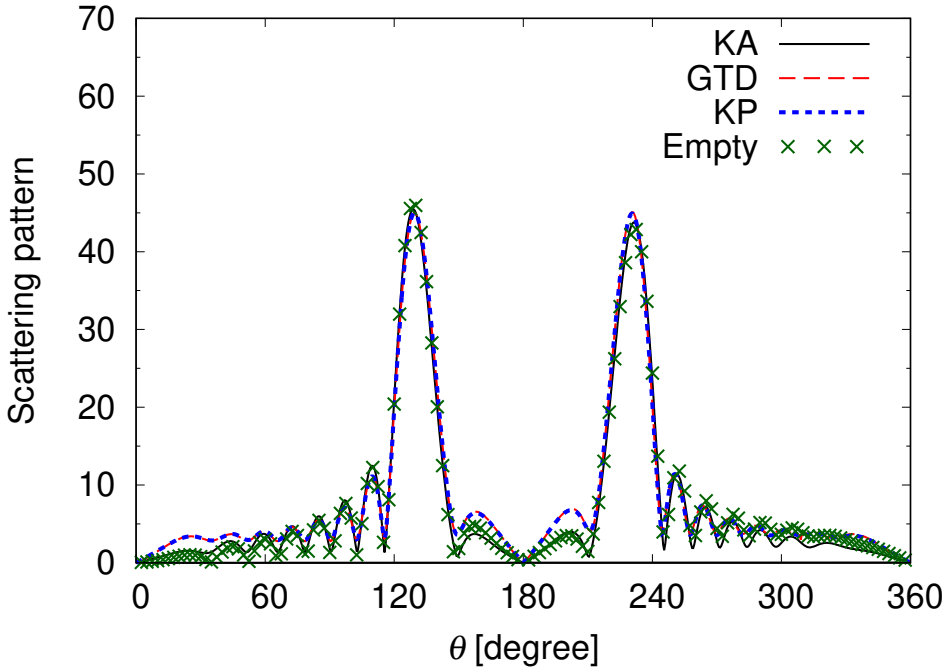

Figure 2.10: Far-field scattering pattern comparison of KA, KP and GTD methods. E polarization. $ka = 30$, $kb_1 = 0$, $kb_2 = kb = 2$, $\varepsilon_r = 3$, $\theta_0 = 50°$.

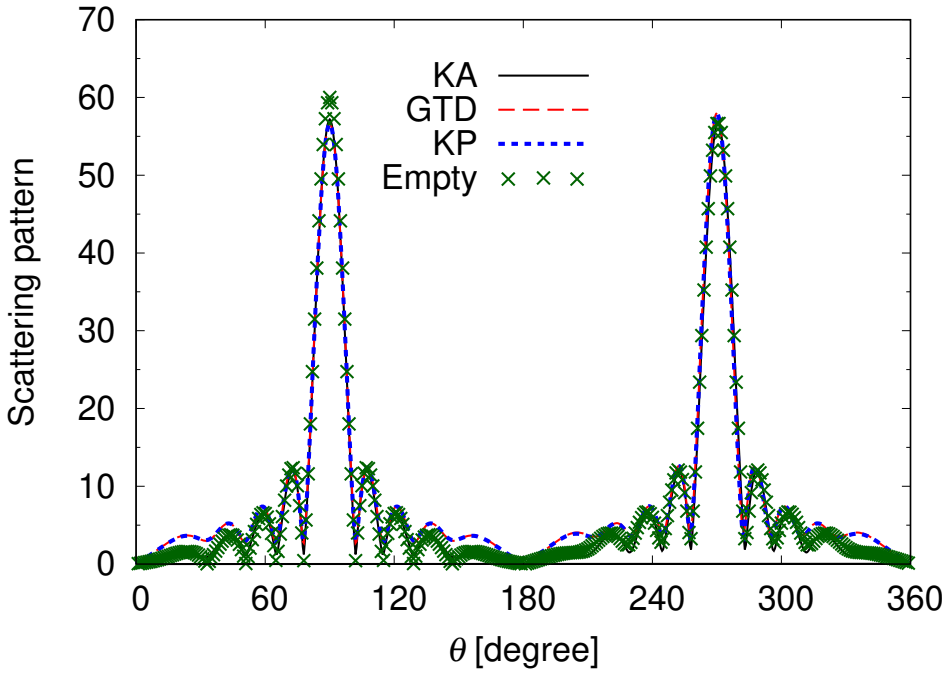

Figure 2.11: Far-field scattering pattern comparison of KA, KP and GTD methods. E polarization. $ka = 30$, $kb_1 = 0$, $kb_2 = kb = 2$, $\varepsilon_r = 3$, $\theta_0 = 90°$.

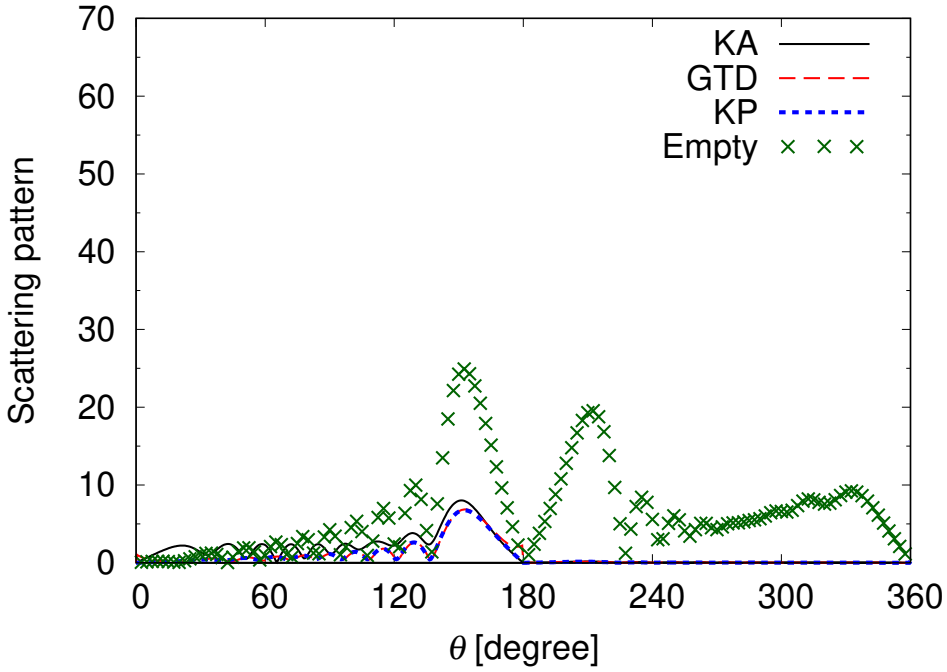

Figure 2.12: Far-field scattering pattern comparison of KA, KP and GTD methods. E polarization. $ka = 30$, $kb_1 = 0$, $kb_2 = kb = 4$, $\varepsilon_r = 3 + i4$, $\theta_0 = 20°$.

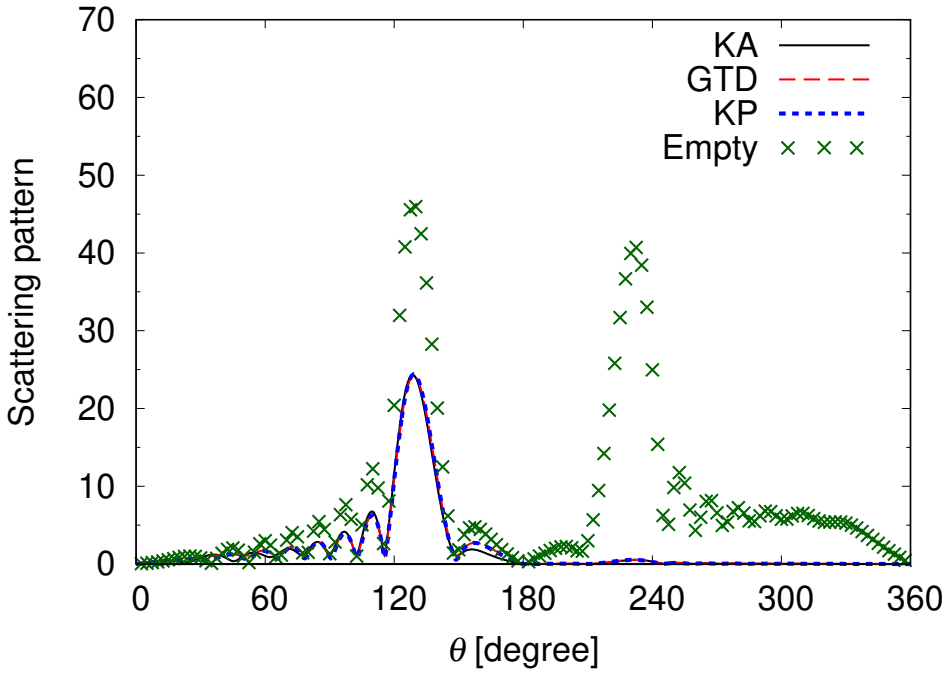

Figure 2.13: Far-field scattering pattern comparison of KA, KP and GTD methods. E polarization. $ka = 30$, $kb_1 = 0$, $kb_2 = kb = 4$, $\varepsilon_r = 3 + i4$, $\theta_0 = 50°$.

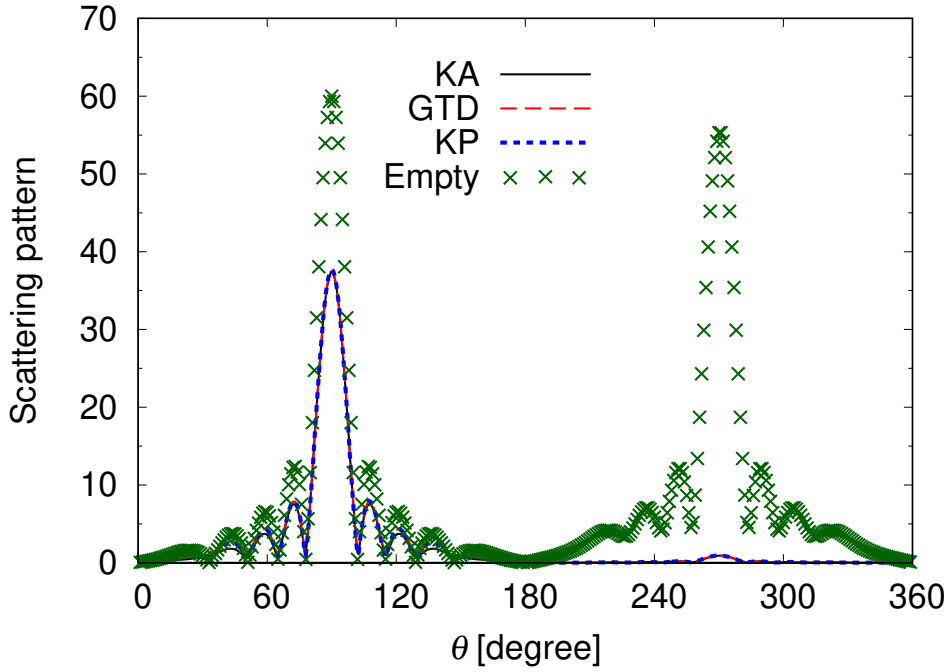

Figure 2.14: Far-field scattering pattern comparison of KA, KP and GTD methods. E polarization. $ka = 30$, $kb_1 = 0$, $kb_2 = kb = 4$, $\varepsilon_r = 3 + i4$, $\theta_0 = 90°$.

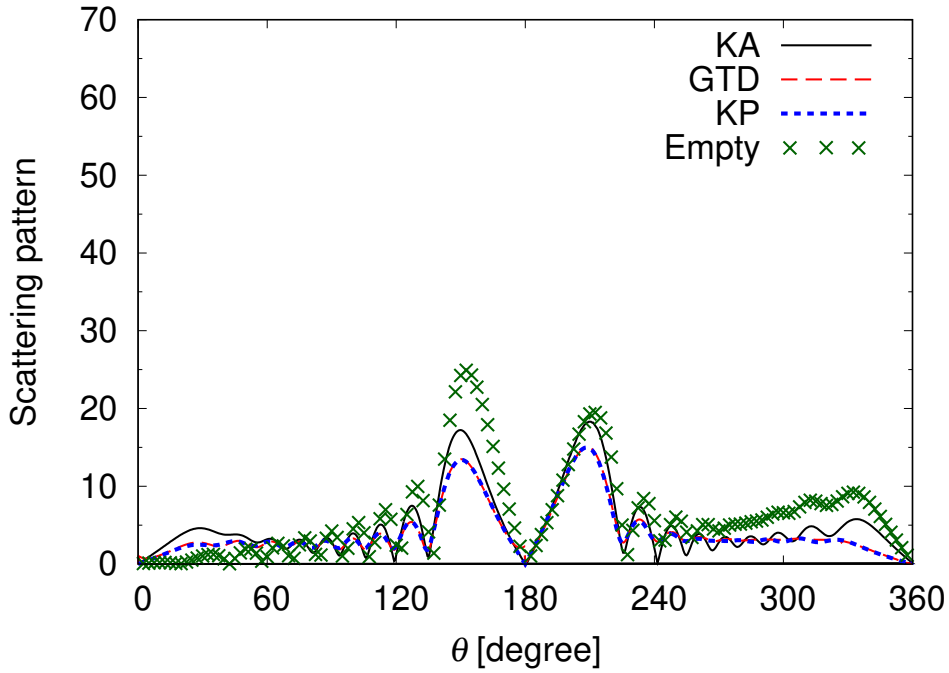

Figure 2.15: Far-field scattering pattern comparison of KA, KP and GTD methods. E polarization. $ka = 30$, $kb_1 = 0$, $kb_2 = kb = 4$, $\varepsilon_r = 3$, $\theta_0 = 20°$.

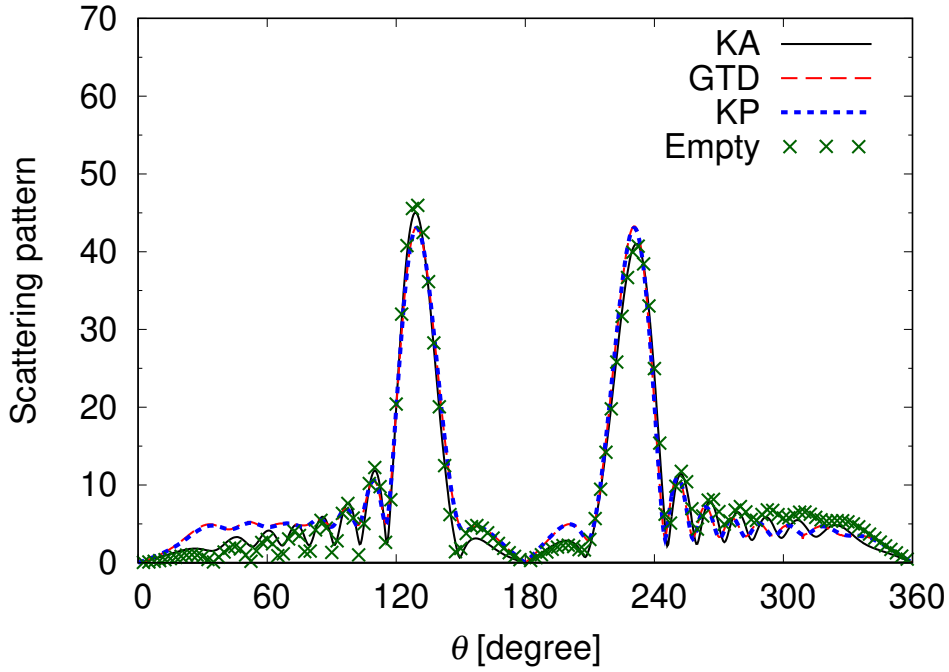

Figure 2.16: Far-field scattering pattern comparison of KA, KP and GTD methods. E polarization. $ka = 30$, $kb_1 = 0$, $kb_2 = kb = 4$, $\varepsilon_r = 3$, $\theta_0 = 50°$.

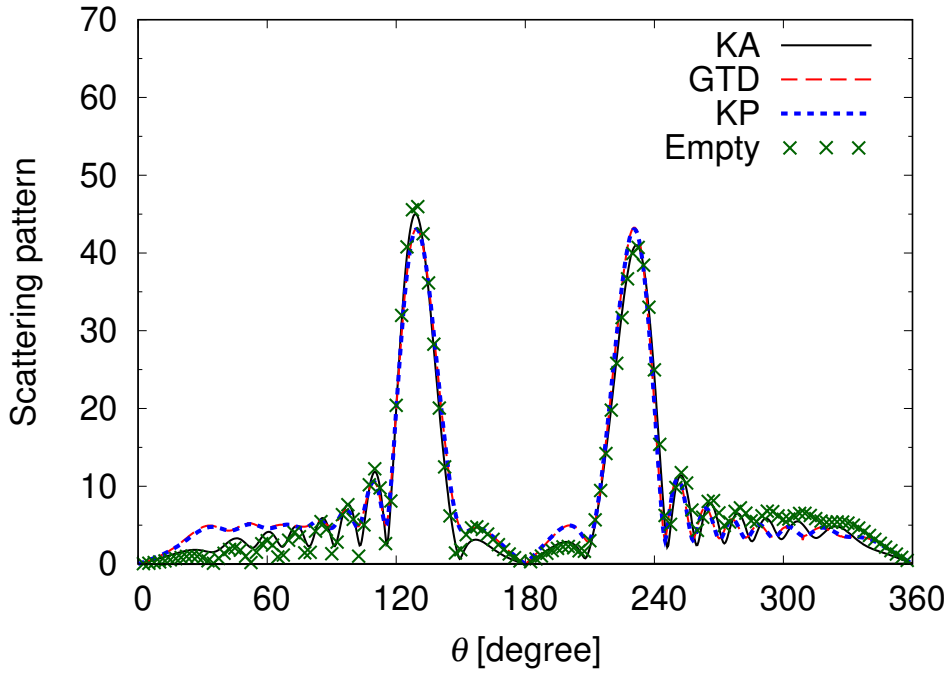

Figure 2.17: Far-field scattering pattern comparison of KA, KP and GTD methods. E polarization. $ka = 30$, $kb_1 = 0$, $kb_2 = kb = 4$, $\varepsilon_r = 3$, $\theta_0 = 90°$.

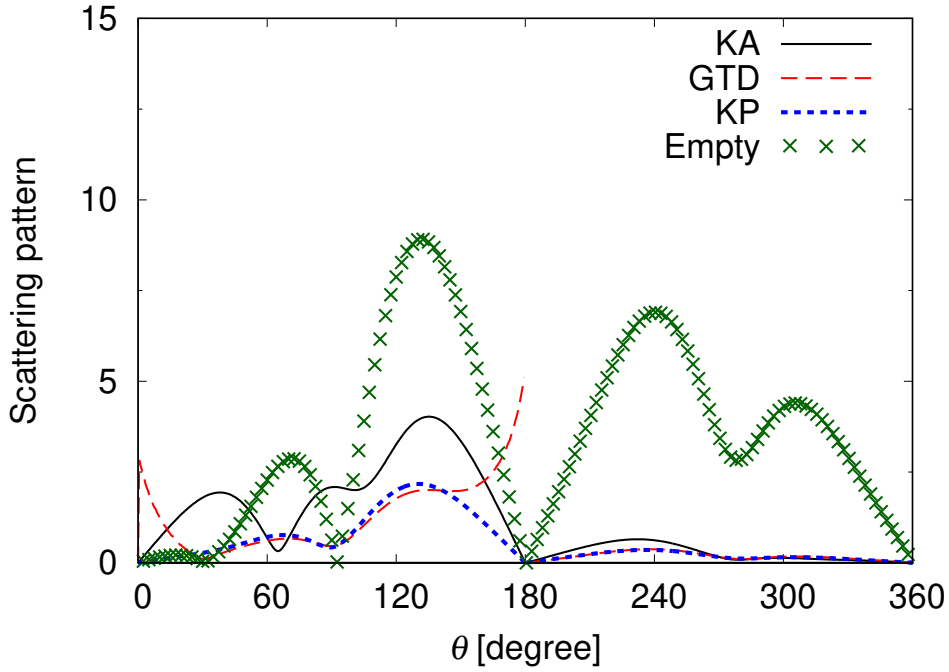

Figure 2.18: Far-field scattering pattern comparison of KA, KP and GTD methods. E polarization. $ka = 7$, $kb_1 = 0$, $kb_2 = kb = 2$, $\varepsilon_r = 3 + i4$, $\theta_0 = 20°$.

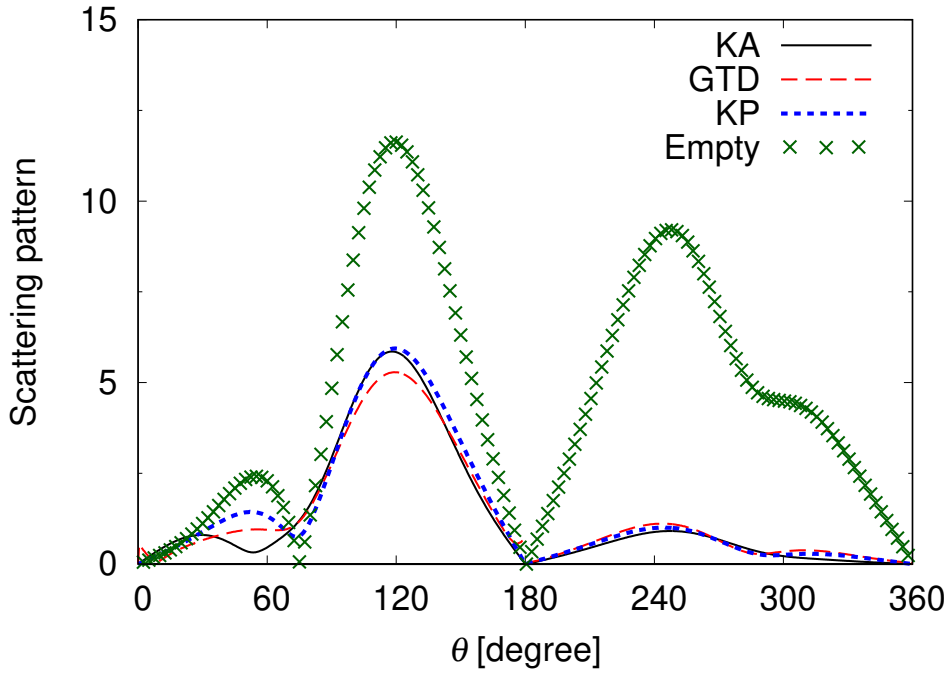

Figure 2.19: Far-field scattering pattern comparison of KA, KP and GTD methods. E polarization. $ka = 7$, $kb_1 = 0$, $kb_2 = kb = 2$, $\varepsilon_r = 3 + i4$, $\theta_0 = 50°$.

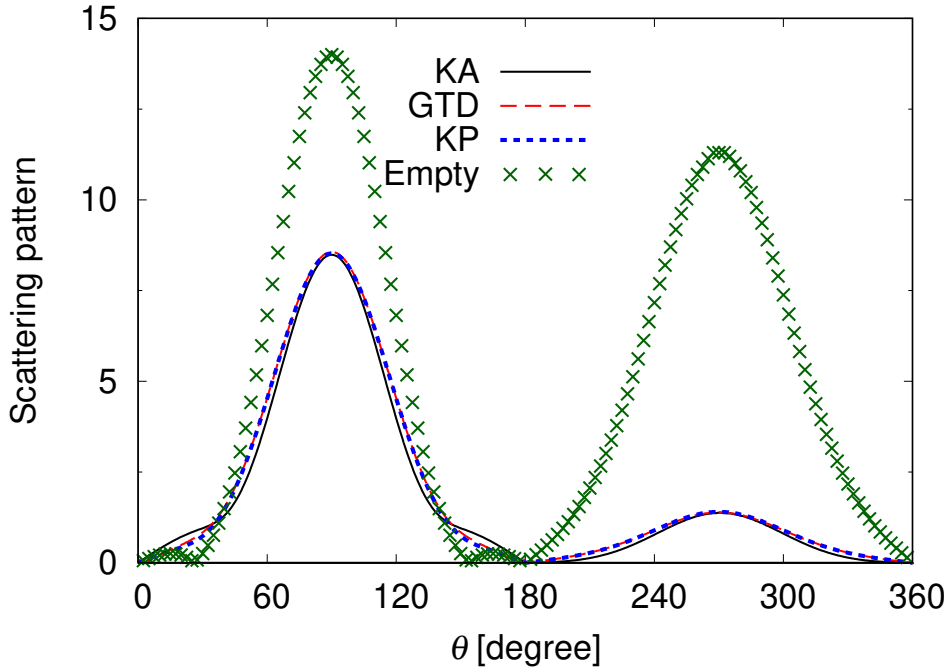

Figure 2.20: Far-field scattering pattern comparison of KA, KP and GTD methods. E polarization. $ka = 7$, $kb_1 = 0$, $kb_2 = kb = 2$, $\varepsilon_r = 3 + i4$, $\theta_0 = 90°$.

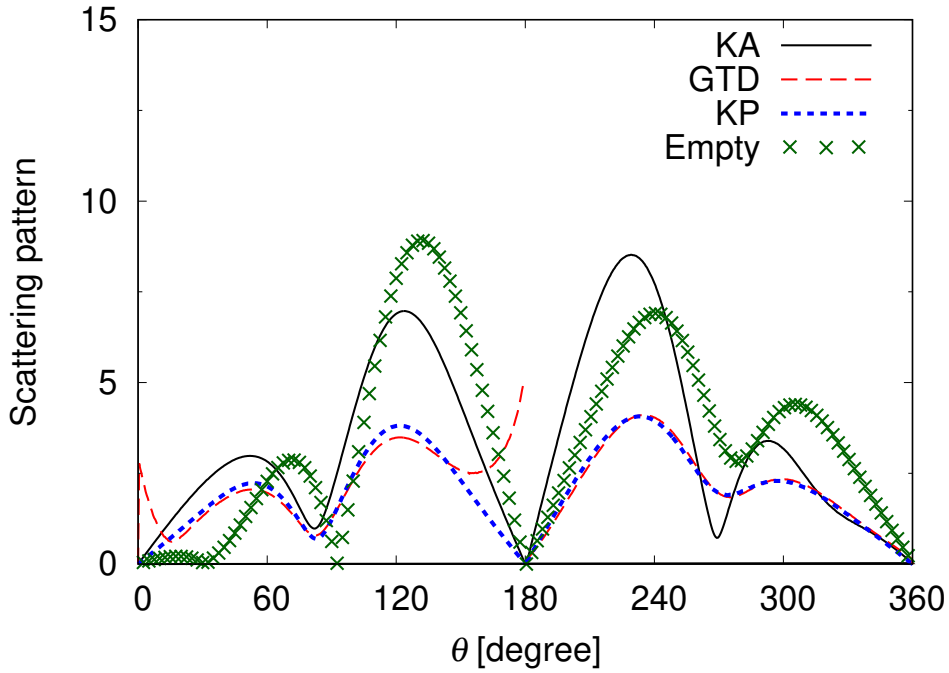

Figure 2.21: Far-field scattering pattern comparison of KA, KP and GTD methods. E polarization. $ka = 7$, $kb_1 = 0$, $kb_2 = kb = 2$, $\varepsilon_r = 3$, $\theta_0 = 20°$.

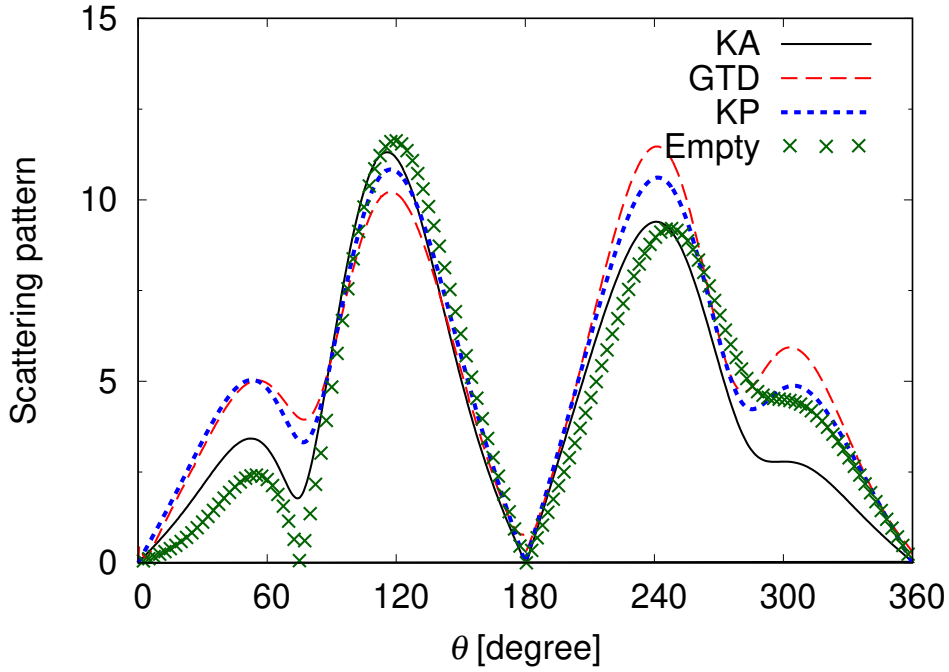

Figure 2.22: Far-field scattering pattern comparison of KA, KP and GTD methods. E polarization. $ka = 7$, $kb_1 = 0$, $kb_2 = kb = 2$, $\varepsilon_r = 3$, $\theta_0 = 50°$.

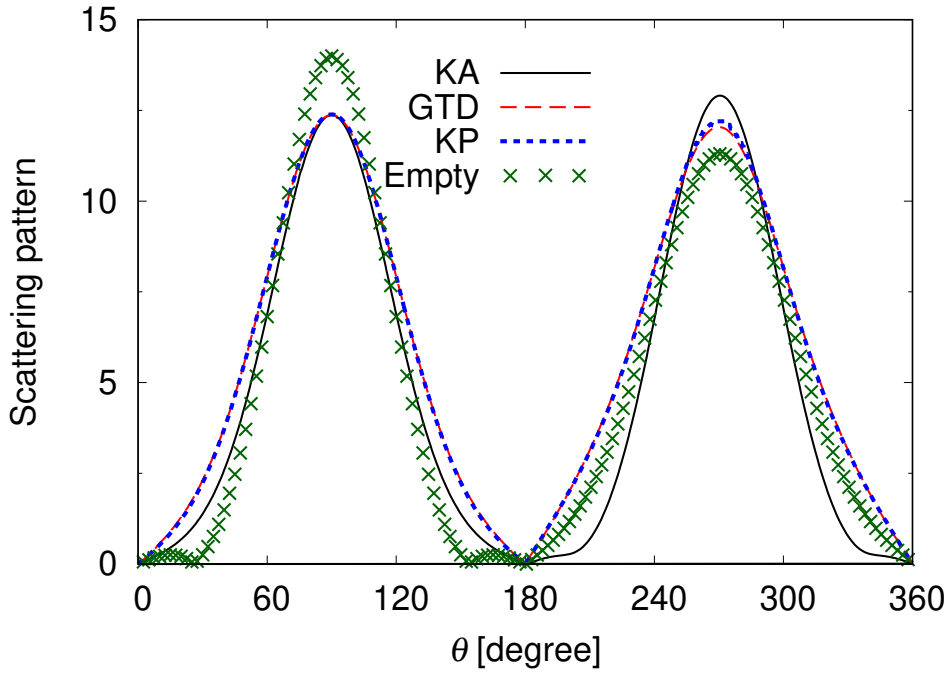

Figure 2.23: Far-field scattering pattern comparison of KA, KP and GTD methods. E polarization. $ka = 7$, $kb_1 = 0$, $kb_2 = kb = 2$, $\varepsilon_r = 3$, $\theta_0 = 90°$.

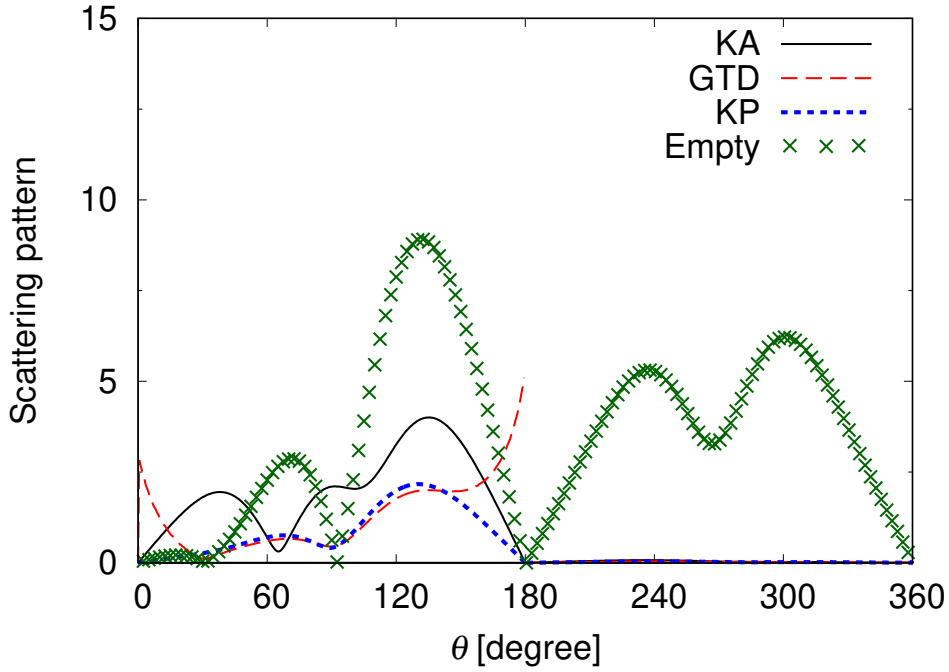

Figure 2.24: Far-field scattering pattern comparison of KA, KP and GTD methods. E polarization. $ka = 7$, $kb_1 = 0$, $kb_2 = kb = 4$, $\varepsilon_r = 3 + i4$, $\theta_0 = 20°$.

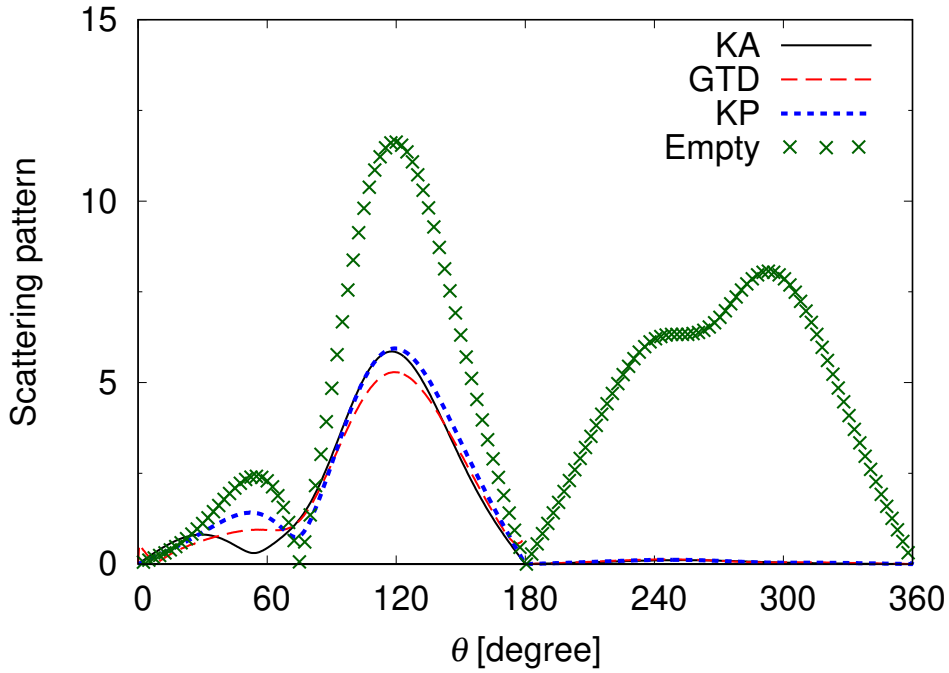

Figure 2.25: Far-field scattering pattern comparison of KA, KP and GTD methods. E polarization. $ka = 7$, $kb_1 = 0$, $kb_2 = kb = 4$, $\varepsilon_r = 3 + i4$, $\theta_0 = 50°$.

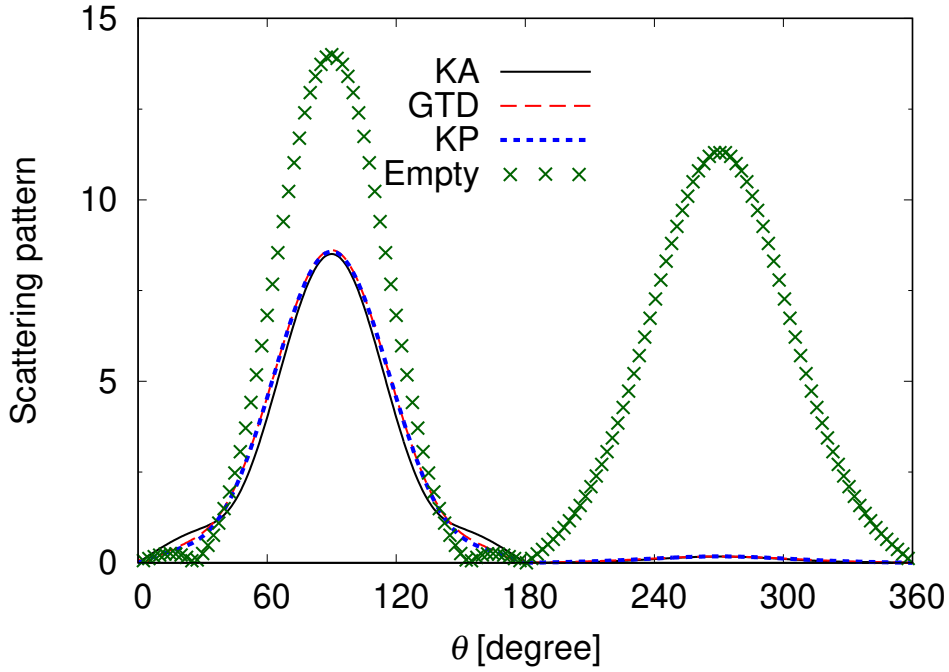

Figure 2.26: Far-field scattering pattern comparison of KA, KP and GTD methods. E polarization. $ka = 7$, $kb_1 = 0$, $kb_2 = kb = 4$, $\varepsilon_r = 3 + i4$, $\theta_0 = 90°$.

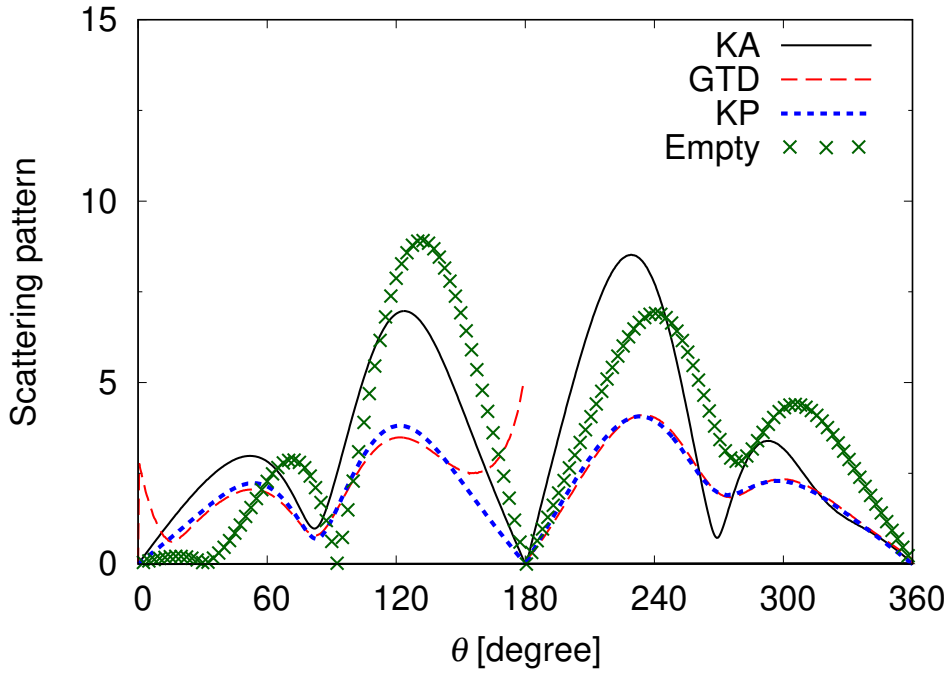

Figure 2.27: Far-field scattering pattern comparison of KA, KP and GTD methods. E polarization. $ka = 7$, $kb_1 = 0$, $kb_2 = kb = 4$, $\varepsilon_r = 3$, $\theta_0 = 20°$.

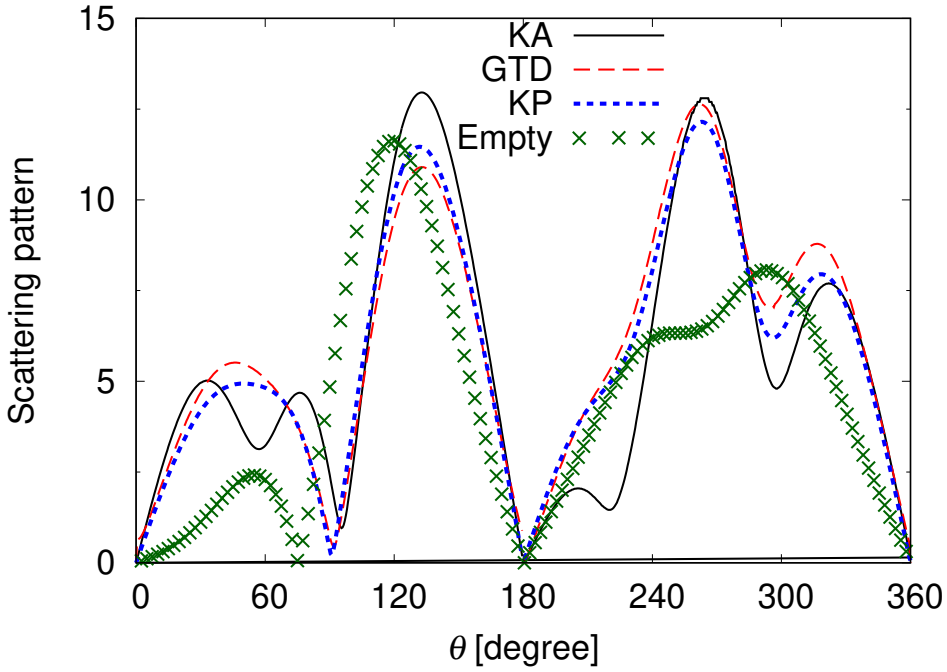

Figure 2.28: Far-field scattering pattern comparison of KA, KP and GTD methods. E polarization. $ka = 7$, $kb_1 = 0$, $kb_2 = kb = 4$, $\varepsilon_r = 3$, $\theta_0 = 50°$.

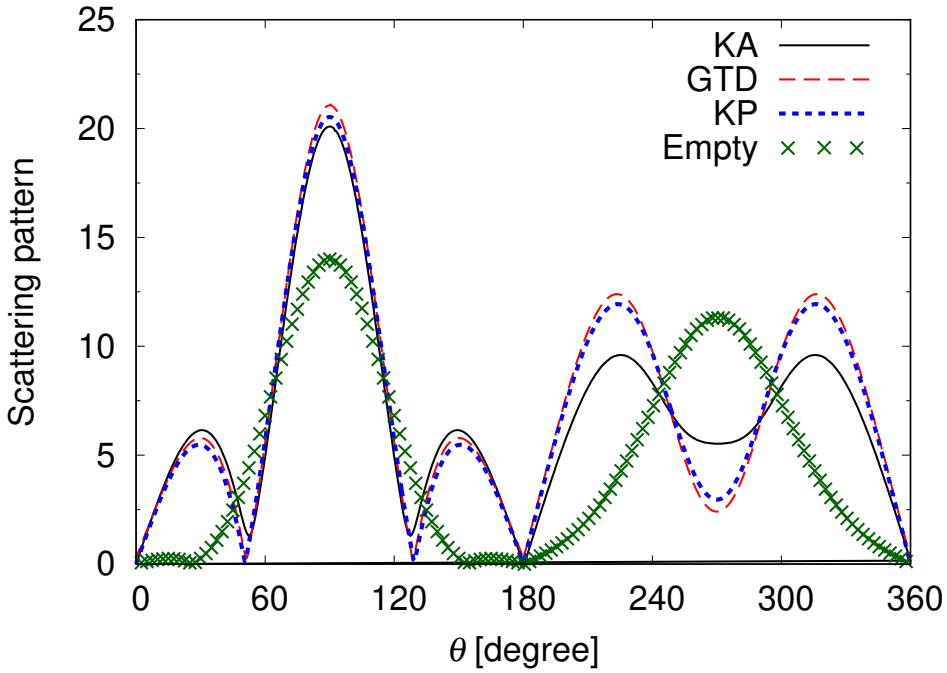

Figure 2.29: Far-field scattering pattern comparison of KA, KP and GTD methods. E polarization. $ka = 7$, $kb_1 = 0$, $kb_2 = kb = 4$, $\varepsilon_r = 3$, $\theta_0 = 90°$.

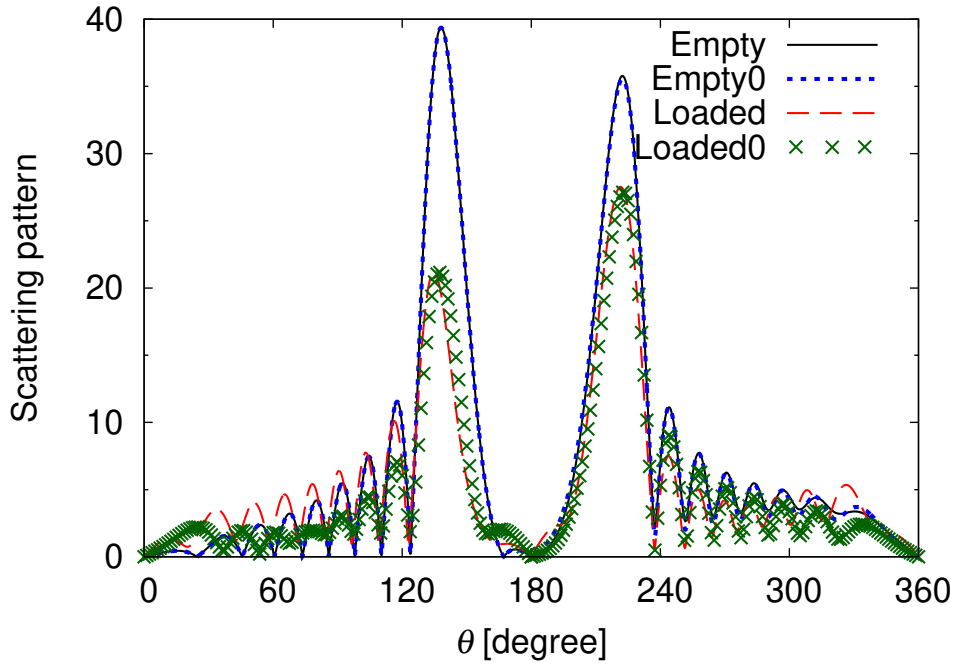

Figure 2.30: Far-field patterns of partially lossless loaded slit. $ka = 30$, $kb_1 = kb/3 = 2/3$, $kb_2 = 2kb/3 = 4/3$, $\varepsilon_r = 3$, $\theta_0 = 40°$.

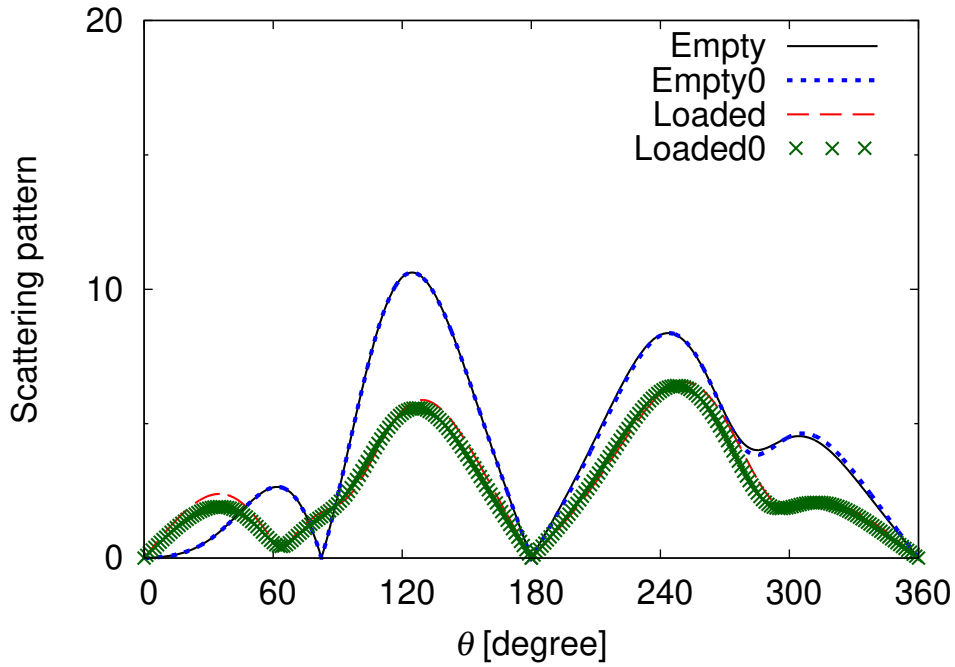

Figure 2.31: Far-field patterns of partially lossless loaded slit. $ka = 7$, $kb_1 = kb/3 = 2/3$, $kb_2 = 2kb/3 = 4/3$, $\varepsilon_r = 3$, $\theta_0 = 40°$.

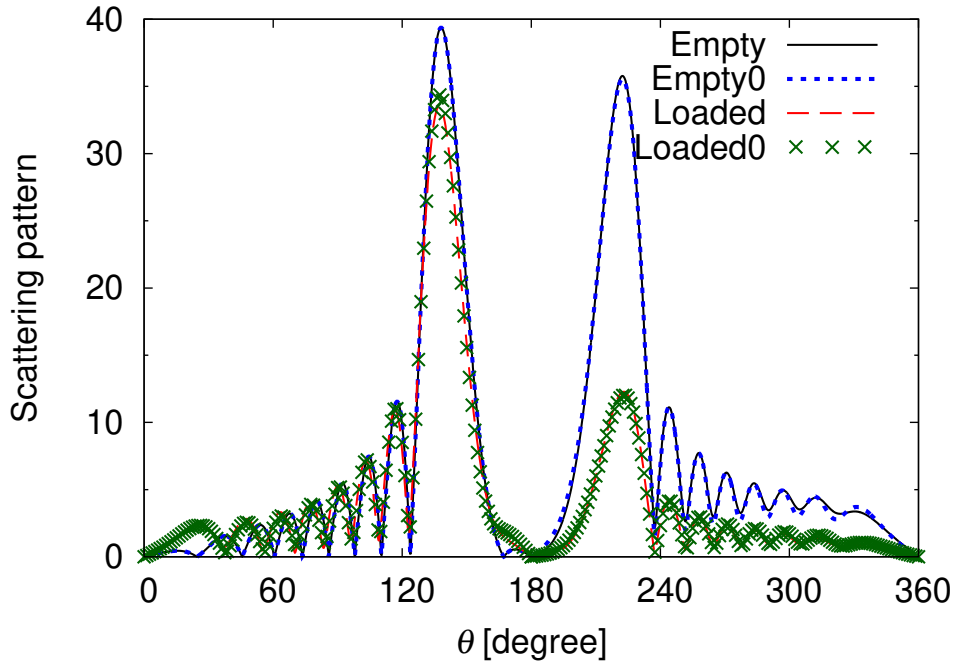

Figure 2.32: Far-field patterns of partially lossy loaded slit. $ka = 30$, $kb_1 = kb/3 = 2/3$, $kb_2 = 2kb/3 = 4/3$, $\varepsilon_r = 3 + i4$, $\theta_0 = 40°$.

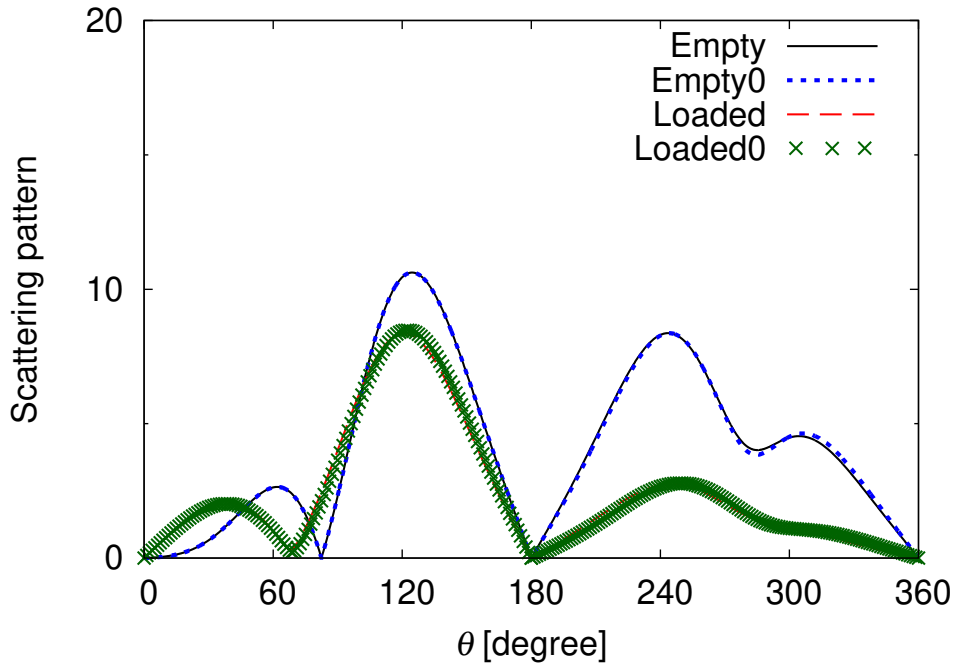

Figure 2.33: Far-field patterns of partially lossy loaded slit. $ka = 7$, $kb_1 = kb/3 = 2/3$, $kb_2 = 2kb/3 = 4/3$, $\varepsilon_r = 3 + i4$, $\theta_0 = 40°$.

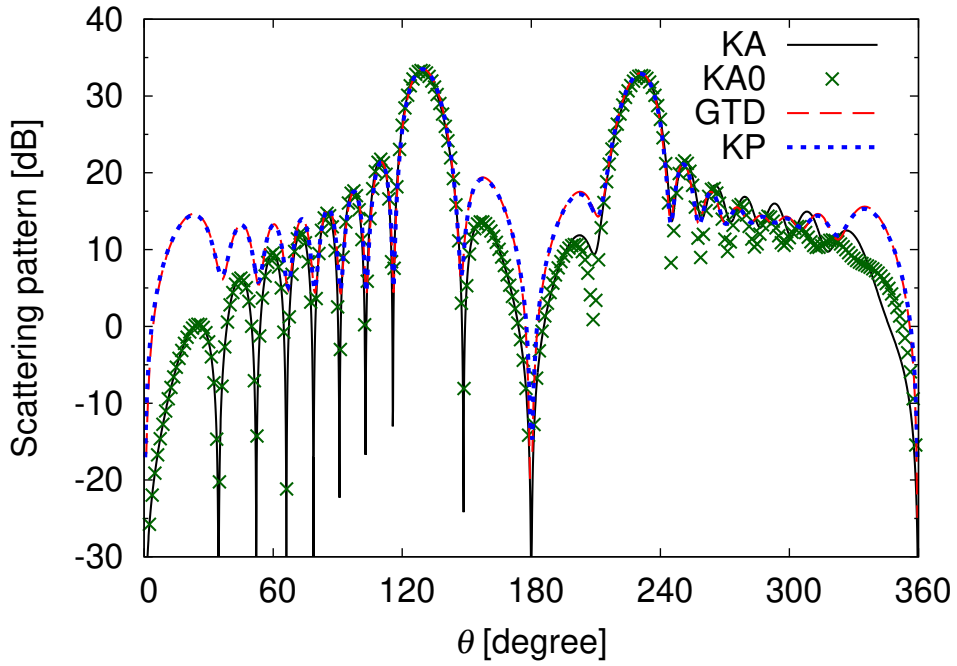

Figure 2.34: Far-field scattering pattern comparison in dB of KA, KP and GTD methods of empty slit. E polarization. $ka = 30$, $kb = 2$, $\theta_0 = 50°$.

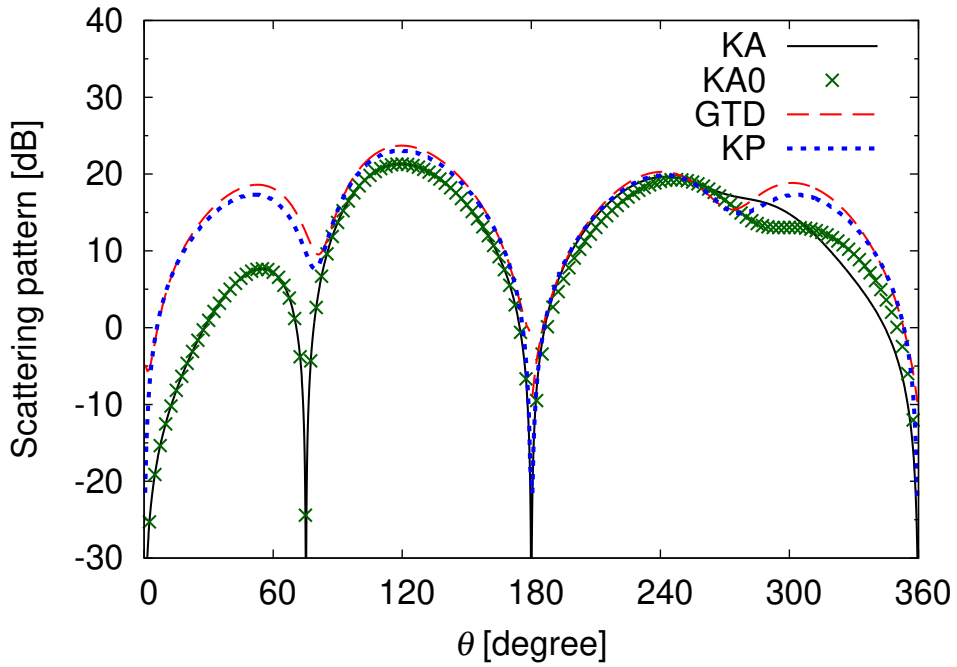

Figure 2.35: Far-field scattering pattern comparison in dB of KA, KP and GTD methods of empty slit. E polarization. $ka = 7$, $kb = 2$, $\theta_0 = 50°$.

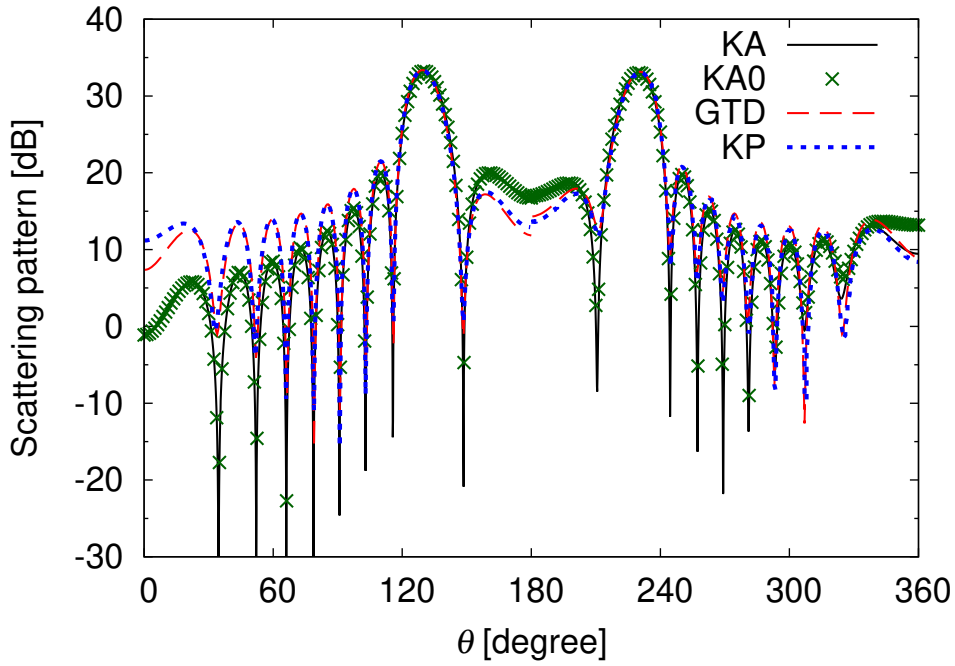

Figure 2.36: Far-field scattering pattern comparison in dB of KA, KP and GTD methods of empty slit. H polarization. $ka = 30$, $kb = 2$, $\theta_0 = 50°$.

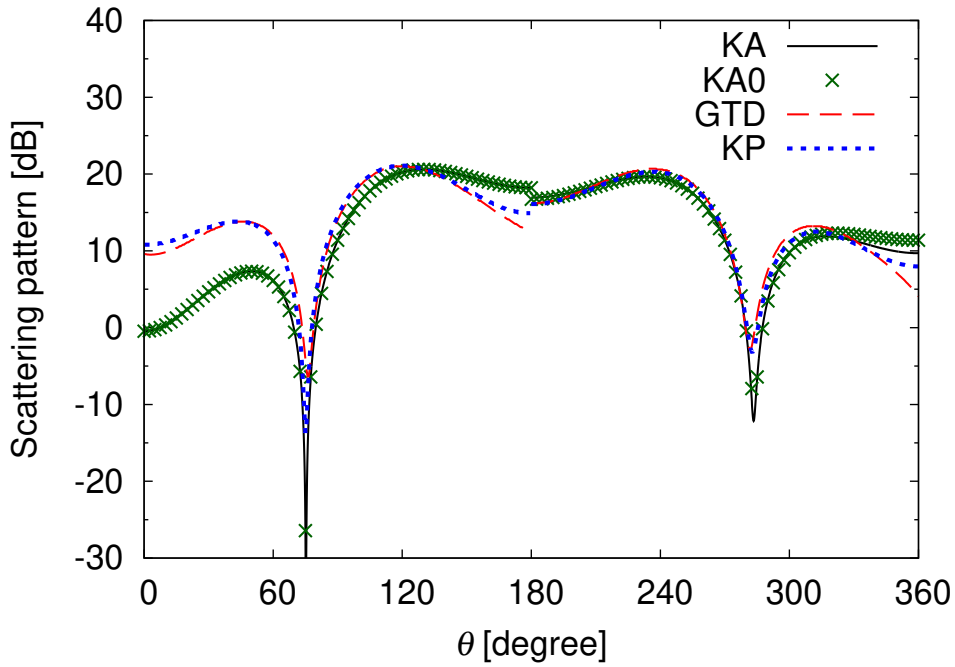

Figure 2.37: Far-field scattering pattern comparison in dB of KA, KP and GTD methods of empty slit. H polarization. $ka = 7$, $kb = 2$, $\theta_0 = 50°$.

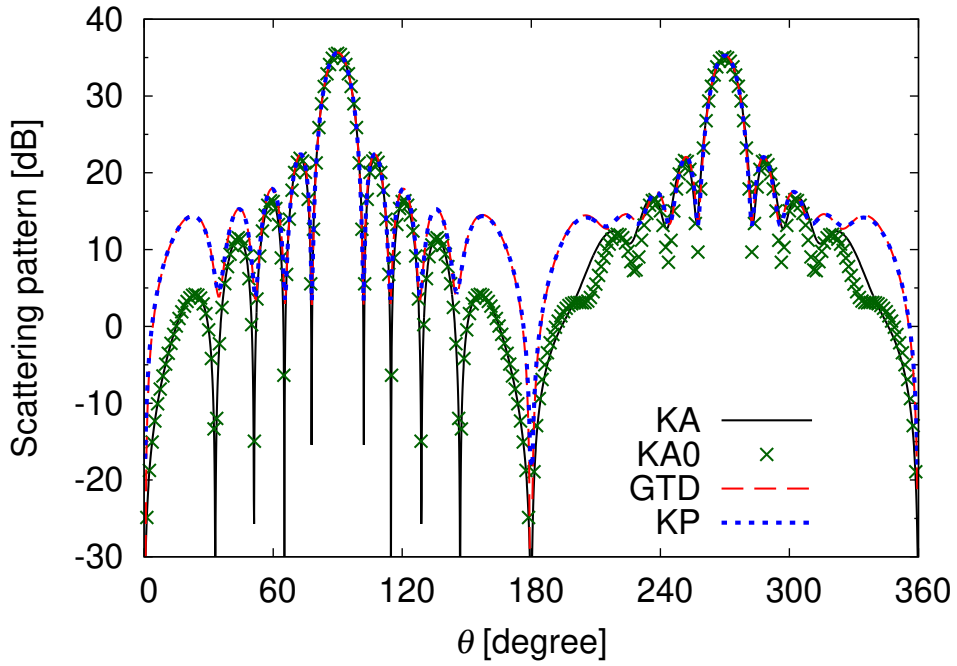

Figure 2.38: Far-field scattering pattern comparison in dB of KA, KP and GTD methods of empty slit. E polarization. $ka = 30$, $kb = 2$, $\theta_0 = 90°$.

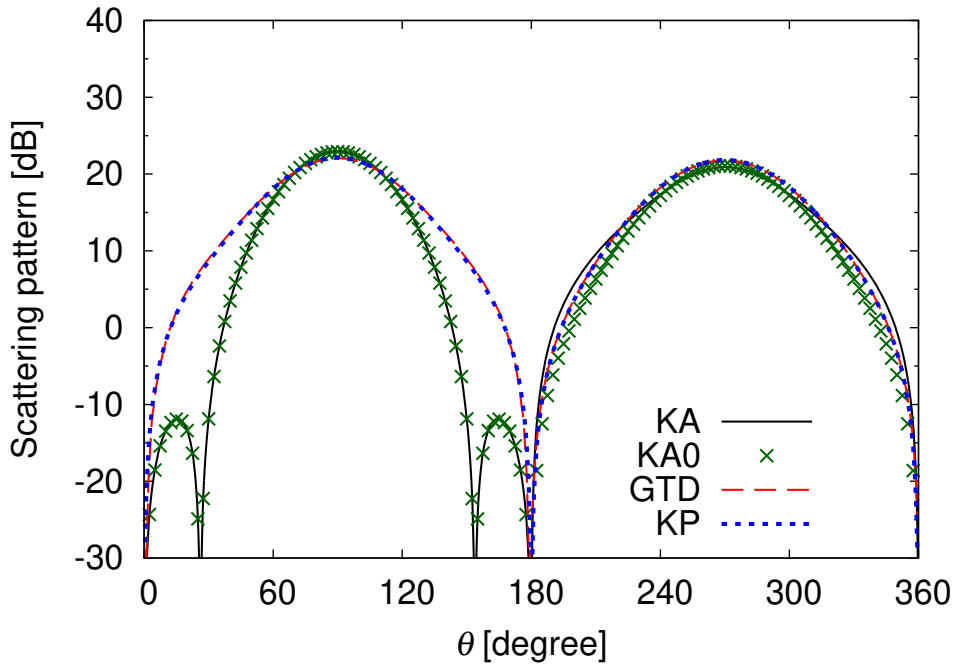

Figure 2.39: Far-field scattering pattern comparison in dB of KA, KP and GTD methods of empty slit. E polarization. $ka = 7$, $kb = 2$, $\theta_0 = 90°$.

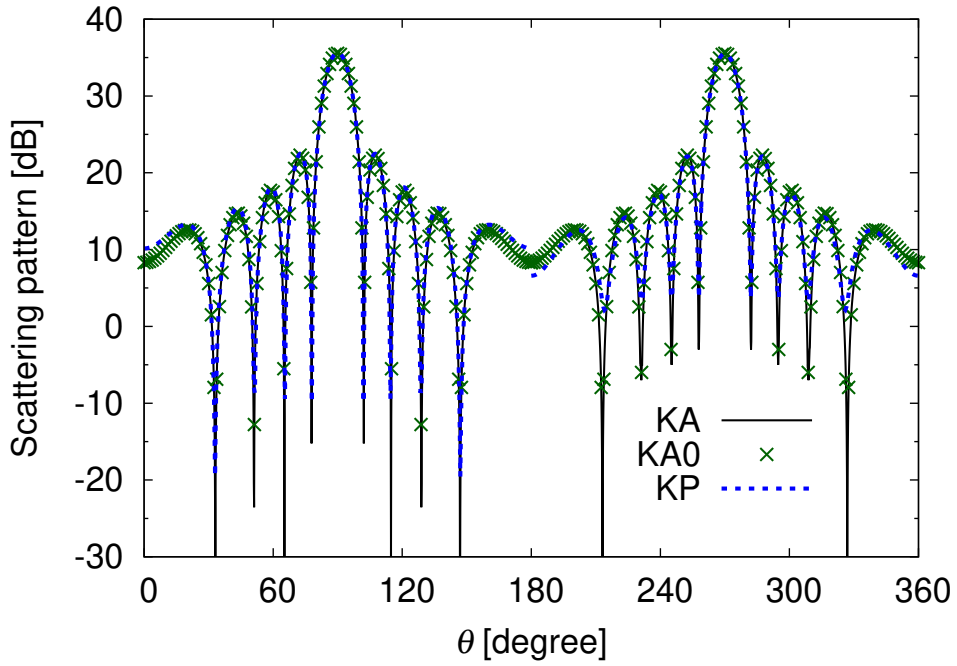

Figure 2.40: Far-field scattering pattern comparison in dB of KA, KP and GTD methods of empty slit. H polarization. $ka = 30$, $kb = 2$, $\theta_0 = 90°$.

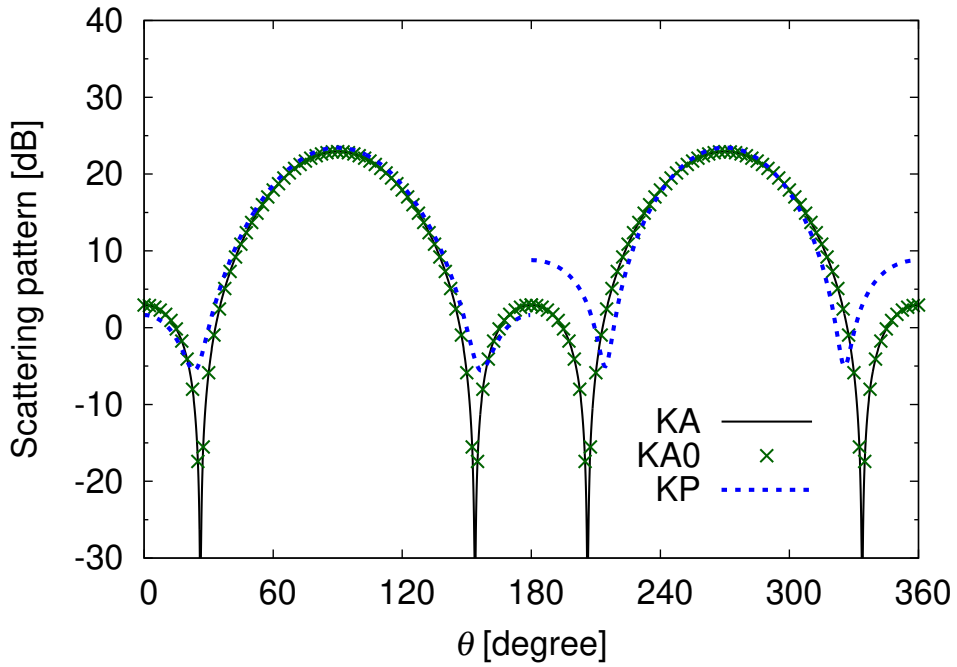

Figure 2.41: Far-field scattering pattern comparison in dB of KA, KP and GTD methods of empty slit. H polarization. $ka = 7$, $kb = 2$, $\theta_0 = 90°$.

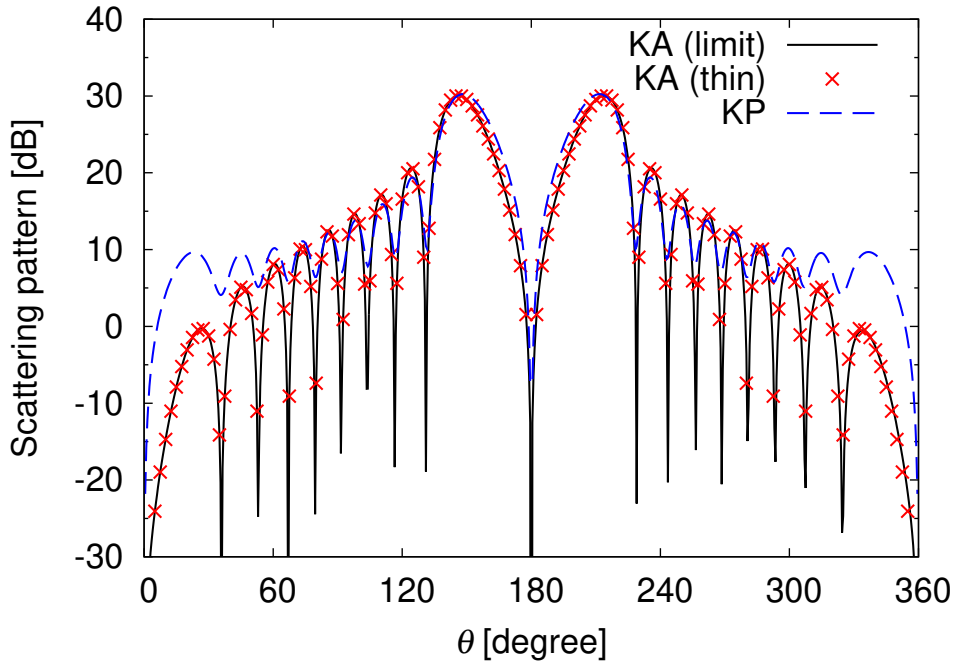

Figure 2.42: Far-field scattering pattern comparison in thin slit case. E polarization. $ka = 30$, $kb \to 0$, $\theta_0 = 30°$.

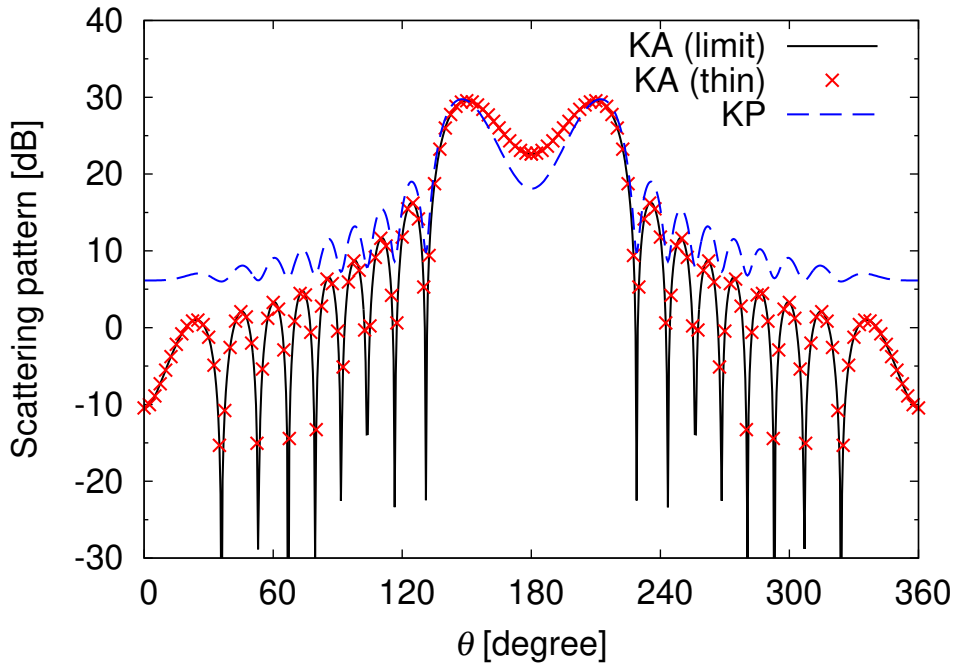

Figure 2.43: Far-field scattering pattern comparison in thin slit case. H polarization. $ka = 30$, $kb \to 0$, $\theta_0 = 30°$.

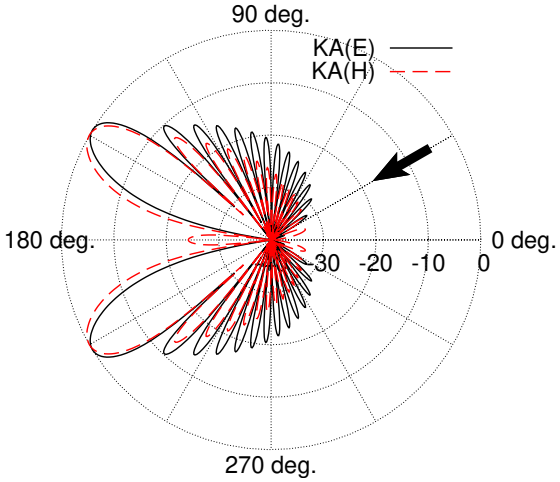

(a)

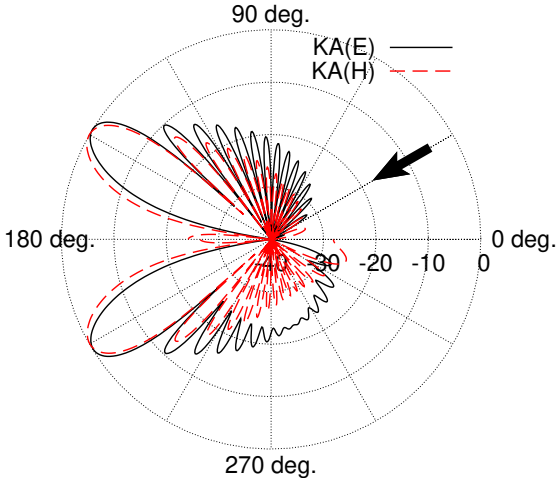

(b)

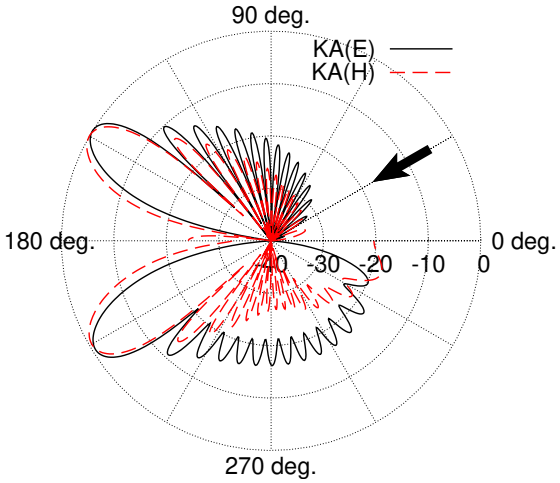

(c)

Figure 2.44: Normalized far-field scattering pattern change from thin slits in dB. $\theta_0 = 30°$, $ka = 50$. (a) $kb = 0$. (b) $kb = 1.0$. (c) $kb = 2.5$.

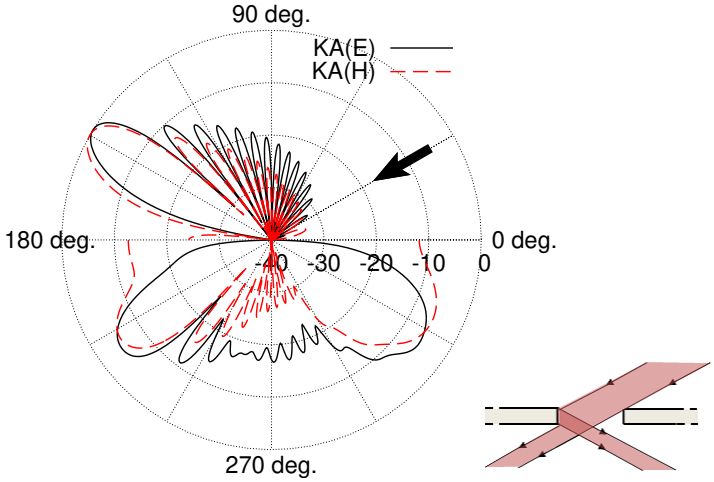

(a)

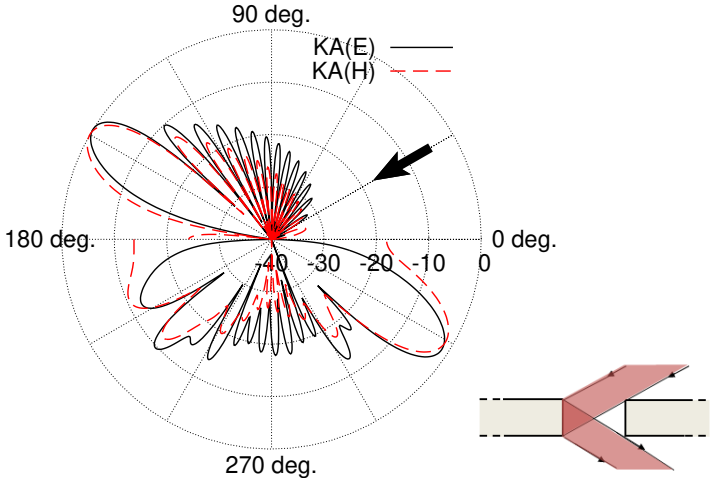

(b)

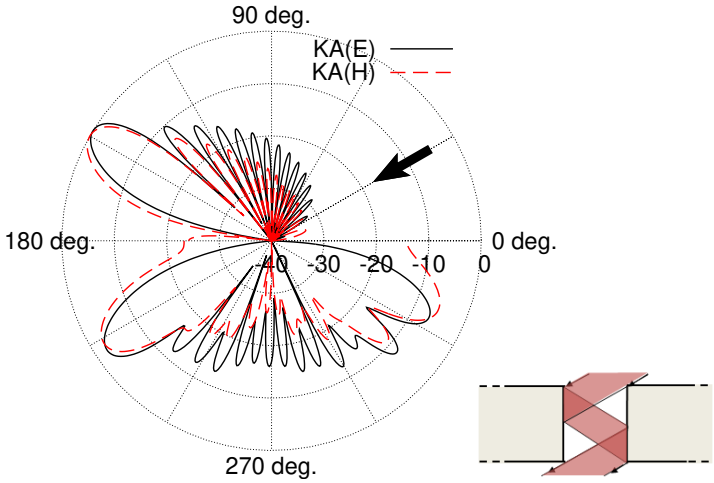

(c)

Figure 2.45: Normalized far-field scattering pattern change from thick empty slits in dB. $\theta_0 = 30°$, $ka = 50$. (a) $kb = 25/\sqrt{3}$. (b) $kb = 50/\sqrt{3}$. (c) $kb = 100/\sqrt{3}$.

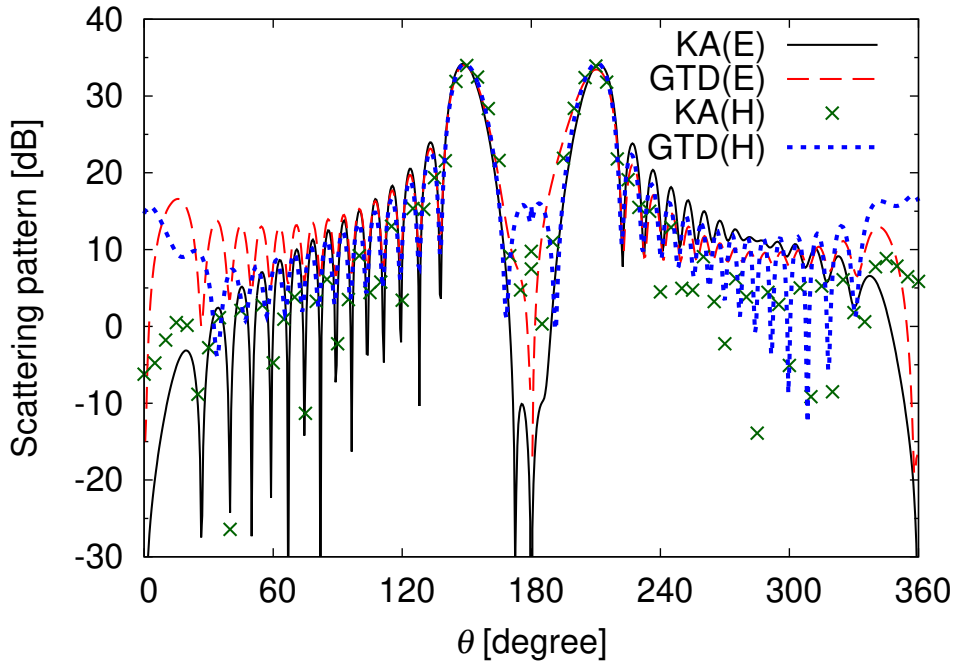

Figure 2.46: Far-field scattering pattern comparison of KA and GTD methods in thick slit case. $ka = 50$, $kb = 50/\sqrt{3}$, $\theta_0 = 30°$.

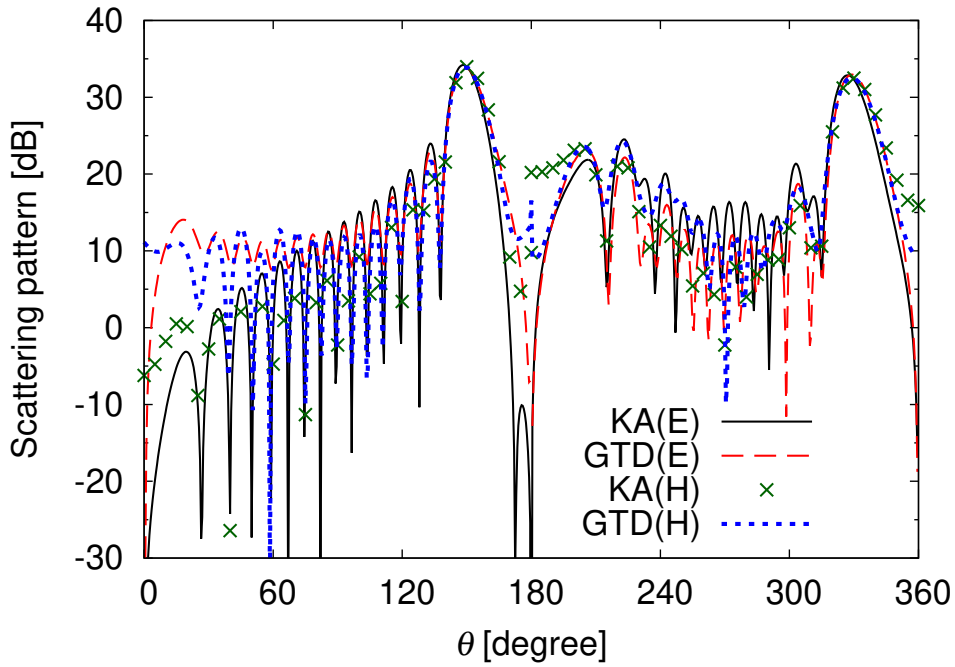

Figure 2.47: Far-field scattering pattern comparison of KA and GTD methods in thin slit case. $ka = 50$, $kb = 1$, $\theta_0 = 30°$.

Chapter 3

Analysis of Plane Wave Scattering by Rectangular Hole in a Thick Conducting Screen

In this chapter, KA method has been extended to solve plane wave scattering problem by a rectangular hole in a thick conducting screen. The scattering field can be resulted from the radiation from equivalent magnetic current sources assumed on the aperture of the hole. Equivalent magnetic currents are also applied to formulate the fields penetrating inside the hole and the subsequent transmitted field to the lower half-space. Both E and H polarized incident plane wave have been formulated, and formulation of a special case of infinite screen has been derived. The formulas derived in Sect. 3.1 and 3.2 are used to obtain some numerical results for the far-field scattering patterns in Sect. 3.4. The KA method results have been compared with those of KP method for validation. Sect. 3.3 shows the relation between three-dimensional and two-dimensional scattering formulation.

Figure 3.1 shows a plane wave impinging upon a rectangular hole perforated on a thick conducting screen. The length, width and thickness parameters of the hole are a, b and c, respectively. Spherical coordinate system has been used where

$$\hat{\boldsymbol{r}} = \sin\theta\cos\phi\ \hat{\boldsymbol{x}} + \sin\theta\sin\phi\ \hat{\boldsymbol{y}} + \cos\theta\ \hat{\boldsymbol{z}}, \tag{3.1}$$

$$\hat{\boldsymbol{\theta}} = \cos\theta\cos\phi\ \hat{\boldsymbol{x}} + \cos\theta\sin\phi\ \hat{\boldsymbol{y}} - \sin\theta\ \hat{\boldsymbol{z}}, \tag{3.2}$$

$$\hat{\boldsymbol{\phi}} = -\sin\phi\ \hat{\boldsymbol{x}} + \cos\phi\ \hat{\boldsymbol{y}}. \tag{3.3}$$

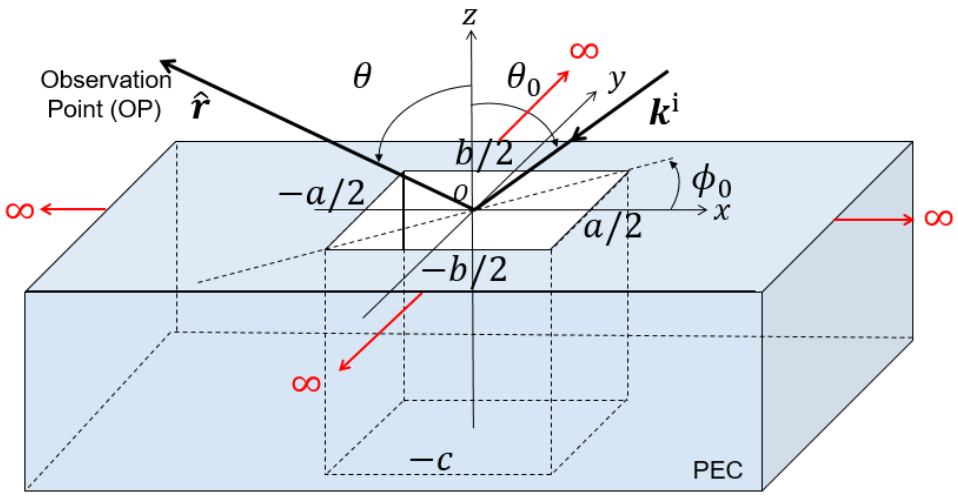

Figure 3.1: Plane wave scattering by a rectangular hole in a thick conducting screen. (θ_0,ϕ_0) denote the angles of incidence.

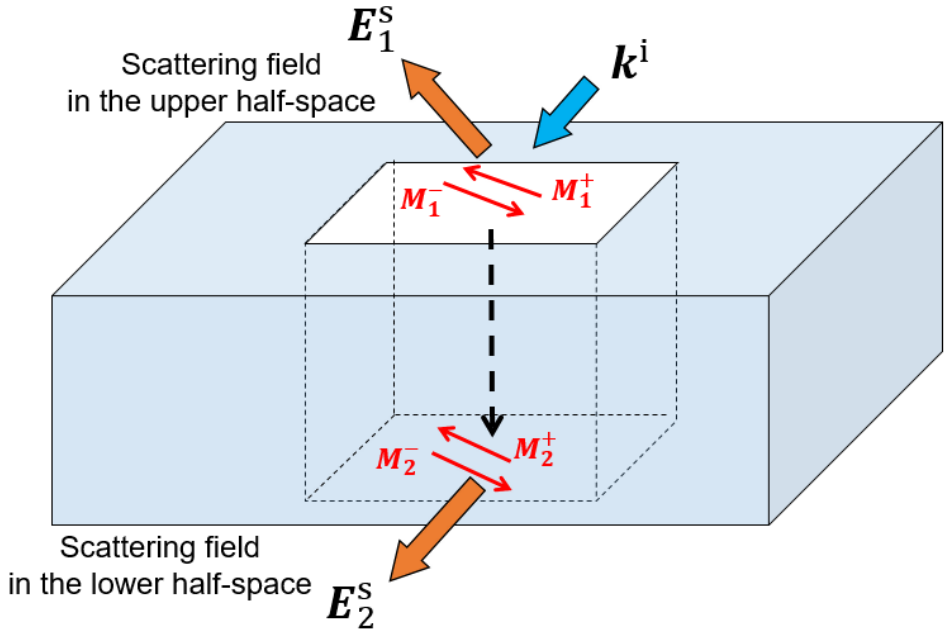

Figure 3.2: Scattering field at upper and lower regions of the hole (radiation from the equivalent magnetic current sources at the hole apertures).

The arbitrary incident plane wave may be decomposed into the transverse electric (TE) and the transverse magnetic (TM) components with respect to the incident plane as

$$\boldsymbol{E}^{\mathrm{i}} = (E^{\mathrm{TM}}\hat{\boldsymbol{\theta}}_0 + E^{\mathrm{TE}}\hat{\boldsymbol{\phi}}_0)e^{i\boldsymbol{k}^{\mathrm{i}}\cdot\boldsymbol{r}}, \tag{3.4}$$

$$\boldsymbol{H}^{\mathrm{i}} = \sqrt{\frac{\varepsilon_0}{\mu_0}}(-E^{\mathrm{TM}}\hat{\boldsymbol{\phi}}_0 + E^{\mathrm{TE}}\hat{\boldsymbol{\theta}}_0)e^{i\boldsymbol{k}^{\mathrm{i}}\cdot\boldsymbol{r}}, \tag{3.5}$$

where '$\hat{}$' denotes the corresponding unit vector,

$$\boldsymbol{k}^{\mathrm{i}} = -k\sin\theta_0\cos\phi_0\ \hat{\boldsymbol{x}} - k\sin\theta_0\sin\phi_0\ \hat{\boldsymbol{y}} - k\cos\theta_0\ \hat{\boldsymbol{z}}, \tag{3.6}$$

$$\boldsymbol{r} = x\ \hat{\boldsymbol{x}} + y\ \hat{\boldsymbol{y}} + z\ \hat{\boldsymbol{z}}, \tag{3.7}$$

(with $|\boldsymbol{k}^{\mathrm{i}}| = k = \omega\sqrt{\varepsilon_0\mu_0}$), $\boldsymbol{r}$, ε_0 and μ_0 represent the free space incident wave number vector, the position vector to the observation point, the free space permittivity, and permeability, respectively. These TE and TM polarizations are independently analyze in the following derivation.

Accordingy, the KA formulation allows scattering field to be derived from radiations from the equivalent magnetic current sources exist on the closing apertures, as shown in Fig. 3.2. There is a reflected field on the upper half-space ($z > 0$) due to the reflection from the screen's surface $z = 0$. This contribution will be omitted in the following diffraction analysis.

3.1 E Polarization

When the TE polarized plane wave of a unit amplitude illuminates, Eqs. (3.4) and (3.5) become

$$\boldsymbol{E}^{\mathrm{i}} = \hat{\boldsymbol{\phi}}_0 e^{i\boldsymbol{k}^{\mathrm{i}}\cdot\boldsymbol{r}}, \tag{3.8}$$

$$\boldsymbol{H}^{\mathrm{i}} = \sqrt{\frac{\varepsilon_0}{\mu_0}}\hat{\boldsymbol{\theta}}_0 e^{i\boldsymbol{k}^{\mathrm{i}}\cdot\boldsymbol{r}}, \tag{3.9}$$

In the KA derivation, the equivalent magnetic current sources $\boldsymbol{M}_1^{\pm}$ exist on the closing upper aperture ($z = 0$). The equivalent magnetic currents $\boldsymbol{M}_1^{\pm}$ may be given with the wave number $\boldsymbol{k}^{\mathrm{i}}$ as

$$\begin{aligned}\boldsymbol{M}_1^{\pm}(x, y, z = 0_{\pm}) =& \boldsymbol{E}^{\mathrm{i}}\big|_{z=0_{\pm}} \times (\pm\hat{\boldsymbol{z}}) = e^{i\boldsymbol{k}^{\mathrm{i}}\cdot\boldsymbol{r}}\hat{\boldsymbol{\phi}}_0\big|_{z=0_{\pm}} \times (\pm\hat{\boldsymbol{z}}) \\ =& \pm e^{-ik(x\sin\theta_0\cos\phi_0 + y\sin\theta_0\sin\phi_0)}(\cos\phi_0\ \hat{\boldsymbol{x}} + \sin\phi_0\ \hat{\boldsymbol{y}}), \\ & \left(|x| < \frac{a}{2}, |y| < \frac{b}{2}, z = 0_{\pm}\right).\end{aligned} \tag{3.10}$$

3.1.1 Scattering Far-field in Incoming Region ($z > 0$)

The upper scattering field $\boldsymbol{E}_1^{\mathrm{s}}$ resulted from the above equivalent magnetic current $\boldsymbol{M}_1^+$may be obtained from a vector potential $\boldsymbol{F}_1$ as [36]

$$\boldsymbol{E}_1^{\mathrm{s}} = -\frac{1}{\varepsilon_0}\nabla \times \boldsymbol{F}_1. \tag{3.11}$$

Vector potential $\boldsymbol{F}_1$ can be expressed in terms of equivalent magnetic current $\boldsymbol{M}_1^+(\boldsymbol{r'})$ by:

$$\boldsymbol{F}_1 = \frac{\varepsilon_0}{2\pi}\int_{S'} \boldsymbol{M}_1^+(\boldsymbol{r'})\frac{e^{ik|\boldsymbol{r}-\boldsymbol{r'}|}}{|\boldsymbol{r}-\boldsymbol{r'}|}dS'. \tag{3.12}$$

Considering the far-field derivation, the vector potential $\boldsymbol{F}_1$ due to the magnetic source can be approximately given as

$$\boldsymbol{F}_1 \sim \varepsilon_0 G\int_{S'} \boldsymbol{M}_1^+(\boldsymbol{r'})e^{-ik\boldsymbol{r'}\cdot\hat{\boldsymbol{r}}}dS' = \varepsilon_0 G\boldsymbol{D}_1(\theta,\phi), \tag{3.13}$$

where

$$\boldsymbol{D}_1(\theta,\phi) = \int_{S'} \boldsymbol{M}_1^+(\boldsymbol{r'})e^{-ik(x'\sin\theta\cos\phi+y'\sin\theta\sin\phi+z'\cos\theta)}dS', \tag{3.14}$$

and G is three-dimensional half-space Green's function:

$$G = \frac{e^{ikr}}{2\pi r}. \tag{3.15}$$

Then

$$\begin{aligned}\boldsymbol{F}_1 &\sim \frac{\varepsilon_0 e^{ikr}}{2\pi r}\int_{S'} \boldsymbol{M}_1^+(\boldsymbol{r'})e^{-ik\boldsymbol{r'}\cdot\hat{\boldsymbol{r}}}dS' \\ &= \frac{\varepsilon_0 e^{ikr}}{2\pi r}\int_{S'} \boldsymbol{M}_1^+(\boldsymbol{r'})e^{-ik(x'\sin\theta\cos\phi+y'\sin\theta\sin\phi)}dS',\end{aligned} \tag{3.16}$$

where

$$\boldsymbol{r'} = x'\ \hat{\boldsymbol{x}} + y'\ \hat{\boldsymbol{y}} + z'\ \hat{\boldsymbol{z}}, \tag{3.17}$$

$$\hat{\boldsymbol{r}} = \sin\theta\cos\phi\ \hat{\boldsymbol{x}} + \sin\theta\sin\phi\ \hat{\boldsymbol{y}} + \cos\theta\ \hat{\boldsymbol{z}}, \tag{3.18}$$

and S' denotes the hole aperture ($|x'| < a/2$, $|y'| < b/2$, $z' = 0_+$) where the equivalent magnetic current source $\boldsymbol{M}_1^+$ expressed in Eq. (3.10) exists. $\boldsymbol{r'}$ is the position vector to the aperture source point $(x', y', z' = 0)$ on S', and $\hat{\boldsymbol{r}}$ is the unit vector directed to the observation point. The vector potential $\boldsymbol{F}_1$ can be derived by analytically executing the integral in Eq. (3.16). Substituting $\boldsymbol{F}_1$ into Eq. (3.11), omitting the terms of r^{-2} due

to far-field consideration, one obtains the upper scattering field $\boldsymbol{E}_1^{\mathrm{s}}$. First, we derive $\boldsymbol{D}_1$ in Eq. (3.14). For the far reflection field calculation, we only consider the source on the upper side of the conducting plate. From Eq. (3.10),

$$\begin{aligned} M_{1x}^{+}e^{-ik(x'\sin\theta\cos\phi+y'\sin\theta\sin\phi)} &= \cos\phi_0 e^{-ik\{x'(\sin\theta_0\cos\phi_0+\sin\theta\cos\phi)+y'(\sin\theta_0\sin\phi_0+\sin\theta\sin\phi)\}} \\ &= \cos\phi_0 e^{-ik(x'\alpha+y'\beta)}, \end{aligned} \tag{3.19}$$

$$\begin{aligned} M_{1y}^{+}e^{-ik(x'\sin\theta\cos\phi+y'\sin\theta\sin\phi)} &= \sin\phi_0 e^{-ik\{x'(\sin\theta_0\cos\phi_0+\sin\theta\cos\phi)+y'(\sin\theta_0\sin\phi_0+\sin\theta\sin\phi)\}} \\ &= \sin\phi_0 e^{-ik(x'\alpha+y'\beta)}, \end{aligned} \tag{3.20}$$

where:

$$\alpha = \sin\theta_0\cos\phi_0 + \sin\theta\cos\phi, \tag{3.21}$$

$$\beta = \sin\theta_0\sin\phi_0 + \sin\theta\sin\phi. \tag{3.22}$$

x and y components of $\boldsymbol{D}_1$ are respectively:

$$\begin{aligned} D_{1x} &= \int_{-b/2}^{b/2}\int_{-a/2}^{a/2} M_{1x}^{+}e^{-ik(x'\sin\theta\cos\phi+y'\sin\theta\sin\phi)}dx'dy' \\ &= \cos\phi_0\int_{-b/2}^{b/2}\int_{-a/2}^{a/2} e^{-ik(x'\alpha+y'\beta)}dx'dy' \\ &= \frac{\cos\phi_0}{ik\alpha}\int_{-b/2}^{b/2}(e^{ik(a\alpha/2-y'\beta)} - e^{-ik(a\alpha/2)+y'\beta})dy' \\ &= -\frac{\cos\phi_0}{k^2\alpha\beta}\left\{e^{ik(a\alpha/2+b\beta/2\beta)} + e^{-ik(a\alpha/2+b\beta/2)} - e^{ik(a\alpha/2-b\beta/2\beta)} - e^{-ik(a\alpha/2-b\beta/2)}\right\} \\ &= -\frac{2\cos\phi_0}{k^2\alpha\beta}\left[\cos\left\{k\left(\frac{a}{2}\alpha+\frac{b}{2}\beta\right)\right\} - \cos\left\{k\left(\frac{a}{2}\alpha-\frac{b}{2}\beta\right)\right\}\right] \\ &= \frac{4\cos\phi_0}{k^2\alpha\beta}\sin\left(\frac{ka}{2}\alpha\right)\sin\left(\frac{kb}{2}\beta\right), \end{aligned} \tag{3.23}$$

$$D_{1y} = \frac{4\sin\phi_0}{k^2\alpha\beta}\sin\left(\frac{ka}{2}\alpha\right)\sin\left(\frac{kb}{2}\beta\right), \tag{3.24}$$

where from Eq. (3.13), we derive the components of vector potential $\boldsymbol{F}_1$ in the sphere coordinates (r,θ,ϕ)

$$\begin{aligned} F_{1r} &= F_{1x}\sin\theta\cos\phi + F_{1y}\sin\theta\sin\phi \\ &= \varepsilon_0 G(D_{1x}\sin\theta\cos\phi + D_{1y}\sin\theta\sin\phi), \end{aligned} \tag{3.25}$$

$$\begin{aligned} F_{1\theta} &= F_{1x}\cos\theta\cos\phi + F_{1y}\cos\theta\sin\phi \\ &= \varepsilon_0 G(D_{1x}\cos\theta\cos\phi + D_{1y}\cos\theta\sin\phi), \end{aligned} \tag{3.26}$$

$$\begin{aligned} F_{1\phi} &= -F_{1x}\sin\phi + F_{1y}\cos\phi \\ &= \varepsilon_0 G(-D_{1x}\sin\phi + D_{1y}\cos\phi). \end{aligned} \tag{3.27}$$

Then

$$F_{1r} = \frac{2\varepsilon_0}{\pi k^2 r\alpha\beta}\sin\theta\cos(\phi_0-\phi)\sin\left(\frac{ka}{2}\alpha\right)\sin\left(\frac{kb}{2}\beta\right)e^{ikr}, \tag{3.28}$$

$$F_{\theta} = \frac{2\varepsilon_0}{\pi k^2 r\alpha\beta}\cos\theta\cos(\phi_0-\phi)\sin\left(\frac{ka}{2}\alpha\right)\sin\left(\frac{kb}{2}\beta\right)e^{ikr}, \tag{3.29}$$

$$F_{\phi} = \frac{2\varepsilon_0}{\pi k^2 r\alpha\beta}\sin(\phi_0-\phi)\sin\left(\frac{ka}{2}\alpha\right)\sin\left(\frac{kb}{2}\beta\right)e^{ikr}. \tag{3.30}$$

Assuming the observation point is sufficiently far away, we ignore the terms of r^{-2}, then we derive

$$\begin{aligned}\boldsymbol{\nabla}\times\boldsymbol{F}_1 =& \frac{1}{r\sin\theta}\left\{\frac{\partial(F_{1\phi}\sin\theta)}{\partial\theta}-\frac{\partial F_{1\theta}}{\partial\phi}\right\}\hat{\boldsymbol{r}}+\frac{1}{r}\left\{\frac{1}{\sin\theta}\frac{\partial F_{1r}}{\partial\phi}-\frac{\partial(rF_{1\phi})}{\partial r}\right\}\hat{\boldsymbol{\theta}}\\ &+\frac{1}{r}\left\{\frac{\partial(rF_{1\theta})}{\partial r}-\frac{\partial F_{1r}}{\partial\theta}\right\}\hat{\boldsymbol{\phi}}\\ \sim& -\frac{1}{r}\frac{\partial(rF_{1\phi})}{\partial r}\hat{\boldsymbol{\theta}}+\frac{1}{r}\frac{\partial(rF_{1\theta})}{\partial r}\hat{\boldsymbol{\phi}}.\end{aligned} \tag{3.31}$$

From Eqs. (3.11) and (3.31) we derive electric far field components caused by the source at the upper side of the conducting plate

$$\begin{aligned}E_{1r} \sim& 0,\\ E_{1\theta} \sim& \frac{2i}{\pi kr\alpha\beta}e^{ikr}\sin(\phi_0-\phi)\sin\left(\frac{ka}{2}\alpha\right)\sin\left(\frac{kb}{2}\beta\right)\\ =& \frac{2i\sin(\phi_0-\phi)e^{ikr}}{\pi kr}\frac{\sin\{ka(\sin\theta_0\cos\phi_0+\sin\theta\cos\phi)/2\}}{\sin\theta_0\cos\phi_0+\sin\theta\cos\phi}\\ &\cdot\frac{\sin\{kb(\sin\theta_0\sin\phi_0+\sin\theta\sin\phi)/2\}}{\sin\theta_0\sin\phi_0+\sin\theta\sin\phi},\end{aligned} \tag{3.32}$$

$$\begin{aligned}E_{1\phi} \sim& -\frac{2i}{\pi kr\alpha\beta}e^{ikr}\cos\theta\cos(\phi_0-\phi)\sin\left(\frac{ka}{2}\alpha\right)\sin\left(\frac{kb}{2}\beta\right)\\ =& -\frac{2i\cos\theta\cos(\phi_0-\phi)e^{ikr}}{\pi kr}\frac{\sin\{ka(\sin\theta_0\cos\phi_0+\sin\theta\cos\phi)/2\}}{\sin\theta_0\cos\phi_0+\sin\theta\cos\phi}\\ &\cdot\frac{\sin\{kb(\sin\theta_0\sin\phi_0+\sin\theta\sin\phi)/2\}}{\sin\theta_0\sin\phi_0+\sin\theta\sin\phi},\end{aligned} \tag{3.33}$$

or

$$E_{1r}^{\mathrm{s}} \sim 0, \tag{3.34}$$

$$E_{1\theta}^{\mathrm{s}} \sim \frac{2i\sin(\phi_0-\phi)e^{ikr}}{\pi kr}A, \tag{3.35}$$

$$E_{1\phi}^{\mathrm{s}} \sim -\frac{2i\cos\theta\cos(\phi_0-\phi)e^{ikr}}{\pi kr}A, \tag{3.36}$$

$$\begin{aligned} A =& \frac{\sin\{ka(\sin\theta_0\cos\phi_0+\sin\theta\cos\phi)/2\}}{\sin\theta_0\cos\phi_0+\sin\theta\cos\phi} \\ & \cdot \frac{\sin\{kb(\sin\theta_0\sin\phi_0+\sin\theta\sin\phi)/2\}}{\sin\theta_0\sin\phi_0+\sin\theta\sin\phi}. \end{aligned} \tag{3.37}$$

The corresponding magnetic scattering field $\boldsymbol{H}^s$ can be found by the following relationship

$$H_\phi = \sqrt{\frac{\varepsilon_0}{\mu_0}}E_\theta, \tag{3.38}$$

$$H_\theta = -\sqrt{\frac{\varepsilon_0}{\mu_0}}E_\phi. \tag{3.39}$$

3.1.2 Electromagnetic Field in Hole Region ($-c < z < 0$)

The proposed model of rectangular hole in a thick conducting screen can be considered as a three-dimensional rectangular waveguide. Consequently, one can formulate the electromagnetic field inside the hole region as the fields propagate inside the waveguide region. If we assume a pair of electric dipole current $\boldsymbol{J}$ and magnetic dipole current $\boldsymbol{M}$ at the apertures, we can derive the electromagnetic field inside the waveguide (not at the aperture) caused by that source by using Hertz vectors [37]:

$$\boldsymbol{E}(\boldsymbol{r},\boldsymbol{r'}) = \nabla\times\nabla\times\hat{\boldsymbol{z}}\Pi'(\boldsymbol{r},\boldsymbol{r'}) + i\omega\mu\nabla\times\hat{\boldsymbol{z}}\Pi''(\boldsymbol{r},\boldsymbol{r'}), \tag{3.40}$$

$$\boldsymbol{H}(\boldsymbol{r},\boldsymbol{r'}) = -i\omega\mu\nabla\times\hat{\boldsymbol{z}}\Pi'(\boldsymbol{r},\boldsymbol{r'}) + \nabla\times\nabla\times\hat{\boldsymbol{z}}\Pi''(\boldsymbol{r},\boldsymbol{r'}), \tag{3.41}$$

where Π', Π'' are called Herts vectors, expressed by scalar potentials $\mathcal{S}', \mathcal{S}''$ and wave source $\boldsymbol{J}\delta(\boldsymbol{r}-\boldsymbol{r'}), \boldsymbol{M}\delta(\boldsymbol{r}-\boldsymbol{r'})$

$$\Pi'(\boldsymbol{r},\boldsymbol{r'}) = \frac{-1}{i\omega\varepsilon}\boldsymbol{J}\cdot\nabla'\times\nabla'\times\hat{\boldsymbol{z}}\mathcal{S}'(\boldsymbol{r},\boldsymbol{r'}) - \boldsymbol{M}\cdot\nabla'\times\hat{\boldsymbol{z}}\mathcal{S}'(\boldsymbol{r},\boldsymbol{r'}), \tag{3.42}$$

$$\Pi''(\boldsymbol{r},\boldsymbol{r'}) = \boldsymbol{J}\cdot\nabla'\times\hat{\boldsymbol{z}}\mathcal{S}''(\boldsymbol{r},\boldsymbol{r'}) + \frac{-1}{i\omega\mu}\boldsymbol{M}\cdot\nabla'\times\nabla'\times\hat{\boldsymbol{z}}\mathcal{S}''(\boldsymbol{r},\boldsymbol{r'}), \tag{3.43}$$

where ∇', ∇ are operators applied for coordinate (x', y', z') and (x, y, z), respectively. If we assume that there are electric and magnetic sources inside the waveguide $\boldsymbol{J}(x', y') =$

$J_x(x',y')\hat{\boldsymbol{x}} + J_y(x',y')\hat{\boldsymbol{y}}, \boldsymbol{M}(x',y') = M_x\hat{\boldsymbol{x}} + M_y\hat{\boldsymbol{y}}$, we can derive

$$\Pi'(\boldsymbol{r},\boldsymbol{r'}) = (\frac{-1}{i\omega\varepsilon}\boldsymbol{J}(x',y')\frac{\partial}{\partial z'} + \boldsymbol{M}(x',y')\times\hat{\boldsymbol{z}})\cdot\nabla_t'\mathcal{S}'(\boldsymbol{r},\boldsymbol{r'}), \tag{3.44}$$

$$\Pi''(\boldsymbol{r},\boldsymbol{r'}) = (\hat{\boldsymbol{z}}\times\boldsymbol{J}(x',y') + \frac{-1}{i\omega\mu}\boldsymbol{M}(x',y')\frac{\partial}{\partial z'})\cdot\nabla_t'\mathcal{S}''(\boldsymbol{r},\boldsymbol{r'}). \tag{3.45}$$

In addition, using eigenmode expansion of the cross section, scalar potential $\mathcal{S}'$, $\mathcal{S}''$ can be expressed, respectively, as

$$\mathcal{S}'(\boldsymbol{r},\boldsymbol{r'}) = \sum_{m=1}^{\infty}\sum_{n=1}^{\infty}\frac{2i}{\kappa_{m,n}ab}e^{i\kappa_{m,n}|z-z'|} \cdot\frac{\sin\frac{m\pi}{a}(x+\frac{a}{2})\sin\frac{n\pi}{b}(y+\frac{b}{2})\sin\frac{m\pi}{a}(x'+\frac{a}{2})\sin\frac{n\pi}{b}(y'+\frac{b}{2})}{(\frac{m\pi}{a})^2+(\frac{n\pi}{b})^2}, \tag{3.46}$$

$$\mathcal{S}''(\boldsymbol{r},\boldsymbol{r'}) = \sum_{m=0}^{\infty}\sum_{n=0}^{\infty}\frac{\epsilon_m\epsilon_n i}{2\kappa_{m,n}ab}e^{i\kappa_{m,n}|z-z'|} \cdot\frac{\cos\frac{m\pi}{a}(x+\frac{a}{2})\cos\frac{n\pi}{b}(y+\frac{b}{2})\cos\frac{m\pi}{a}(x'+\frac{a}{2})\cos\frac{n\pi}{b}(y'+\frac{b}{2})}{(\frac{m\pi}{a})^2+(\frac{n\pi}{b})^2}, \tag{3.47}$$

where the wave number inside the hole,

$$\kappa_{m,n} = \sqrt{k^2-(\frac{m\pi}{a})^2-(\frac{n\pi}{b})^2}, \tag{3.48}$$

$$\epsilon_m = \begin{cases} 1 & (m=0) \\ 2 & (m>0). \end{cases} \tag{3.49}$$

To derive electromagnetic field expression given by Eqs. (3.40) and (3.41), one needs Hertz vectors in Eqs.(3.44) and (3.45). Those expressions can be written as:

$$\Pi' = \frac{-1}{i\omega\varepsilon}(J_x\frac{\partial(\nabla_t'\mathcal{S}')_x}{\partial z'} + J_y\frac{\partial(\nabla_t'\mathcal{S}')_y}{\partial z'}) + M_y(\nabla_t'\mathcal{S}')_x - M_x(\nabla_t'\mathcal{S}')_y, \tag{3.50}$$

$$\Pi'' = -J_y(\nabla_t'\mathcal{S}'')_x + J_x(\nabla_t'\mathcal{S}'')_y + \frac{-1}{i\omega\mu}(M_x\frac{\partial(\nabla_t'\mathcal{S}'')_x}{\partial z'} + M_y\frac{\partial(\nabla_t'\mathcal{S}'')_y}{\partial z'}). \tag{3.51}$$

According to Eqs. (3.46), (3.47), we consider the wave propagation along the z-axis negative direction. Thus, $e^{i\kappa_{m,n}|z-z'|} = e^{-i\kappa_{m,n}(z-z')}$ and

$$(\nabla_t'\mathcal{S}')_x = \sum_{m=1}^{\infty}\sum_{n=1}^{\infty}\frac{2im\pi}{\kappa_{m,n}a^2b}e^{-i\kappa_{m,n}(z-z')} \cdot\frac{\sin\frac{m\pi}{a}(x+\frac{a}{2})\sin\frac{n\pi}{b}(y+\frac{b}{2})\cos\frac{m\pi}{a}(x'+\frac{a}{2})\sin\frac{n\pi}{b}(y'+\frac{b}{2})}{(\frac{m\pi}{a})^2+(\frac{n\pi}{b})^2}, \tag{3.52}$$

$$(\nabla_t'\mathcal{S}')_y = \sum_{m=1}^{\infty}\sum_{n=1}^{\infty}\frac{2in\pi}{\kappa_{m,n}ab^2}e^{-i\kappa_{m,n}(z-z')} \cdot\frac{\sin\frac{m\pi}{a}(x+\frac{a}{2})\sin\frac{n\pi}{b}(y+\frac{b}{2})\sin\frac{m\pi}{a}(x'+\frac{a}{2})\cos\frac{n\pi}{b}(y'+\frac{b}{2})}{(\frac{m\pi}{a})^2+(\frac{n\pi}{b})^2}, \tag{3.53}$$

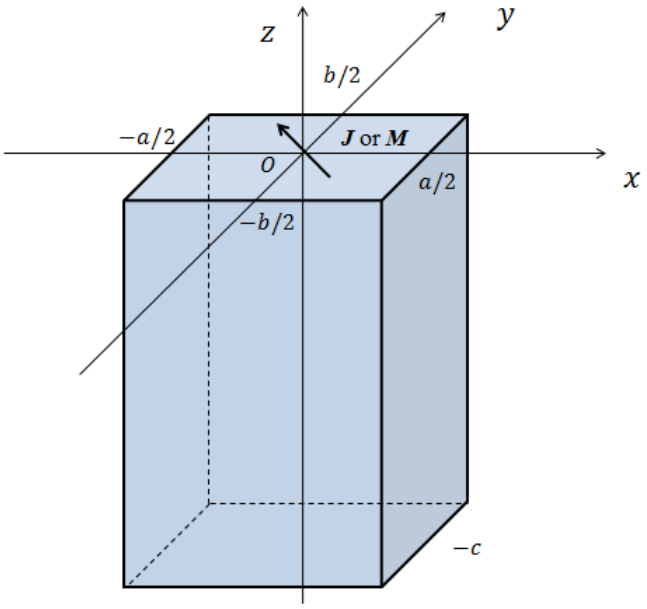

Figure 3.3: Semi-infinite rectangular waveguide with the sources on $z = 0$

$$\frac{\partial(\nabla_t' \mathcal{S}')_x}{\partial z'} = \sum_{m=1}^{\infty}\sum_{n=1}^{\infty} \frac{-2m\pi}{a^2 b} e^{-i\kappa_{m,n}(z-z')} \cdot \frac{\sin\frac{m\pi}{a}(x+\frac{a}{2})\sin\frac{n\pi}{b}(y+\frac{b}{2})\cos\frac{m\pi}{a}(x'+\frac{a}{2})\sin\frac{n\pi}{b}(y'+\frac{b}{2})}{(\frac{m\pi}{a})^2+(\frac{n\pi}{b})^2}, \quad (3.54)$$

$$\frac{\partial(\nabla_t' \mathcal{S}')_y}{\partial z'} = \sum_{m=1}^{\infty}\sum_{n=1}^{\infty} \frac{-2n\pi}{ab^2} e^{-i\kappa_{m,n}(z-z')} \cdot \frac{\sin\frac{m\pi}{a}(x+\frac{a}{2})\sin\frac{n\pi}{b}(y+\frac{b}{2})\sin\frac{m\pi}{a}(x'+\frac{a}{2})\cos\frac{n\pi}{b}(y'+\frac{b}{2})}{(\frac{m\pi}{a})^2+(\frac{n\pi}{b})^2}, \quad (3.55)$$

$$(\nabla_t' \mathcal{S}'')_x = \sum_{m=0}^{\infty}\sum_{n=0}^{\infty} \frac{-\epsilon_m\epsilon_n i m\pi}{2\kappa_{m,n} a^2 b} e^{-i\kappa_{m,n}(z-z')} \cdot \frac{\cos\frac{m\pi}{a}(x+\frac{a}{2})\cos\frac{n\pi}{b}(y+\frac{b}{2})\sin\frac{m\pi}{a}(x'+\frac{a}{2})\cos\frac{n\pi}{b}(y'+\frac{b}{2})}{(\frac{m\pi}{a})^2+(\frac{n\pi}{b})^2}, \quad (3.56)$$

$$(\nabla_t' \mathcal{S}'')_y = \sum_{m=0}^{\infty}\sum_{n=0}^{\infty} \frac{-\epsilon_m\epsilon_n i n\pi}{2\kappa_{m,n} ab^2} e^{-i\kappa_{m,n}(z-z')} \cdot \frac{\cos\frac{m\pi}{a}(x+\frac{a}{2})\cos\frac{n\pi}{b}(y+\frac{b}{2})\cos\frac{m\pi}{a}(x'+\frac{a}{2})\sin\frac{n\pi}{b}(y'+\frac{b}{2})}{(\frac{m\pi}{a})^2+(\frac{n\pi}{b})^2}, \quad (3.57)$$

$$\frac{\partial(\nabla_t' \mathcal{S}'')_x}{\partial z'} = \sum_{m=0}^{\infty}\sum_{n=0}^{\infty} \frac{\epsilon_m\epsilon_n m\pi}{2a^2 b} e^{-i\kappa_{m,n}(z-z')} \cdot \frac{\cos\frac{m\pi}{a}(x+\frac{a}{2})\cos\frac{n\pi}{b}(y+\frac{b}{2})\sin\frac{m\pi}{a}(x'+\frac{a}{2})\cos\frac{n\pi}{b}(y'+\frac{b}{2})}{(\frac{m\pi}{a})^2+(\frac{n\pi}{b})^2}, \quad (3.58)$$

$$\frac{\partial(\nabla_t'\mathcal{S}'')_y}{\partial z'} = \sum_{m=0}^{\infty}\sum_{n=0}^{\infty}\frac{\epsilon_m\epsilon_n n\pi}{2ab^2}e^{-i\kappa_{m,n}(z-z')} \cdot \frac{\cos\frac{m\pi}{a}(x+\frac{a}{2})\cos\frac{n\pi}{b}(y+\frac{b}{2})\cos\frac{m\pi}{a}(x'+\frac{a}{2})\sin\frac{n\pi}{b}(y'+\frac{b}{2})}{(\frac{m\pi}{a})^2+(\frac{n\pi}{b})^2}. \quad (3.59)$$

In Kirchhoff approximation method, we first assume that there are equivalent magnetic sources $\boldsymbol{M}_1$ only (no electric sources $\boldsymbol{J}$) at the upper aperture of the waveguide. In detail, the sources at the lower side of upper aperture $\boldsymbol{M}_1^-$ with x, y components as follow lead to the field propagating inside the waveguide.

$$\boldsymbol{M}_1^-(x',y') = M_{1x}^-\hat{\boldsymbol{x}} + M_{1y}^-\hat{\boldsymbol{y}}. \quad (3.60)$$

Substuting Eqs.(3.52)$\sim$(3.59) into Eqs. (3.50) and (3.51), one gets:

$$\Pi' = \sum_{m=1}^{\infty}\sum_{n=1}^{\infty}\bar{\alpha}\sin\frac{m\pi}{a}\left(x+\frac{a}{2}\right)\sin\frac{n\pi}{b}\left(y+\frac{b}{2}\right)e^{-i\kappa_{m,n}(z-z')}, \quad (3.61)$$

$$\bar{\alpha} = \frac{2}{ab(k^2-\kappa_{m,n}^2)}\left\{\frac{i}{\kappa_{m,n}}M_{1y}^-\frac{m\pi}{a}\cos\frac{m\pi}{a}\left(x'+\frac{a}{2}\right)\sin\frac{n\pi}{b}\left(y'+\frac{b}{2}\right) - \frac{i}{\kappa_{m,n}}M_{1x}^-\frac{n\pi}{b}\sin\frac{m\pi}{a}\left(x'+\frac{a}{2}\right)\cos\frac{n\pi}{b}\left(y'+\frac{b}{2}\right)\right\}, \quad (3.62)$$

$$\Pi'' = \sum_{m=0}^{\infty}\sum_{n=0}^{\infty}\bar{\beta}\cos\frac{m\pi}{a}\left(x+\frac{a}{2}\right)\cos\frac{n\pi}{b}\left(y+\frac{b}{2}\right)e^{-i\kappa_{m,n}(z-z')}, \quad (3.63)$$

$$\bar{\beta} = \frac{\epsilon_m\epsilon_n}{2ab(k^2-\kappa_{m,n}^2)}\left\{-\frac{1}{i\omega\mu}M_{1y}^-\frac{n\pi}{b}\cos\frac{m\pi}{a}\left(x'+\frac{a}{2}\right)\sin\frac{n\pi}{b}\left(y'+\frac{b}{2}\right) + \frac{1}{i\omega\mu}M_{1x}^-\frac{m\pi}{a}\sin\frac{m\pi}{a}\left(x'+\frac{a}{2}\right)\cos\frac{n\pi}{b}\left(y'+\frac{b}{2}\right)\right\}. \quad (3.64)$$

Besides, Eqs. (3.40) and (3.41) can be written as:

$$\boldsymbol{E} = \left(\frac{\partial}{\partial z}\frac{\partial\Pi'}{\partial x}+i\omega\mu\frac{\partial\Pi''}{\partial y}\right)\hat{\boldsymbol{x}} + \left(\frac{\partial}{\partial z}\frac{\partial\Pi'}{\partial y}-i\omega\mu\frac{\partial\Pi''}{\partial x}\right)\hat{\boldsymbol{y}} - \left(\frac{\partial^2\Pi'}{\partial x^2}+\frac{\partial^2\Pi'}{\partial y^2}\right)\hat{\boldsymbol{z}}, \quad (3.65)$$

$$\boldsymbol{H} = \left(\frac{\partial}{\partial z}\frac{\partial\Pi''}{\partial x}-i\omega\varepsilon\frac{\partial\Pi'}{\partial y}\right)\hat{\boldsymbol{x}} + \left(\frac{\partial}{\partial z}\frac{\partial\Pi''}{\partial y}+i\omega\varepsilon\frac{\partial\Pi'}{\partial x}\right)\hat{\boldsymbol{y}} - \left(\frac{\partial^2\Pi''}{\partial x^2}+\frac{\partial^2\Pi''}{\partial y^2}\right)\hat{\boldsymbol{z}}. \quad (3.66)$$

One can derive field components in z-direction:

$$\begin{aligned}
E_z =& -\left(\frac{\partial^2\Pi'}{\partial x^2}+\frac{\partial^2\Pi'}{\partial y^2}\right)\\
=& \sum_{m=1}^{\infty}\sum_{n=1}^{\infty} C_{m,n}\sin\frac{m\pi}{a}\left(x+\frac{a}{2}\right)\sin\frac{n\pi}{b}\left(y+\frac{b}{2}\right)e^{-i\kappa_{m,n}(z-z')}, \qquad (3.67)\\
C_{m,n} =& \frac{2}{abi}\Bigg\{-\frac{1}{\kappa_{m,n}}M_{1y}^{-}\frac{m\pi}{a}\cos\frac{m\pi}{a}\left(x'+\frac{a}{2}\right)\sin\frac{n\pi}{b}\left(y'+\frac{b}{2}\right)\\
&+\frac{1}{\kappa_{m,n}}M_{1x}^{-}\frac{n\pi}{b}\sin\frac{m\pi}{a}\left(x'+\frac{a}{2}\right)\cos\frac{n\pi}{b}\left(y'+\frac{b}{2}\right)\Bigg\}, \qquad (3.68)\\
H_z =& -\left(\frac{\partial^2\Pi''}{\partial x^2}+\frac{\partial^2\Pi''}{\partial y^2}\right),\\
=& \sum_{m=0}^{\infty}\sum_{n=0}^{\infty} F_{m,n}\cos\frac{m\pi}{a}\left(x+\frac{a}{2}\right)\cos\frac{n\pi}{b}\left(y+\frac{b}{2}\right)e^{-i\kappa_{m,n}(z-z')} \qquad (3.69)\\
F_{m,n} =& \frac{\epsilon_m\epsilon_n}{2abi}\Bigg\{-\frac{1}{\omega\mu}M_{1y}^{-}\frac{n\pi}{b}\cos\frac{m\pi}{a}\left(x'+\frac{a}{2}\right)\sin\frac{n\pi}{b}\left(y'+\frac{b}{2}\right)\\
&-\frac{1}{\omega\mu}M_{1x}^{-}\frac{m\pi}{a}\sin\frac{m\pi}{a}\left(x'+\frac{a}{2}\right)\cos\frac{n\pi}{b}\left(y'+\frac{b}{2}\right)\Bigg\}. \qquad (3.70)
\end{aligned}$$

If the incident wave is plane wave, then the equivalent magnetic current components at the aperture ($-a/2 < x' < a/2, -b/2 < y' < b/2, z' = 0_-$) are derived from Eq. (3.10) as

$$M_{1x}^{-} = -\cos\phi_0 e^{-ik(x'\sin\theta_0\cos\phi_0+y'\sin\theta_0\sin\phi_0)}, \qquad (3.71)$$

$$M_{1y}^{-} = -\sin\phi_0 e^{-ik(x'\sin\theta_0\cos\phi_0+y'\sin\theta_0\sin\phi_0)}. \qquad (3.72)$$

Taking the integral at the upper aperture, for our assumption, we have only the magnetic current source $\boldsymbol{M}_1$ and no electric current. Accordingly, one has to consider imaging effect of the source on the conducting surface, then we derive electromagnetic field in the waveguide from source at the upper aperture:

$$\begin{aligned}
E_z^{\mathrm{w}} =& -\left(\frac{\partial^2\Pi'}{\partial x^2}+\frac{\partial^2\Pi'}{\partial y^2}\right)\\
=& \sum_{m=1}^{\infty}\sum_{n=1}^{\infty} C_{m,n}^{\mathrm{w}}\sin\frac{m\pi}{a}\left(x+\frac{a}{2}\right)\sin\frac{n\pi}{b}\left(y+\frac{b}{2}\right)e^{-i\kappa_{m,n}(z-z')}, \qquad (3.73)
\end{aligned}$$

$$
\begin{aligned}
C^{\mathrm{w}}_{m,n} =& \int_{-a/2}^{a/2}\int_{-b/2}^{b/2} C_{mn}dx'dy' \\
=& \frac{2}{abi\kappa_{m,n}}\Bigg\{ \int_{-a/2}^{a/2} -M^{-}_{1y}\frac{m\pi}{a}\cos\frac{m\pi}{a}\left(x'+\frac{a}{2}\right)\sin\frac{n\pi}{b}\sin\left(y'+\frac{b}{2}\right) \\
&+ \int_{-b/2}^{b/2} M^{-}_{1x}\frac{n\pi}{b}\sin\frac{m\pi}{a}\left(x'+\frac{a}{2}\right)\cos\frac{n\pi}{b}\sin\left(y'+\frac{b}{2}\right)\Bigg\} \\
=& \frac{4}{abi\kappa_{m,n}} \\
&\cdot\Bigg\{ \sin\phi_0\frac{m\pi}{a}\int_{-a/2}^{a/2}\cos\frac{m\pi}{a}\left(x'+\frac{a}{2}\right)e^{-ik\sin\theta_0\cos\phi_0 x'}dx' \\
&\qquad\qquad \cdot\int_{-b/2}^{b/2}\sin\frac{n\pi}{b}\left(y'+\frac{b}{2}\right)e^{-ik\sin\theta_0\sin\phi_0 y'}dy' \\
&+(-\cos\phi_0)\frac{n\pi}{b}\int_{-a/2}^{a/2}\sin\frac{m\pi}{a}\left(x'+\frac{a}{2}\right)e^{-ik\sin\theta_0\cos\phi_0 x'}dx' \\
&\qquad\qquad \cdot\int_{-b/2}^{b/2}\cos\frac{n\pi}{b}\left(y'+\frac{b}{2}\right)e^{-ik\sin\theta_0\sin\phi_0 y'}dy'\Bigg\} \\
=& \frac{4}{abi\kappa_{m,n}} \\
&\cdot\Bigg\{ (\sin\phi_0)\frac{m\pi}{a}\frac{-ik\sin\theta_0\cos\phi_0}{(-ik\sin\theta_0\cos\phi_0)^2+(m\pi/a)^2} \\
&\cdot(e^{(-ika\sin\theta_0\cos\phi_0)/2}\cos m\pi - e^{(ika\sin\theta_0\cos\phi_0)/2}) \\
&\cdot\frac{-n\pi/b}{(-ik\sin\theta_0\sin\phi_0)^2+(n\pi/b)^2}(e^{(-ikb\sin\theta_0\sin\phi_0)/2}\cos n\pi - e^{(ikb\sin\theta_0\sin\phi_0)/2}) \\
&+(-\cos\phi_0)\frac{n\pi}{b}\frac{-m\pi/a}{(-ik\sin\theta_0\cos\phi_0)^2+(m\pi/a)^2} \\
&\cdot(e^{(-ika\sin\theta_0\cos\phi_0)/2}\cos m\pi - e^{(ika\sin\theta_0\cos\phi_0)/2}) \\
&\cdot\frac{-ik\sin\theta_0\sin\phi_0}{(-ik\sin\theta_0\sin\phi_0)^2+(n\pi/b)^2}(e^{(-ikb\sin\theta_0\sin\phi_0)/2}\cos n\pi - e^{(ikb\sin\theta_0\sin\phi_0)/2})\Bigg\} \\
=& \frac{4ik}{abi\kappa_{m,n}}\frac{\frac{m\pi}{a}\frac{n\pi}{b}}{\left\{(-ik\sin\theta_0\cos\phi_0)^2+(\frac{m\pi}{a})^2\right\}\left\{(-ik\sin\theta_0\sin\phi_0)^2+(\frac{n\pi}{b})^2\right\}} \\
&\cdot(e^{(-ika\sin\theta_0\cos\phi_0)/2}\cos m\pi - e^{(ika\sin\theta_0\cos\phi_0)/2}) \\
&\cdot(e^{(-ikb\sin\theta_0\sin\phi_0)/2}\cos n\pi - e^{(ikb\sin\theta_0\sin\phi_0)/2}) \\
&\cdot(\sin\phi_0\sin\theta_0\cos\phi_0 - \cos\phi_0\sin\theta_0\sin\phi_0) \\
=& 0. \qquad (3.74)
\end{aligned}
$$

Similarly,

$$
\begin{aligned}
H_z^{\mathrm{w}} =& -\left(\frac{\partial^2\Pi''}{\partial x^2}+\frac{\partial^2\Pi''}{\partial y^2}\right)\\
=& \sum_{m=0}^{\infty}\sum_{n=0}^{\infty} F_{m,n}^{\mathrm{w}} \cos\frac{m\pi}{a}\left(x+\frac{a}{2}\right)\cos\frac{n\pi}{b}\left(y+\frac{b}{2}\right)e^{-i\kappa_{m,n}(z)}, \qquad (3.75)\\
F_{m,n}^{\mathrm{w}} =& \int_{-a/2}^{a/2}\int_{-b/2}^{b/2} F_{mn}dx'dy'\\
=& -\frac{\epsilon_m\epsilon_n}{2abi\omega\mu}\left\{\int_{-a/2}^{a/2}\int_{-b/2}^{b/2} M_{1y}^{-}\frac{n\pi}{b}\cos\frac{m\pi}{a}\left(x'+\frac{a}{2}\right)\sin\frac{n\pi}{b}\left(y'+\frac{b}{2}\right)dx'dy'\right.\\
&\left.+\int_{-a/2}^{a/2}\int_{-b/2}^{b/2} M_{1x}^{-}\frac{m\pi}{a}\sin\frac{m\pi}{a}\left(x'+\frac{a}{2}\right)\cos\frac{n\pi}{b}\left(y'+\frac{b}{2}\right)dx'dy'\right\}\\
=& -\frac{2\epsilon_m\epsilon_n}{2abi\omega\mu}\\
&\cdot\left\{(-\sin\phi_0)\frac{n\pi}{b}\int_{-a/2}^{a/2}\cos\frac{m\pi}{a}\left(x'+\frac{a}{2}\right)e^{-ik\sin\theta_0\cos\phi_0 x'}dx'\right.\\
&\cdot\int_{-b/2}^{b/2}\sin\frac{n\pi}{b}\left(y'+\frac{b}{2}\right)e^{-ik\sin\theta_0\sin\phi_0 y'}dy'\\
&+(-\cos\phi_0)\frac{m\pi}{a}\int_{-a/2}^{a/2}\sin\frac{m\pi}{a}\left(x'+\frac{a}{2}\right)e^{-ik\sin\theta_0\cos\phi_0 x'}dx'\\
&\left.\cdot\int_{-b/2}^{b/2}\cos\frac{n\pi}{b}\left(y'+\frac{b}{2}\right)e^{-ik\sin\theta_0\sin\phi_0 y'}dy'\right\}\\
=& -\frac{2\epsilon_m\epsilon_n}{2abi\omega\mu}\left\{(-\sin\phi_0)\frac{n\pi}{b}\frac{-ik\sin\theta_0\cos\phi_0}{(-ik\sin\theta_0\cos\phi_0)^2+(m\pi/a)^2}\right.\\
&\cdot(e^{(-ika\sin\theta_0\cos\phi_0)/2}\cos m\pi-e^{(ika\sin\theta_0\cos\phi_0)/2})\\
&\cdot\frac{-n\pi/b}{(-ik\sin\theta_0\sin\phi_0)^2+(n\pi/b)^2}(e^{(-ikb\sin\theta_0\sin\phi_0)/2}\cos n\pi-e^{(ikb\sin\theta_0\sin\phi_0)/2})\\
&+(-\cos\phi_0)\frac{m\pi}{a}\frac{-m\pi/a}{(-ik\sin\theta_0\cos\phi_0)^2+(m\pi/a)^2}\\
&\cdot(e^{(-ika\sin\theta_0\cos\phi_0)/2}\cos m\pi-e^{(ika\sin\theta_0\cos\phi_0)/2})\\
&\left.\cdot\frac{-ik\sin\theta_0\sin\phi_0}{(-ik\sin\theta_0\sin\phi_0)^2+(n\pi/b)^2}(e^{(-ikb\sin\theta_0\sin\phi_0)/2}\cos n\pi-e^{(ikb\sin\theta_0\sin\phi_0)/2})\right\}\\
=&\frac{2\epsilon_m\epsilon_n}{2abi\omega\mu}\frac{1}{\left\{(-ik\sin\theta_0\cos\phi_0)^2+\left(\frac{m\pi}{a}\right)^2\left\{\left\{(-ik\sin\theta_0\sin\phi_0)^2+\left(\frac{n\pi}{b}\right)^2\right\}\right.}\\
&\cdot\left\{\sin\phi_0(ik\sin\theta_0\cos\phi_0)\left(\frac{n\pi}{b}\right)^2+\cos\phi_0(ik\sin\theta_0\sin\phi_0)\left(\frac{m\pi}{a}\right)^2\right\}\\
&\cdot(e^{(-ika\sin\theta_0\cos\phi_0)/2}\cos m\pi-e^{(ika\sin\theta_0\cos\phi_0)/2})\\
&\cdot(e^{(-ikb\sin\theta_0\sin\phi_0)/2}\cos n\pi-e^{(ikb\sin\theta_0\sin\phi_0)/2})
\end{aligned}
$$

$$
\begin{aligned}
=&\frac{2\epsilon_m\epsilon_n}{2abi\omega\mu}\frac{a^2b^2}{\{(aik\sin\theta_0\cos\phi_0)^2+(m\pi)^2\}\{(bik\sin\theta_0\sin\phi_0)^2+(n\pi)^2\}}\\
&\cdot(ik\sin\theta_0\sin\phi_0\cos\phi_0)\Big\{\left(\frac{m\pi}{a}\right)^2+\left(\frac{n\pi}{b}\right)^2\Big\}\\
&\cdot\left\{e^{(-ika\sin\theta_0\cos\phi_0)/2}(-1)^m-e^{(ika\sin\theta_0\cos\phi_0)/2}\right\}\\
&\cdot\left\{e^{(-ikb\sin\theta_0\sin\phi_0)/2}(-1)^n-e^{(ikb\sin\theta_0\sin\phi_0)/2}\right\}\\
=&\sqrt{\frac{\varepsilon_0}{\mu_0}}\frac{\epsilon_m\epsilon_n ab(k^2-\kappa_{m,n}^2)\sin\theta_0\cos\phi_0\sin\phi_0}{\{(m\pi)^2-(ka\sin\theta_0\cos\phi_0)^2\}\{(n\pi)^2-(kb\sin\theta_0\sin\phi_0)^2\}}\\
&\cdot\left\{(-1)^{m+1}e^{(-ika\sin\theta_0\cos\phi_0)/2}+e^{(ika\sin\theta_0\cos\phi_0)/2}\right\}\\
&\cdot\left\{(-1)^{n+1}e^{(-ikb\sin\theta_0\sin\phi_0)/2}+e^{(ikb\sin\theta_0\sin\phi_0)/2}\right\}. \qquad (3.76)
\end{aligned}
$$

In addition, according to Maxwell's equations, one can derive other electric components $E_x^{\mathrm{w}}, E_y^{\mathrm{w}}$ from magnetic component H_z^{w}:

$$
E_x^{\mathrm{w}}=\frac{i\omega\mu}{k^2-\kappa_{m,n}^2}\frac{\partial H_z^{\mathrm{w}}}{\partial y}, E_y^{\mathrm{w}}=-\frac{i\omega\mu}{k^2-\kappa_{m,n}^2}\frac{\partial H_z^{\mathrm{w}}}{\partial x}, \qquad (3.77)
$$

Substuting Eqs. (3.75) and (3.76) into Eq. (3.77), we can derive

$$
\begin{aligned}
E_x^{\mathrm{w}}=&\sum_{m=0}^{\infty}\sum_{n=0}^{\infty}F_{mnx}^{\mathrm{w}}\cos\frac{m\pi}{a}\left(x+\frac{a}{2}\right)\sin\frac{n\pi}{b}\left(y+\frac{b}{2}\right)e^{-i\kappa_{m,n}z}, \qquad (3.78)\\
F_{mnx}^{\mathrm{w}}=&-\frac{i\epsilon_m\epsilon_n kan\pi\sin\theta_0\cos\phi_0\sin\phi_0}{\{(m\pi)^2-(ka\sin\theta_0\cos\phi_0)^2\}\{(n\pi)^2-(kb\sin\theta_0\sin\phi_0)^2\}}\\
&\cdot\left\{(-1)^{m+1}e^{(-ika\sin\theta_0\cos\phi_0)/2}+e^{(ika\sin\theta_0\cos\phi_0)/2}\right\}\\
&\cdot\left\{(-1)^{n+1}e^{(-ikb\sin\theta_0\sin\phi_0)/2}+e^{(ikb\sin\theta_0\sin\phi_0)/2}\right\}, \qquad (3.79)\\
E_y^{\mathrm{w}}=&\sum_{m=0}^{\infty}\sum_{n=0}^{\infty}F_{mny}^{\mathrm{w}}\sin\frac{m\pi}{a}\left(x+\frac{a}{2}\right)\cos\frac{n\pi}{b}\left(y+\frac{b}{2}\right)e^{-i\kappa_{m,n}z}, \qquad (3.80)\\
F_{mny}^{\mathrm{w}}=&\frac{i\epsilon_m\epsilon_n kbm\pi\sin\theta_0\cos\phi_0\sin\phi_0}{\{(m\pi)^2-(ka\sin\theta_0\cos\phi_0)^2\}\{(n\pi)^2-(kb\sin\theta_0\sin\phi_0)^2\}}\\
&\cdot\left\{(-1)^{m+1}e^{(-ika\sin\theta_0\cos\phi_0)/2}+e^{(ika\sin\theta_0\cos\phi_0)/2}\right\}\\
&\cdot\left\{(-1)^{n+1}e^{(-ikb\sin\theta_0\sin\phi_0)/2}+e^{(ikb\sin\theta_0\sin\phi_0)/2}\right\}. \qquad (3.81)
\end{aligned}
$$

On the other hand, the equivalent magnetic source $\boldsymbol{M}_2^+$ at the upper side of the lower aperture ($z=-c_+$):

$$
\boldsymbol{M}_2^+=\boldsymbol{E}^{\mathrm{w}}\times\hat{\boldsymbol{z}}=E_y^{\mathrm{w}}\hat{\boldsymbol{x}}-E_x^{\mathrm{w}}\hat{\boldsymbol{y}}, \qquad (3.82)
$$

and at the lower side ($z=-c_-$):

$$
\boldsymbol{M}_2^-=\boldsymbol{E}^{\mathrm{w}}\times(-\hat{\boldsymbol{z}})=-E_y^{\mathrm{w}}\hat{\boldsymbol{x}}+E_x^{\mathrm{w}}\hat{\boldsymbol{y}}, \qquad (3.83)
$$

where $\boldsymbol{E}^{\mathrm{w}}$ is the electric field propagates inside the waveguide calculated in Eqs.(3.78)$\sim$(3.81).

3.1.3 Scattering Far-field in Transmitted Region ($z < -c$)

We now derive the electric far-field components in the lower region caused by the sources. Considering the lower side of the lower aperture, from Eqs. (3.78)∼(3.81) and Eq. (3.83) x, y components of $\boldsymbol{M_2^-}$ are:

$$\begin{aligned}
M_{2x}^- =& -E_y^{\mathrm{w}}\big|_{x=x',y=y',z=-c} \\
=& \sum_{m=0}^{\infty}\sum_{n=0}^{\infty} -F_{mny}^{\mathrm{w}} \sin\frac{m\pi}{a}\left(x'+\frac{a}{2}\right)\cos\frac{n\pi}{b}\left(y'+\frac{b}{2}\right)e^{i\kappa_{m,n}c}, \qquad (3.84)\\
F_{mny}^{\mathrm{w}} =& \frac{i\epsilon_m\epsilon_n kbm\pi \sin\theta_0\cos\phi_0\sin\phi_0}{\{(m\pi)^2-(ka\sin\theta_0\cos\phi_0)^2\}\{(n\pi)^2-(kb\sin\theta_0\sin\phi_0)^2\}} \\
& \cdot\left\{(-1)^{m+1}e^{(-ika\sin\theta_0\cos\phi_0)/2}+e^{(ika\sin\theta_0\cos\phi_0)/2}\right\} \\
& \cdot\left\{(-1)^{n+1}e^{(-ikb\sin\theta_0\sin\phi_0)/2}+e^{(ikb\sin\theta_0\sin\phi_0)/2}\right\}, \qquad (3.85)\\
M_{2y}^- =& E_x^{\mathrm{w}}\big|_{x=x',y=y',z=-c} \\
=& \sum_{m=0}^{\infty}\sum_{n=0}^{\infty} F_{mnx}^{\mathrm{w}} \cos\frac{m\pi}{a}\left(x'+\frac{a}{2}\right)\sin\frac{n\pi}{b}\left(y'+\frac{b}{2}\right)e^{i\kappa_{m,n}c}, \qquad (3.86)\\
F_{mnx}^{\mathrm{w}} =& -\frac{i\epsilon_m\epsilon_n kan\pi \sin\theta_0\cos\phi_0\sin\phi_0}{\{(m\pi)^2-(ka\sin\theta_0\cos\phi_0)^2\}\{(n\pi)^2-(kb\sin\theta_0\sin\phi_0)^2\}} \\
& \cdot\left\{(-1)^{m+1}e^{(-ika\sin\theta_0\cos\phi_0)/2}+e^{(ika\sin\theta_0\cos\phi_0)/2}\right\} \\
& \cdot\left\{(-1)^{n+1}e^{(-ikb\sin\theta_0\sin\phi_0)/2}+e^{(ikb\sin\theta_0\sin\phi_0)/2}\right\}. \qquad (3.87)
\end{aligned}$$

Then, we derive $\boldsymbol{D}_2$ for lower scattering field derivation using

$$\boldsymbol{D}_2(\theta,\phi) = \int_{S''} \boldsymbol{M}_2^-(\boldsymbol{r'})e^{-ik(x'\sin\theta\cos\phi+y'\sin\theta\sin\phi+z'\cos\theta)}dS'', \qquad (3.88)$$

where S'' is the aperture ($|x'| < a/2$, $|y'| < b/2$, $z' = -c_-$) on which the equivalent source $\boldsymbol{M}_2^-$ expressed in Eqs. (3.84) and (3.86) exists. x, y components of $\boldsymbol{D}_2$ are:

$$\begin{aligned}
D_{2x} =& \int_{-b/2}^{b/2}\int_{-a/2}^{a/2} M_{2x}^- e^{-ik(x'\sin\theta\cos\phi+y'\sin\theta\sin\phi-c\cos\theta)}dx'dy' \\
=& \int_{-b/2}^{b/2}\int_{-a/2}^{a/2} -\sum_{m=0}^{\infty}\sum_{n=0}^{\infty} F_{mny}^{\mathrm{w}} \sin\frac{m\pi}{a}\left(x'+\frac{a}{2}\right)\cos\frac{n\pi}{b}\left(y'+\frac{b}{2}\right)e^{i\kappa_{m,n}c} \\
& \qquad \cdot e^{-ik(x'\sin\theta\cos\phi+y'\sin\theta\sin\phi-c\cos\theta)}dx'dy' \\
=& -\sum_{m=0}^{\infty}\sum_{n=0}^{\infty} F_{mny}^{\mathrm{w}} \int_{-a/2}^{a/2} \sin\frac{m\pi}{a}\left(x'+\frac{a}{2}\right)e^{-ik\sin\theta\cos\phi x'}dx' \\
& \qquad \cdot \int_{-b/2}^{b/2} \cos\frac{n\pi}{b}\left(y'+\frac{b}{2}\right)e^{-ik\sin\theta\sin\phi y'}dy' e^{i(k\cos\theta+\kappa_{m,n})c}
\end{aligned}$$

$$
\begin{aligned}
&= -\sum_{m=0}^{\infty}\sum_{n=0}^{\infty} F^{\mathrm{w}}_{mny}\frac{-m\pi/a}{(-ik\sin\theta\cos\phi)^2+(m\pi/a)^2}(e^{(-ika\sin\theta\cos\phi)/2}\cos m\pi - e^{(ika\sin\theta\cos\phi)/2})\\
&\quad\cdot\frac{-ik\sin\theta\sin\phi}{(-ik\sin\theta\sin\phi)^2+(n\pi/b)^2}(e^{(-ikb\sin\theta\sin\phi)/2}\cos n\pi - e^{(ikb\sin\theta\sin\phi)/2})e^{i(k\cos\theta+\kappa_{m,n})c}\\
&=\sum_{m=0}^{\infty}\sum_{n=0}^{\infty}\frac{\epsilon_m\epsilon_n k^2ab^3m^2\pi^2\sin\theta_0\cos\phi_0\sin\phi_0}{\{(m\pi)^2-(ka\sin\theta_0\cos\phi_0)^2\}\{(n\pi)^2-(kb\sin\theta_0\sin\phi_0)^2\}}\\
&\quad\cdot\frac{\sin\theta\sin\phi}{\{(m\pi)^2-(ka\sin\theta\cos\phi)^2\}\{(n\pi)^2-(kb\sin\theta\sin\phi)^2\}}\\
&\quad\cdot\left\{(-1)^{m+1}e^{(-ika\sin\theta_0\cos\phi_0)/2}+e^{(ika\sin\theta_0\cos\phi_0)/2}\right\}\\
&\quad\cdot\left\{(-1)^{n+1}e^{(-ikb\sin\theta_0\sin\phi_0)/2}+e^{(ikb\sin\theta_0\sin\phi_0)/2}\right\}\\
&\quad\cdot\left\{(-1)^{m+1}e^{(-ika\sin\theta\cos\phi)/2}+e^{(ika\sin\theta\cos\phi)/2}\right\}\\
&\quad\cdot\left\{(-1)^{n+1}e^{(-ikb\sin\theta\sin\phi)/2}+e^{(ikb\sin\theta_0\sin\phi)/2}\right\}e^{i(k\cos\theta+\kappa_{m,n})c},
\end{aligned}
\tag{3.89}
$$

$$
\begin{aligned}
D_{2y} &= \int_{-b/2}^{b/2}\int_{-a/2}^{a/2} M^{-}_{2y}e^{-ik(x'\sin\theta\cos\phi+y'\sin\theta\sin\phi-c\cos\theta)}dx'dy'\\
&= \int_{-b/2}^{b/2}\int_{-a/2}^{a/2}\sum_{m=0}^{\infty}\sum_{n=0}^{\infty}F^{\mathrm{w}}_{mnx}\cos\frac{m\pi}{a}\left(x'+\frac{a}{2}\right)\sin\frac{n\pi}{b}\left(y'+\frac{b}{2}\right)e^{i\kappa_{m,n}c}\\
&\qquad\qquad\cdot e^{-ik(x'\sin\theta\cos\phi+y'\sin\theta\sin\phi-c\cos\theta)}dx'dy'\\
&= \sum_{m=0}^{\infty}\sum_{n=0}^{\infty}F^{\mathrm{w}}_{mnx}\int_{-a/2}^{a/2}\cos\frac{m\pi}{a}\left(x'+\frac{a}{2}\right)e^{-ik\sin\theta\cos\phi x'}dx'\\
&\qquad\qquad\cdot\int_{-b/2}^{b/2}\sin\frac{n\pi}{b}\left(y'+\frac{b}{2}\right)e^{-ik\sin\theta\sin\phi y'}dy'e^{i(k\cos\theta+\kappa_{m,n})c}\\
&= \sum_{m=0}^{\infty}\sum_{n=0}^{\infty}F^{\mathrm{w}}_{mnx}\frac{-ik\sin\theta\cos\phi}{(-ik\sin\theta\cos\phi)^2+(m\pi/a)^2}(e^{(-ika\sin\theta\cos\phi)/2}\cos m\pi - e^{(ika\sin\theta\cos\phi)/2})\\
&\quad\cdot\frac{-n\pi/b}{(-ik\sin\theta\sin\phi)^2+(n\pi/b)^2}(e^{(-ikb\sin\theta\sin\phi)/2}\cos n\pi - e^{(ikb\sin\theta\sin\phi)/2})e^{i(k\cos\theta+\kappa_{m,n})c}\\
&= \sum_{m=0}^{\infty}\sum_{n=0}^{\infty}\frac{\epsilon_m\epsilon_n k^2a^3bn^2\pi^2\sin\theta_0\cos\phi_0\sin\phi_0}{\{(m\pi)^2-(ka\sin\theta_0\cos\phi_0)^2\}\{(n\pi)^2-(kb\sin\theta_0\sin\phi_0)^2\}}\\
&\quad\cdot\frac{\sin\theta\cos\phi}{\{(m\pi)^2-(ka\sin\theta\cos\phi)^2\}\{(n\pi)^2-(kb\sin\theta\sin\phi)^2\}}\\
&\quad\cdot\left\{(-1)^{m+1}e^{(-ika\sin\theta_0\cos\phi_0)/2}+e^{(ika\sin\theta_0\cos\phi_0)/2}\right\}\\
&\quad\cdot\left\{(-1)^{n+1}e^{(-ikb\sin\theta_0\sin\phi_0)/2}+e^{(ikb\sin\theta_0\sin\phi_0)/2}\right\}\\
&\quad\cdot\left\{(-1)^{m+1}e^{(-ika\sin\theta\cos\phi)/2}+e^{(ika\sin\theta\cos\phi)/2}\right\}\\
&\quad\cdot\left\{(-1)^{n+1}e^{(-ikb\sin\theta\sin\phi)/2}+e^{(ikb\sin\theta_0\sin\phi)/2}\right\}e^{i(k\cos\theta+\kappa_{m,n})c}.
\end{aligned}
\tag{3.90}
$$

From Eqs.(3.11)∼(3.13) and (3.31), we can calculate electric field $\boldsymbol{E}_2^{\rm s}$ from $\boldsymbol{D}_2$ as

$$\begin{aligned}\boldsymbol{E}_2^{\rm s} \sim & -\left\{\frac{ik}{2\pi r}(D_{2x}\sin\phi - D_{2y}\cos\phi)e^{ikr}\right\}\hat{\boldsymbol{\theta}} \\ & -\left\{\frac{ik}{2\pi r}(D_{2x}\cos\theta\cos\phi + D_{2y}\cos\theta\sin\phi)e^{ikr}\right\}\hat{\boldsymbol{\phi}}. \end{aligned} \tag{3.91}$$

The electric far-field components contributed by the source $\boldsymbol{M}_2^-$ at the lower side of the lower aperture are:

$$E_{2r} \sim 0, \tag{3.92}$$

$$\begin{aligned} E_{2\theta} \sim & \frac{ikabe^{ikr}}{2\pi r}\sum_{m=0}^{\infty}\sum_{n=0}^{\infty}\frac{\epsilon_m\epsilon_n\sin\theta_0\cos\phi_0\sin\phi_0}{\{(m\pi)^2-(ka\sin\theta_0\cos\phi_0)^2\}\{(n\pi)^2-(kb\sin\theta_0\sin\phi_0)^2\}} \\ & \cdot\frac{\sin\theta\{-(kbm\pi\sin\phi)^2+(kan\pi\cos\phi)^2\}}{\{(m\pi)^2-(ka\sin\theta\cos\phi)^2\}\{(n\pi)^2-(kb\sin\theta\sin\phi)^2\}} \\ & \cdot\left\{(-1)^{m+1}e^{(-ika\sin\theta_0\cos\phi_0)/2}+e^{(ika\sin\theta_0\cos\phi_0)/2}\right\} \\ & \cdot\left\{(-1)^{n+1}e^{(-ikb\sin\theta_0\sin\phi_0)/2}+e^{(ikb\sin\theta_0\sin\phi_0)/2}\right\} \\ & \cdot\left\{(-1)^{m+1}e^{(-ika\sin\theta\cos\phi)/2}+e^{(ika\sin\theta\cos\phi)/2}\right\} \\ & \cdot\left\{(-1)^{n+1}e^{(-ikb\sin\theta\sin\phi)/2}+e^{(ikb\sin\theta_0\sin\phi)/2}\right\}e^{i(k\cos\theta+\kappa_{m,n})c}, \end{aligned} \tag{3.93}$$

$$\begin{aligned} E_{2\phi} \sim & \frac{ikabe^{ikr}}{2\pi r}\sum_{m=0}^{\infty}\sum_{n=0}^{\infty}\frac{\epsilon_m\epsilon_n\sin\theta_0\cos\phi_0\sin\phi_0}{\{(m\pi)^2-(ka\sin\theta_0\cos\phi_0)^2\}\{(n\pi)^2-(kb\sin\theta_0\sin\phi_0)^2\}} \\ & \cdot\frac{\sin\theta\cos\theta\sin\phi\cos\phi\{-(kbm\pi)^2-(kan\pi)^2\}}{\{(m\pi)^2-(ka\sin\theta\cos\phi)^2\}\{(n\pi)^2-(kb\sin\theta\sin\phi)^2\}} \\ & \cdot\left\{(-1)^{m+1}e^{(-ika\sin\theta_0\cos\phi_0)/2}+e^{(ika\sin\theta_0\cos\phi_0)/2}\right\} \\ & \cdot\left\{(-1)^{n+1}e^{(-ikb\sin\theta_0\sin\phi_0)/2}+e^{(ikb\sin\theta_0\sin\phi_0)/2}\right\} \\ & \cdot\left\{(-1)^{m+1}e^{(-ika\sin\theta\cos\phi)/2}+e^{(ika\sin\theta\cos\phi)/2}\right\} \\ & \cdot\left\{(-1)^{n+1}e^{(-ikb\sin\theta\sin\phi)/2}+e^{(ikb\sin\theta_0\sin\phi)/2}\right\}e^{i(k\cos\theta+\kappa_{m,n})c}. \end{aligned} \tag{3.94}$$

or

$$E_{2r}^{\rm s} \sim 0, \tag{3.95}$$

$$\begin{aligned} E_{2\theta}^{\rm s} \sim & -\frac{i\omega\mu_0 e^{ik(r+c\cos\theta)}}{2\pi r}\sum_{m=0}^{\infty}\sum_{n=0}^{\infty}\frac{F_{mn}^{\rm w}}{k^2-\kappa_{m,n}^2}e^{i\kappa_{m,n}c} \\ & \cdot\left\{(m\pi kb\sin\phi)^2-(n\pi ka\cos\phi)^2\right\}\sin\theta \\ & \cdot\frac{(-1)^{m+1}e^{-ik(a/2)\sin\theta\cos\phi}+e^{ik(a/2)\sin\theta\cos\phi}}{(m\pi)^2-(ka\sin\theta\cos\phi)^2} \\ & \cdot\frac{(-1)^{n+1}e^{-ik(b/2)\sin\theta\sin\phi}+e^{ik(b/2)\sin\theta\sin\phi}}{(n\pi)^2-(kb\sin\theta\sin\phi)^2}, \end{aligned} \tag{3.96}$$

$$E^{\mathrm{s}}_{2\phi} \sim -\frac{i\omega\mu_0 e^{ik(r+c\cos\theta)}}{2\pi r}\sum_{m=0}^{\infty}\sum_{n=0}^{\infty}\frac{F^{\mathrm{w}}_{mn}}{k^2-\kappa^2_{m,n}}e^{i\kappa_{m,n}c}$$
$$\cdot\{(m\pi kb)^2+(n\pi ka)^2\}\sin\theta\cos\theta\sin\phi\cos\phi$$
$$\cdot\frac{(-1)^{m+1}e^{-ik(a/2)\sin\theta\cos\phi}+e^{ik(a/2)\sin\theta\cos\phi}}{(m\pi)^2-(ka\sin\theta\cos\phi)^2}$$
$$\cdot\frac{(-1)^{n+1}e^{-ik(b/2)\sin\theta\sin\phi}+e^{ik(b/2)\sin\theta\sin\phi}}{(n\pi)^2-(kb\sin\theta\sin\phi)^2}. \tag{3.97}$$

where F^{w}_{mn} is the excitation coefficient expressed in Eq. (3.76).

3.1.4 Scattering Far-field from Infinitely Thin Screen

It is important to self-validate the above scattering formulation by deriving a special circumstance of an infinitely thin screen. In KA method, the upper scattering field in this case stay the same since there are no dependences of upper scattering field $\boldsymbol{E}^{\mathrm{s}}_1$ on the screen thickness according to Eqs. (3.35) and 3.36. For the lower scattering field, one can take the limit $c \to 0$ in Eqs. (3.96) and 3.97. On the other hand, the lower scattering field in this case $\boldsymbol{\phi}^{\mathrm{ss}}_2 = \boldsymbol{E}^{\mathrm{ss}}_2$ can be derived directly from $\boldsymbol{M}^{-}_1$ in Eq. (3.10) in the similar way of deriving $\boldsymbol{E}^{\mathrm{s}}_1$ in Sect. 3.1.1 with $\boldsymbol{M}^{+}_1$ replaced by $\boldsymbol{M}^{-}_1$ in Eq. (3.16). Since $\boldsymbol{M}^{-}_1 = -\boldsymbol{M}^{+}_1$, one gets for $\theta > \pi/2$

$$E^{\mathrm{ss}}_{2y} = -E^{\mathrm{s}}_{1y}, \tag{3.98}$$

or

$$E^{\mathrm{ss}}_{2r} \sim 0, \tag{3.99}$$
$$E^{\mathrm{ss}}_{2\theta} \sim -\frac{2i\sin(\phi_0-\phi)e^{ikr}}{\pi kr}A, \tag{3.100}$$
$$E^{\mathrm{ss}}_{2\phi} \sim \frac{2i\cos\theta\cos(\phi_0-\phi)e^{ikr}}{\pi kr}A, \tag{3.101}$$
$$A = \frac{\sin\{ka(\sin\theta_0\cos\phi_0+\sin\theta\cos\phi)/2\}}{\sin\theta_0\cos\phi_0+\sin\theta\cos\phi}$$
$$\cdot\frac{\sin\{kb(\sin\theta_0\sin\phi_0+\sin\theta\sin\phi)/2\}}{\sin\theta_0\sin\phi_0+\sin\theta\sin\phi}. \tag{3.102}$$

The comparison of results from these two calculations will be shown in Sect. 3.4.

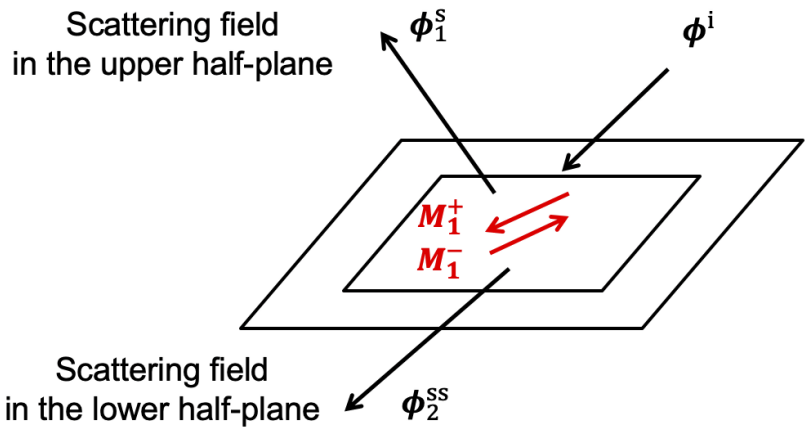

Figure 3.4: Plane wave scattering by an infinitely thin screen.

3.2 H Polarization

When the TM polarized plane wave of a unit amplitude illuminates, Eqs. (3.4) and (3.5) become

$$\boldsymbol{E}^{\mathrm{i}} = \hat{\boldsymbol{\theta}}_0 e^{i\boldsymbol{k}^{\mathrm{i}}\cdot\boldsymbol{r}}, \tag{3.103}$$

$$\boldsymbol{H}^{\mathrm{i}} = -\sqrt{\frac{\varepsilon_0}{\mu_0}}\hat{\boldsymbol{\phi}}_0 e^{i\boldsymbol{k}^{\mathrm{i}}\cdot\boldsymbol{r}}, \tag{3.104}$$

If one starts from $\boldsymbol{H}^{\mathrm{i}}$, the corresponding $\boldsymbol{E}_{\mathrm{i}}$ can be derived based on Ampere's equation as in Appendix B. In the KA derivation, the equivalent magnetic current sources $\boldsymbol{M}_1^{\pm}$ exist on the closing upper aperture ($z = 0$). The equivalent magnetic currents $\boldsymbol{M}_1^{\pm}$ may be expressed in terms of the wave number $\boldsymbol{k}^{\mathrm{i}}$ as

$$\begin{aligned}\boldsymbol{M}_1^{\pm}(x, y, z = 0_{\pm}) =& \boldsymbol{E}^{\mathrm{i}}\big|_{z=0_{\pm}} \times (\pm\hat{\boldsymbol{z}}) = e^{i\boldsymbol{k}^{\mathrm{i}}\cdot\boldsymbol{r}}\hat{\boldsymbol{\theta}}_0\big|_{z=0_{\pm}} \times (\pm\hat{\boldsymbol{z}}) \\ =& \pm e^{-ik(x\sin\theta_0\cos\phi_0 + y\sin\theta_0\sin\phi_0)}(\sin\phi_0\cos\theta_0\ \hat{\boldsymbol{x}} - \cos\phi_0\sin\theta_0\ \hat{\boldsymbol{y}}), \\ & \left(|x| < \frac{a}{2}, |y| < \frac{b}{2}, z = 0_{\pm}\right).\end{aligned} \tag{3.105}$$

3.2.1 Scattering Far-field in Incoming Region ($z > 0$)

The upper scattering field $\boldsymbol{E}_1^{\mathrm{s}}$ resulted from the above equivalent magnetic current $\boldsymbol{M}_1^+$ can also be obtained from a vector potential $\boldsymbol{F}_1$ as [36]

$$\boldsymbol{E}_1^{\mathrm{s}} = -\frac{1}{\varepsilon_0}\nabla \times \boldsymbol{F}_1. \tag{3.106}$$

Vector potential $\boldsymbol{F}_1$ can be derived from equivalent magnetic current $\boldsymbol{M}_1^+(\boldsymbol{r'})$ by:

$$\boldsymbol{F}_1 = \frac{\varepsilon_0}{2\pi}\int_{S'} \boldsymbol{M}_1^+(\boldsymbol{r'})\frac{e^{ik|\boldsymbol{r}-\boldsymbol{r'}|}}{|\boldsymbol{r}-\boldsymbol{r'}|}dS' \tag{3.107}$$

With far-field consideration, the vector potential $\boldsymbol{F}_1$ due to the magnetic source can be approximated as

$$\boldsymbol{F}_1 \sim \varepsilon_0 G\int_{S'} \boldsymbol{M}_1^+(\boldsymbol{r'})e^{-ik\boldsymbol{r'}\cdot\hat{\boldsymbol{r}}}dS' = \varepsilon_0 G\boldsymbol{D}_1(\theta,\phi), \tag{3.108}$$

where

$$\boldsymbol{D}_1(\theta,\phi) = \int_{S'} \boldsymbol{M}_1^+(\boldsymbol{r'})e^{-ik(x'\sin\theta\cos\phi+y'\sin\theta\sin\phi+z'\cos\theta)}dS', \tag{3.109}$$

and G is three-dimensional half-space Green's function:

$$G = \frac{e^{ikr}}{2\pi r}. \tag{3.110}$$

Then

$$\begin{aligned}\boldsymbol{F}_1 &\sim \frac{\varepsilon_0 e^{ikr}}{2\pi r}\int_{S'} \boldsymbol{M}_1^+(\boldsymbol{r'})e^{-ik\boldsymbol{r'}\cdot\hat{\boldsymbol{r}}}dS' \\ &= \frac{\varepsilon_0 e^{ikr}}{2\pi r}\int_{S'} \boldsymbol{M}_1^+(\boldsymbol{r'})e^{-ik(x'\sin\theta\cos\phi+y'\sin\theta\sin\phi)}dS',\end{aligned} \tag{3.111}$$

where

$$\boldsymbol{r'} = x'\,\hat{\boldsymbol{x}} + y'\,\hat{\boldsymbol{y}} + z'\,\hat{\boldsymbol{z}}, \tag{3.112}$$

$$\hat{\boldsymbol{r}} = \sin\theta\cos\phi\,\hat{\boldsymbol{x}} + \sin\theta\sin\phi\,\hat{\boldsymbol{y}} + \cos\theta\,\hat{\boldsymbol{z}}, \tag{3.113}$$

and S' denotes the aperture ($|x'| < a/2$, $|y'| < b/2$, $z' = 0_+$) where the current $\boldsymbol{M}_1^+$ given in Eq. (3.105) exists. $\boldsymbol{r'}$ is the position vector to the aperture source point $(x', y', z' = 0)$ on S', and $\hat{\boldsymbol{r}}$ is the unit vector directed to the observation point. The integral in Eq. (3.111) is analytically solved to obtain $\boldsymbol{F}_1$. Again, substituting $\boldsymbol{F}_1$ into Eq. (3.106), considering far-field condition, one can obtain the scattering field $\boldsymbol{E}_1^{\mathrm{s}}$ in upper region.

First, we derive $\boldsymbol{D}_1$ in Eq. (3.109). For the far reflection field calculation, we only consider the source on the upper side of the conducting plate. From Eq. (3.105),

$$\begin{aligned}M_{1x}^+e^{-ik(x'\sin\theta\cos\phi+y'\sin\theta\sin\phi)} &= \sin\phi_0\cos\theta_0 e^{-ik\{x'(\sin\theta_0\cos\phi_0+\sin\theta\cos\phi)+y'(\sin\theta_0\sin\phi_0+\sin\theta\sin\phi)\}} \\ &= \sin\phi_0\cos\theta_0 e^{-ik(x'\alpha+y'\beta)},\end{aligned} \tag{3.114}$$

$$\begin{aligned}M_{1y}^+e^{-ik(x'\sin\theta\cos\phi+y'\sin\theta\sin\phi)} &= -\cos\phi_0\cos\theta_0 e^{-ik\{x'(\sin\theta_0\cos\phi_0+\sin\theta\cos\phi)+y'(\sin\theta_0\sin\phi_0+\sin\theta\sin\phi)\}} \\ &= -\cos\phi_0\cos\theta_0 e^{-ik(x'\alpha+y'\beta)},\end{aligned} \tag{3.115}$$

where:

$$\alpha = \sin\theta_0 \cos\phi_0 + \sin\theta\cos\phi, \tag{3.116}$$

$$\beta = \sin\theta_0 \sin\phi_0 + \sin\theta\sin\phi. \tag{3.117}$$

x and y components of $\boldsymbol{D}_1$ are respectively:

$$\begin{aligned}
D_{1x} &= \int_{-b/2}^{b/2}\int_{-a/2}^{a/2} M_{1x}^{+} e^{-ik(x'\sin\theta\cos\phi + y'\sin\theta\sin\phi)} dx'dy' \\
&= \sin\phi_0\cos\theta_0 \int_{-b/2}^{b/2}\int_{-a/2}^{a/2} e^{-ik(x'\alpha+y'\beta)} dx'dy' \\
&= \frac{\sin\phi_0\cos\theta_0}{ik\alpha}\int_{-b/2}^{b/2}(e^{ik(a\alpha/2-y'\beta)} - e^{-ik(a\alpha/2)+y'\beta)})dy' \\
&= -\frac{\sin\phi_0\cos\theta_0}{k^2\alpha\beta}\left\{e^{ik(a\alpha/2+b\beta/2\beta)} + e^{-ik(a\alpha/2+b\beta/2)} - e^{ik(a\alpha/2-b\beta/2\beta)} - e^{-ik(a\alpha/2-b\beta/2)}\right\} \\
&= -\frac{2\sin\phi_0\cos\theta_0}{k^2\alpha\beta}\left[\cos\left\{k\left(\frac{a}{2}\alpha + \frac{b}{2}\beta\right)\right\} - \cos\left\{k\left(\frac{a}{2}\alpha - \frac{b}{2}\beta\right)\right\}\right] \\
&= \frac{4\sin\phi_0\cos\theta_0}{k^2\alpha\beta}\sin\left(\frac{ka}{2}\alpha\right)\sin\left(\frac{kb}{2}\beta\right),
\end{aligned} \tag{3.118}$$

$$D_{1y} = -\frac{4\cos\phi_0\cos\theta_0}{k^2\alpha\beta}\sin\left(\frac{ka}{2}\alpha\right)\sin\left(\frac{kb}{2}\beta\right), \tag{3.119}$$

where from Eq. (3.108), we derive the components of vector potential $\boldsymbol{F}_1$ in the sphere coordinates (r, θ, ϕ)

$$\begin{aligned}
F_{1r} &= F_{1x}\sin\theta\cos\phi + F_{1y}\sin\theta\sin\phi \\
&= \varepsilon_0 G(D_{1x}\sin\theta\cos\phi + D_{1y}\sin\theta\sin\phi),
\end{aligned} \tag{3.120}$$

$$\begin{aligned}
F_{1\theta} &= F_{1x}\cos\theta\cos\phi + F_{1y}\cos\theta\sin\phi \\
&= \varepsilon_0 G(D_{1x}\cos\theta\cos\phi + D_{1y}\cos\theta\sin\phi),
\end{aligned} \tag{3.121}$$

$$\begin{aligned}
F_{1\phi} &= -F_{1x}\sin\phi + F_{1y}\cos\phi \\
&= \varepsilon_0 G(-D_{1x}\sin\phi + D_{1y}\cos\phi).
\end{aligned} \tag{3.122}$$

Then

$$F_{1r} = \frac{2\varepsilon_0}{\pi k^2 r\alpha\beta}\sin\theta\cos\theta_0\sin(\phi-\phi_0)\sin\left(\frac{ka}{2}\alpha\right)\sin\left(\frac{kb}{2}\beta\right)e^{ikr}, \tag{3.123}$$

$$F_{\theta} = \frac{2\varepsilon_0}{\pi k^2 r\alpha\beta}\cos\theta\cos\theta_0\sin(\phi-\phi_0)\sin\left(\frac{ka}{2}\alpha\right)\sin\left(\frac{kb}{2}\beta\right)e^{ikr}, \tag{3.124}$$

$$F_{\phi} = \frac{2\varepsilon_0}{\pi k^2 r\alpha\beta}\cos\theta_0\cos(\phi-\phi_0)\sin\left(\frac{ka}{2}\alpha\right)\sin\left(\frac{kb}{2}\beta\right)e^{ikr}. \tag{3.125}$$

Assuming the observation point is sufficiently far away, we ignore the terms of r^{-2}, then we derive

$$\begin{aligned}\nabla \times \boldsymbol{F}_1 =& \frac{1}{r\sin\theta}\left\{\frac{\partial(F_{1\phi}\sin\theta)}{\partial\theta} - \frac{\partial F_{1\theta}}{\partial\phi}\right\}\hat{\boldsymbol{r}} + \frac{1}{r}\left\{\frac{1}{\sin\theta}\frac{\partial F_{1r}}{\partial\phi} - \frac{\partial(rF_{1\phi})}{\partial r}\right\}\hat{\boldsymbol{\theta}} \\ &+ \frac{1}{r}\left\{\frac{\partial(rF_{1\theta})}{\partial r} - \frac{\partial F_{1r}}{\partial\theta}\right\}\hat{\boldsymbol{\phi}} \\ &\sim -\frac{1}{r}\frac{\partial(rF_{1\phi})}{\partial r}\hat{\boldsymbol{\theta}} + \frac{1}{r}\frac{\partial(rF_{1\theta})}{\partial r}\hat{\boldsymbol{\phi}}. \end{aligned} \tag{3.126}$$

From Eqs. (3.106) and (3.126) we derive electric far field components caused by the source at the upper side of the conducting screen in H polarization as

$$\begin{aligned} E_{1r} \sim& 0, \\ E_{1\theta} \sim& -\frac{2i}{\pi kr\alpha\beta}e^{ikr}\sin(\phi_0-\phi)\sin\left(\frac{ka}{2}\alpha\right)\sin\left(\frac{kb}{2}\beta\right) \\ =& -\frac{2i\cos\theta_0\cos(\phi_0-\phi)e^{ikr}}{\pi kr}\frac{\sin\{ka(\sin\theta_0\cos\phi_0+\sin\theta\cos\phi)/2\}}{\sin\theta_0\cos\phi_0+\sin\theta\cos\phi} \\ &\cdot\frac{\sin\{kb(\sin\theta_0\sin\phi_0+\sin\theta\sin\phi)/2\}}{\sin\theta_0\sin\phi_0+\sin\theta\sin\phi}, \end{aligned} \tag{3.127}$$

$$\begin{aligned} E_{1\phi} \sim& -\frac{2i}{\pi kr\alpha\beta}e^{ikr}\cos\theta\cos(\phi_0-\phi)\sin\left(\frac{ka}{2}\alpha\right)\sin\left(\frac{kb}{2}\beta\right) \\ =& -\frac{2i\cos\theta_0\cos\theta\sin(\phi_0-\phi)e^{ikr}}{\pi kr}\frac{\sin\{ka(\sin\theta_0\cos\phi_0+\sin\theta\cos\phi)/2\}}{\sin\theta_0\cos\phi_0+\sin\theta\cos\phi} \\ &\cdot\frac{\sin\{kb(\sin\theta_0\sin\phi_0+\sin\theta\sin\phi)/2\}}{\sin\theta_0\sin\phi_0+\sin\theta\sin\phi}, \end{aligned} \tag{3.128}$$

or

$$E_{1r}^{\mathrm{s}} \sim 0, \tag{3.129}$$

$$E_{1\theta}^{\mathrm{s}} \sim -\frac{2i\cos\theta_0\cos(\phi_0-\phi)e^{ikr}}{\pi kr}A, \tag{3.130}$$

$$E_{1\phi}^{\mathrm{s}} \sim -\frac{2i\cos\theta_0\cos\theta\sin(\phi_0-\phi)e^{ikr}}{\pi kr}A, \tag{3.131}$$

$$\begin{aligned} A =& \frac{\sin\{ka(\sin\theta_0\cos\phi_0+\sin\theta\cos\phi)/2\}}{\sin\theta_0\cos\phi_0+\sin\theta\cos\phi} \\ &\cdot\frac{\sin\{kb(\sin\theta_0\sin\phi_0+\sin\theta\sin\phi)/2\}}{\sin\theta_0\sin\phi_0+\sin\theta\sin\phi}. \end{aligned} \tag{3.132}$$

The corresponding magnetic scattering fields can be derived from electric fields using the relationship in Eqs. (3.38) and (3.39).

3.2.2 Electromagnetic Field in Hole Region ($-c < z < 0$)

The proposed model of rectangular hole in a thick conducting screen can be considered as a three-dimensional rectangular waveguide. Consequently, one can formulate the electromagnetic field inside the hole region as the fields propagate inside the waveguide region. Using exactly the same derivation process from Eqs. (3.40) to Eq. (3.66) One gets the field components inside the hole in z-direction for H polarization incidence as

$$\begin{aligned} E_z =& -\left(\frac{\partial^2\Pi'}{\partial x^2}+\frac{\partial^2\Pi'}{\partial y^2}\right) \\ =& \sum_{m=1}^{\infty}\sum_{n=1}^{\infty} C_{m,n}\sin\frac{m\pi}{a}\left(x+\frac{a}{2}\right)\sin\frac{n\pi}{b}\left(y+\frac{b}{2}\right)e^{-i\kappa_{m,n}(z-z')}, \end{aligned} \tag{3.133}$$

$$\begin{aligned} C_{m,n} =& \frac{2}{abi}\Bigg\{-\frac{1}{\kappa_{m,n}}M_{1y}^{-}\frac{m\pi}{a}\cos\frac{m\pi}{a}\left(x'+\frac{a}{2}\right)\sin\frac{n\pi}{b}\left(y'+\frac{b}{2}\right) \\ &+\frac{1}{\kappa_{m,n}}M_{1x}^{-}\frac{n\pi}{b}\sin\frac{m\pi}{a}\left(x'+\frac{a}{2}\right)\cos\frac{n\pi}{b}\left(y'+\frac{b}{2}\right)\Bigg\}, \end{aligned} \tag{3.134}$$

$$\begin{aligned} H_z =& -\left(\frac{\partial^2\Pi''}{\partial x^2}+\frac{\partial^2\Pi''}{\partial y^2}\right), \\ =& \sum_{m=0}^{\infty}\sum_{n=0}^{\infty} F_{m,n}\cos\frac{m\pi}{a}\left(x+\frac{a}{2}\right)\cos\frac{n\pi}{b}\left(y+\frac{b}{2}\right)e^{-i\kappa_{m,n}(z-z')} \end{aligned} \tag{3.135}$$

$$\begin{aligned} F_{m,n} =& \frac{\epsilon_m\epsilon_n}{2abi}\Bigg\{-\frac{1}{\omega\mu}M_{1y}^{-}\frac{n\pi}{b}\cos\frac{m\pi}{a}\left(x'+\frac{a}{2}\right)\sin\frac{n\pi}{b}\left(y'+\frac{b}{2}\right) \\ &-\frac{1}{\omega\mu}M_{1x}^{-}\frac{m\pi}{a}\sin\frac{m\pi}{a}\left(x'+\frac{a}{2}\right)\cos\frac{n\pi}{b}\left(y'+\frac{b}{2}\right)\Bigg\}. \end{aligned} \tag{3.136}$$

If the incident wave is plane wave, then the equivalent magnetic current components at the aperture ($-a/2 < x' < a/2, -b/2 < y' < b/2, z' = 0_{-}$) are derived from Eq. (3.10) as

$$M_{1x}^{-} = -\sin\phi_0\cos\theta_0 e^{-ik(x'\sin\theta_0\cos\phi_0+y'\sin\theta_0\sin\phi_0)}, \tag{3.137}$$

$$M_{1y}^{-} = \cos\phi_0\cos\theta_0 e^{-ik(x'\sin\theta_0\cos\phi_0+y'\sin\theta_0\sin\phi_0)}. \tag{3.138}$$

Taking the integral at the upper aperture, for our assumption, we have only the magnetic current source $\boldsymbol{M}_1$ and no electric current. Accordingly, one has to consider imaging effect of the source on the conducting surface, then we derive electromagnetic field in the waveguide from source at the upper aperture:

$$\begin{aligned} E_z^{\mathrm{w}} =& -\left(\frac{\partial^2\Pi'}{\partial x^2}+\frac{\partial^2\Pi'}{\partial y^2}\right) \\ =& \sum_{m=1}^{\infty}\sum_{n=1}^{\infty} C_{m,n}^{\mathrm{w}}\sin\frac{m\pi}{a}\left(x+\frac{a}{2}\right)\sin\frac{n\pi}{b}\left(y+\frac{b}{2}\right)e^{-i\kappa_{m,n}z}, \end{aligned} \tag{3.139}$$

$$
\begin{aligned}
C^{\mathrm{w}}_{m,n} =& \int_{-a/2}^{a/2}\int_{-b/2}^{b/2} C_{mn}dx'dy' \\
=& \frac{2}{abi\kappa_{m,n}}\left\{ \int_{-a/2}^{a/2} -M^{-}_{1y}\frac{m\pi}{a}\cos\frac{m\pi}{a}\left(x'+\frac{a}{2}\right)\sin\frac{n\pi}{b}\sin\left(y'+\frac{b}{2}\right)\right. \\
&\left. + \int_{-b/2}^{b/2} M^{-}_{1x}\frac{n\pi}{b}\sin\frac{m\pi}{a}\left(x'+\frac{a}{2}\right)\cos\frac{n\pi}{b}\sin\left(y'+\frac{b}{2}\right)\right\} \\
=& \frac{4}{abi\kappa_{m,n}} \\
&\cdot\left\{ -\cos\phi_0\cos\theta_0\frac{m\pi}{a}\int_{-a/2}^{a/2}\cos\frac{m\pi}{a}\left(x'+\frac{a}{2}\right)e^{-ik\sin\theta_0\cos\phi_0 x'}dx'\right. \\
&\cdot\int_{-b/2}^{b/2}\sin\frac{n\pi}{b}\left(y'+\frac{b}{2}\right)e^{-ik\sin\theta_0\sin\phi_0 y'}dy' \\
&+(\sin\phi_0\cos\theta_0)\frac{n\pi}{b}\int_{-a/2}^{a/2}\sin\frac{m\pi}{a}\left(x'+\frac{a}{2}\right)e^{-ik\sin\theta_0\cos\phi_0 x'}dx' \\
&\left.\cdot\int_{-b/2}^{b/2}\cos\frac{n\pi}{b}\left(y'+\frac{b}{2}\right)e^{-ik\sin\theta_0\sin\phi_0 y'}dy'\right\} \\
=& \frac{4}{abi\kappa_{m,n}} \\
&\cdot\left\{(-\cos\phi_0\cos\theta_0)\frac{m\pi}{a}\frac{-ik\sin\theta_0\cos\phi_0}{(-ik\sin\theta_0\cos\phi_0)^2+(m\pi/a)^2}\right. \\
&\cdot(e^{-(ika\sin\theta_0\cos\phi_0)/2}\cos m\pi - e^{(ika\sin\theta_0\cos\phi_0)/2}) \\
&\cdot\frac{-n\pi/b}{(-ik\sin\theta_0\sin\phi_0)^2+(n\pi/b)^2}(e^{(-ikb\sin\theta_0\sin\phi_0)/2}\cos n\pi - e^{(ikb\sin\theta_0\sin\phi_0)/2}) \\
&+(\sin\phi_0\cos\theta_0)\frac{n\pi}{b}\frac{-m\pi/a}{(-ik\sin\theta_0\cos\phi_0)^2+(m\pi/a)^2} \\
&\cdot(e^{(-ika\sin\theta_0\cos\phi_0)/2}\cos m\pi - e^{(ika\sin\theta_0\cos\phi_0)/2}) \\
&\left.\cdot\frac{-ik\sin\theta_0\sin\phi_0}{(-ik\sin\theta_0\sin\phi_0)^2+(n\pi/b)^2}(e^{(-ikb\sin\theta_0\sin\phi_0)/2}\cos n\pi - e^{(ikb\sin\theta_0\sin\phi_0)/2})\right\} \\
=& \frac{4mn\pi^2 k\sin\theta_0\cos\theta_0}{\kappa_{m,n}} \\
&\cdot\frac{(-1)^{m+1}e^{-ik(a/2)\sin\theta_0\cos\phi_0}+e^{ik(a/2)\sin\theta_0\cos\phi_0}}{(m\pi)^2-(ka\sin\theta_0\cos\phi_0)^2} \\
&\cdot\frac{(-1)^{n+1}e^{-ik(b/2)\sin\theta_0\sin\phi_0}+e^{ik(b/2)\sin\theta_0\sin\phi_0}}{(n\pi)^2-(kb\sin\theta_0\sin\phi_0)^2}.
\end{aligned}
\tag{3.140}
$$

Similarly,

$$
\begin{aligned}
H_z^{\mathrm{w}} &= -\left(\frac{\partial^2\Pi''}{\partial x^2}+\frac{\partial^2\Pi''}{\partial y^2}\right)\\
&= \sum_{m=0}^{\infty}\sum_{n=0}^{\infty} F_{m,n}^{\mathrm{w}} \cos\frac{m\pi}{a}\left(x+\frac{a}{2}\right)\cos\frac{n\pi}{b}\left(y+\frac{b}{2}\right)e^{-i\kappa_{m,n}z}, \qquad (3.141)\\
F_{m,n}^{\mathrm{w}} &= \int_{-a/2}^{a/2}\int_{-b/2}^{b/2} F_{mn}dx'dy'\\
&= -\frac{\epsilon_m\epsilon_n}{2abi\omega\mu}\left\{\int_{-a/2}^{a/2}\int_{-b/2}^{b/2} M_{1y}^{-}\frac{n\pi}{b}\cos\frac{m\pi}{a}(x'+\frac{a}{2})\sin\frac{n\pi}{b}(y'+\frac{b}{2})dx'dy'\right.\\
&\quad \left.+\int_{-a/2}^{a/2}\int_{-b/2}^{b/2} M_{1x}^{-}\frac{m\pi}{a}\sin\frac{m\pi}{a}(x'+\frac{a}{2})\cos\frac{n\pi}{b}(y'+\frac{b}{2})dx'dy'\right\}\\
&= -\frac{2\epsilon_m\epsilon_n}{2abi\omega\mu}\\
&\quad \cdot\left\{(\cos\phi_0\cos\theta_0)\frac{n\pi}{b}\int_{-a/2}^{a/2}\cos\frac{m\pi}{a}(x'+\frac{a}{2})e^{-ik\sin\theta_0\cos\phi_0 x'}dx'\right.\\
&\quad \cdot\int_{-b/2}^{b/2}\sin\frac{n\pi}{b}(y'+\frac{b}{2})e^{-ik\sin\theta_0\sin\phi_0 y'}dy'\\
&\quad +(-\sin\phi_0\sin\theta)\frac{m\pi}{a}\int_{-a/2}^{a/2}\sin\frac{m\pi}{a}(x'+\frac{a}{2})e^{-ik\sin\theta_0\cos\phi_0 x'}dx'\\
&\quad \left.\cdot\int_{-b/2}^{b/2}\cos\frac{n\pi}{b}(y'+\frac{b}{2})e^{-ik\sin\theta_0\sin\phi_0 y'}dy'\right\}\\
&= -\frac{2\epsilon_m\epsilon_n}{2abi\omega\mu}\\
&\quad \cdot\left\{\cos\phi_0\cos\theta_0\frac{n\pi}{b}\frac{-ik\sin\theta_0\cos\phi_0}{(-ik\sin\theta_0\cos\phi_0)^2+(m\pi/a)^2}\right.\\
&\quad \cdot(e^{(-ika\sin\theta_0\cos\phi_0)/2}\cos m\pi - e^{(ika\sin\theta_0\cos\phi_0)/2})\\
&\quad \cdot\frac{-n\pi/b}{(-ik\sin\theta_0\sin\phi_0)^2+(n\pi/b)^2}(e^{(-ikb\sin\theta_0\sin\phi_0)/2}\cos n\pi - e^{(ikb\sin\theta_0\sin\phi_0)/2})\\
&\quad +\sin\phi_0\cos\theta_0\frac{m\pi}{a}\frac{m\pi/a}{(-ik\sin\theta_0\cos\phi_0)^2+(m\pi/a)^2}\\
&\quad \cdot(e^{(-ika\sin\theta_0\cos\phi_0)/2}\cos m\pi - e^{(ika\sin\theta_0\cos\phi_0)/2})\\
&\quad \left.\cdot\frac{-ik\sin\theta_0\sin\phi_0}{(-ik\sin\theta_0\sin\phi_0)^2+(n\pi/b)^2}(e^{(-ikb\sin\theta_0\sin\phi_0)/2}\cos n\pi - e^{(ikb\sin\theta_0\sin\phi_0)/2})\right\}
\end{aligned}
$$

$$
\begin{aligned}
=&\sqrt{\frac{\varepsilon_0}{\mu_0}}\frac{\epsilon_m\epsilon_n\pi^2(n^2a^2\cos^2\phi_0-m^2b^2\sin^2\phi_0)\sin\theta_0\cos\theta_0}{ab}\\
&\cdot\frac{(-1)^{m+1}e^{-ik(a/2)\sin\theta_0\cos\phi_0}+e^{ik(a/2)\sin\theta_0\cos\phi_0}}{(m\pi)^2-(ka\sin\theta_0\cos\phi_0)^2}\\
&\cdot\frac{(-1)^{n+1}e^{-ik(b/2)\sin\theta_0\sin\phi_0}+e^{ik(b/2)\sin\theta_0\sin\phi_0}}{(n\pi)^2-(kb\sin\theta_0\sin\phi_0)^2}.
\end{aligned}
\tag{3.142}
$$

Here, $C^{\mathrm{w}}_{m,n}$ and $F^{\mathrm{w}}_{m,n}$ are the excitation coefficients of the $\mathrm{TE_{mn}}$ and $\mathrm{TM_{mn}}$ modal field. In addition, according to Maxwell's equations, one can derive other electric components $E^{\mathrm{w}}_x, E^{\mathrm{w}}_y$ from magnetic component H^{w}_z:

$$
E^{\mathrm{w}}_x=\frac{i\omega\mu}{k^2-\kappa^2_{m,n}}\frac{\partial H^{\mathrm{w}}_z}{\partial y}, E^{\mathrm{w}}_y=-\frac{i\omega\mu}{k^2-\kappa^2_{m,n}}\frac{\partial H^{\mathrm{w}}_z}{\partial x},
\tag{3.143}
$$

Substuting Eqs. (3.141) and (3.142) into Eq. (3.143), we can derive

$$
\begin{aligned}
E^{\mathrm{w}}_x=&\sum_{m=1}^{\infty}\sum_{n=1}^{\infty}\alpha^{\mathrm{w}}_1\cos\frac{m\pi}{a}\left(x+\frac{a}{2}\right)\sin\frac{n\pi}{b}\left(y+\frac{b}{2}\right)e^{-i\kappa_{m,n}z},\\
&+\sum_{m=0}^{\infty}\sum_{n=0}^{\infty}\beta^{\mathrm{w}}_1\cos\frac{m\pi}{a}\left(x+\frac{a}{2}\right)\sin\frac{n\pi}{b}\left(y+\frac{b}{2}\right)e^{-i\kappa_{m,n}z},
\end{aligned}
\tag{3.144}
$$

where

$$
\begin{aligned}
\alpha^{\mathrm{w}}_1=&-\frac{2ik}{k^2-\kappa_{mn}}\sin\theta_0\cos\theta_0\left(\frac{m\pi}{a}\right)^2\frac{n\pi}{b}\\
&\cdot\frac{ab}{\{(m\pi)^2-(ka\sin\theta_0\cos\phi_0)^2\}\{(n\pi)^2-(kb\sin\theta_0\sin\phi_0)^2\}}\\
&\cdot\left\{(-1)^{m+1}e^{(-ika\sin\theta_0\cos\phi_0)/2}+e^{(ika\sin\theta_0\cos\phi_0)/2}\right\}\\
&\cdot\left\{(-1)^{n+1}e^{(-ikb\sin\theta_0\sin\phi_0)/2}+e^{(ikb\sin\theta_0\sin\phi_0)/2}\right\},
\end{aligned}
\tag{3.145}
$$

$$
\begin{aligned}
\beta^{\mathrm{w}}_1=&-\frac{\epsilon_m\epsilon_n ik}{2(k^2-\kappa_{mn})}\sin\theta_0\cos\theta_0\frac{n\pi}{b}\left\{-\left(\frac{n\pi}{b}\cos\phi_0\right)^2+\left(\frac{m\pi}{a}\right)^2\right\}\\
&\cdot\frac{ab}{\{(m\pi)^2-(ka\sin\theta_0\cos\phi_0)^2\}\{(n\pi)^2-(kb\sin\theta_0\sin\phi_0)^2\}}\\
&\cdot\left\{(-1)^{m+1}e^{(-ika\sin\theta_0\cos\phi_0)/2}+e^{(ika\sin\theta_0\cos\phi_0)/2}\right\}\\
&\cdot\left\{(-1)^{n+1}e^{(-ikb\sin\theta_0\sin\phi_0)/2}+e^{(ikb\sin\theta_0\sin\phi_0)/2}\right\}.
\end{aligned}
\tag{3.146}
$$

$$
\begin{aligned}
E^{\mathrm{w}}_y=&\sum_{m=1}^{\infty}\sum_{n=1}^{\infty}\alpha^{\mathrm{w}}_2\sin\frac{m\pi}{a}\left(x+\frac{a}{2}\right)\cos\frac{n\pi}{b}\left(y+\frac{b}{2}\right)e^{-i\kappa_{m,n}z},\\
&+\sum_{m=0}^{\infty}\sum_{n=0}^{\infty}\beta^{\mathrm{w}}_2\sin\frac{m\pi}{a}\left(x+\frac{a}{2}\right)\cos\frac{n\pi}{b}\left(y+\frac{b}{2}\right)e^{-i\kappa_{m,n}z},
\end{aligned}
\tag{3.147}
$$

where

$$\begin{aligned}\alpha_2^{\mathrm{w}} =& -\frac{2ik}{k^2-\kappa_{mn}}\sin\theta_0\cos\theta_0\frac{m\pi}{a}\left(\frac{n\pi}{b}\right)^2\\ &\cdot\frac{ab}{\{(m\pi)^2-(ka\sin\theta_0\cos\phi_0)^2\}\{(n\pi)^2-(kb\sin\theta_0\sin\phi_0)^2\}}\\ &\cdot\left\{(-1)^{m+1}e^{(-ika\sin\theta_0\cos\phi_0)/2}+e^{(ika\sin\theta_0\cos\phi_0)/2}\right\}\\ &\cdot\left\{(-1)^{n+1}e^{(-ikb\sin\theta_0\sin\phi_0)/2}+e^{(ikb\sin\theta_0\sin\phi_0)/2}\right\},\end{aligned} \tag{3.148}$$

$$\begin{aligned}\beta_2^{\mathrm{w}} =&\frac{\epsilon_m\epsilon_n ik}{2(k^2-\kappa_{mn})}\sin\theta_0\cos\theta_0\frac{m\pi}{a}\left\{-\left(\frac{n\pi}{b}\cos\phi_0\right)^2-\left(\frac{m\pi}{a}\sin\phi_0\right)^2\right\}\\ &\cdot\frac{ab}{\{(m\pi)^2-(ka\sin\theta_0\cos\phi_0)^2\}\{(n\pi)^2-(kb\sin\theta_0\sin\phi_0)^2\}}\\ &\cdot\left\{(-1)^{m+1}e^{(-ika\sin\theta_0\cos\phi_0)/2}+e^{(ika\sin\theta_0\cos\phi_0)/2}\right\}\\ &\cdot\left\{(-1)^{n+1}e^{(-ikb\sin\theta_0\sin\phi_0)/2}+e^{(ikb\sin\theta_0\sin\phi_0)/2}\right\}.\end{aligned} \tag{3.149}$$

On the other hand, the equivalent magnetic source $\boldsymbol{M}_2^+$ at the upper side of the lower aperture ($z=-c_+$):

$$\boldsymbol{M}_2^+ = \boldsymbol{E}^{\mathrm{w}}\times\hat{\boldsymbol{z}} = E_y^{\mathrm{w}}\hat{\boldsymbol{x}} - E_x^{\mathrm{w}}\hat{\boldsymbol{y}}, \tag{3.150}$$

and at the lower side ($z=-c_-$):

$$\boldsymbol{M}_2^- = \boldsymbol{E}^{\mathrm{w}}\times(-\hat{\boldsymbol{z}}) = -E_y^{\mathrm{w}}\hat{\boldsymbol{x}} + E_x^{\mathrm{w}}\hat{\boldsymbol{y}}, \tag{3.151}$$

where $\boldsymbol{E}^{\mathrm{w}}$ is the electric field propagates inside the waveguide calculated in Eqs.(3.144) and (3.147).

3.2.3 Scattering Far-field in Transmitted Region ($z<-c$)

We now derive the electric far-field components in the lower region caused by the sources. Considering the lower side of the lower aperture, from Eqs. (3.144), (3.147) and Eq. (3.151) x, y components of $\boldsymbol{M_2^-}$ are:

$$\begin{aligned}M_{2x}^- =& -E_y^{\mathrm{w}}\big|_{x=x',y=y',z=-c}\\ =& -\sum_{m=1}^{\infty}\sum_{n=1}^{\infty}\alpha_2^{\mathrm{w}}\sin\frac{m\pi}{a}\left(x+\frac{a}{2}\right)\cos\frac{n\pi}{b}\left(y+\frac{b}{2}\right)e^{-i\kappa_{m,n}z},\\ &-\sum_{m=0}^{\infty}\sum_{n=0}^{\infty}\beta_2^{\mathrm{w}}\sin\frac{m\pi}{a}\left(x+\frac{a}{2}\right)\cos\frac{n\pi}{b}\left(y+\frac{b}{2}\right)e^{i\kappa_{m,n}c},\end{aligned} \tag{3.152}$$

$$
\begin{aligned}
M_{2y}^{-} =& E_x^{\mathrm{w}}\big|_{x=x',y=y',z=-c} \\
=& \sum_{m=1}^{\infty}\sum_{n=1}^{\infty} \alpha_1^{\mathrm{w}} \cos\frac{m\pi}{a}\left(x+\frac{a}{2}\right)\sin\frac{n\pi}{b}\left(y+\frac{b}{2}\right)e^{-i\kappa_{m,n}z}, \\
&+\sum_{m=0}^{\infty}\sum_{n=0}^{\infty} \beta_1^{\mathrm{w}} \cos\frac{m\pi}{a}\left(x+\frac{a}{2}\right)\sin\frac{n\pi}{b}\left(y+\frac{b}{2}\right)e^{i\kappa_{m,n}c}.
\end{aligned} \tag{3.153}
$$

Then, we derive $\boldsymbol{D}_2$ for lower scattering field derivation using

$$
\boldsymbol{D}_2(\theta,\phi) = \int_{S''} \boldsymbol{M}_2^{-}(\boldsymbol{r'}) e^{-ik(x'\sin\theta\cos\phi + y'\sin\theta\sin\phi + z'\cos\theta)} dS'', \tag{3.154}
$$

where S'' is the aperture ($|x'| < a/2$, $|y'| < b/2$, $z' = -c_-$) on which the equivalent source $\boldsymbol{M}_2^{-}$ expressed in Eqs. (3.152) and (3.153) exists. x, y components of $\boldsymbol{D}_2$ are:

$$
\begin{aligned}
D_{2x} =& \int_{-b/2}^{b/2}\int_{-a/2}^{a/2} M_{2x}^{-} e^{-ik(x'\sin\theta\cos\phi + y'\sin\theta\sin\phi - c\cos\theta)} dx'dy' \\
=& \int_{-b/2}^{b/2}\int_{-a/2}^{a/2} -\Bigg\{ \sum_{m=1}^{\infty}\sum_{n=1}^{\infty} \alpha_2^{\mathrm{w}} \sin\frac{m\pi}{a}\left(x'+\frac{a}{2}\right)\cos\frac{n\pi}{b}\left(y'+\frac{b}{2}\right)e^{i\kappa_{m,n}c} \\
&+ \sum_{m=0}^{\infty}\sum_{n=0}^{\infty} \beta_2^{\mathrm{w}} \sin\frac{m\pi}{a}\left(x'+\frac{a}{2}\right)\cos\frac{n\pi}{b}\left(y'+\frac{b}{2}\right)e^{i\kappa_{m,n}c} \Bigg\} \\
&\cdot e^{-ik(x'\sin\theta\cos\phi + y'\sin\theta\sin\phi - c\cos\theta)} dx'dy' \\
=& -\sum_{m=1}^{\infty}\sum_{n=1}^{\infty} \alpha_2^{\mathrm{w}} \int_{-a/2}^{a/2} \sin\frac{m\pi}{a}\left(x'+\frac{a}{2}\right) e^{-ik\sin\theta\cos\phi x'} dx' \\
&\qquad \cdot \int_{-b/2}^{b/2} \cos\frac{n\pi}{b}\left(y'+\frac{b}{2}\right) e^{-ik\sin\theta\sin\phi y'} dy' e^{i(k\cos\theta+\kappa_{m,n})c} \\
&-\sum_{m=0}^{\infty}\sum_{n=0}^{\infty} \beta_2^{\mathrm{w}} \int_{-a/2}^{a/2} \sin\frac{m\pi}{a}\left(x'+\frac{a}{2}\right) e^{-ik\sin\theta\cos\phi x'} dx' \\
&\qquad \cdot \int_{-b/2}^{b/2} \cos\frac{n\pi}{b}\left(y'+\frac{b}{2}\right) e^{-ik\sin\theta\sin\phi y'} dy' e^{i(k\cos\theta+\kappa_{m,n})c} \\
=& -\sum_{m=1}^{\infty}\sum_{n=1}^{\infty} \alpha_2^{\mathrm{w}} \frac{-m\pi/a}{(-ik\sin\theta\cos\phi)^2 + (m\pi/a)^2} (e^{(-ika\sin\theta\cos\phi)/2}\cos m\pi - e^{(ika\sin\theta\cos\phi)/2}) \\
&\cdot \frac{-ik\sin\theta\sin\phi}{(-ik\sin\theta\sin\phi)^2 + (n\pi/b)^2} (e^{(-ikb\sin\theta\sin\phi)/2}\cos n\pi - e^{(ikb\sin\theta\sin\phi)/2}) e^{i(k\cos\theta+\kappa_{m,n})c} \\
&-\sum_{m=0}^{\infty}\sum_{n=0}^{\infty} \beta_2^{\mathrm{w}} \frac{-m\pi/a}{(-ik\sin\theta\cos\phi)^2 + (m\pi/a)^2} (e^{(-ika\sin\theta\cos\phi)/2}\cos m\pi - e^{(ika\sin\theta\cos\phi)/2}) \\
&\cdot \frac{-ik\sin\theta\sin\phi}{(-ik\sin\theta\sin\phi)^2 + (n\pi/b)^2} (e^{(-ikb\sin\theta\sin\phi)/2}\cos n\pi - e^{(ikb\sin\theta\sin\phi)/2}) e^{i(k\cos\theta+\kappa_{m,n})c}.
\end{aligned} \tag{3.155}
$$

$$
\begin{aligned}
D_{2y} &= \int_{-b/2}^{b/2}\int_{-a/2}^{a/2} M_{2y}^{-} e^{-ik(x'\sin\theta\cos\phi+y'\sin\theta\sin\phi-c\cos\theta)}dx'dy' \\
&= \int_{-b/2}^{b/2}\int_{-a/2}^{a/2}\left\{\sum_{m=1}^{\infty}\sum_{n=1}^{\infty}\alpha_1^{\mathrm{w}}\cos\frac{m\pi}{a}\left(x'+\frac{a}{2}\right)\sin\frac{n\pi}{b}\left(y'+\frac{b}{2}\right)e^{i\kappa_{m,n}c}\right. \\
&\quad \left.+\sum_{m=0}^{\infty}\sum_{n=0}^{\infty}\beta_1^{\mathrm{w}}\cos\frac{m\pi}{a}\left(x'+\frac{a}{2}\right)\sin\frac{n\pi}{b}\left(y'+\frac{b}{2}\right)e^{i\kappa_{m,n}c}\right\} \\
&\quad \cdot e^{-ik(x'\sin\theta\cos\phi+y'\sin\theta\sin\phi-c\cos\theta)}dx'dy' \\
&= \sum_{m=1}^{\infty}\sum_{n=1}^{\infty}\alpha_1^{\mathrm{w}}\int_{-a/2}^{a/2}\cos\frac{m\pi}{a}\left(x'+\frac{a}{2}\right)e^{-ik\sin\theta\cos\phi x'}dx' \\
&\qquad\qquad \cdot\int_{-b/2}^{b/2}\sin\frac{n\pi}{b}\left(y'+\frac{b}{2}\right)e^{-ik\sin\theta\sin\phi y'}dy'e^{i(k\cos\theta+\kappa_{m,n})c} \\
&\quad +\sum_{m=0}^{\infty}\sum_{n=0}^{\infty}\beta_1^{\mathrm{w}}\int_{-a/2}^{a/2}\cos\frac{m\pi}{a}\left(x'+\frac{a}{2}\right)e^{-ik\sin\theta\cos\phi x'}dx' \\
&\qquad\qquad \cdot\int_{-b/2}^{b/2}\sin\frac{n\pi}{b}\left(y'+\frac{b}{2}\right)e^{-ik\sin\theta\sin\phi y'}dy'e^{i(k\cos\theta+\kappa_{m,n})c} \\
&= \sum_{m=1}^{\infty}\sum_{n=1}^{\infty}\alpha_1^{\mathrm{w}}\frac{-ik\sin\theta\cos\phi}{(-ik\sin\theta\cos\phi)^2+(m\pi/a)^2}(e^{(-ika\sin\theta\cos\phi)/2}\cos m\pi-e^{(ika\sin\theta\cos\phi)/2}) \\
&\quad \cdot\frac{-n\pi/b}{(-ik\sin\theta\sin\phi)^2+(n\pi/b)^2}(e^{(-ikb\sin\theta\sin\phi)/2}\cos n\pi-e^{(ikb\sin\theta\sin\phi)/2})e^{i(k\cos\theta+\kappa_{m,n})c} \\
&\quad +\sum_{m=0}^{\infty}\sum_{n=0}^{\infty}\beta_1^{\mathrm{w}}\frac{-ik\sin\theta\cos\phi}{(-ik\sin\theta\cos\phi)^2+(m\pi/a)^2}(e^{(-ika\sin\theta\cos\phi)/2}\cos m\pi-e^{(ika\sin\theta\cos\phi)/2}) \\
&\quad \cdot\frac{-n\pi/b}{(-ik\sin\theta\sin\phi)^2+(n\pi/b)^2}(e^{(-ikb\sin\theta\sin\phi)/2}\cos n\pi-e^{(ikb\sin\theta\sin\phi)/2})e^{i(k\cos\theta+\kappa_{m,n})c}.
\end{aligned}
\tag{3.156}
$$

From Eqs.(3.11)$\sim$(3.13) and (3.31), we can calculate electric field $\boldsymbol{E}_2^{\mathrm{s}}$ from $\boldsymbol{D}_2$ as

$$
\begin{aligned}
\boldsymbol{E}_2^{\mathrm{s}} \sim &-\left\{\frac{ik}{2\pi r}(D_{2x}\sin\phi-D_{2y}\cos\phi)e^{ikr}\right\}\hat{\boldsymbol{\theta}} \\
&-\left\{\frac{ik}{2\pi r}(D_{2x}\cos\theta\cos\phi+D_{2y}\cos\theta\sin\phi)e^{ikr}\right\}\hat{\boldsymbol{\phi}}.
\end{aligned}
\tag{3.157}
$$

The electric far-field components contributed by the source $\boldsymbol{M}_2^{-}$ at the lower side of the lower aperture are:

$$
E_{2r}^{\mathrm{s}} \sim 0, \tag{3.158}
$$

$$
\begin{aligned}
E^{\mathrm{s}}_{2\theta} \sim & \frac{-ie^{ik(r+c\cos\theta)}}{2\pi r}\sum_{m=0}^{\infty}\sum_{n=0}^{\infty}\frac{(ka)^2(kb)^2\sin\theta}{k^2-\kappa^2_{m,n}}e^{i\kappa_{m,n}c} \\
& \cdot\left[\omega\mu_0\left\{\left(\frac{m\pi}{ka}\right)^2\sin^2\phi-\left(\frac{n\pi}{kb}\right)^2\cos^2\phi\right\}F^{\mathrm{w}}_{m,n}-\kappa_{m,n}\frac{m\pi}{ka}\frac{n\pi}{kb}C^{\mathrm{w}}_{m,n}\right] \\
& \cdot\frac{(-1)^{m+1}e^{-ik(a/2)\sin\theta\cos\phi}+e^{ik(a/2)\sin\theta\cos\phi}}{(m\pi)^2-(ka\sin\theta\cos\phi)^2} \\
& \cdot\frac{(-1)^{n+1}e^{-ik(b/2)\sin\theta\sin\phi}+e^{ik(b/2)\sin\theta\sin\phi}}{(n\pi)^2-(kb\sin\theta\sin\phi)^2},
\end{aligned}
\tag{3.159}
$$

$$
\begin{aligned}
E^{\mathrm{s}}_{2\phi} \sim & \frac{-ie^{ik(r+c\cos\theta)}}{2k\pi r}\sum_{m=0}^{\infty}\sum_{n=0}^{\infty}F^{\mathrm{w}}_{m,n}e^{i\kappa_{m,n}c} \\
& \cdot(ka)^2(kb)^2\sin\theta\cos\theta\sin\phi\cos\phi \\
& \cdot\frac{(-1)^{m+1}e^{-ik(a/2)\sin\theta\cos\phi}+e^{ik(a/2)\sin\theta\cos\phi}}{(m\pi)^2-(ka\sin\theta\cos\phi)^2} \\
& \cdot\frac{(-1)^{n+1}e^{-ik(b/2)\sin\theta\sin\phi}+e^{ik(b/2)\sin\theta\sin\phi}}{(n\pi)^2-(kb\sin\theta\sin\phi)^2}.
\end{aligned}
\tag{3.160}
$$

where $C^{\mathrm{w}}_{m,n}$ and $F^{\mathrm{w}}_{m,n}$is the excitation coefficient expressed in Eqs. (3.140) and (3.142).

3.2.4 Scattering Far-field from Infinitely Thin Screen

It is important to self-validate the above scattering formulation by deriving a special circumstance of an infinitely thin screen. In KA method, the upper scattering field in this case stay the same since there are no dependences of upper scattering field $\boldsymbol{E}^{\mathrm{s}}_1$ on the screen thickness according to Eqs. (3.130) and (3.131). For the lower scattering field, one can take the limit $c \to 0$ in Eqs. (3.159) and (3.160). On the other hand, the lower scattering field in this case $\boldsymbol{\phi}^{\mathrm{ss}}_2 = \boldsymbol{E}^{\mathrm{ss}}_2$ can be derived directly from $\boldsymbol{M}^{-}_1$ in Eq. (3.10) in the similar way of deriving $\boldsymbol{E}^{\mathrm{s}}_1$ in Sect. 3.1.1 with $\boldsymbol{M}^{+}_1$ replaced by $\boldsymbol{M}^{-}_1$ in Eq. (3.16). Since $\boldsymbol{M}^{-}_1 = -\boldsymbol{M}^{+}_1$, one gets for $\theta > \pi/2$

$$
E^{\mathrm{ss}}_2 = -E^{\mathrm{s}}_1, \tag{3.161}
$$

or

$$
E^{\mathrm{ss}}_{2r} \sim 0, \tag{3.162}
$$

$$
E^{\mathrm{ss}}_{2\theta} \sim \frac{2i\cos\theta_0\cos(\phi_0-\phi)e^{ikr}}{\pi kr}A, \tag{3.163}
$$

$$
E^{\mathrm{ss}}_{2\phi} \sim \frac{2i\cos\theta_0\cos\theta\sin(\phi_0-\phi)e^{ikr}}{\pi kr}A, \tag{3.164}
$$

$$
A = \frac{\sin\{ka(\sin\theta_0\cos\phi_0+\sin\theta\cos\phi)/2\}}{\sin\theta_0\cos\phi_0+\sin\theta\cos\phi}\frac{\sin\{kb(\sin\theta_0\sin\phi_0+\sin\theta\sin\phi)/2\}}{\sin\theta_0\sin\phi_0+\sin\theta\sin\phi}. \tag{3.165}
$$

The comparison of results from these two calculations will be shown in Sect. 3.4.

3.3 Relation between Three-dimensional and Two-dimensional Scattering Formulation

As a validation step, the scattering field relation between three and two-dimensional formulation is discussed in this section to validate the previous derivation, not only for rectangular hole scattering derivation but also that of the slit. Based on this assessment, one can be confident to apply the proposed KA method for more practical problems in the future. Here, the final three-dimensional formulation of scattering by rectangular hole in a thick conducting screen is expressed again in a special case that is close to two-dimensional problem and then compared with the formulation of scattering by thick conducting empty slits. If one restricts that the incident plane wave and the observation point P are both located in x-z ($y = 0$) plane for the three-dimensional formulation, the cross-sectional configuration becomes exactly the same as two-dimensional thick empty slit. In this section, the 3D-2D relation has been shown for E polarization case. A similar procedure can be applied for the H polarization. Since the relation between 2D and 3D formulation is shown, one can estimate the scattering field by practical three-dimensional object by using less complicated equations. It plays an important role in analyzing and calculation time reduction. A related 2D-3D conversion has been used for estimating 3D radar cross section from 2D analytical results [38], [39].

According to previous sections, the upper scattering field from the three-dimensional rectangular hole in a thick conducting screen is

$$E^{\mathrm{s}}_{1\theta} \sim \frac{2i\sin(\phi_0-\phi)e^{ikr}}{\pi kr}A, \tag{3.166}$$

$$E^{\mathrm{s}}_{1\phi} \sim -\frac{2i\cos\theta\cos(\phi_0-\phi)e^{ikr}}{\pi kr}A, \tag{3.167}$$

$$A = \frac{\sin\{ka(\sin\theta_0\cos\phi_0+\sin\theta\cos\phi)/2\}}{\sin\theta_0\cos\phi_0+\sin\theta\cos\phi}\frac{\sin\{kb(\sin\theta_0\sin\phi_0+\sin\theta\sin\phi)/2\}}{\sin\theta_0\sin\phi_0+\sin\theta\sin\phi}. \tag{3.168}$$

The lower scattering field from the three-dimensional rectangular hole in a thick conduct-

ing screen is

$$E_{2\theta}^{\mathrm{s}} \sim -\frac{i\omega\mu_0 e^{ik(r+c\cos\theta)}}{2\pi r}\sum_{m=0}^{\infty}\sum_{n=0}^{\infty}\frac{F_{mn}^{\mathrm{w}}}{k^2-\kappa_{m,n}^2}e^{i\kappa_{m,n}c}$$
$$\cdot\left\{(m\pi kb\sin\phi)^2-(n\pi ka\cos\phi)^2\right\}\sin\theta$$
$$\cdot\frac{(-1)^{m+1}e^{-ik(a/2)\sin\theta\cos\phi}+e^{ik(a/2)\sin\theta\cos\phi}}{(m\pi)^2-(ka\sin\theta\cos\phi)^2}\frac{(-1)^{n+1}e^{-ik(b/2)\sin\theta\sin\phi}+e^{ik(b/2)\sin\theta\sin\phi}}{(n\pi)^2-(kb\sin\theta\sin\phi)^2}, \tag{3.169}$$

$$E_{2\phi}^{\mathrm{s}} \sim -\frac{i\omega\mu_0 e^{ik(r+c\cos\theta)}}{2\pi r}\sum_{m=0}^{\infty}\sum_{n=0}^{\infty}\frac{F_{mn}^{\mathrm{w}}}{k^2-\kappa_{m,n}^2}e^{i\kappa_{m,n}c}$$
$$\cdot\left\{(m\pi kb)^2+(n\pi ka)^2\right\}\sin\theta\cos\theta\sin\phi\cos\phi$$
$$\cdot\frac{(-1)^{m+1}e^{-ik(a/2)\sin\theta\cos\phi}+e^{ik(a/2)\sin\theta\cos\phi}}{(m\pi)^2-(ka\sin\theta\cos\phi)^2}\frac{(-1)^{n+1}e^{-ik(b/2)\sin\theta\sin\phi}+e^{ik(b/2)\sin\theta\sin\phi}}{(n\pi)^2-(kb\sin\theta\sin\phi)^2}. \tag{3.170}$$

where F_{mn}^{w} is the excitation coefficient expressed in Eq. (3.76).

The upper scattering field from the two-dimensional conducting thick empty slit (loaded layer reflection coefficient $R_m = 0$, transmission coefficient $T_m = 1$) is

$$E_{1y}^{\mathrm{s}} = \frac{-4i\sin\theta\sin\left\{ka(\cos\theta_0+\cos\theta)/2\right\}}{\cos\theta_0+\cos\theta}C(k\rho), \tag{3.171}$$

$$C(k\rho) = \sqrt{\frac{1}{8\pi k\rho}}e^{ik\rho+i\pi/4}. \tag{3.172}$$

The lower scattering field from the two-dimensional conducting thick empty slit is

$$E_{2y}^{s} = 4ika\sin\theta C(k\rho)$$
$$\sum_{m=1}^{\infty}\frac{(m\pi)^2}{\{(m\pi)^2-(ka\cos\theta_0)^2\}\{(m\pi)^2-(ka\cos\theta)^2\}}$$
$$\cdot\left\{(-1)^m e^{(-ika\cos\theta_0)/2}-e^{(ika\cos\theta_0)/2}\right\}\left\{(-1)^m e^{(-ika\cos\theta)/2}-e^{(ika\cos\theta)/2}\right\}$$
$$\cdot e^{i\zeta_m b+ikb\sin\theta}. \tag{3.173}$$

By setting $\phi_0 = 0$, $\phi = (0,\pi)$, $r = \rho$, $\vartheta_0 = \pi/2-\theta_0$, $\vartheta = \pi/2\mp\theta$ $(0<|\vartheta|<\pi/2)$, and replacing the three-dimensional half-space Green's function $e^{ikr}/(2\pi r)$ by the corresponding two-dimensional half-space one $e^{ik\rho+i\pi/4}/\sqrt{2\pi k\rho} = 2C(k\rho)$, one can see from Eq. (3.166) that the three-dimensional $E_{1\theta}^{\mathrm{s}}(\phi=\phi_0=0,\pi)$ component equals to 0, $E_{2\theta}^{\mathrm{s}}(\phi=\phi_0=0,\pi)$ component also equals to 0 due to the following derivation

i) In case of $n \neq 0$:

The excitation coefficient

$$\begin{aligned} F^{\mathrm{w}}_{m,n} =& \frac{\epsilon_m \epsilon_n \pi^2 k (m^2 b^2 + n^2 a^2) \cos\vartheta \sin\phi_0}{ab\omega\mu_0} \\ & \cdot \frac{(-1)^{m+1} e^{(-ika\cos\vartheta_0)/2} + e^{(ika\cos\vartheta_0)/2}}{(m\pi)^2 - (ka\cos\vartheta_0)^2} \frac{(-1)^{n+1} e^{(-ikb\cos\vartheta_0 \sin\phi_0)/2} + e^{(ikb\cos\vartheta_0 \sin\phi_0)/2}}{(n\pi)^2 - (kb\cos\vartheta \sin\phi_0)^2} \\ =& 0. \end{aligned} \tag{3.174}$$

Then

$$E^{\mathrm{s}}_{2\theta}\Big|_{n\neq 0} = E^{\mathrm{s}}_{2\phi}\Big|_{n\neq 0} = 0. \tag{3.175}$$

ii) In case of $n = 0$:

$$F^{\mathrm{s}}_{m,0} = \frac{-i\epsilon_m \pi^2 m^2 b}{a\omega\mu_0} \frac{(-1)^{m+1} e^{(-ika\cos\vartheta_0)/2} + e^{(ika\cos\vartheta_0)/2}}{(m\pi)^2 - (ka\cos\vartheta_0)^2}. \tag{3.176}$$

Then

$$\begin{aligned} E^{\mathrm{s}}_{2\theta}\Big|_{n=0} =& -\omega\mu_0 e^{ikc\sin\vartheta} 2C(k\rho) \sum_{m=0}^{\infty} \frac{F^{\mathrm{w}}_{m,0}}{k^2 - \kappa_{m,0}} e^{i\kappa_{m,0}c} \\ & \cdot (m\pi kb \sin\phi)^2 (\pm\cos\vartheta) \\ & \cdot \frac{(-1)^{m+1} e^{(-ika\cos\vartheta)/2} + e^{(ika\cos\vartheta)/2}}{(m\pi)^2 - (ka\cos\vartheta)^2} \frac{\pm 2i \sin\left(\frac{kb}{2}\cos\vartheta\sin\phi\right)}{-(kb\cos\vartheta\sin\phi)^2} \\ =& -\omega\mu_0 e^{ikc\sin\vartheta} 2C(k\rho) \sum_{m=0}^{\infty} \frac{F^{\mathrm{w}}_{m,0}}{k^2 - \kappa_{m,0}} e^{i\kappa_{m,0}c} \\ & \cdot (m\pi kb)^2 \\ & \cdot \frac{(-1)^{m+1} e^{(-ika\cos\vartheta)/2} + e^{(ika\cos\vartheta)/2}}{(m\pi)^2 - (ka\cos\vartheta)^2} \frac{2i \sin\left(\frac{kb}{2}\cos\vartheta\sin\phi\right)}{-(kb)^2\cos\vartheta} \\ =& 0. \end{aligned} \tag{3.177}$$

On the other hand, $E^{\mathrm{s}}_{\phi}(\phi = \phi_0 = 0, \pi)$ component may be related to the two-dimensional E^{s}_{y} component as following derivation. The derivation is established separately in 4 quadrants. One notes that $F^{\mathrm{w}}_{0,0} = 0$ then $E^{\mathrm{s}}_{2\phi}\Big|_{m=n=0} = 0$.

i) In the first quadrant: Set $\phi = 0$, $\vartheta = \frac{\pi}{2} - \theta$ ($\vartheta < \frac{\pi}{2}$), then one gets $\sin\theta = \cos\vartheta$, $\cos\theta = \sin\vartheta$. Scattering field in the first quadrant becomes

$$\begin{aligned} E^{\mathrm{s}}_{1\phi} =& \frac{-4ib\sin\vartheta \sin\{ka(\cos\vartheta_0 + \cos\vartheta)/2\}}{\cos\vartheta_0 + \cos\vartheta} C(k\rho) \\ \to& bE^{\mathrm{s}}_{1y}, \quad \left(E^{\mathrm{s}}_{1y} \text{ in Eq. (3.171) }\right) \end{aligned} \tag{3.178}$$

ii) In the second quadrant: Set $\phi = \pi$, $\vartheta = \frac{\pi}{2} + \theta$ ($\frac{\pi}{2} < \vartheta < \pi$), then one gets $\sin\theta = -\cos\vartheta$, $\cos\theta = \sin\vartheta$. Scattering field in the second quadrant becomes

$$\begin{aligned} E^{\rm s}_{1\phi} =& \frac{4ib\sin\vartheta\sin\{ka(\cos\vartheta_0+\cos\vartheta)/2\}}{\cos\vartheta_0+\cos\vartheta} C(k\rho) \\ \to& -bE^{\rm s}_{1y}, \quad \left(E^{\rm s}_{1y} \text{ in Eq. (3.171)}\right) \end{aligned} \tag{3.179}$$

iii) In the third quadrant: Set $\phi = \pi$, $\vartheta = \frac{\pi}{2} + \theta$ ($\pi < \vartheta < \frac{3\pi}{2}$), then one gets $\sin\theta = -\cos\vartheta$, $\cos\theta = \sin\vartheta$. Scattering field in the third quadrant becomes

$$\begin{aligned} E^{\rm s}_{2\phi} =& E^{\rm s}_{2\phi}\Big|_{m\neq 0, n=0} \\ =& -i\omega\mu_0 e^{ikc\sin\vartheta} 2C(k\rho) \sum_{m=1}^{\infty} \frac{F^{\rm w}_{m,0}}{k^2-\kappa_{m,0}} e^{i\kappa_{m,0}c} \\ & \cdot (m\pi kb\sin\phi)^2(-\cos\vartheta)\sin\vartheta\sin\phi(-1) \\ & \cdot \frac{(-1)^{m+1}e^{(-ika\cos\vartheta)/2} + e^{(ika\cos\vartheta)/2}}{(m\pi)^2-(ka\cos\vartheta)^2} \frac{2i\sin\left(\frac{kb}{2}(-\cos\vartheta)\sin\phi\right)}{-(kb(-\cos\vartheta)\sin\phi)^2}, \\ \lim_{\substack{\phi_0\to 0\\ \phi\to\pi}} E^{\rm s}_{2\phi} =& -4ikab\sin\vartheta C(k\rho) \\ & \sum_{m=1}^{\infty} \frac{(m\pi)^2}{\{(m\pi)^2-(ka\cos\vartheta_0)^2\}\{(m\pi)^2-(ka\cos\vartheta)^2\}} \\ & \cdot \left\{(-1)^m e^{(-ika\cos\vartheta_0)/2} - e^{(ika\cos\vartheta_0)/2}\right\} \\ & \cdot \left\{(-1)^m e^{(-ika\cos\vartheta)/2} - e^{(ika\cos\vartheta)/2}\right\} \\ & \cdot e^{i\kappa_{m,0}c + ikc\sin\theta}. \end{aligned} \tag{3.180}$$

$$\to -bE^{\rm s}_{2y}, \quad \left(E^{\rm s}_{2y} \text{ in Eq. (3.173)}\right),$$

$$\kappa_{m,0} = \zeta_m = \sqrt{k^2 - \left(\frac{m\pi}{a}\right)^2}. \tag{3.181}$$

iv) In the fourth quadrant: Set $\phi = 0$, $\vartheta = \frac{\pi}{2} - \theta$ ($\vartheta > \frac{3\pi}{2}$), then one gets $\sin\theta = \cos\vartheta$, $\cos\theta = \sin\vartheta$. Scattering field in the fourth quadrant becomes

$$\begin{aligned} E^{\rm s}_{2\phi} =& E^{\rm s}_{2\phi}\Big|_{m\neq 0, n=0} \\ =& -i\omega\mu_0 e^{ikc\sin\vartheta} 2C(k\rho) \sum_{m=1}^{\infty} \frac{F^{\rm w}_{m,0}}{k^2-\kappa_{m,0}} e^{i\kappa_{m,0}c} \\ & \cdot (m\pi kb\sin\phi)^2(-\cos\vartheta)\sin\vartheta\sin\phi(-1) \\ & \cdot \frac{(-1)^{m+1}e^{(-ika\cos\vartheta)/2} + e^{(ika\cos\vartheta)/2}}{(m\pi)^2-(ka\cos\vartheta)^2} \frac{2i\sin\left(\frac{kb}{2}(-\cos\vartheta)\sin\phi\right)}{-(kb(-\cos\vartheta)\sin\phi)^2}, \end{aligned}$$

$$\lim_{\substack{\phi_0\to 0\\ \phi\to 0}} E^{\mathrm{s}}_{2\phi} = 4ikab\sin\vartheta C(k\rho)$$

$$\sum_{m=1}^{\infty} \frac{(m\pi)^2}{\{(m\pi)^2-(ka\cos\vartheta_0)^2\}\{(m\pi)^2-(ka\cos\vartheta)^2\}}$$

$$\cdot\left\{(-1)^m e^{(-ika\cos\vartheta_0)/2} - e^{(ika\cos\vartheta_0)/2}\right\}$$

$$\cdot\left\{(-1)^m e^{(-ika\cos\vartheta)/2} - e^{(ika\cos\vartheta)/2}\right\}$$

$$\cdot\, e^{i\kappa_{m,0}c+ikc\sin\theta}. \tag{3.182}$$

$$\to bE^{\mathrm{s}}_{2y}, \quad \left(E^{\mathrm{s}}_{2y} \text{ in Eq. (3.173) }\right) \tag{3.183}$$

In conclusion, one gets $E^{\mathrm{s}}_{1,2\phi} = bE^{\mathrm{s}}_{1,2y}$ for the first and fourth quadrants ($\phi = 0$), and $E^{\mathrm{s}}_{1,2\phi} = -bE^{\mathrm{s}}_{1,2y}$ for the second and third quadrants ($\phi = \pi$). The difference is only the longitudinal (y-direction) hole's width b.

3.4 Numerical Results and Discussion

Some representative numerical results of the far-field scattering by rectangular hole in a thick conducting screen have been obtained using the previously obtained formulas. The contribution of the reflected plane wave is omitted in the following results. Firstly, the figures which include numerical results from both KA and KP methods are shown to validate the formulation obtained by the proposed KA method. After that, the other aspects of the scattering feature analyzed by the KA method have been shown.

Figures 3.5, 3.6 and 3.8 show the far-field scattering patterns for a square hole ($a = b$) in the incident plane for TE and TM polarizations, respectively. The field component $E_\phi(E_\theta)$ represents the co-polarization component for the scattering field in case of TE(TM) polarized incidence. In this observation plane, there are no contributions of corresponding cross-polarization components according to the formulation. For the comparison with results obtained by the KP method, the hole width parameters are chosen to be $ka = kb = 30, 10$, $kc = 2$ is for the thickness, and the angles of incidence are set as ($\theta_0 = 30°$), (ϕ_0=$0°, 45°$). As revealed in those figures, the larger ka and kb parameters are, the higher and sharper the scattering patterns can be obtained especially at the main lobe directions. Also, more diffraction lobes are formed as a result of the interference between the radiation fields excited at the hole's edges. One can observe that the main lobes direct the corresponding reflected and incident shadow boundary directions near (θ, ϕ)=($30°, 180°$) and

(θ, ϕ)=$(150°, 180°)$ in Fig. 3.5, (θ, ϕ)=$(30°, 225°)$ and (θ, ϕ)=$(150°, 225°)$ in Figs. 3.6, 3.8. The above results include corresponding patterns derived by the KP method [14] for the comparison. As mentioned before, the eigenfunction expansion KP method is known to be an effective solution for small apertures, while the proposed KA method is effective in a high frequency regime for large aperture objects such as the building windows. However, our KA results show agreement with those of the KP method particularly at the main lobe directions in all considered cases of the aperture width. One still finds some differences in the figures at some low angle side lobes. This difference can be explained by the fact that the KA solution does not satisfy the boundary condition [35], and the multiple edge diffraction terms have not been considered. The TE and TM polarization difference occurs at the vicinity of boundary direction at $\theta = 90°$ due to the boundary conditions.

The scattering far-fields in the cross-section which is perpendicular to the incident plane for TE and TM polarizations are shown in Figs. 3.7 and 3.9, respectively. In this perpendicular cross-section, the scattering patterns are found to be symmetric with respect to the normal z-axis. Since the thickness ($kc = 2$) can be considered to be pretty thin, one can observe that the scattering patterns become roughly symmetric with respect to the boundary (x-y) plane, as mentioned before. It is also a similarity of scattering features between patterns shown in Figs. 3.6, 3.8 and Figs. 3.7, 3.9.

For the effect of the conducting screen thickness, one can observe the change of the scattering patterns in the transmitted region, for example in case of $ka = kb = 30$ for TE polarization, in Fig. 3.10. The pattern in the upper region is independent of the screen's thickness since the upper scattering fields excited by $\boldsymbol{M}_1^+$ contain no information on the screen's thickness kc in the KA method. Two representative thickness parameters are chosen here to show clearly the incident beam reflection through the hole on the conducting wall. The incident plane wave partly impinges in the hole and experiences the internal reflection at the internal hole's wall. Here, one may trace the internal bouncing by geometrical optics (GO) beams to predict the reflection direction. In case of $kc = \sqrt{6}ka$, the single GO beam reflection occurs in Fig. 3.10(a), and the double bouncing GO beam propagation can be observed in Fig. 3.10(b) for $kc = 2\sqrt{6}ka$. The single and double bouncing phenomenon also occurs at various screen thicknesses depend on the incident angle. The incident plane wave in the hole's aperture is changed into the waveguide

modes according to the KA derivation, the lower scattering patterns confirm that the modal re-radiation field correctly illustrates the GO beam bouncing prediction. However, in the other arbitrary thickness values, the transmitted fields are more complicated due to the waveguide mode summation which is difficult to predict by simple GO beams.

Figure 3.11 shows the pattern change, for both TE and TM polarization incidences, in co-polarization cross section by the aperture shape transition from a symmetric aperture ($ka = kb = 30$) to a un-symmetric one ($ka = 60$, $kb = 15$). As can be assessed from the scattering field coefficient A in Eq. (3.37), it is a multiplication of sinc functions of x and y variables, each of which has periodical nulls as the aperture size a or b becomes large. The maximum value of A is

$$A_{\max} = \frac{k^2 ab}{4}, \tag{3.184}$$

as the dominator of A becomes zero. This maximum value occurs at the forward scattering direction. Because of the same area ($k^2 ab = 900$) between two apertures, the scattering peaks accordingly describe the same maximum value. However, due to the characteristic of sinc functions in the coefficient A in Eq. (3.37), the pattern has more nulls and rapid oscillation when the aperture is a rectangular ($a \neq b$). These scattering patterns are nearly symmetric with respect to the screen due to pretty thin value of the screen thickness ($kc = 2$), as mentioned before. Figure 3.12 shows the pattern change of the cross-polarization component in the plane normal to the incident plane. The symmetricity with respect to z-axis deteriorates as the aperture is changed from a symmetric aperture ($a = b$) to an un-symmetric one ($a \neq b$).

A consideration of the scattering fields in a special circumstance of an infinitely thin screen is necessary to self-check the KA formulation accuracy. For this case, the scattering field $\boldsymbol{E}_2^{\mathrm{ss}}$ in the lower half-space can be derived directly from $\boldsymbol{M}_1^-$ in Eq. (3.10) for E polarization and in Eq. (3.105) for H polarization in similar way of deriving $\boldsymbol{E}_1^{\mathrm{s}}$. As a result, one does not need to consider the thickness of the screen. Consequently, one finds for $\theta > \pi/2$

$$\boldsymbol{E}_2^{\mathrm{ss}} \;=\; -\boldsymbol{E}_1^{\mathrm{s}}. \tag{3.185}$$

Based on this result, the scattering patterns are exactly symmetric with respect to the screen for the infinitely thin screen. Besides, one can also take a limit of the finite thickness

c of our lower scattering field $\boldsymbol{E}_2^{\mathrm{s}}$ formulation in Eqs. (3.96), (3.97), (3.159) and (3.160). Figure 3.13(a) shows the far-field pattern comparison between $\boldsymbol{E}_2^{\mathrm{ss}}$ (infinitely thin case) and $\boldsymbol{E}_2^{\mathrm{s}}$ (limit case) for $\boldsymbol{E}_\phi$ in θ variation. Although the equivalence between them has not been analytically shown, a very good agreement has been observed. These values are similar for most observation angles and a symmetry with respect to the ground plane can also be seen in the three-dimensional view of Fig. 3.13(b).

Figure 3.14 shows the change of scattering pattern peak value and its direction due to the change of aperture width. One can observe the peak value in the result of co-polarization scattering pattern in the incident plane ($\phi = \phi_0, \pi + \phi_0$). In KA method, there are no upper limitations for the positive value of aperture width ka, kb. However, a representative value of $ka = kb = 50$ which reveals that the aperture hole is quite large compared with the wavelength ($a = b \approx 8\lambda$) is chosen to be the maximum value. Screen thickness kc is chosen to be a finite value of $kc = 2$. The black solid line and red dashed line, respectively, shows the value in dB of the scattering peak at the upper and lower half-space which are scaled by the vertical axis on the left. Their corresponding θ direction in degree denoted by blue dot line and green cross line are measured by the vertical axis on the right. For their ϕ direction, according to previous results, the scattering peak always lies on the forward direction of $\phi = 225°$. As can be seen in the figure, the values of both upper and lower scattering peak increase as the aperture width become larger as mentioned in previous results. Considering the far-field pattern at lower half-space, the lower scattering fields are calculated using summation of the successive waveguide mode m and n as in Eq. (3.97). When $ka = kb < 4.5$, there exists only mode $m = 0$ and $n = 0$ which leads to zero value of scattering fields. For the peak direction, the peaks direct the corresponding reflected and incident shadow boundary directions near (θ, ϕ)=$(30°, 225°)$ and (θ, ϕ)=$(150°, 225°)$ for $ka = kb > 5$. In cases of smaller values of ka the scattering peaks tend to direct to higher angles near normal direction. This can be explained by the contribution of radiation fields excited at the hole's edges. One can base on this result to choose an applicable value of aperture width to apply KA method for scattering field calculation.

The change of scattering pattern peak value and its direction due to the change of screen thickness is shown in Fig. 3.15. One mentioned that the upper scattering field does not depend on the thickness parameter, thus only lower scattering peak values are

shown here. A large value of aperture width $ka = kb = 30$ is chosen which is the main reason for the peak value range from 50dB to 58dB. It becomes more difficult to predict exactly the peak direction of the transmitted fields by general geometrical optics due to the complicated summation of waveguide fields contribution as the screen thickness becomes larger. Then the θ direction of the peak, in this case, cannot be exactly equal to 135°. Also, depending on a certain value of screen thickness, the waveguide internal reflection occurs differently which leads to ϕ direction of the peak equals to 45° or 225° as analyzed in Fig. 3.10.

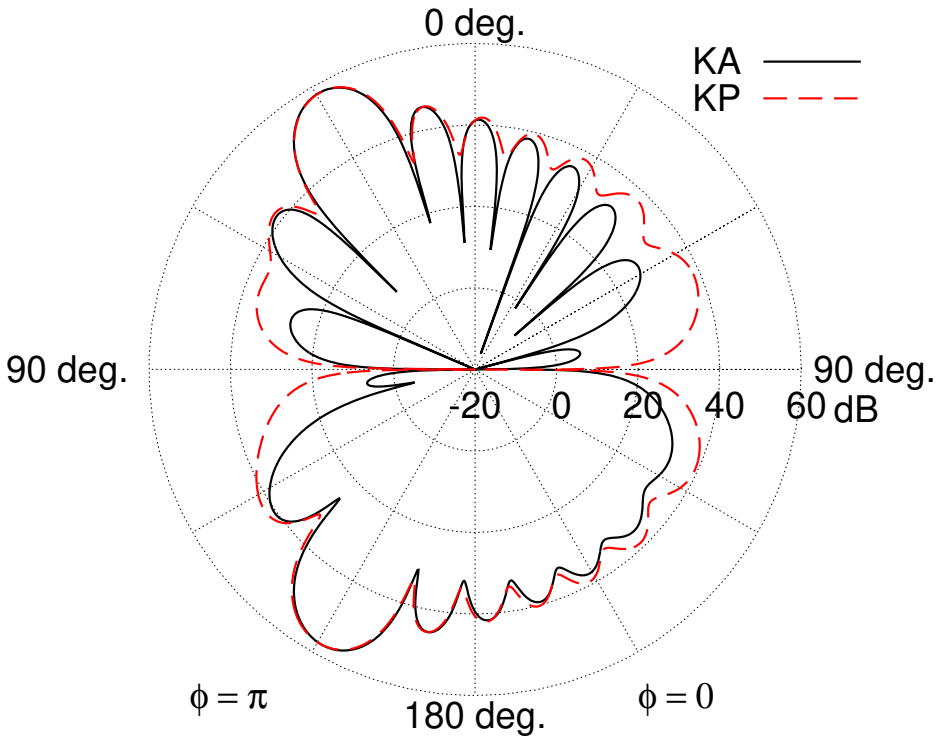

(a)

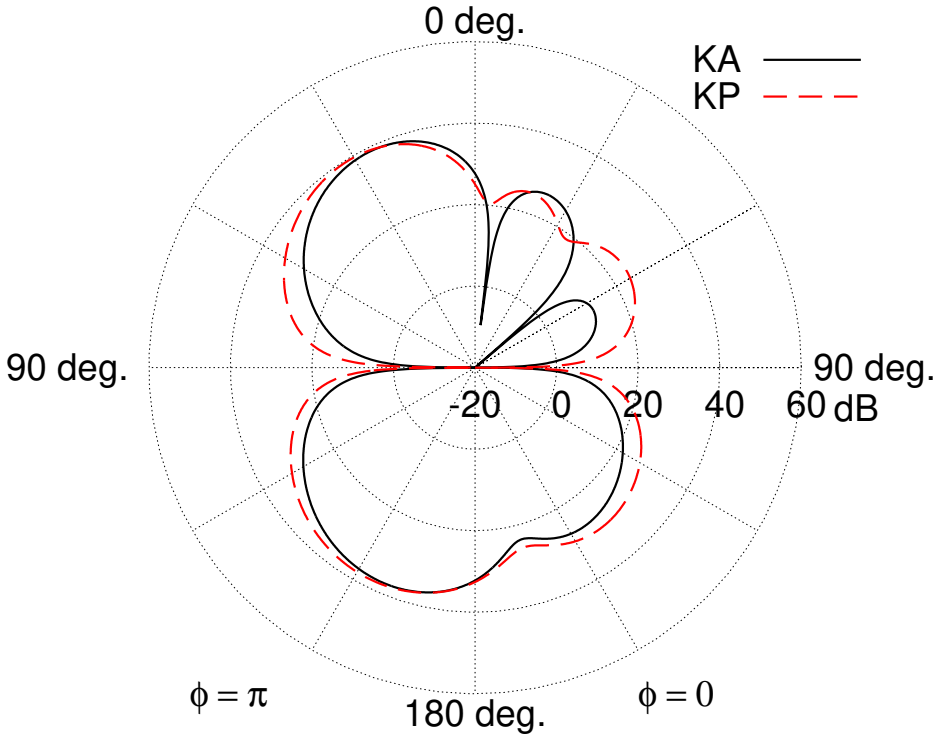

(b)

Figure 3.5: Co-polarization far-field scattering pattern comparison by KA and KP methods (E_ϕ) in θ variation for TE polarization in the incident plane ($\phi = \phi_0, \pi+\phi_0$), $\theta_0 = \pi/6$, $\phi_0 = 0$, $kc = 2$. (a) $ka = kb = 30$. (b) $ka = kb = 10$.

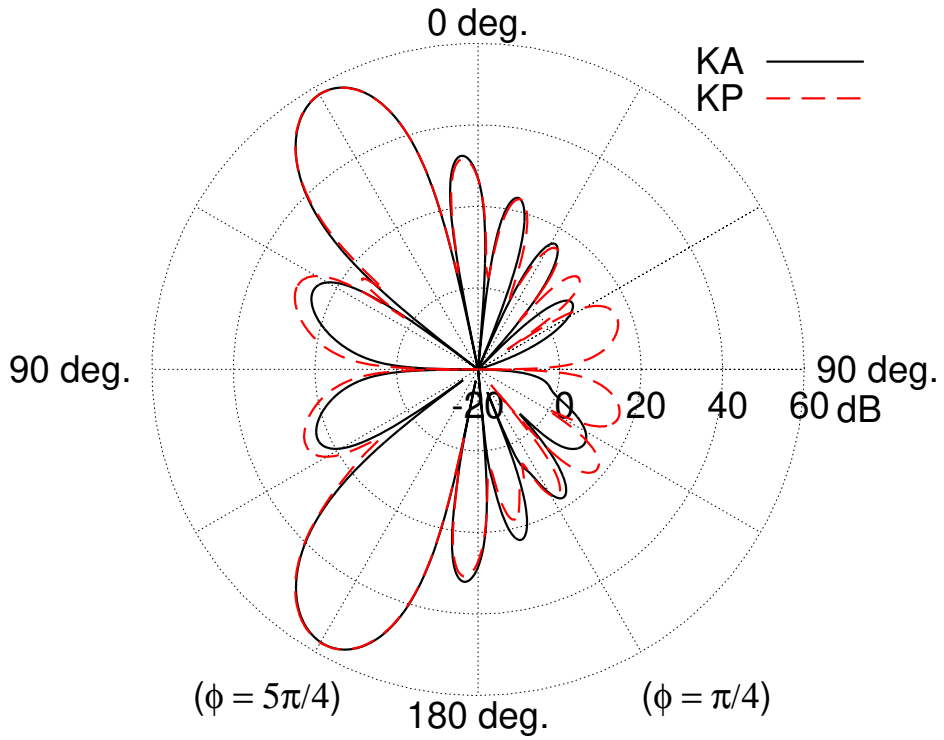

(a)

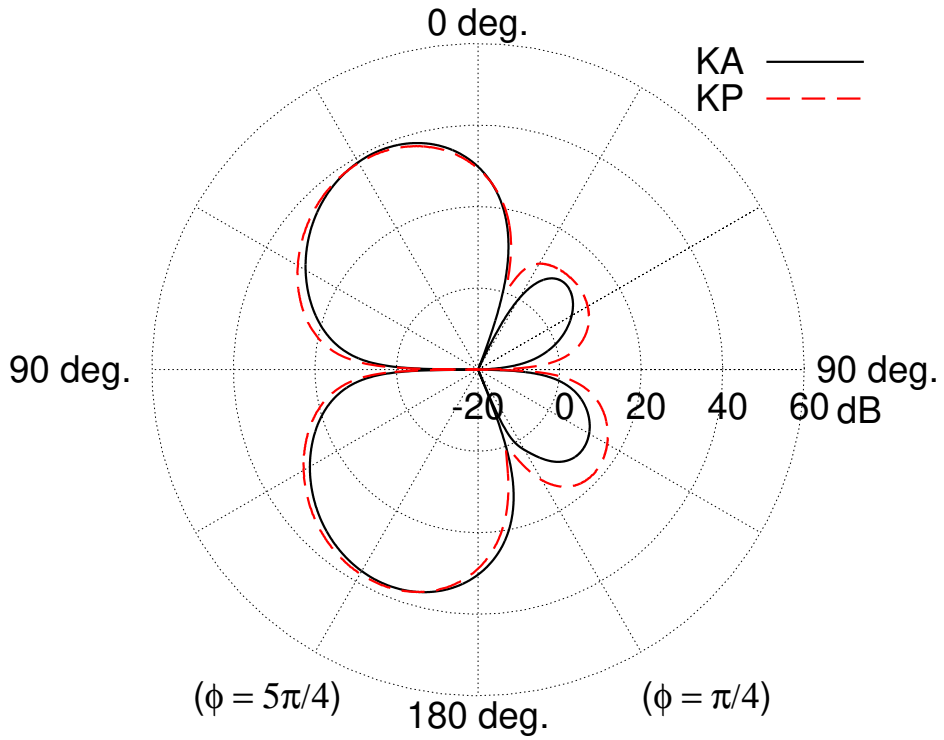

(b)

Figure 3.6: Far-field scattering pattern comparison (E_ϕ) in θ variation for TE polarization in different observation planes. $\theta_0 = \pi/6$, $\phi_0 = \pi/4$, $kc = 2$. (a) $ka = kb = 30$. (b) $ka = kb = 10$.

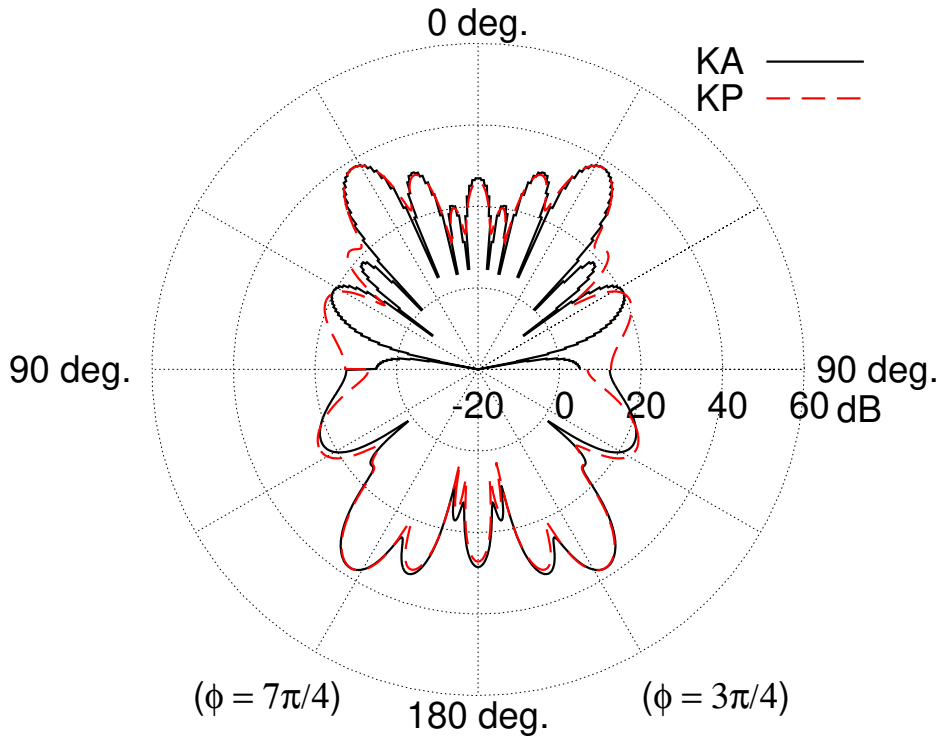

(a)

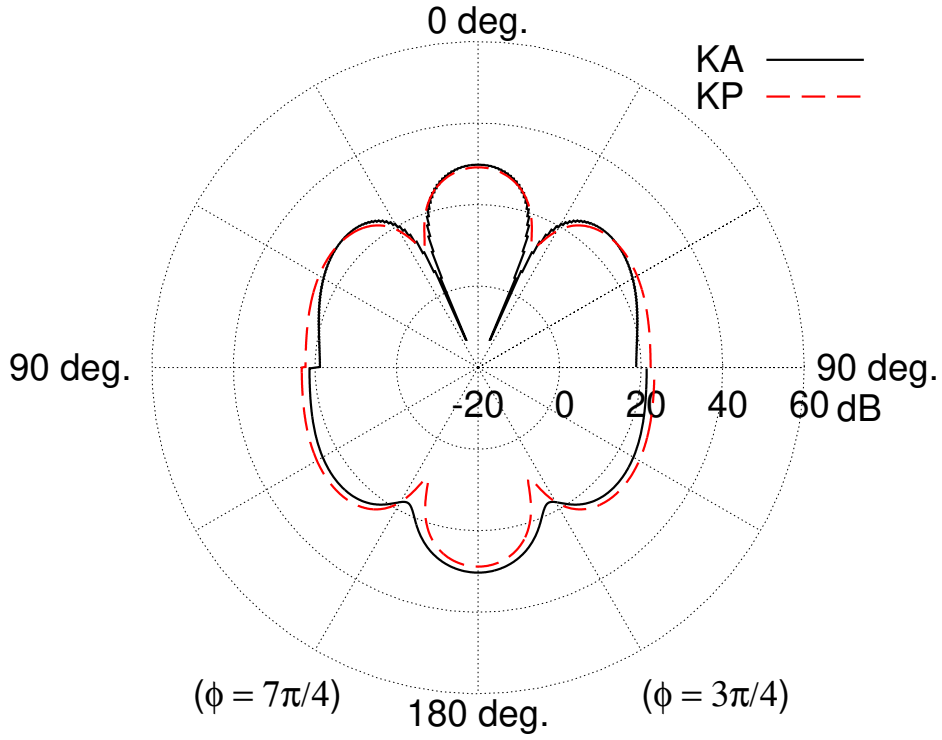

(b)

Figure 3.7: Cross-polarization far-field scattering pattern comparison (E_θ) in θ variation for TE polarization in the plane normal to the incident plane ($\phi = \pi/2 + \phi_0, 3\pi/2 + \phi_0$), $\theta_0 = \pi/6$, $\phi_0 = \pi/4$, $kc = 2$. (a) $ka = kb = 30$. (b) $ka = kb = 10$.

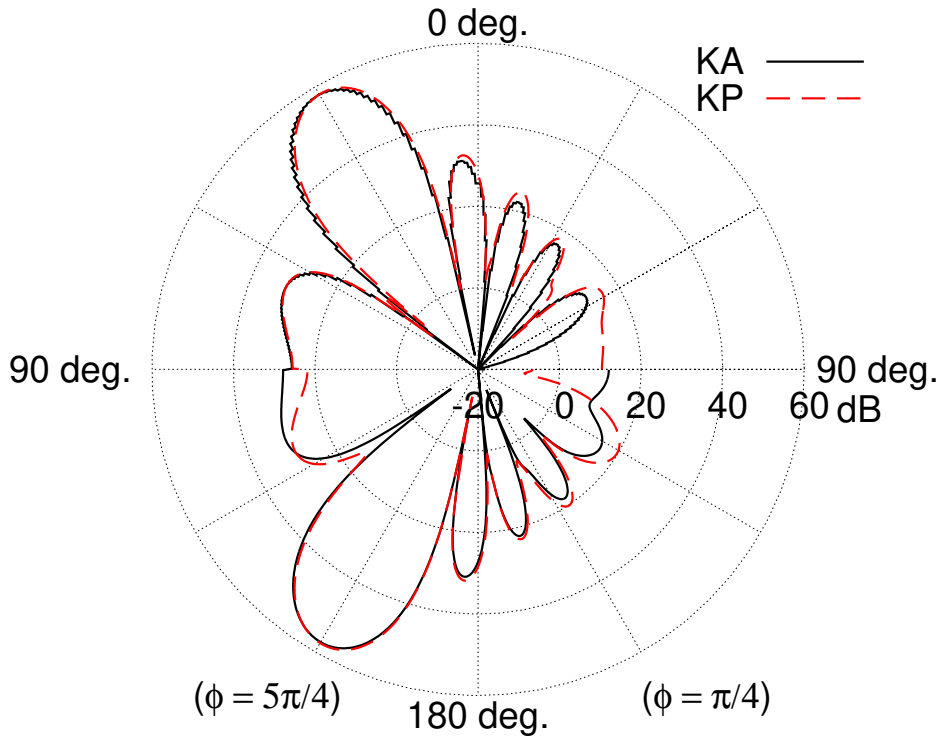

(a)

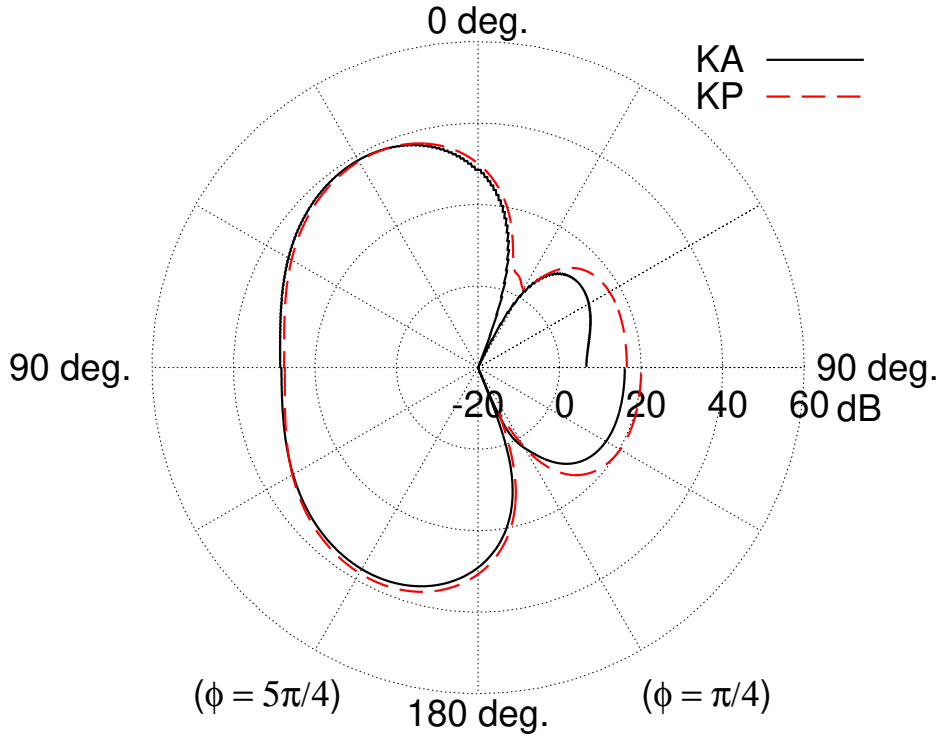

(b)

Figure 3.8: Co-polarization far-field scattering pattern comparison by KA and KP methods (E_θ) in θ variation for TM polarization in the incident plane ($\phi = \phi_0, \pi+\phi_0$), $\theta_0 = \pi/6$, $\phi_0 = \pi/4$, $kc = 2$. (a) $ka = kb = 30$. (b) $ka = kb = 10$.

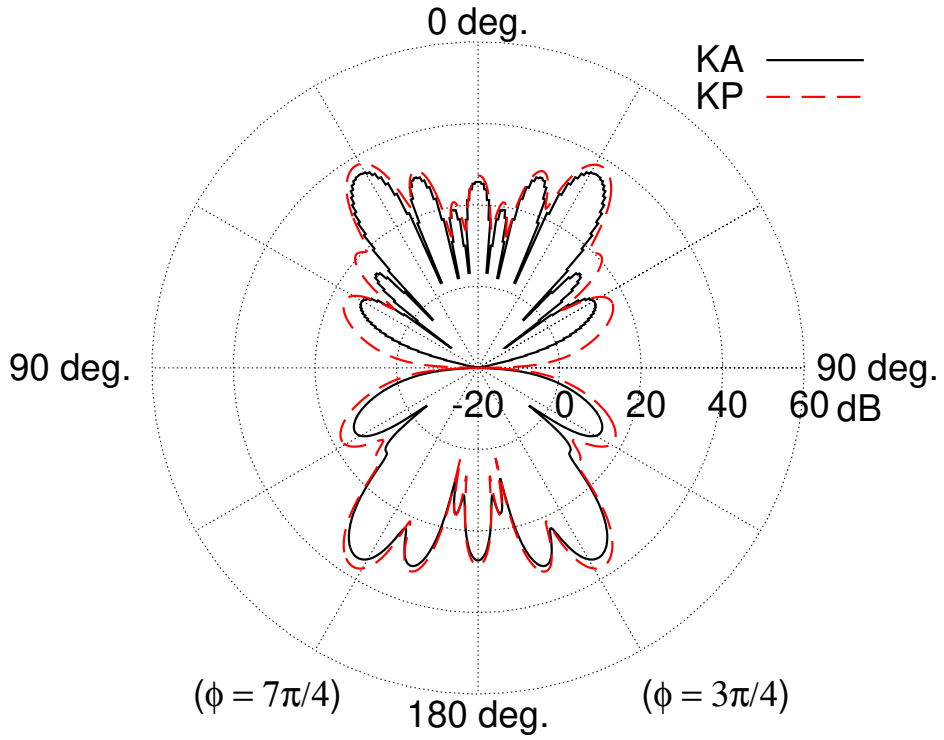

(a)

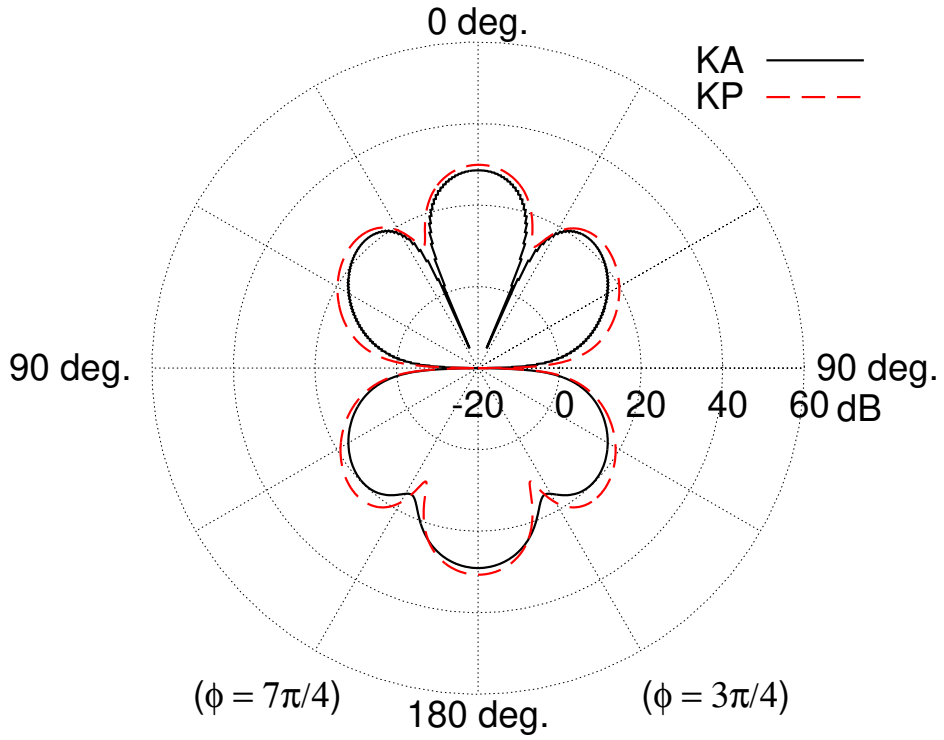

(b)

Figure 3.9: Cross-polarization far-field scattering pattern (E_ϕ) in θ variation for TM polarization in the plane normal to the incident plane ($\phi = \pi/2+\phi_0, 3\pi/2+\phi_0$), $\theta_0 = \pi/6$, $\phi_0 = \pi/4$, $kc = 2$. (a) $ka = kb = 30$. (b) $ka = kb = 10$.

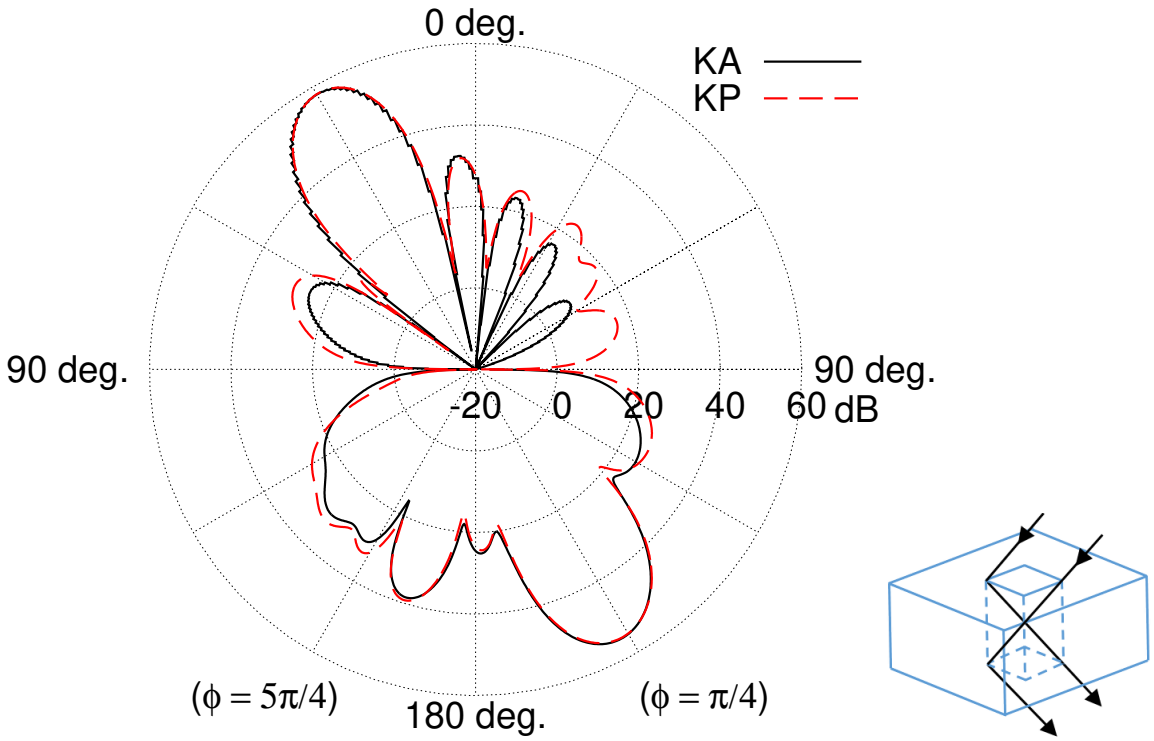

(a)

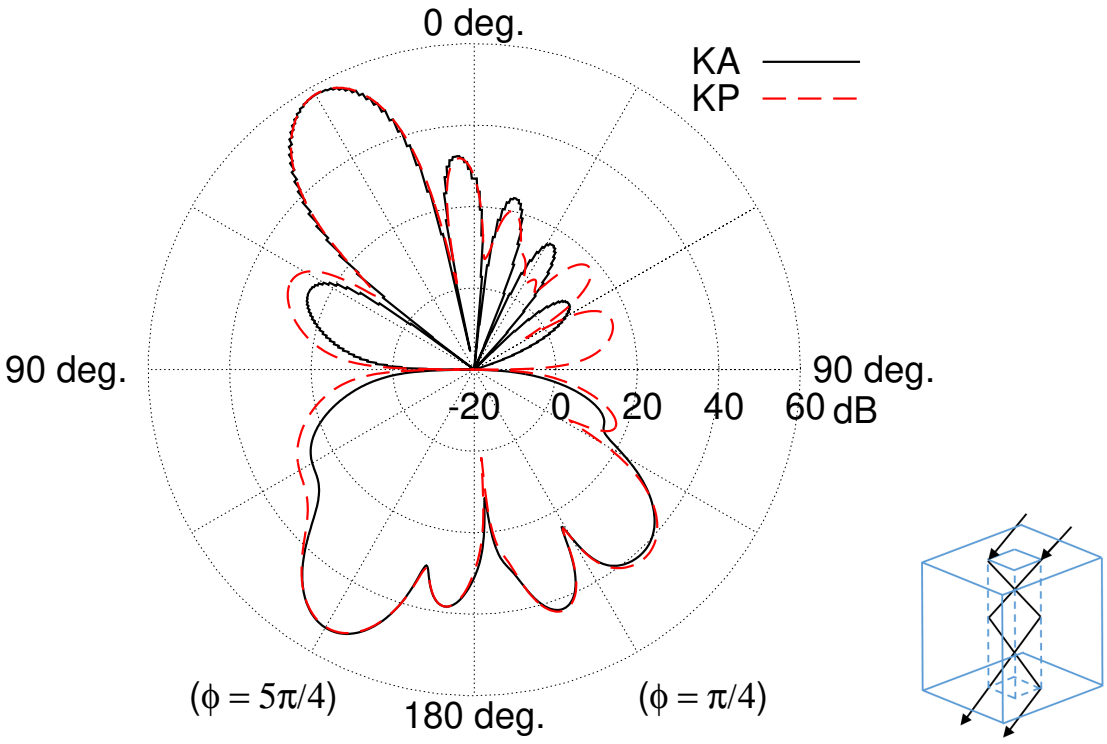

(b)

Figure 3.10: Far-field scattering pattern comparison (E_ϕ) in θ variation of the thick screen cases for TE polarization in the incident plane ($\phi = \phi_0, \pi + \phi_0$), $\theta_0 = \pi/6$, $\phi_0 = \pi/4$, $ka = kb = 30$. (a) $kc = \sqrt{6}ka$. (b) $kc = 2\sqrt{6}ka$.

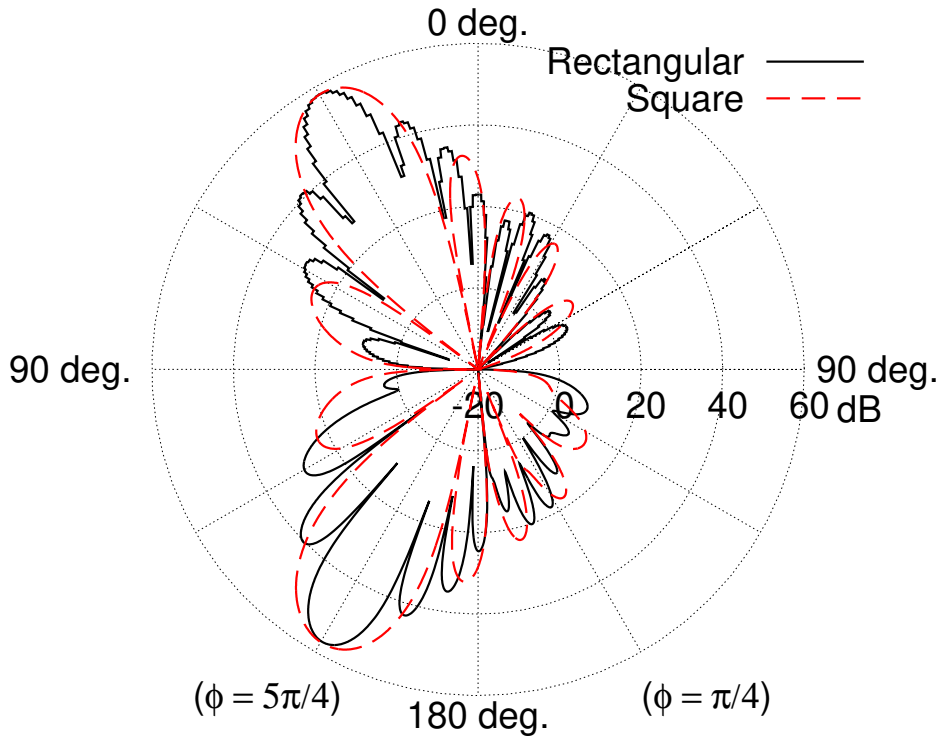

(a)

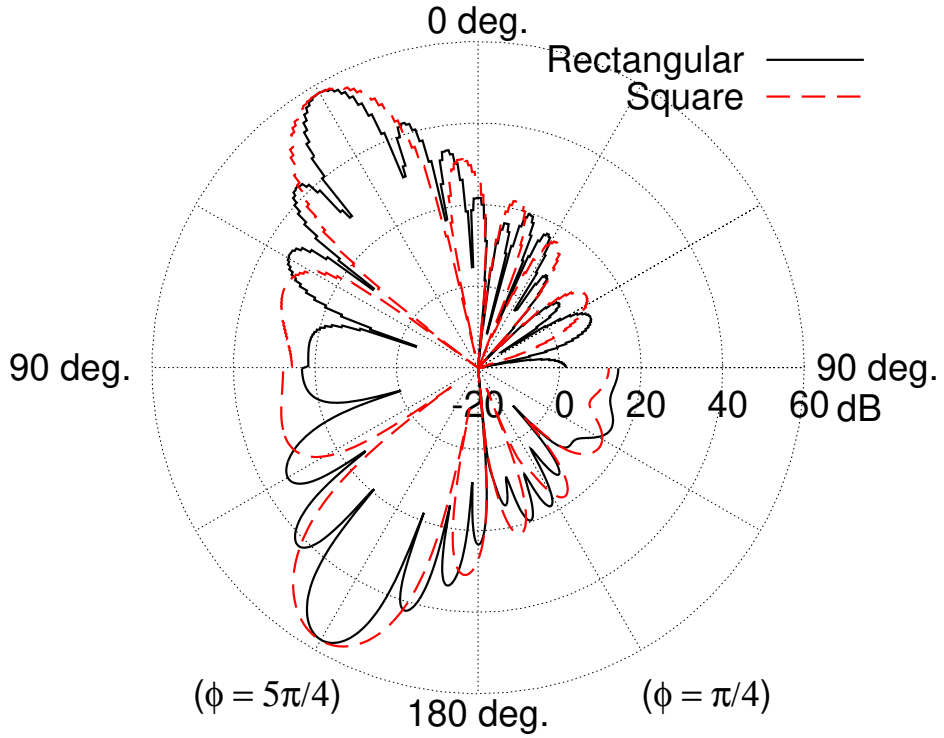

(b)

Figure 3.11: Co-polarization far-field scattering patterns by KA method in the incident plane from a rectangular aperture ($ka/2 = 2kb = 30$) and a square aperture ($ka = kb = 30$). $\theta_0 = \pi/6$, $\phi_0 = \pi/4$, $kc = 2$. (a) E_ϕ for TE polarization. (b) E_θ for TM polarization.

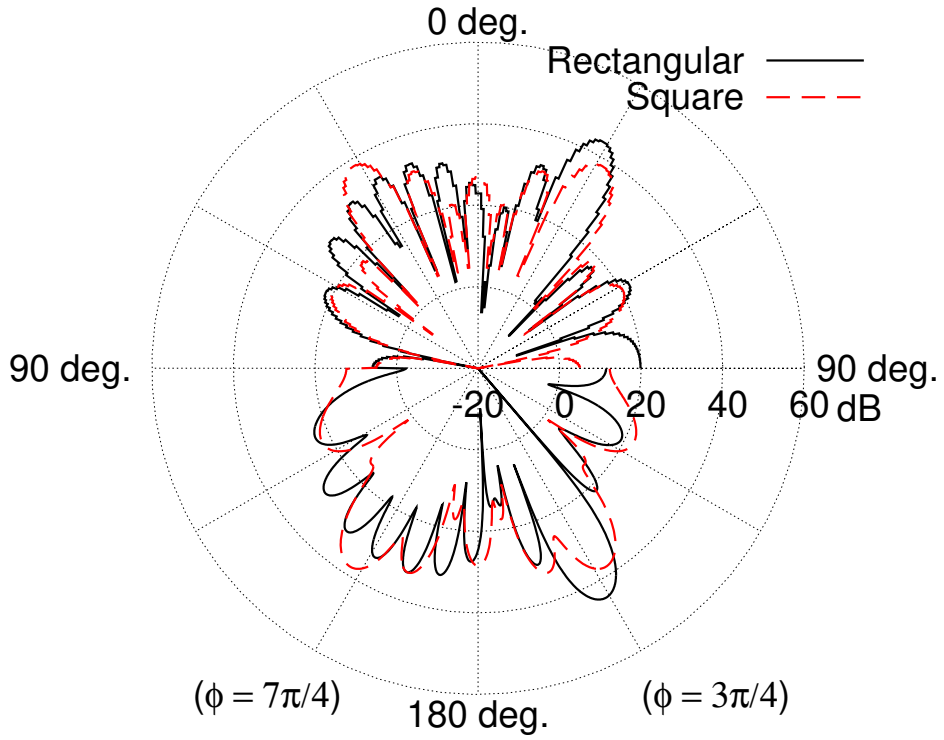

(a)

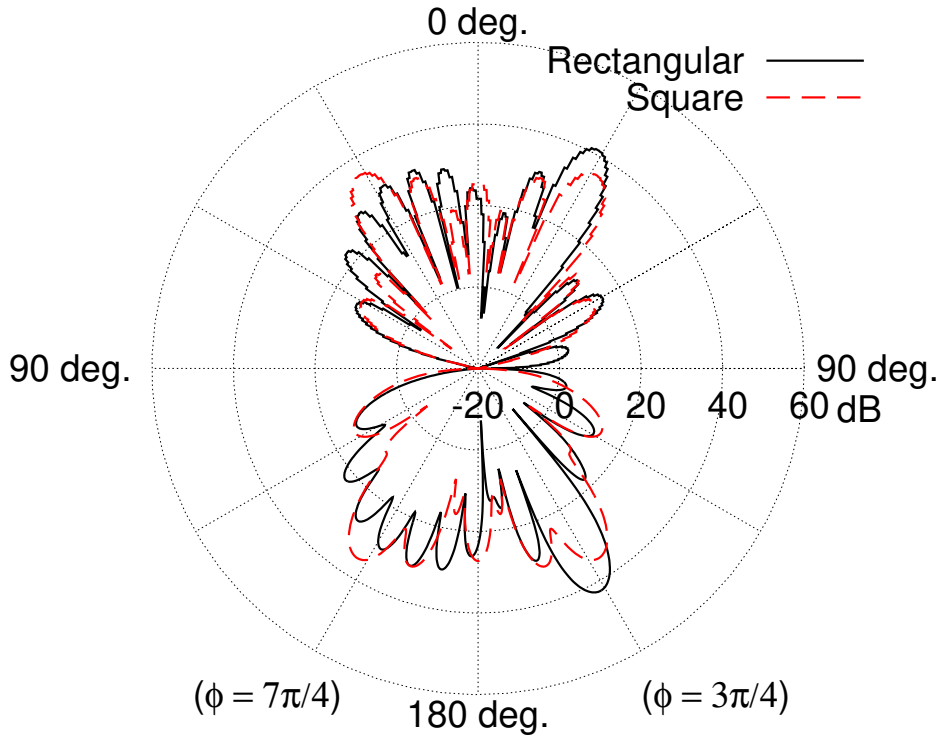

(b)

Figure 3.12: Cross-polarization far-field scattering patterns by KA method in the plane normal to the incident plane from a rectangular aperture ($ka/2 = 2kb = 30$) and a square aperture ($ka = kb = 30$). $\theta_0 = \pi/6$, $\phi_0 = \pi/4$, $kc = 2$. (a) E_θ for TE polarization. (b) E_ϕ for TM polarization.

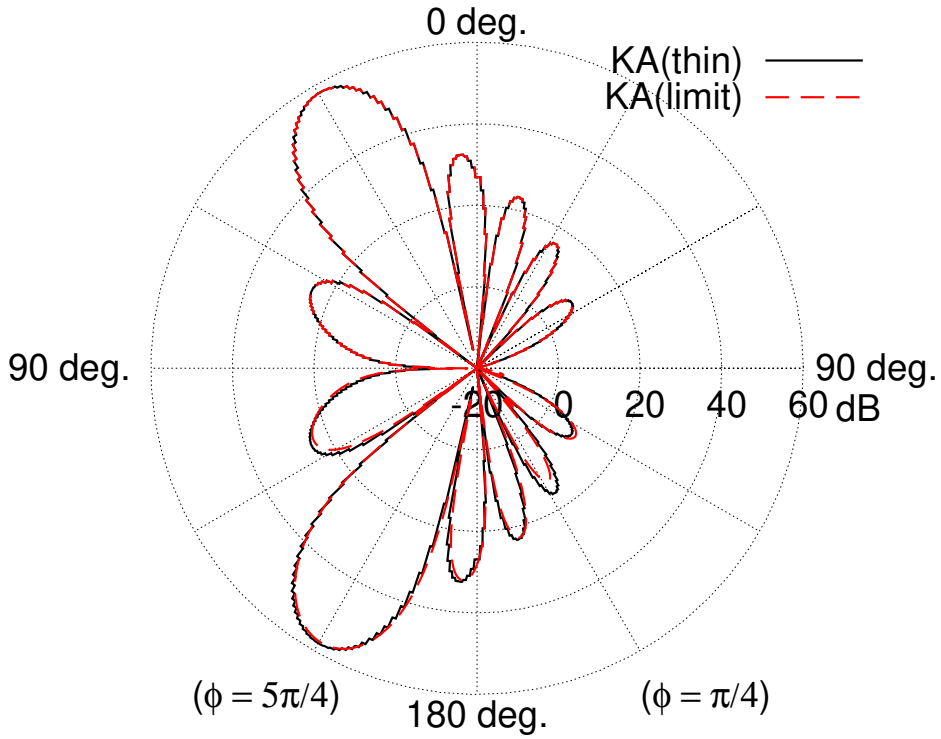

(a)

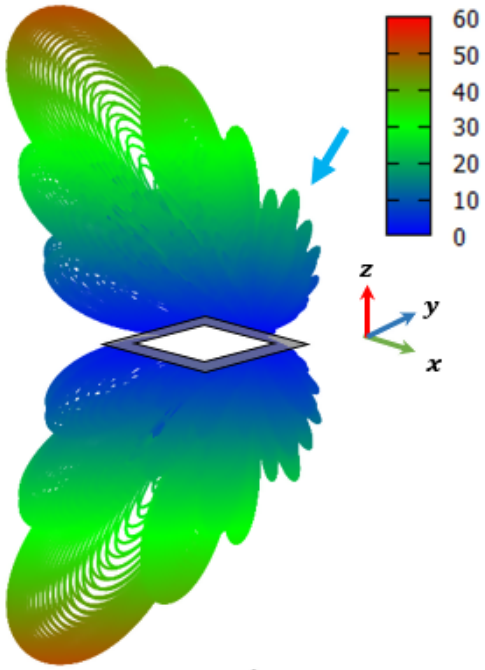

(b)

Figure 3.13: Far-field scattering patterns by KA method (E_ϕ) in θ variation (infinitely thin screen). TE polarization, $\theta_0 = 30°$, $\phi_0 = 45°$, $ka = kb = 30$. (a) Cross sectional view in the incident plane ($\phi = \phi_0, \pi + \phi_0$). Comparison between an infinitely thin and a limit ($c \to 0$) cases. (b) Three-dimensional view.

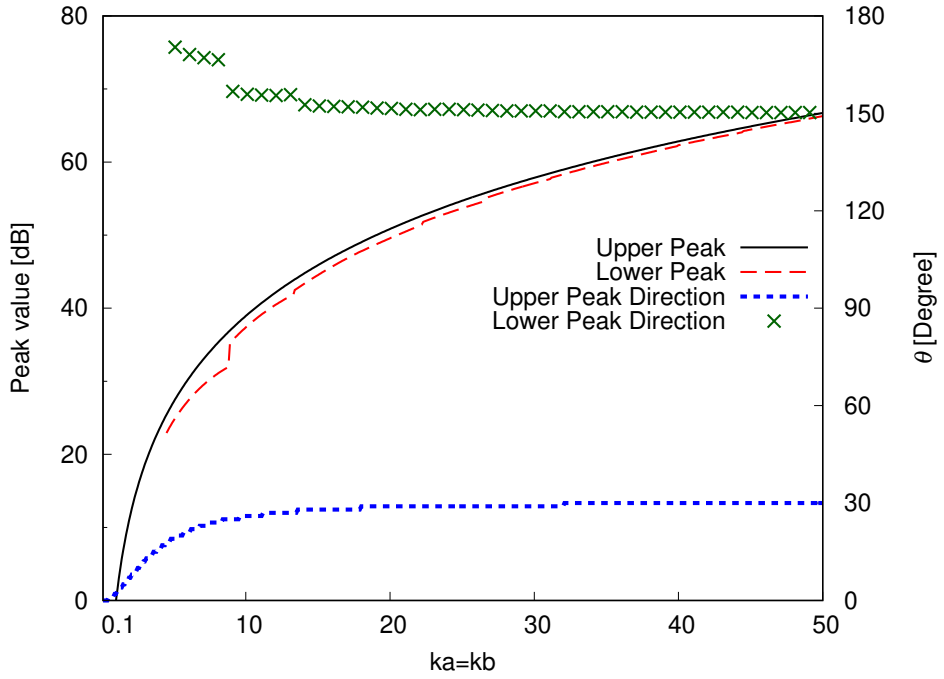

Figure 3.14: Peak value and peak direction of co-polarization far-field scattering pattern in the incident plane ($\phi = \phi_0, \pi + \phi_0$) at upper and lower half-space in aperture width variation. TE polarization, $kc = 2$, $\theta_0 = 30°$, $\phi_0 = 45°$.

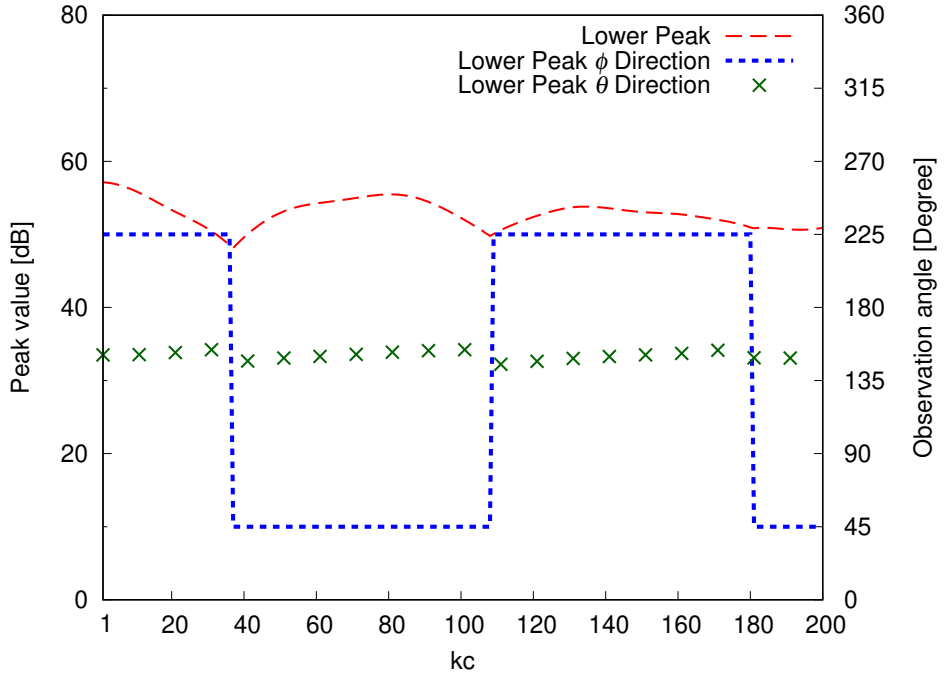

Figure 3.15: Peak value and peak direction of co-polarization far-field scattering pattern in the incident plane ($\phi = \phi_0, \pi + \phi_0$) at lower half-space in screen thickness variation. TE polarization, $ka = kb = 30$, $\theta_0 = 30°$, $\phi_0 = 45°$.

Chapter 4

Concluding Remarks

Kirchhoff approximation - a high frequency approximation method to analyze the electromagnetic plane wave scattering by aperture on conducting screen has been proposed. This method is based on assumption that scattering fields can be considered as field radiations from equivalent magnetic current sources postulated on the closing apertures.

Firstly, the plane wave scattering by a two-dimensional aperture model of loaded conducting thick slits has been formulated using the KA method in Chapter 2. The scattering fields result from the equivalent magnetic current sources exist on the slit's apertures. Scattering characteristics in many aspects such as various aperture width, slit's thickness, incident wave's direction, incident wave's polarization, and glass layer effect has been analyzed. The agreement between numerical results derived by the proposed KA method with those from GTD and KP method in most circumstances ensures the KA formulation accuracy. The accuracy is also confirmed by analytical assessment in special circumstance (infinitely thin slit) and in relation with the corresponding results of three-dimensional analysis in Chapter 3. The validation is important to extend the KA method to solve more practical scattering problem.

In Chapter 3, the KA method has been successfully extended to solve more complicated scattered object of three-dimensional rectangular hole perforated in a thick conducting screen. The scattering fields can also be obtained from equivalent magnetic current sources on the hole apertures in both E and H polarization cases of the incident plane waves. Since the analytical derivation process for three-dimensional scattering fields in the KA method is lengthy and complicated, the final results have been checked by those from the KP method in many circumstances of aperture width, screen thickness, polarization,

incident angles, and observation angles. A relation between KA three-dimensional and two-dimensional formulation has also been shown to confirm the accuracy.

The efficiency of the KA method in aperture scattering high frequency analysis has been shown in the thesis. Based on the obtained results, one can confidently extend our formulation to more practical scattering prediction, such as multiple apertures, inverse scattering problems to estimate the physical parameters. This study is directed to build an effective wave propagation model to predict the outdoor-indoor transmitted signals accurately. KA method could be an effective tool for examining radio propagation characteristics through building windows in outdoor-indoor environment.

Acknowledgment

I truly appreciate that MEXT and Chuo University have provided me the great opportunity to study in Japan. And I would like to express my reverence to Prof. Hiroshi Shirai for his guidance, inspiration and academic advice during my doctoral course. I have duly noticed and appreciated his kindnesses and patience over these years. He has set a standard of professional and ethical excellence to emulate. His continued guidance and support led me the right way.

I also want to thank Prof. Keiji Goto from the National Defense Academy, Prof. Ryoichi Sato from Niigata University, Prof. Kazuya Kobayashi from Chuo University, and Prof. Hirohide Serizawa from Numazu College for their advice and comments that led to important improvements in this thesis and my research.

I would like to express my deepest gratitude to my family and Shirai Lab's members, especially my parents, my wife, my colleagues including Dr. Quang Ngoc Hieu, Mr. Ta Quang Ngoc, Mr. Masayuki Shimizu, and Mr. Haruchika Kimura. The encouragement from them is the main source of motivation and resilience for me to overcome tough times, to finish the research and to write this thesis.

References

[1] M. Kerker, *The Scattering of Light*, Academic, 1969.

[2] Lord Rayleigh, "On the electromagnetic theory of light," *Philos. Mag.12(73)*, pp. 81–101, 1881.

[3] L. Lorenz, *Videnskabernes Selskab Skrifter*, Vol. 6, p. 142, 1890. [Reprinted in L. Lorenz, Oeuvres Scientifiques, Librairie Lehmann, Copenhagen, Vol. 1, p. 405, 1896 (Reprinted by Johnson, New York, 1964).]

[4] J. J. Thomson, *Recent Researches in Electricity and Magnetism*, Oxford University, 1893.

[5] G. Mie, "Beitrage zur Optik truber medien, speziell kolloidaler Metallosungen," *Ann. Phys. 330*,pp. 377–445, 1908.

[6] J. A. Stratton, *Electromagnetic Theory*, McGraw-Hill, 1941.

[7] J. G. Van Bladel, *Electromagnetic Fields*, 2nd ed., Wiley, 2007.

[8] C. F. Bohren and D. R. Huffman, *Absorption and Scattering of Light by Small Particles*, Wiley, 1940.

[9] L. Tsang, J. A. Kong, and K. H. Ding, *Scattering of Electromagnetic Waves: Theory and Applications*, Wiley, 2000.

[10] P. M. Morse and P. J. Rubenstein, "The diffraction of waves by ribbons and by slits," *Phys. Rev.*, vol. 54, no. 11, pp. 895–898, 1938.

[11] Y. Nomura and S. Katsura, "Diffraction of electromagnetic waves by ribbon and slit. I," *J. Phys. Soc. Jpn.*, vol. 12, no. 2, pp. 190–200, 1957.

[12] K. Hongo, "Diffraction of electromagnetic plane wave by infinite slit perforated in a conducting screen with finite thickness," *Trans. IECE*, vol. 54B, no. 7, pp. 419–425, Jul. 1971 (in Japanese).

[13] K. Hongo and G. Ishii, "Diffraction of an electromagnetic plane wave by a thick slit," *IEEE Trans. Antennas Propag.*, vol. 26, no.3, pp. 494–499, May 1978.

[14] H. Serizawa, "Diffraction by a rectangular hole in a thick conducting screen," Open access peer-reviewed chapter, IntechOpen, 2019.

[15] S. Kashyap and M. A. K. Hamid, "Diffraction characteristics of a slit in a thick conducting screen," *IEEE Trans. on Antennas and Propag.*, vol. 19, no. 4, pp. 499–507, Jul. 1971.

[16] S. H. Kang, H. J. Eom, and T. J. Park, "TM scattering from a slit in a thick conducting screen: Revisited," *IEEE Trans. Microw. Theory Techn.*, vol. 41, no. 5, pp. 895–899, May 1993.

[17] T. J. Park, S. H. Kang, and H. J. Eom, "TE scattering from a slit in a thick conducting screen: Revisited," *IEEE Trans. on Antennas and Propag.*, vol. 42, no. 1, pp. 112–114, Jan. 1994.

[18] M. A. Morgan, *Finite Element and Finite Difference Methods in Electromagnetic Scattering*, Elsevier, New York 1989.

[19] D. L. Colton and R. Kress, *Inverse Acoustic and Electromagnetic Scattering Theory*, Springer–Verlag, 1992.

[20] S. Bilbao, *Wave and Scattering: Methods for Numerical Simulation*, John Wiley & Sons, 2004.

[21] A. V. Osipov and S. A. Tretyakov, *Modern Electromagnetic Scattering Theory with Applications*, John Wiley & Sons, 2017.

[22] M. Tomita and K. Yasuura, "Numerical analysis of plane wave scattering from dielectric cylinders," *IEICE Trans. Commun.,* vol. J62–B, no. 2, pp. 132–139, 1979. (in Japanese).

[23] T. Yamasaki, T. Hinata and T. Hosono, "Scattering of plane wave electromagnetic waves by a conducting rectangular cylinder –Point matching method considering edged condition–," *IEICE Trans. Electron.,* vol. J72–C–I, no. 11, pp. 703–710, 1989. (in Japanese).

[24] W. Kishida, R. Ozaki and T. Yamasaki, "Scattering of electromagnetic wave by a dielectric rectangular cylinder with conducting strip," *Technical Report on Electromagnetic Theory*, IEEJ, EMT-17-60, pp. 37–40, 2017. (in Japanese).

[25] S. N. Karp and A. Russek, "Diffraction by a wide slit," *J. Appl. Phys.*, vol.27, no.8, pp.886–894, Aug. 1956.

[26] P. C. Clemmow, "A method for the exact solution of a class of two dimensional diffraction problem," *Proc. roy. Soc.*, A 205, 281, 1951.

[27] H. Levine, "Diffraction by an infinite slit," *Technical Report No. 61*, Applied Mathematics and Statistics Laboratory, Stanford University.

[28] S. R. Seshadri, "High-frequency diffraction of plane waves by an infinite slit –I and II," *Proc. Nat. Inst. Sci. India, Ser. A*, 25, 301 (1959); 25, 322 (1959).

[29] S. R. Seshadri and T. T. Wu, "High-frequency diffraction of plane waves by an infinite slit for grazing incidence," *IRE Transactions on Antennas and Propagation*, vol.8, no.1, pp. 37–42, Jan. 1960.

[30] S. Koshikawa, K. Kobayashi and T. Eizawa, "Wiener-Hopf analysis of the high-frequency diffraction by a strip: Higher order asymptotics," *T. IEE Japan*, vol.113-A, no.3, pp. 157–166, 1993.

[31] H. Shirai and R. Sato, "High frequency ray-mode coupling analysis of plane wave diffraction by a wide and thick slit on a conducting screen," *IEICE Trans. Electron.*, vol.E95-C, no.1, pp.10–15, Jan. 2012.

[32] H. Shirai, M. Shimizu and R. Sato, "Hybrid ray-mode analysis of E-polarized plane wave diffraction by a thick slit," *IEEE Trans. Antennas and Propag.*, vol.64, no.11, pp.4828–4835, Nov. 2016.

[33] M. Shimizu, H. Shirai and R. Sato, "Electromagnetic scattering analysis by a window model on a building wall," *IEICE Trans. Electron.*, vol.J100-C, no.7, pp.295–301, July 2017 (in Japanese).

[34] H. Shirai and L. B. Felsen, "Rays, modes and beams for plane wave coupling into a wide open-ended parallel-plane waveguide," *Wave motion*, vol. 9, no. 4, pp. 301–317, Jul. 1987.

[35] H. Shirai, *Geometrical Theory of Diffraction*, Corona Publishing Co.,Ltd., 2015 (in Japanese).

[36] C. A. Balanis, *Advanced Engineering Electromagnetics*, 2nd ed., Wiley, NJ, 2012.

[37] L. B. Felsen and N. Marcuvitz, *Radiation and Scattering of Waves*, Prentice-Hall, NJ, 1973.

[38] R. A. Ross, "Radar cross section of rectangular flat plates as a function of aspect angle," *IEEE Trans. Antennas and Propag.*, vol.AP-14, no.3, pp.329–335, May 1966.

[39] H. N. Quang and H. Shirai, "High frequency electromagnetic scattering analysis by rectangular cylinders," *IEICE Trans. Electron.*, vol.E102-C, no.1, pp.21–29, Jan. 2019.

List of Publications

Journal Papers

[1] K. N. Nguyen and H. Shirai, "Kirchhoff Approximation Analysis of Plane Wave Scattering by Conducting Thick Slits," *IEICE Trans. Electron.*, Vol. 102-C, No. 1, pp. 12–20, Jan. 2019.

[2] K. N. Nguyen, H. Shirai and H. Serizawa, "Electromagnetic Scattering Analysis from a Rectangular Hole in a Thick Conducting Screen," Accepted and to be published on *IEICE Trans. Electron.*, Vol. 104-C, No. 4, Apr. 2021.

Proceedings of International Conferences

[1] K. N. Nguyen, and H. Shirai, "Electromagnetic Plane Wave Scattering by a Rectangular Hole in a Thick Conducting Screen," *Proc. of 2017 International Conference on Electromagnetics and Advanced Applications*, pp. 394–396, Verona, Italy.

[2] K. N. Nguyen and H. Shirai, "H-polarized Plane Wave Diffraction by Thick Conducting Slits," *Proc. of 2018 IEEE International Conference on Communications and Electronics (ICCE 2018)*, pp. 433–436, Hue, Vietnam.

[3] K. N. Nguyen and H. Shirai, "H-polarized Plane Wave Diffraction by Thick Conducting Slits," *Proc. of 2018 Progress in Electromagnetics Research Symposium (PIERS 2018)*, pp. 553–558, Toyama, Japan.

[4] K. N. Nguyen and H. Shirai, "Electromagnetic Plane Wave Diffraction by Thick Conducting Slits -E Polarization Case-," *Proc. of 2018 International Symposium on Antennas and Propagation (ISAP 2018)*, CDROM, Busan, Korea.

[5] K. N. Nguyen and H. Shirai, "High Frequency Diffraction by Rectangular Hole in a Thick Conducting Screen -H Polarization Case-," *Proc. of 2019 Progress in Electromagnetics Research Symposium (PIERS 2019)*, pp. 100–104, Rome, Italy.

[6] K. N. Nguyen and H. Shirai, "High Frequency Diffraction by Thick Loaded Conducting Slits -H Polarization Case-," *Proc. of 2019 IEEE International Symposium on Antennas and Propagation (APS/URSI 2019)*, pp. 497–498, Atlanta, USA.

[7] K. N. Nguyen and H. Shirai, "High Frequency Diffraction by a Rectangular Hole in a Thick Conducting Screen -E Polarization Case-," *Proc. of 2020 IEEE International Symposium on Antennas and Propagation (APS/URSI 2020)*, CDROM, Montreal, Canada.

[8] K. N. Nguyen and H. Shirai, "TE Plane Wave Diffraction by Window Aperture on a Thick Conducting Wall," *Proc. of 2020 IEEE International Conference on Advanced Technologies for Communication (ATC 2020)*, CDROM, Nha Trang, Vietnam.

Presentation at Domestic Conferences

[1] K. N. Nguyen and H. Shirai, "Plane Wave Diffraction by a Rectangular Hole in a Thick Conducting Screen," *IEICE Technical Report on Electromagnetic Theory (EMT)*, EMT2017-66, pp. 171–176, Yamagata, Japan.

[2] K. N. Nguyen and H. Shirai, "Plane Wave Diffraction by Loaded Slit in a Thick Conducting Screen," *IEICE Technical Report on Electromagnetic Theory (EMT)*, EMT2018-52, pp. 65–70, Tottori, Japan.

Academic Awards

[1] Japanese Government (MEXT) Scholarship for Research Student (September 2015–March 2016), Master Student (April 2016–March 2018), and Doctoral Student (April 2018–March 2021).

[2] Best Student Paper Award (2nd Prize) of *2018 Progress In Electromagnetics Research Symposium (PIERS 2018)*, August 1-4, 2018 at Toyama, Japan.

[3] International Conference Attendance Grant of *NEC C&C Foundation*, October 2018.

[4] Best Student Paper Award (Finalist) of *2018 International Symposium on Antennas and Propagation (ISAP 2018)*, October 23-26, 2018 at Busan, Korea.

[5] 24th Chuo University Katsuma Funaki Academic Encouragement Award, March 14th, 2019.

[6] Best Student Paper Award (Honorable Mention) of *2019 PhotonIcs and Electromagnetics Research Symposium (PIERS 2019)*, June 17-20, 2019 at Rome, Italy.

[7] Best Paper Award by the *Institute of Electronics, Information and Communication Engineers (IEICE)*, June 4th, 2020.

[8] 2020 Research Scholarship of *Hakumon Schorlarship Society*, June 23rd, 2020.